PACKING OF GRANULAR MATERIALS

by

Riccardo Isola

Thesis submitted to the University of Nottingham

for the degree of Doctor of Philosophy

January 2008

ABSTRACT

Granular materials are prevalent in the world at macro and micro scales, from the macro-scale of construction materials to the micro-scale of chemical powders. The properties of assemblages of grains are heavily controlled by the interparticle contacts. In order to assist with the better understanding of the means by which granular assemblages behave, this thesis seeks to develop understanding of the number, type and geometrical distribution of the contact points between individual grains.

The study has been limited to assemblages of spheres in psuedo-random packing arrangements as these simulate the arrangements often encountered in real situations. Assemblages comprising equal-sized and two-sized spheres have been studied.

The work reported herein analyses various types of packings simulated by algorithms purposely developed during this research, focusing on fundamental geometrical parameters such as packing density, coordination number and radial distribution function in order to develop basic concepts and relationships to be used for future applications. Particular attention is given to the study of bidisperse packings, which can be considered as a simplification of a variably graded mixture.

The thesis describes how the statistical distribution of partial coordination numbers are strictly related to each other and originate from a common normal distribution

that has herein been called "characteristic distribution". This concept allows the development of a model for the prediction of partial coordination numbers in the packings simulated. The concept of superficial distribution of contact points is also introduced to represent the evenness of the distribution of these contacts on a particle's surface.

Furthermore, the radial distribution function of monodisperse and bidisperse packings is studied in order to investigate long-range relationships between particles and to compare the simulated packings to the numerical reconstruction of a real assembly of spherical particles scanned by an X-Ray CT.

Finally, the thesis proposes sensible follow-on activity that could develop the study further.

Keywords: granular material, particles, packing, spheres, coordination, contact.

ACKNOWLEDGEMENTS

The present project was carried out at the NTEC - Nottingham Transportation Engineering Centre (former NCPE – Nottingham Centre for Pavement Engineering), School of Civil Engineering, under the supervision of Mr. Andrew R. Dawson from the same university. The conclusion of this dissertation has been possible thanks to the collaboration of several individuals and entities to whom I would like to express my gratitude.

First of all, I would like to thank Mr. Andrew Dawson for his constant interest in this relatively new subject, his encouragement to pursue knowledge, his invaluable contributions during the numerous discussions and his careful reading of this text.

I would also like to thank the department of the Nottingham Transportation Engineering Centre in the person of Prof. Andy Collop, who provided the facilities needed for the research and an ideal working place. Thanks are also due to the technical and secretarial staff of the NTEC, particularly to Chris Fox for his assistance with the work carried out on the X-Ray CT.

I cannot forget the financial support provided by my personal sponsor, the local government of Sardinia, Italy. Without its scholarship this research project and my whole experience in the United Kingdom would still be a dream.

My gratitude also goes to the TRL - Transport Research Laboratory, where I have the pleasure and honour to work, and in particular Mr. Ian Carswell, who believe in me supported me in the last period of my research.

I would like to express my personal thanks to Prof. Mauro Coni of the University of Cagliari, Sardinia, for his wise mentoring and friendship during these years.

A special thank to all my friends at the research office, in no particular order, Joel, Joe, Mohamed, Lelio, James, Salah, Pierpaolo, Ted, Poranic, Phil, Muslich, York, Dave, Nono, Junwei and Jed, with whom I have shared many enjoyable times.

Finally, all my gratitude goes to my girlfriend Camila, for her love, understanding and constant encouragement, and to my family Fausto, Miriam and Cristina, for their precious support and sacrifice. They are my giants.

TABLE OF CONTENT

TABLE OF FIGURES

LIST OF TABLES

LIST OF SYMBOLS AND ABBREVIATIONS

ρ	packing density
FCC	face-centered cubic packing
HCP	hexagonal close-packed packing
LRP	loose random packing
DRP	dense random packing
RCP	random close packing
DEM	discrete element modelling
V_V	volume of a particle's Voronoi cell
D	superficial distribution
P	parking number for equal spheres
P_{ij}	parking number of j-type spheres on an i-type sphere
P_{ij}'	modified parking number
C	coordination number for equal spheres
C_{ij}	coordination number of an i-type sphere with j-type spheres
$<C_{ij}>$	average C_{ij}
C_{ijmax}	maximum C_{ij}
$C_{ij}^{kn}{}_{max}$	C_{ijmax} when n k-type spheres are also on the i-type sphere
$<C_{ij}^*>$	mean of the normal distribution of which the distribution of C_{ij} is the non-negative part
C_{ij}'	normalised C_{ij}
D_{ijk}	theoretical disturbance
$f(C_{ij},C_{ik})$	relative distribution of C_{ij} for a given value of C_{ik}, with $k \neq j$
$F(C_{ij})$	total distribution of C_{ij}
RDF, g(r)	radial distribution function
$g_{s90}(r)$	RDF of small spheres in a bidisperse packing with 90% of the solid volume occupied by small spheres
α	percentage of uncaged particles

1 INTRODUCTION

1.1 A very brief history of granular packing

«It's a great invention, but who would want to use it anyway?»

Rutherford B. Hayes, U.S. President, after a demonstration of Alexander Bell's telephone, 1878.

This is a granular world, it has always been. In the past millennia we have learnt how to use granular materials to build houses and roads, to measure time (hourglass), to feed all of us (rice, flour, Maltesers chocolates…) and we have learnt how to vacuum them! They are so common that we breathe them (pollen, dust, gases; Brilliantov et al 1996), drink them (pharmaceutical powders; Fu et al 2006) and play with them (sand; Seidler et al 2000, snow; University of Bristol 2007) and we don't even realise it. Ultimately, it seems that every system formed by numerous parts can be studied as a granular structure (proteins; Pollastri et al 2002, cells; Aste et al 1996a; Aste et al 1996b).

Cunning roman salesmen used to keep a vertical stick at the centre of barrels while filling them with beans, knowing that this would make them looser, lighter and more profitable, since they were going to be sold by volume. Ever since then, people acknowledged there could be something to gain in understanding and manipulating the properties of such materials.

Granules, or grains, are usually imagined as spheres, since this is supposed to be the most simple, perfect, beautiful and widely studied geometric solid we could ever think of. Thanks to its natural charm, spheres have always attracted scientific attention. In 1611, for instance, Kepler suggested, without proof, that equal spheres can never be packed together occupying more than 74% of the available volume, while in 1694 two of the leading scientists of the day – Isaac Newton and David Gregory – started a famous argument about whether the maximum possible number of equal spheres that can be placed around a central one of the same size should be 12 (Newton) or 13 (Gregory) (Pfender & Ziegler 2004; Plus Magazine 2003).

That was a long time ago, nonetheless the answer to both of these apparently simple geometrical problems could not be given until, some years ago, the following appeared (Figure 1.1):

```
From hales@math.lsa.umich.edu Wed Aug 19 02:43:02 1998
Date: Sun, 9 Aug 1998 09:54:56 -0400 (EDT)
From: Tom Hales <hales@math.lsa.umich.edu>
To:

Subject: Kepler conjecture


Dear colleagues,


I have started to distribute copies of a series of papers
giving a solution to the Kepler conjecture, the oldest
problem in discrete geometry. These results are still
preliminary in the sense that they have not been refereed
and have not even been submitted for publication, but the
proofs are to the best of my knowledge correct and complete.

Nearly four hundred years ago, Kepler asserted that no
packing of congruent spheres can have a density greater than
the density of the face-centred cubic packing. This
assertion has come to be known as the Kepler conjecture. In
1900, Hilbert included the Kepler conjecture in his famous
list of mathematical problems.

...

The full proof appears in a series of papers totalling well
over 250 pages. The computer files containing the computer
code and data files for combinatorics, interval arithmetic,
and linear programs require over 3 gigabytes of space for
storage.

Tom Hales
```

Figure 1-1 First Announcement of a solution to the Kepler conjecture given by Thomas C. Hales, University of Pittsburgh, in 1998 [62, 90]

Hales, University of Pittsburgh, in 1998 (Sloane 1998; University of Pittsburgh 1998).

This thesis describes my humble efforts to contribute, from three years of study, to this incredibly wide subject, rich in history, applications and possibilities. For those that have found this introduction interesting, here is a little treat: the answer to the argument is 12.

Newton was right once again.

1.2 Granular Mechanics in Engineering

As mentioned before, the granular form is probably one of the most common of those in which some materials are found in nature, and for this reason researches on the mechanics of granular materials can be found in many different fields.

Aggregates used in civil constructions are generally found in granular form and it is well known that their characteristics depend on the physical properties of the single grains and on the way these grains interact with each other. Thom and Brown (1988), for instance, investigated the influence of grading and dry density on the aggregate behaviour performing repeated loading triaxial tests. They observed that while the resilient properties seem to be ruled by the material itself, permanent deformation and shear strength can be considered to be highly influenced by geometric factors such as grading, void ratio, degree of interlocking and friction angle between the particles. Hecht (2000a; 2004b) studied the geomechanical properties of an aggregate (density, elastic modulus…) comparing different gradings and referring to some classical packing models.

A change in grading and density can be expected to result in a different value of the coordination number (number of contact points between a particle and its neighbours) leading to a different stress distribution over the particle's surface: a coarse aggregate consisting of grains of the same size with a small fine fraction will load each particle with higher tensile stresses than if the same particles were conveniently surrounded by an appropriate number of smaller particles. As shown by McDowell (1996a, p. 2098-2101), "the probability of fracture is a function of applied

stress, particle size and coordination number. When the effect of coordination number dominates over particle size in determining the probability of fracture for a particle, the resulting particle size distributions are fractal in nature. By choosing appropriate particle parameters, it is possible to obtain normal compression curves which resemble those found experimentally". (See also Jiang et al 2005; Lim 2004; McDowell & Humphreys 2002; McDowell 1998b; McDowell 2000c)

Beside the more traditional research fields such as geotechnics, food industry and chemistry (Brilliantov et al 1996; Fu et al 2006; Ohlenbush et al 1988; University of Bristol 2007), the recent development of Discrete Element Modelling techniques (DEM) has shown that more general materials can be simulated using packings of hard spheres and modelling the behaviour of the contacts between the particles. DEM has proved to be a promising tool but, in order to be able to make the most out of it, a deep understanding of its elements (packings of spheres) is desirable. At an early stage of this research some observations attracted the attention of the author:

a. Although it appears clear that the contacts between the particles are, in this type of simulation, the most important part of the models, little was known about their number (coordination number) and their superficial distribution on a particle, which are parameters that should influence the aggregate performance and the probability of fracture (Cheng et al 2003; Lim 2004; McDowell 1996a).

b. Most of the existing knowledge refers to the monodisperse case, i.e. the case of identical spheres, while being able to distinguish between at least two

types of spheres (bidisperse packings) could bring great advantages to future researches. The two types can differ in size or in physical properties: for instance, one type could be harder than the other, simulating a mixed aggregate formed by two types of material. In this case, it is clear that the contact between two hard particles should be modelled in a different way than the contact between a hard and a soft particle or between two soft ones. The possibility to predict, given the quantities of the two materials, how many contacts of each type will appear would be a very useful tool when studying their behaviour.

Given the importance that the contacts between particles have for these structures, the ultimate aim is to be able to estimate their number and position for the most general case of uniform grading and various particle shapes. However, the actual state of research knowledge requires a more basic approach to be taken at this stage. Many researchers work on this topic trying to enhance the level of detail (and the complexity) from different point of views, some of them modelling particles of shapes more complex than spherical (spherocylinders (Williams, & Philipse 2003), ellipsoids (Antony et al 2005; Bezrukov, A. and Stoyan 2006; Ting et al 1995), rods (Philipse 1996) and even arbitrary shapes (Frenkel et al 2008; Gan et al 2004; Luchnikov et al 1999), others considering compressible particles (Makse et al 2000) or a wide size distribution (Kansal et al 2002; Kong & Lannutti 2000; Yang et al 2000a; Yang et al 2003b; Zou et al 2003a), nonetheless more fundamental issues like those expressed in a. and b. (above) still need to be understood. The aim of this research, therefore, cannot be to supply an answer for all the possible issues that arise about the packing of granular materials, but rather to contribute to the enhancement

of the knowledge and the understanding of, at least, some basic aspects of this vast topic, studying monodisperse and bidisperse packings of spheres as a foundation for engineering studies. Although in a generalised and simplified manner, this research is designed to bring new results and help developing original concepts that can, ultimately, be of great importance for this and other fields.

Ultimately, a better understanding of the way particles interact with each other and of the quantity, type and characteristics of their reciprocal contact points will be, in future, used to design stronger, cheaper and more durable aggregate mixtures, model porous materials and any other possible application for which these packings have been studied in the last four centuries.

1.3 Aims & objectives

The aims of this research can be summarised as follows:

- To describe what is currently known about monodisperse and bidisperse packings of spheres in order to identify gaps of knowledge, particularly focusing on parameters of engineering interest.
- To describe the methods that are generally employed in these studies and consider limitations and advantages.
- To develop algorithms to produce the packings that will be subject of this study. These algorithms must be able to deliver an accurate spatial description of different types of configurations of groups of spheres.
- To analyse the packings produced focusing on parameters of interest, such as coordination number and packing density, and possibly develop a way to describe the position of the contact points, with other spheres, on the surface of a sphere.
- To study the differences between monodisperse and bidisperse packings and investigate in detail the coordination number of bidisperse packings distinguishing between different types of contact.
- To consider ways to relate the simulated structures to packings of real particles, either simulating more realistic packings or by means of physical experiments, possibly by means of x-ray tomography equipment, recently acquired at the University of Nottingham.

- Ultimately, to supply a better understanding of these structures, indicate applications of the observations made and supply a solid basis for further developments.

As will be discussed in more detail in the methodology presented in Chapter 3, most of the results examined in this research will be obtained by computer simulation, using algorithms developed for the purpose in Visual Basic or Matlab languages.

While, on one hand, this approach allows the treatment of a very large and accurate amount of data, on the other hand constant checks are desirable to ensure that what is being analysed bears some relation to that which can be observed in the real world. This will be achieved by comparison with previous researches, critical observation and by performing some physical experiments.

1.4 Thesis layout

This thesis is organised as follows:

Chapter 1 – Introduction

The current chapter introduces the topic of study and states the general aims of the research.

Chapter 2 – Literature Review

Introduces the main technical concepts used in the research showing what is known and identifying gaps in knowledge.

Chapter 3 – Methodology

Expresses the general ideas underneath the research and the approach taken to achieve the aims proposed.

Chapter 4 – Coordination Number

Presents the results of the analysis of coordination number for clusters, monodisperse packings ("sticky" and "diluted") and bidisperse packings.

Chapter 5 – Superficial Distribution

Introduces a parameter able to describe the superficial distribution of contact points, analysing it for clusters and bidisperse packings.

Chapter 6 – Radial Distribution Function

Presents the results of the analysis of the radial distribution function for the monodisperse and bidisperse packings simulated.

Chapter 7 – X-Ray Experiment

Describes the experimental study of a packing of spherical particles performed using an X-Ray CT equipment.

Chapter 8 – Discussion

Collects the findings from the other chapters and shows how some of them can be used to take the analysis further.

Chapter 9 – Conclusions

Summarises the main results from the research, discusses which targets have been met and to what extent and suggests implications of the work done and ideas for future studies.

Several algorithms have been developed by the author in order to reach the findings presented in this thesis. They are described conceptually in Chapters 2 and 3 and more in detail into a series of Appendices. As well as containing all the information about the algorithms employed, they also contain a more complete presentation of the numerous results of which, for reasons of clarity and brevity, only some examples have been included in the main body of the thesis.

2 LITERATURE REVIEW

2.1 Algorithms for Sphere Packings Simulation

The following is a brief review of the main algorithms that are generally employed in the studies that involve numerical simulations of sphere packings:

Mechanical Contraction.

A set of spheres is generated randomly in a container i gravity-less space, occupying a height much larger than what will be the height of the final packing. This extremely loose assembly is then densified (see Figure 2.1) under the effect of strong vertical forces and rearrangements due to the spheres' interactions, until a stable structure is achieved.

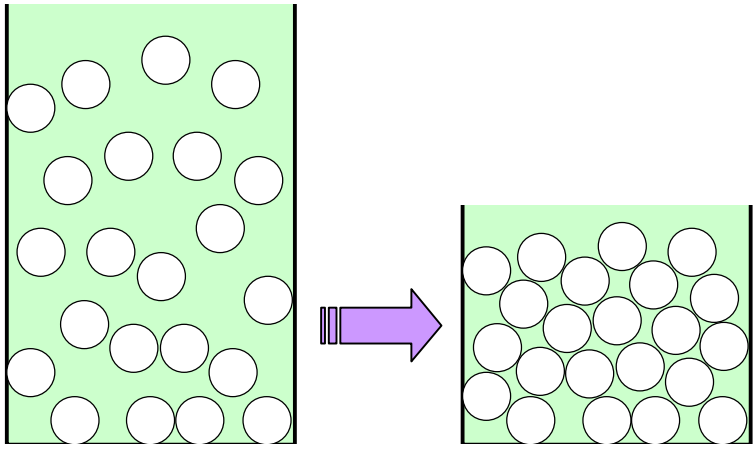

Figure 2-1 Mechanical Contraction algorithm

Monte Carlo.

A set of small spheres is generated randomly in a container, occupying approximately the volume that would produce the desired packing density if the spheres were of the correct (target) size. The spheres are then expanded by small increments (see Figure 2.2) and constantly rearranged to minimise overlapping until the target sphere size and packing density are reached.

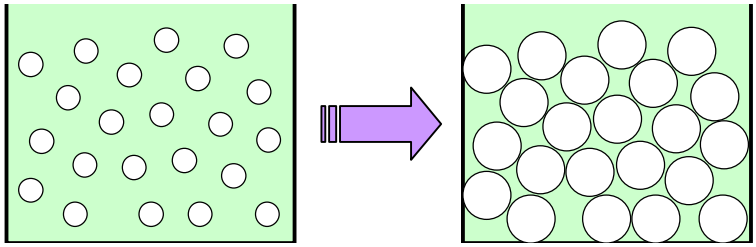

Figure 2-2 Monte Carlo algorithm

Drop and Roll.

It simulates the arrangement of spheres dropped one by one in a container under gravity. In general, the initial horizontal position of the sphere is chosen randomly as a "dropping point", then the sphere is left free to roll until a position of stable equilibrium is reached (see Figure 2.3).

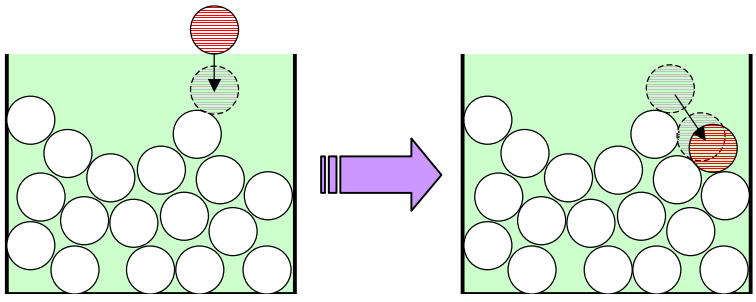

Figure 2-3 Drop-and-Roll algorithm

Spherical Growth.

The procedure is similar to the Drop and Roll algorithm, the main difference being the packing geometry. The spheres sediment centripetally (see Figure 2.4) on an initial "seed" from any direction, making the packing grow spherically instead of vertically.

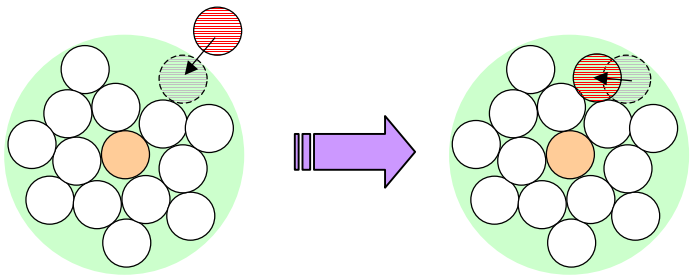

Figure 2-4 Spherical Growth algorithm

2.2 Packing Density

In engineering practice, packing density or its related parameters such as porosity can often alone satisfactorily characterise a packing. Being generally defined as the ratio between solid volume and total volume, this parameter can be estimated at local or global scale. At a local level, the estimation of the portion of space "belonging" to each sphere of a monodisperse packing can be done by means of the Voronoï tessellation.

In a system of spheres (*A*) of same size, the Voronoï cell belonging to one particular sphere (*a*) is defined as the total of the space's points which are closer to the centre of *a* than to the centre of any other sphere of the system *A*. To state it in another way, it is the smallest polyhedron totally enclosed by the planes which are perpendicular bisectors of lines joining the centre of sphere *a* to all other sphere centres (Troadec et al 1998a). This concept is illustrated by a two-dimensional example in Figure 2.5 and in 3D in Figure 2.6 (Gervois et al 1992).

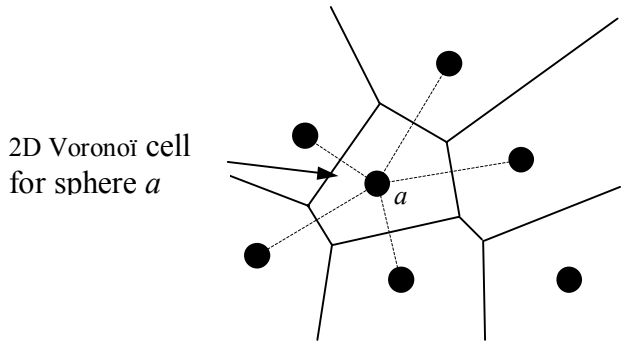

Figure 2-5 2D example of Voronoi tessellation

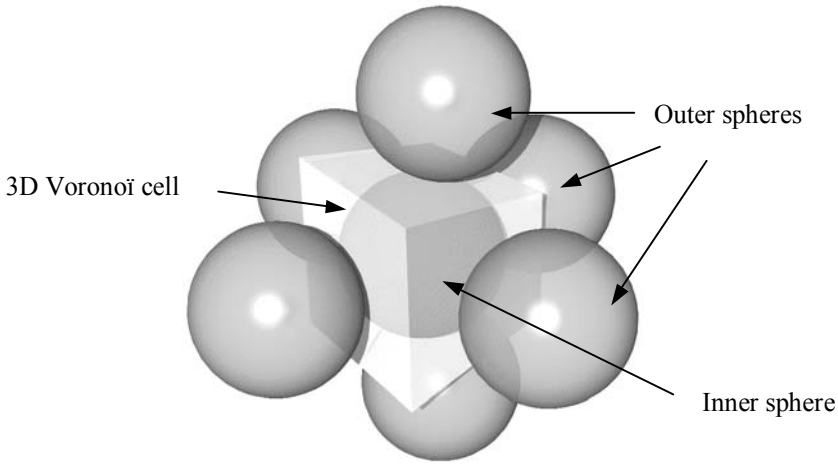

Figure 2-6 3D example of Voronoi cell

The modern use of the Voronoï construction began with crystallography, but since then it has become much more generally applied, proving its efficacy in disciplines like geography, ecology, and politics. Basically, it can be applied everywhere spatial patterns are analysed to identify regions of activity or influence (Aste & Weaire 2000).

"Nevertheless, for polydisperse assemblies of spheres this tessellation is not a good choice as planes may cut the large spheres (see Figure 2.7)." To overcome this problem, it is possible to adopt two generalisations of the Voronoï tessellation: the Radical Tessellation (Annic et al 1994) and the Navigation Map. It is appropriate to quote from Richard et al (2001a) at this point as illustrated by Figure 2.7.

> "Radical tessellation was introduced by Gellatly and Finney and used by Telley. It consists in choosing as separation plane between two spheres the radical plane, i.e. the points with equal tangent

relative to the two spheres. This plane is outside the spheres and orthogonal to the centreline. In the particular case of equal spheres we recover the bisecting plane.

The navigation map was introduced by Medvedev. It consists in taking as faces of the generalised Voronoï cells the sets of points equidistant from the surface of the spheres. The faces are then no longer planes as for the radical tessellation but, in general, pieces of hyperboloids. Of course, for equal spheres hyperboloids are replaced by bisecting planes." (Richard et al 2001a, p. 296)

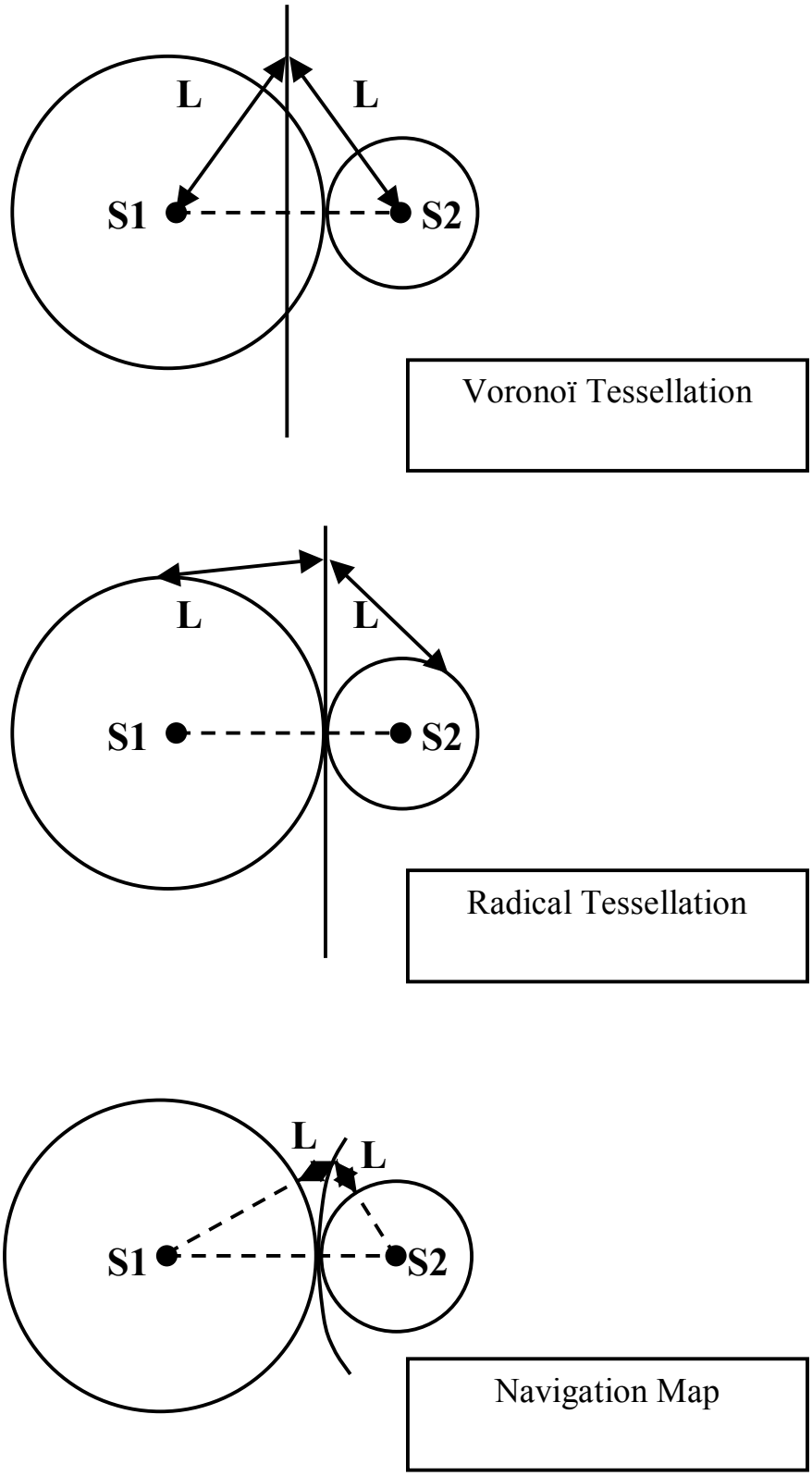

Figure 2-7 Different tessellations for packings of spheres of different sizes

Obviously, the local measurement of packing density can only be done if the positions of the spheres (i.e. the spatial coordinates of their centres) are known with a certain precision. This is often not the case for experimental packings where, especially before the introduction of new techniques such as confocal microscopy and x-ray microtomography, this quantity is usually measured as an average over the whole packing.

Being the most directly measurable and descriptive parameter of sphere packings, numerous studies have investigated packing density and its role in the assembly's physical behaviour. A recent publication by Aste (2005) presents a very comprehensive and clear summary of most of these works, therefore its structure will be followed here, integrated with comments from the present author and citations from others.

> "When equal balls are packed in a container under gravity they occupy a fraction between 55% and 74% of the volume depending on the way the packing is formed and organised at grain level. The densest packing is achieved by an ordered (crystalline) stack of balls in parallel hexagonal layers forming the so-called Barlow packing at density $\rho = \pi / \sqrt{18} \approx 0.74$. Volume fractions between 0.74 and 0.64 can be produced by introducing a certain amount of disorder (vacancies, crystalline defects, polycrystalline regions etc) starting from an ordered Barlow packing" (Aste 2005, p. S2363)

Richard et al. (1999b)

> "have studied the crystallisation of disordered packings and observed that the crystalline structure contains both FCC and HCP[1] regions. The fraction of HCP symmetry in the packing decreases to zero as the propensity of the packing to crystallise increases. This shows, as expected, that for hard sphere systems the FCC structure is more stable than the HCP structure" (Richard et al 1999b. p. 420)

Aste (2005) reports that

> "on the other hand, if the balls are poured into the container they arrange themselves in a disorderly fashion and the packing results typically in densities between 0.61 and 0.62 (depending on the kinds of balls, the shape of the container, the speed and height from which they are poured). Larger densities up to around 0.63 can be reached by gently tapping the container, whereas to achieve the so-called random close packing limit at approximately 0.64 it seems necessary to add a small compression from above while tapping" (Aste 2005, p. S2363-S2364)

[1] Face-centered cubic (FCC) and hexagonal close-packed (HCP) are the two regular configurations of spheres that achieve the largest density. They are two versions of what is above called Barlow packing. Relative to a reference exagonal packing layer with positioning A, two more positionings B and C are possible. Every sequence of A, B, and C without immediate repetition of the same one is possible and gives an equally dense packing for spheres of a given radius. The most regular ones are ABABABA (HCP) and ABCABCA (FCC). In both arrangements each sphere has twelve neighbors.

Clarke & Jonsson (1993) reports that

> "Scott and co-workers poured ball bearings into cylindrical tubes and carefully measured the packing density as a function of the container size. By extrapolating to infinite size, they arrived at values for the packing densities in two reproducible limits. By gently rotating the cylinder into a vertical position, the spheres assembled in a low density packing (Loose Random Packing, LRP) with a measured packing density of 0.60. by vibrating the cylinders at a suitable frequency for a few minutes, the density had increased to a high density limit (Dense Random Packing, DRP) with packing density of 0.637" (Clarke & Jonsson 1993, p. 3975)

Scott (1960 in Onoda & Liniger 1990, p. 2727) concluded that "it seems unlikely that there are other stable random-packing arrangements for equal spheres in space which have packing densities outside these limits".

> "Controlled vertical tapping of a stack of grains in a tube has been used in several works to induce progressive densification in the system and it has been noted that a steady plateau at densities comparable to the density obtained by simply pouring the grains can be obtained in a reproducible way by tuning the induced maximal acceleration to between 1 and 6 times the gravitational one. All the available data in the literature indicate that densities

> above 0.64 cannot be achieved without partial crystallization" (Aste 2005, p. S2364)

Philippe & Bideau (2002, p. 677) observed that "the evolution of the mean volume fraction and of the mean potential energy of a granular packing under consecutive vertical taps presents a slow densification until a final steady state". This densification process has been investigated by Novak et al. (1998. p. 1971), who report that if a pile of monodisperse spherical beads is shaken vertically its density "slowly reaches a final steady-state value about which the density fluctuates".

> "Densities below 0.60 can only be achieved by special treatments of the system. Loose packing densities in the range of 0.577-0.583 have been obtained by dry nitrogen passed through the container from the bottom. Loose packings at densities 0.58-0.59 can be also produced by using a special technique which has been known for thousands of years and it was used by the sellers of dry grains to increase profits by improving of about 10% the volume occupied by the granular packing. This technique consists in pouring the spheres into the container with a stick inserted inside and slowly removing the stick after pouring. Intermediate densities (0.59-0.61) can be produced by shaking these loose structures. However these intermediate values are not stable under shaking and any action tends to densify the system up to the region between 0.61 and 0.63 within which the density can be increased or decreased in a reversible way depending on the kind of action performed on the system. The lowest achievable limit for a stable packing is 0.555

> (which coincides with the dilatancy onset) but such a limit can only be reached by reducing the effect of gravity" (Aste 2005, p. S2364)

After being introduced by Scott (1962), the two concepts of LRP and DRP (also known as Random Close Packing RCP) have been the subject of numerous studies. Nonetheless, their definition is still debateable and no rigorous analytical solution has been given. The LRP is generally defined as the lowest packing density achievable by a mechanically stable random packing. As observed by Onoda & Liniger (1990, p. 2727),

> "important for the concept of LRP is the exclusion of cases where attractive forces exist between spheres, as with colloids. If spheres are strongly bonded, very loose, stable structures are possible, due to linear chains and other arrangements that would not be stable if the bonding forces were not present. The term 'mechanically stable' means that the packing of spheres is in static equilibrium under an existing set of external applied forces. In the case of macroscopic, spherical balls poured in a container, the external forces are due to gravity and [due to] the reaction forces of the container walls".

Berryman (1982, p. 1053) defined random close packing as the structure that occurs at

> "the minimum packing density ρ for which the median nearest-neighbour radius equals the diameter of the spheres. Using the radial distribution function (see Section) at more dilute concentrations to estimate median nearest-neighbour radii, lower

> bounds on the critical packing density ρ_{rcp} are obtained and the value ρ_{rcp} is estimated by extrapolation. Random close packing is predicted to occur for $\rho_{rcp} = 0.64 \pm 0.02$ in three dimensions and $\rho_{rcp} = 0.82 \pm 0.02$ in two dimensions. Both of these predictions are shown to be consistent with the available experimental data".

Estimations of DRP come from simulations of variable packings. As reported by Matheson (1974, p. 2569-2570), "packing densities approaching the value of 0.637 have been obtained with a deterministic algorithm by Norman et al (1971), Adams and Matheson (1972) and Bennett (1972). This method, which will subsequently be referred to as the spherical growth procedure, starts with a small quasi-spherical core of touching spheres around the origin of the coordinates system" and proceeds placing each next sphere in the available pocket closest to the origin. The assemblies grown with this method are inhomogeneous:

> "the packing density in very small assemblies of radius equal to 2.5 sphere diameters can be as high as 0.67 and this density falls to 0.628 in a sphere assembly of radius equal to 10 sphere diameters. Bennett (1972) has found that the packing density of a spherical assembly varies linearly with the reciprocal of the radius of the assembly, and has predicted that the density of an assembly of infinite radius would be 0.61" (Matheson 1974, p. 2570).

Liu et al. (1999) have applied the Discrete Elements Method to spherical assemblies of single-size spheres applying a field of centripetal forces to the particles. They show that, in this type of simulation, the initial conditions do not affect the final state

of the packings. As shown by others (Matheson 1974), a packing of spherical growth is not uniform. The local mean porosity increases with the increase of the distance from the packing's centre, R_p.

> "Matheson (1974) suggested that the inhomogeneity results from the packing mechanism involved, i.e. adding spheres to a surface with an inconstant radius of curvature. This consideration obviously also applies to the present packings, although the simulation algorithms are different. [Omissis] The relationship between packing density ρ and packing size Rp can be described by
>
> $$\rho = 0.645 + 0.662 \cdot \left(\frac{1}{R_p} \right)^{2.094} \qquad (1)$$
>
> which suggests that the limit packing density is 0.645, in good agreement with the recent estimate. Obviously, different equations give different extrapolated (limit) packing densities. However, if focused on the data in the region of 1/Rp < 0.15, then a more consistent limit packing density is resulted. In this case, a linear plot of ρ vs. 1/Rp suggests that this limit packing density is 0.637" (Liu et al 1999, p. 441-442).

Recently, Torquato et al. (2000) questioned the legitimacy of Random Close Packing, attributing to its ill-defined characteristics the elusiveness of the calculation of its density. The following is an extract from their publication.

> "The prevailing notion of random close packing (RCP, also known as dense random packing DRP) is that it is the maximum density that a large, random collection of spheres can attain and that this

density is a universal quantity. This traditional view can be summarised as follows: "ball bearings and similar objects have been shaken, settled in oil, stuck with paint, kneaded inside rubber balloons, and all with no better result than a packing density of 0.636". [Omissis] Indeed, in a recent experimental study, it was shown that one can achieve denser (partially crystalline) packings when particles are poured at low rates into horizontally shaken containers. Computer algorithms can be used to generate and study idealised random packings, but the final states are clearly protocol-dependent. For example, a popular rate-dependent densification algorithm achieves ρ between 0.642 and 0.649, a Monte Carlo scheme gives $\rho \approx 0.68$, and a "drop and roll" algorithm yields $\rho \approx 0.60$. It is noteworthy that, in contrast to the last algorithm, the first two algorithms produce configurations in which either the majority or all of the particles are not in contact with one another. We are not aware of any algorithms that truly account for friction between spheres. However, we suggest that the aforementioned inconsistencies and deficiencies of RCP arise because it is an ill-defined state, explaining why, to this day, there is no theoretical determination of the RCP density. This is to be contrasted with the rigor that has been used very recently to prove that the densest possible packing density ρ for identical spheres is $\pi/\sqrt{18} \approx 0.7405$, corresponding to the close-packed face-centred cubic (fcc) lattice or its stacking variants. The term "close packed" implies that the spheres are in contact with one another with the

> highest possible coordination number on average. This is consistent with the view that RCP is the highest possible density that a random packing of close-packed spheres can possess. However, the terms "random" and "close-packed" are at odds with one another. Increasing the degree of coordination, and thus, the bulk system density, comes at an expense of disorder. The precise proportion of each of these competing effects is arbitrary and therein lies the problem" (Torquato et al 2000, p. 2064)

Aste (2005), summarising the information, deduced

> "that there are four rather well defined density regions: 0.55-0.58 where packings can be created only if the effect of gravity is reduced; 0.58-0.61 where packings can be generated but they are unstable under tapping; 0.61-0.64 where reversible structures can be created by pouring grains into the container and tapping for sufficiently long times (however it is not completely established whether the region 0.63-0.64 can be reached only by tapping or whether some combined compression must be added); 0.64-0.74 where crystallization is present" (Aste 2005, p. S2364-S2365)

The definition of these density regions is considered to be of great importance for the study of molecular dynamics, as they clearly represent the different phases in which a granular material can be found. For instance, as shown by To & Stachurski (2004), the ratio of the number of loose (non-caged) to total spheres can be taken, together with packing density, as a measure describing solidity of a packing. Figure 2.8

represents packings of different packing densities obtained with a spherical growth algorithm. "At high packing density the points fall on a steeply inclined straight line, while the other points at lower packing densities are less ordered without a clear pattern. This is suggestive of two regimes of behaviour, that of gas-like and liquid-like. Thus, the gas-to-liquid transition point can be characterised by the two coordinates:

$$\text{Packing density} \approx 0.49, \qquad \frac{loose}{total} \approx 0.8 \qquad (2)$$

Extrapolation of the inclined line downwards points to maximum packing density ≈ 0.61 < 0.64 (DRP)" (To & Stachurski 2004, p. 166)

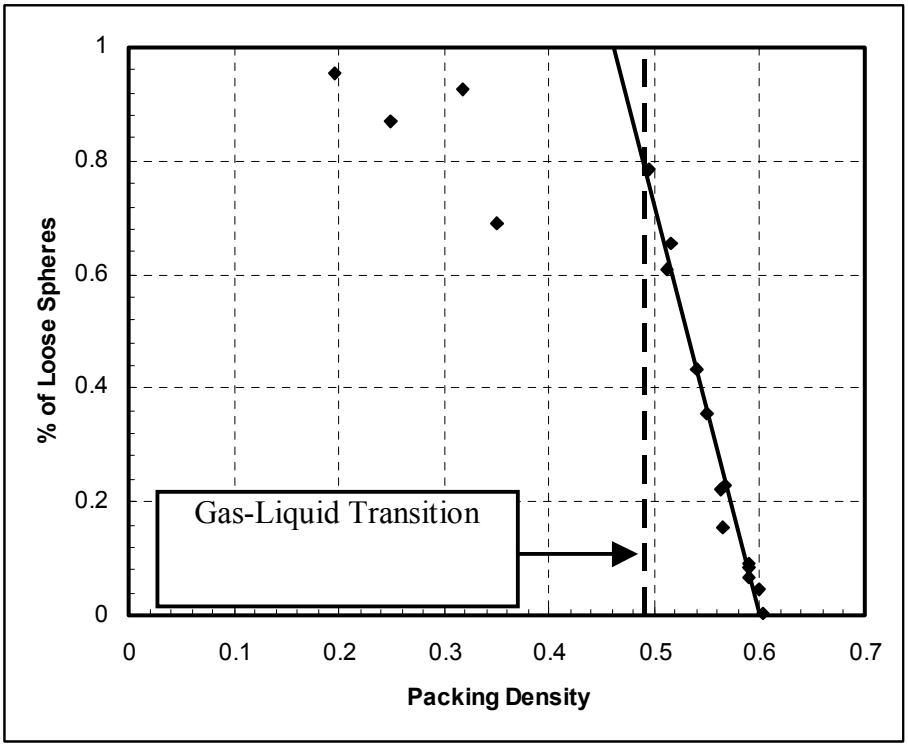

Figure 2-8 Gas-liquid transition observed by To & Stachurki

"Molecular dynamics simulations show that hard sphere systems behave like a gas below ρ ≈ 0.49. Upon compaction, liquid-like

behaviour is observed up to $\rho \approx 0.55$, where crystallisation starts to occur. If crystallisation is avoided, the system undertakes a glass transition at $\rho \approx 0.56$ and then it can be compacted up to $\rho \approx 0.645$ where no further densification can be induced. Empirical and simulated evidence suggest that something very special might happen in the geometry of the packing at densities above $\rho \approx 0.56$; a process which must terminate below $\rho \approx 0.65$. What makes the understanding of this process particularly challenging is that there are no a priori reasons for the densification process to stop around $\rho \approx 0.64$. On the contrary, there are plenty of local configurations which are denser than this limit and any arrangement of spheres in stacked planar hexagonal closed packed layers can reach the density of $\rho = \pi / \sqrt{18} \approx 0.7405$, as achieved in fcc (face-centred cubic) of hcp (hexagonal closed-packed) crystalline packings" (Aste 2004c, p. 2)

2.3 Radial Distribution Function

Aste (2005) has recently published the results of an extremely interesting experimental work on large packings of monodisperse hard spheres. The following is an extract from his section about the Radial Distribution Function, which we believe presents this subject in a very exhaustive way.

> "The radial distribution function $g(r)$ is the probability distribution of finding the centre of a particle in a given position at distance r from a reference one. This measurement is widely used in geometrical characterisation of packing structures and contains information about long range interparticle correlations and their organisation. In order to measure this quantity one must count the number of sphere centres within a radial distance r from a given one. The average of this number, computed over the whole sample ($n_t(r)$), is related to the radial distribution function by
>
> $$n_t(r_1) - n_t(r_0) = \int_{r_0}^{r_1} g(r) 4\pi r^2 dr . \qquad (3)$$
>
> Therefore, given the position of the sphere centres, these two quantities $n_t(r)$ and $g(r)$ can be straightforwardly computed. It is easy to compute that the asymptotic behaviour ($r/d \to \infty$) for the total number of centres of spheres with diameter d inside a spherical region of radius r is $n_t(r) \approx 8\rho(r/d)^3$. Therefore asymptotically one expects $g(r) \to 6\rho/(\pi d^3)$. Such a dependence on packing density and bead size might turn out to be inconvenient

for comparison between different systems. Therefore often a normalised radial distribution function is used instead:

$$\tilde{g}(r) = \frac{\pi d^3}{6\rho} g(r), \qquad (4)$$

which tends to 1 when $r/d \to \infty$.

The first experimental measurement of the radial distribution function in a packing of equal sized spheres was performed by Scott and subsequently reanalysed by Mason. They observed a sharp peak at 1.0 diameters (associated with spheres in contact) and a curious 'square' shape of the second peak between 1.7 and 2.0 diameters. After these first observations, unusual enlargements of the second peak and its 'splitting' in two peaks at $r/d \approx \sqrt{3}$ and $r/d \approx 2$ have been generally observed in several experiments and simulations of monosized sphere packings. The presence of the peaks after the peak at $r = d$ is a clear indication that the system is organised: a characteristic structure with distinct local patterns is present. To understand which kind of local configuration contributes most to each peak of the $g(r)$ is very important in order to work out which kind of local arrangements generate this globally non-ordered structures. For instance, it is easy to verify that a radial distance $r/d \approx \sqrt{3}$ is consistent with configurations made by placing the centres of four spheres on the vertices of two in-plane equilateral triangles (with edge length d) which share one edge (see Figures 2.9 and 2.10). But it was pointed out in (Clarke & Jonsson 1993) that a large contribution to the peak at $r/d \approx \sqrt{3}$

can also come from configurations made of five spheres placed on the vertices of two tetrahedra which share a common face, whereas the peak at $r/d \approx 2$ is due to three or more spheres which are lying along a (rather) straight line." (Aste 2005, p. S2374-S2376)

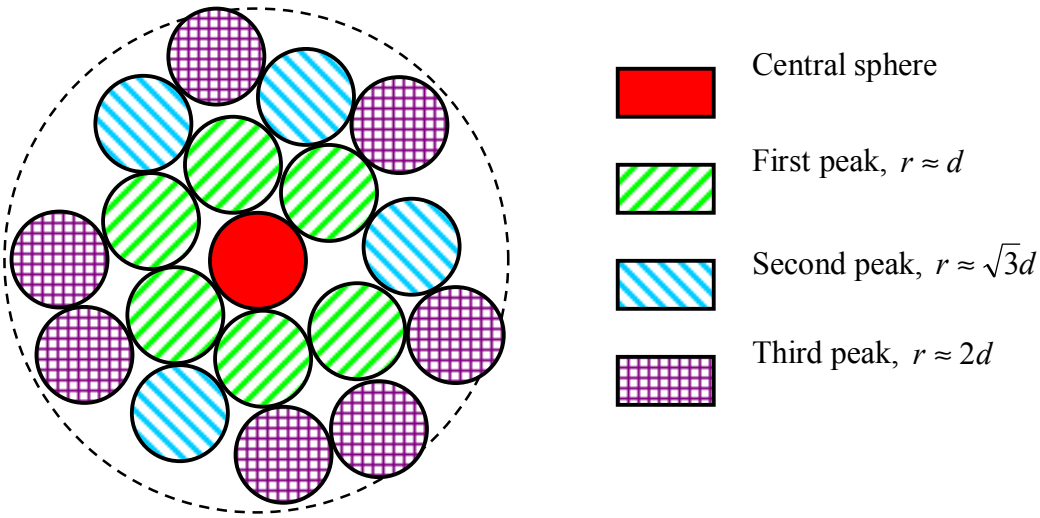

Figure 2-9 2D example of particles contributing to the various peaks of the RDF

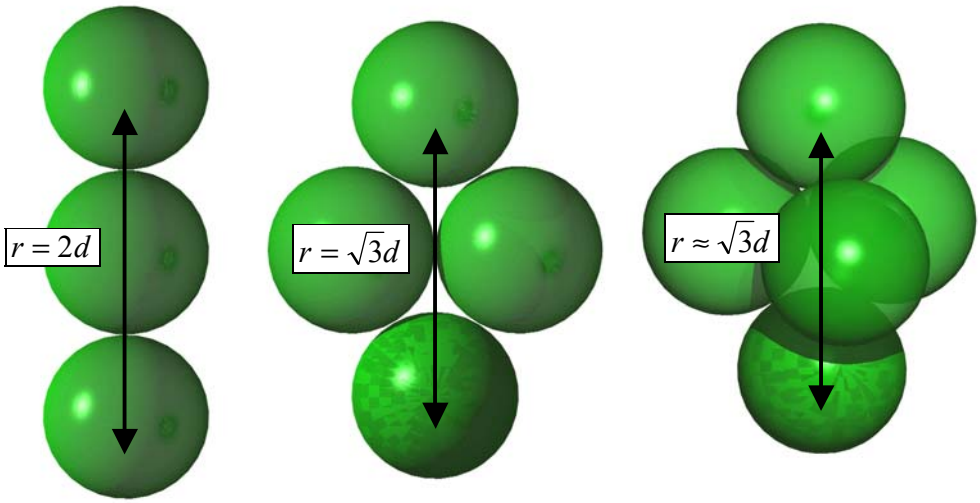

Figure 2-10 Sphere structures contributing to the main peaks of the RDF

The correspondence of the different peaks to particular relative position of the neighbouring spheres is also treated by Kumar & Kumaran (2005), who studied the

occurrence of each different sphere structure and showed their separate contributes to $g(r)$.

Aste (2005) observed that

> "the two peaks at $r = \sqrt{3}d$ and $r = 2d$ both increase in height with the packing density (see Figure 2.11), where packing density increases constantly from packing A to packing F) and, interestingly, the relative growth with the density is faster in the peak at $r = \sqrt{3}d$ with respect to the peak at $r = 2d$. This certainly indicates an increasing organisation in the packing structure." (Aste 2005, p. S2376)

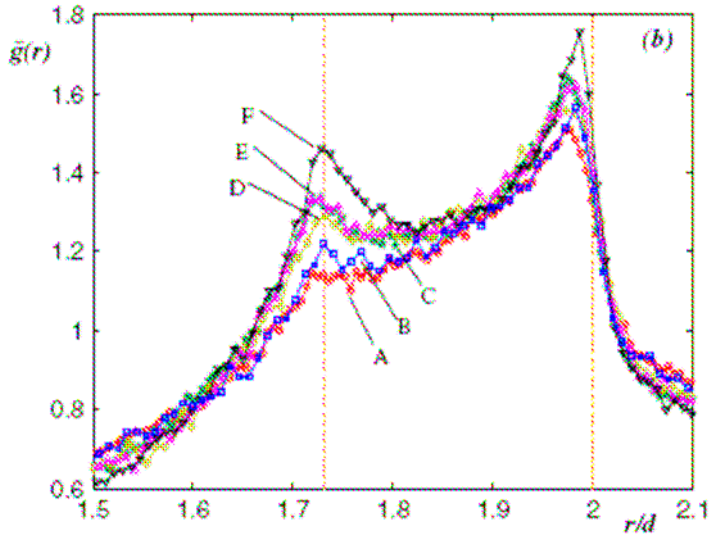

Figure 2-11 Behaviour of the first sub-peak for various packing densities

This experimental evidence confirmed the simulations performed by Clarke & Jonsson (1993). Using a Monte Carlo algorithm they produced sphere packings with packing densities ranging from 0.56 (LRP) to 0.64 (DRP), analysing the different possible sphere configurations and their contributions to the RDF $g(r)$. Moreover,

they pointed out how for $\rho \leq 0.60$ the second peak does not appear to split anymore due to the rapid decrease of the size of the peak at $r = \sqrt{3}d$ (see Figure 2.12).

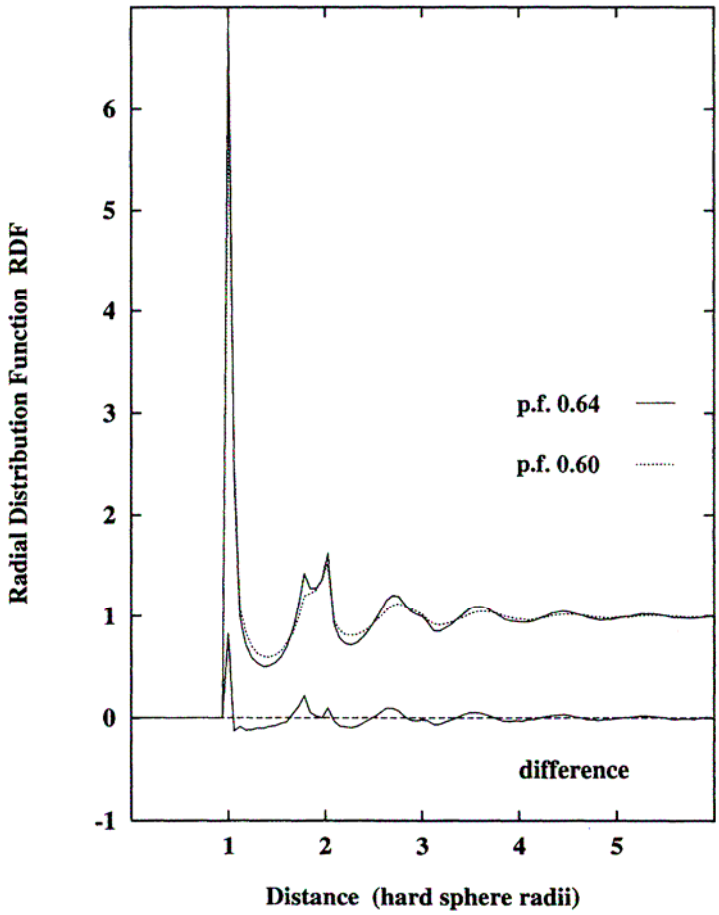

Figure 2-12 Disappearing of first sub-peak for packing densities < 0.60

Similar results have been obtained by Richard et al. (2003c) (from an experimental study of a granular assembly analysed by x-ray computed tomography at various stage of compaction) and by Yang et al. (2000a), who employed a very different simulation algorithm. They generated monodisperse packings of hard spheres by means of a mechanical contraction algorithm. Interparticle forces (van der Waals) affect the packings in different measure according to the sphere size, which ranges from 1000μm to 1μm, resulting in different packing densities and, therefore, different

stable structures. Packings of coarse particles are unaffected by small interparticle forces and achieve higher densities than the packings of fine ones. The comparison of $g(r)$ for these different packings shows (Figure 2.13) that when particle size decreases (Yang et al 2000a):

- the first component of the second peak at $r = \sqrt{3}d$ vanishes when particle size is less than 100μm although the main component at $r = 2d$ is maintained;
- the peaks beyond the second one gradually vanish;
- the first peak becomes narrower, with a sharp decrease to the first minimum.

In general, it is possible to say that packings of smaller spheres will be more affected by interparticle forces. This will result in lower packing densities and, as shown before, flatter $g(r)$ functions. Yang et al., therefore, conclude that, when the packing is subject not only to gravitational but also to interparticle forces, "decreasing particle size can result in a more uniform packing". (Yang et al 2000a)

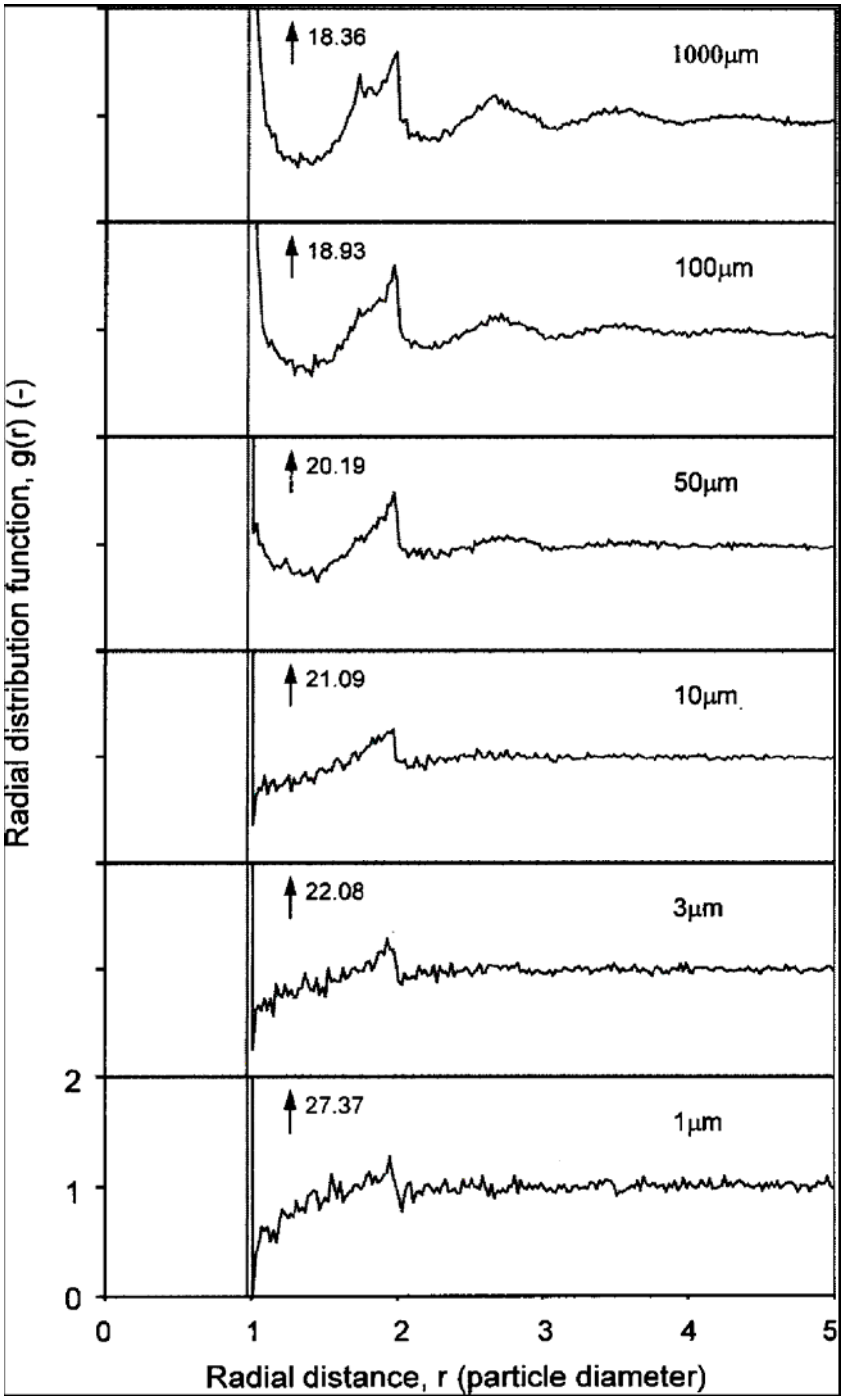

Figure 2-13 RDF for various particle's size in simulated frictional packings

Matheson (1974) reported the same behaviour of the second peak for packings generated with the spherical growth algorithm. He compares (see Figure 2.14) his simulated packing ($\rho \approx 0.607$) to an experimental sphere assembly described by

Finney in 1970 ($\rho \approx 0.637$). It is easy to verify the disappearing of the peak at $r = \sqrt{3}d$ and the flattening of the peaks beyond the second.

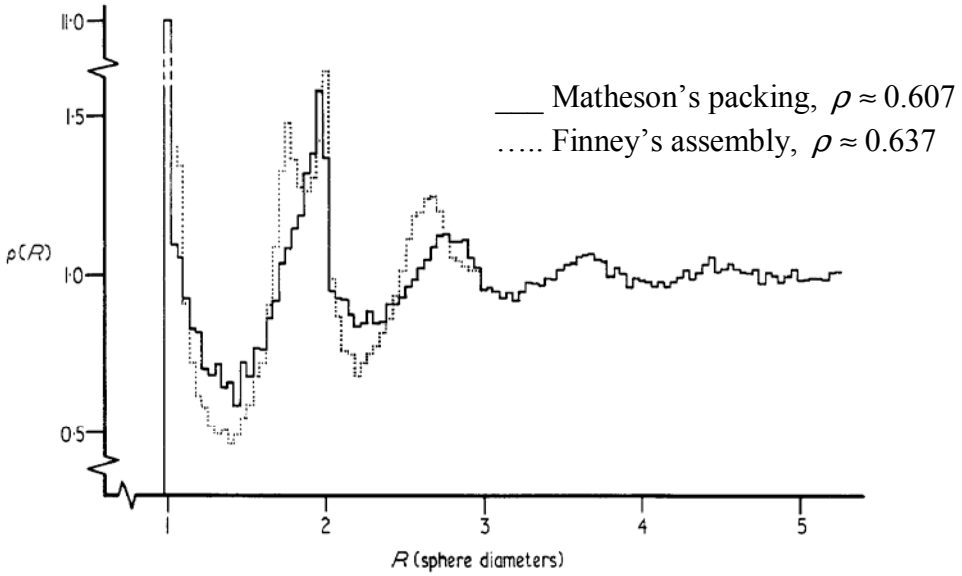

Figure 2-14 Comparison between RDF of a simulated packing and a real assembly

Similar indications can also be found in Bezrukov et al (2001a); Donev et al (2004a); Donev et al (2005b); Liu et al (1999); Silbert et al (2002); Wouterse & Philipse (2006); Yang et al (2003); Yang et al (2003b).

Finally, it is interesting to note (Liu et al 1999, p. 435) that "a sequential addition method cannot simulate the close random packing of packing density 0.64 and/or generate a packing with its radial distribution function of a second split peak."

From the available literature we can observe that the general behaviour and characteristics of the Radial Distribution Function appear to be independent from the method used to produce the packing. Moreover, the comparisons between experimental and numerical results available in the literature show very good

agreement and consistency while, as will be shown later in this chapter, this does not always happen for other parameters (such as coordination number, see further). This consistency of behaviour makes the Radial Distribution Function a potentially useful tool for the study of some topological aspects of these packings, and can have an important role in this research.

2.4 Kissing Number

"The 'kissing number problem' is a basic geometric problem that got its name from billiards: two balls 'kiss' if they touch. The kissing number problem asks 'how many balls can touch one given ball at the same time if all the balls have the same size?'. If one arranges the balls on a pool table, it is easy to show that the answer is exactly 6: six balls just perfectly surround a given ball." (Pfender & Ziegler 2004, p. 2) This hexagonal planar lattice also delivers the highest packing density for an arrangement of two-dimensional hard spheres. However, the solution of this problem in three dimensions is

> "surprisingly hard. Isaac Newton and David Gregory had a famous controversy about it in 1694: Newton said that 12 should be the correct answer, while Gregory thought that 13 balls could fit in. The regular icosahedron yields a configuration of 12 touching balls that has great beauty and symmetry, and leaves considerable gaps between the balls, which are clearly visible in Figure 2.15.

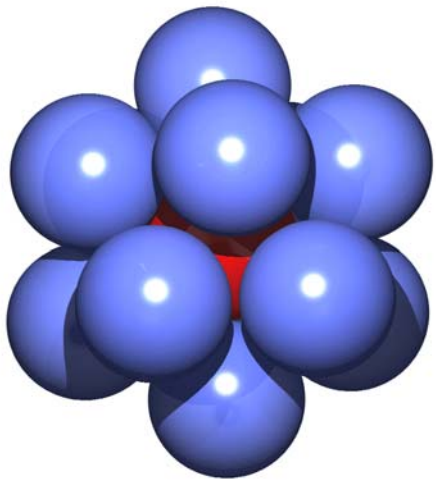

Figure 2-15 Configuration of 12 spheres around a central one - HCP

> So perhaps if you move all of them to one side, would a 13th ball possibly fit in? It is a close call, but the answer is no, 12 is the correct answer. But to prove this is a hard problem, which was finally solved by Schutte and van der Waerden in 1953." (Pfender & Ziegler 2004, p. 2-3)

Mansfield et al (1996) makes a similar point to Pfender & Ziegler, reporting how the kissing number represents a classical problem in mathematical physics and discrete geometry.

The kissing number is a single-valued determinate quantity, in contrast with the distributed values of contact numbers found when placing spheres in randomly chosen positions (see Sections 2.5 for parking number and 2.7 for coordination number).

2.5 Parking Number

The parking number represents the maximum number of probe spheres that can be placed on the surface of a target sphere if tentative sites for each succeeding sphere are selected entirely at random. The estimation of this number is part of "the class of so-called parking problems. For example, how many automobiles can be parked on a long street if the site for each is chosen randomly?" (Mansfield et al 1996, p. 3245)

In other words "the kissing number is the absolute maximum contact number achieved for regular close-packed spheres, while the parking number is a lower constrained maximum that has more relevance for less dense amorphous sphere packings (i.e. for packings that do not show the organised regular structure typical of closely packed spheres). To increase the system's coordination above the parking value the disordered neighbours must be rearranged (at least partly) into a more ordered configuration." (Wouterse et al 2005, p. 1)

In the procedure used for the random selection of attachment sites, "probe spheres diffuse one at a time in the vicinity of the target sphere from a great distance. During this diffusion process, they are not allowed to overlap any previously attached probe spheres, and they attach to the target sphere at the point at which they first make contact. The process continues with the addition of probe spheres until those already in contact prevent any new attachment." (Mansfield et al 1996, p. 3245-3246) The application of this method, also based on previous studies by Bouvard & Lange (1992) and Liniger & Raj (1987), has led Mansfield (1996) to the estimation of the

parking number P as a function of the size ratio r_1/r_2 between target and probe spheres radius:

$$P = 2.187 \cdot \left(\frac{r_1}{r_2} + 1 \right)^2 \qquad (5)$$

In the particular case when the probe spheres have same size of the target sphere, equation leads to P = 8.75.

2.6 Caging Number

When the particles that form a packing are being studied from a physical point of view, where external forces are likely to be applied to their structure, an interesting parameter that can be discussed is the so-called caging number, defined as the average minimum number of randomly placed spheres required to block any translational movement of a central one.

> "One might identify the parking number as the typical number of spheres required to immobilise a sphere in a random packing. However, the parking process is merely a maximisation under the constraint of random positioning and non-overlap which pays no heed to the issue whether or not the target sphere S is able to translate. On average, to achieve this arrest much less spheres are required than the parking number. Thus, to describe the local arrest of a single sphere, a 'caging' number has been introduced defined as the average minimum number of randomly placed spheres that blocks all the translational degrees of freedom of S." … "The main challenge in a geometrical caging problem is to account for excluded volume effects, which cause positions of contacts on a sphere to be strongly correlated. For randomly parked, overlapping neighbour spheres, i.e. for a distribution of completely uncorrelated contact points on the surface of sphere S, caging number have been calculated analytically for spheres of arbitrary dimension. For non-

overlapping hard spheres, however, caging numbers have only been determined by computer simulation." (Wouterse et al 2005, p. 1-2)

Wouterse et al. (2005) propose an analytical estimation of the caging number for three-dimensional hard spheres. "A hard-sphere contact excludes an area (a spherical cap) on the target sphere S surface where no other spheres can be placed

$$A_{excl} = 2\pi\left\{1-\cos\left[2\arcsin\left(\frac{r_2/r_1}{r_2/r_1+1}\right)\right]\right\}. \qquad (6)$$

This area is the area excluded for other sphere centres", but these other spheres can exclude part of this area themselves (the excluded areas or volumes can overlap) and thus the common part of this area would be counted twice. "To get a more meaningful result, the excluded area is taken to be the area that belongs exclusively to a single sphere contact, namely

$$A_{excl} = 2\pi\left\{1-\cos\left[\arcsin\left(\frac{r_2/r_1}{r_2/r_1+1}\right)\right]\right\}." \qquad (7)$$

It has to be observed that n contact points will be able to cage the target sphere S only if they are not on the same hemisphere, i.e. there is not an equator on S such that all the n contact points share the same hemisphere. The probability for n contact points to cage the target sphere S can, therefore, be seen as the probability for at least one point to lay on the opposite hemisphere. The probability for finding n contact points on a three-dimensional hemisphere is approximated by Wouterse et al. as

$$p_{3,n} = \left(\frac{1}{2}n^2 - \frac{1}{2}n + 1\right)\left[\frac{2\pi-(n-1)A_{excl}}{4\pi - nA_{excl}}\right]^{n-1}. \qquad (8)$$

They found that this approximation agrees well with computer simulations over the whole range of size ratios. The caging number found numerically is 4.71 for equal spheres, in good agreement with previous literature.

In their experimental analysis of large packings of monosized spheres, Aste et al. (Aste 2005; Aste et al 2004c; Aste et al 2005d)

> "study a quantity which is relevant for system dynamics: the escape probability which is the probability that a sphere can move outward from a given location without readjusting the positions of its first neighbours. This quantity is calculated by constructing circles through the centres of the three spheres corresponding to the three faces incident at each vertex of the Voronoi polyhedron. If one of these circles has a radius larger than d, it implies that the central sphere can pass through that neighbouring configuration and move outward from its local position without displacing the first neighbours. In other words, the neighbouring cage is open if at least one radius is larger than d; vice versa the cage is closed when all radii are smaller than d. The escape probability is defined as the fraction of open cages. We find that all the samples with $\rho > 0.6$ have zero escape probability, whereas the two samples with $\rho = 0.586$ and 0.595 have very small fractions of open cages (0.1% and 0.06% respectively). This strongly suggests that around $\rho \approx 0.62 \pm 0.01$ an important phase in the system dynamics reaches an end: above this density, local readjustments involving only the

displacement of a single sphere are forbidden and the system compaction can proceed only by involving the collective and correlated readjustment of larger sets of spheres." (Aste 2005, p. 7-8)

2.7 Coordination Number

In general, coordination number is the number of contacts that a particle has with other particles, and is probably the most commonly investigated parameter in the literature on granular packings.

> "Indeed, this is a very simple topological quantity which gives important information about the local configurations and the packing stability and determines the cohesion of the material when capillary bridges between particles are present. Moreover, historically, this was the first topological quantity investigated in these systems" (Aste 2005, p. S2367-S2368)

Although many studies have focused on coordination number, its analytical determination remains elusive. The only generally agreed point seems to be Bennett's (1972) hypothesis that a mean coordination number of 6.0 is a necessary requirement for the stability of random packings of monodisperse frictionless spheres, which was summarised by Aste (2005, p. S2372) as follows:

> "In a stack of grains at mechanical equilibrium, Newton's equations for the balance of the force and torque acting on each grain must be satisfied. In such systems, to achieve stability, the number of degrees of freedom must balance the number of constraints. If we consider a packing of N perfect, smooth spheres, a simple counting gives 3N degrees of freedom (translational modes) and CN/2 constraints (one normal force per contact, C

contacts on average and each contact shared by two spheres). In this case, the balance between freedom and constraints implies that C must be equal to 6. On the other hand, real grains have unavoidably rotational modes and therefore the degrees of freedom number 6N (i.e. in reality each of the N grains has 3 translational modes and 3 rotational modes, while perfect smooth spheres only have the 3 translational ones). Moreover some friction is always present; therefore tangential forces must also be considered yielding 3CN/2 constraints on the contacts (N spheres, three components of the force per contact, C contacts on average and each contact shared by two spheres). In this case the isostaticity equilibrium gives:

$6N = 3CN/2 \rightarrow 3C = 12 \rightarrow C = 4$ (9)

However, it must be noted that this condition for C is neither sufficient nor necessary. Indeed, there can be local configurations which contribute to C but do not contribute to the whole system rigidity (there are, for instance, the rattlers)." (Aste 2005, p. S2372)

More generally, defining a sphere in d-dimensions as the group of d-dimensional points that have the same distance r from the centre, it can be shown that "the minimal average coordination number required to obtain static packings of d-dimensional frictionless (i.e. smooth) spheres that are stable against external perturbations is $C_{smooth} = 2d$, whereas for spheres with friction $C_{frictional} = d + 1$. In three dimensions $C_{smooth} = 6$ and $C_{frictional} = 4$" (Silbert et al 2002). The packings that respect this condition will be called "isostatic", while those with smaller or larger

average coordination number will be called respectively "ipostatic" and "hyperstatic". In their study, Silbert et al. "investigate whether or not sphere packings readily achieve isostaticity under generic packing conditions. This isostaticity hypothesis is important in theories focusing on the macroscopic response of such packings" (Silbert et al 2002, p. 1)

By means of computer simulations, Silbert (2002) has investigated the variation of packings of spheres as a function of their friction coefficient. He observed that, while this isostaticity hypothesis is verified for frictionless hard spheres regardless of the packing method, the packings of frictional hard spheres form a variety of hyperstatic structures ($C > C_f$) that depend on system parameters and construction history. In his simulations the average coordination number decreases smoothly from $C_{smooth} = 6$ assuming values higher than the expected $C_{frictional} = 4$, disagreeing with the isostaticity hypothesis.

The complexity of the problem arises from the fact that coordination number, although simple in its definition, is unavoidably an ill-defined quantity. Given two spheres of radius r_1 and r_2, their touching condition can be expressed as:

$$d = r_1 + r_2 \qquad (10)$$

where d is the distance between the centres of the two spheres. It is evident, therefore, that two spheres can be arbitrarily close (d a little greater than $r_1 + r_2$) without actually being in contact with each other. The problem of the contact evaluation is always encountered in experimental studies (see following section) due

to the unavoidable technical approximations (d can't be precisely measured), while this is not the case for numerical simulations, where the spheres' position and dimension is exactly known. This is the reason why, in this Section, we distinguish between physical experiments and numerical simulations.

Physical experiments.

The following is an extract from a recent paper by Aste (2005), which we believe describes better than anything else the remarkable efforts that, to date, have been made to empirically estimate coordination number.

> "In the literature several physical methods have been used, but they encounter problems all essentially associated with the uncertainty in the correct threshold distance which must be used between touching and non-touching spheres. In an early experiment Smith et al (1929) poured lead shots into a beaker and then filled the beaker with a solution of acetic acid. The acid was then drained but a small ring of liquid was retained by capillarity at each contact point. After a few hours, white circular deposits at the contact positions were visible on the shots. The counting of the number of such marks on each shot led Smith to conclude that the number of contacts increases with the density and it is in the range between 6.9 and 9.14 for five samples with densities from 0.553 to 0.641. However, this early experiment is now considered not completely satisfactory because capillary necks of acids can also form between near but non-touching spheres and because the density of 0.553 appears to be too small for a stable packing of monosized spheres under gravity. A more precise but similar experiment was performed by Bernal and Mason about 30 years later. In this experiment they used ball bearings compressed with a rubber band making a packing with density 0.62. The number of contacts was

> calculated by counting the number of marks left on the balls by a black Japanese paint after drainage. Unlike Smith, they distinguish between touching balls and nearly touching balls, reporting an average number of touching spheres equal to 6.4 over an average number of 8.4 total marks. They estimated that with this method nearly touching balls are registered up to a distance 5% greater than the ball diameter. The same method, applied to a less dense packing with $\rho = 0.6$ (obtained by slowly rolling the balls in the container), gave 5.5 for the average number of touching spheres and 7.1 on adding the nearly touching balls. In another experiment, a different method was adopted by Scott (1962), who poured molten paraffin wax into a heated container filled with the balls packed at $\rho = 0.63$ and allowed the set-up to cool. In this way, after a great effort, he managed to calculate the Cartesian coordinates of a central cluster of about 1000 balls with a remarkable precision of less than 1% of their diameters. From these centre positions he computed an average number of 9.3 spheres within 1.1 diameters from the centres of the test spheres. Surprisingly, after this remarkable experiment by Scott, no further empirical investigations were performed until very recently when new techniques (confocal microscopy and x-ray microtomography) allowed visualization of the inside of the packing structures." (Aste 2005, p. S2368)

Aste et al. (2004c; 2005d) have themselves performed extensive empirical investigations of large packings of monosized spheres (≈ 150,000 beads) using an X-

ray computer tomography apparatus. As the identification of touching spheres is, in general, an ill-defined problem from an experimental point of view, in their analysis they "assume that the spheres in contact are located at a radial distance between the diameter d and d + v, where v is the voxel-size", i.e. the size of the pixels used during the image acquisition. Table 1 and Figure 2.16 show the values of the average number of contacting neighbours N_c computed at three different radial distances (d, d + v/2 and d + v).

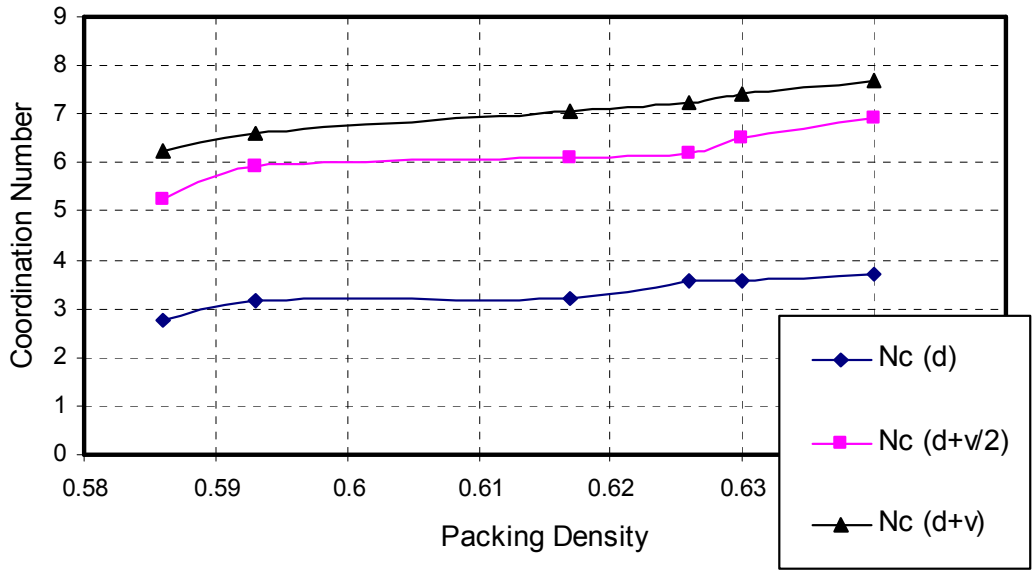

Figure 2-16 Coordination number changes greatly changing the distance threshold

Table 1 Number of contacts between particles for different threshold distances

Packing Density (ρ)	Number of Contacts		
	N_c (d)	N_c (d + v/2)	N_c (d + v)
0.586	2.75	5.26	6.22
0.593	3.15	5.91	6.61
0.617	3.23	6.11	7.05
0.626	3.56	6.18	7.25
0.630	3.58	6.51	7.40
0.640	3.73	6.94	7.69

Bezrukov et al. (2002b) report that, for packings of real spheres, Stoyan et al. give for a porosity of 0.36, which they identify with a random close packing, an average value of coordination number of 6.4, while for a porosity of 0.36, which they call "loose" random packing, an average value of coordination number of 5.5.

Numerical simulations.

Clarke & Jonsson (1993) generated packings of single size sphere assemblies with a wide range of densities using a Monte Carlo algorithm that minimises sphere overlapping and periodically "vibrates" the spheres by giving each of them a small random displacement. They analyse structures starting from a Loose Random Packing (LRP) with a packing density of 0.56 until the Dense Random Packing limit with a packing density of 0.64 is reached, proceeding by density increments of 0.02. Using a cut-off distance to define "contact" of 1.057 diameters they reported contact statistics which are in good agreement with the previous work by Bernal and Mason, reported in (Aste 2005), who suggested a distance threshold 5% higher than the spheres diameter. They observed that "not only does the distribution of coordination number shift to a larger number of contacts as the packing is densified, but it also changes shape", passing from a symmetric distribution at low packing density to a highly asymmetric distribution at higher densities.

In an early study, Matheson (1974) combined the spherical growth method with a drop and roll algorithm to simulate a random monodisperse packing of hard spheres. The results of his computation showed that "the mean coordination number at 1.1 diameters is 7.82, a value which is significantly lower than the value of 8.85 obtained for a shaken ball-bearing assembly of higher density by Bernal (1967). It falls to 6.19 if only spheres within 1.01 diameters are considered, and for true contacts the mean coordination number is 5.99. In this latter case, half of the spheres were found to have exactly six contacts, while only 2% have four contacts, the minimum number for stability. This value of the mean coordination number supports Bennett's (1972)

hypothesis that a mean coordination number of 6.0 is a necessary requirement for a true random packing of single spheres". Moreover, the three different distributions of coordination number for the different values of distance were found to be Gaussian in general character.

To & Stachurski (2004) have simulated packings of monodisperse spheres with various packing densities using a spherical growth algorithm. Their approach differs from previous ones as they count the number of contacts differentiating between caged and uncaged spheres. Figures 2.17-2.19 show some of their results.

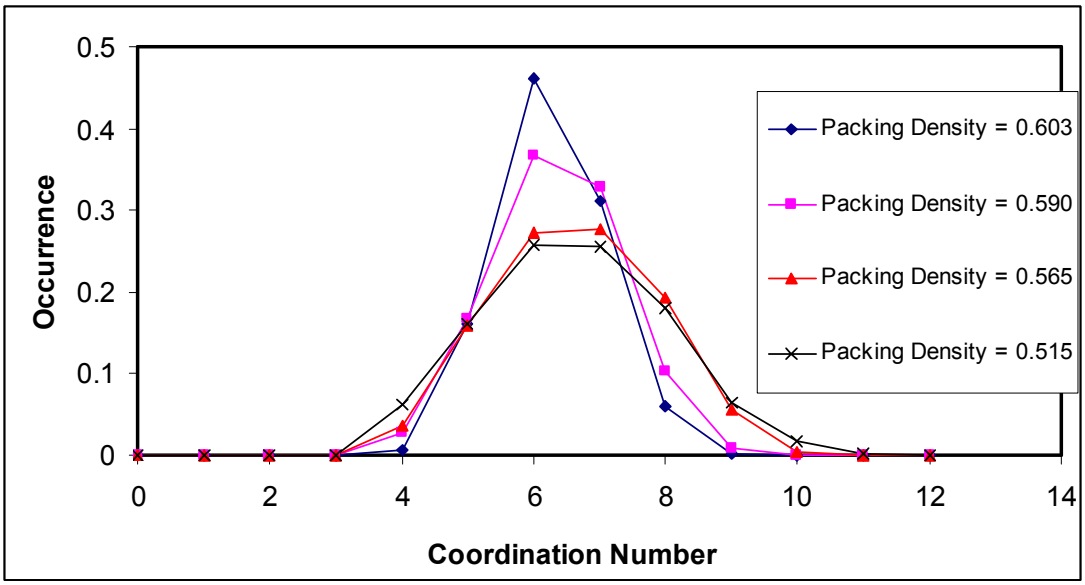

Figure 2-17 Coordination number distribution for caged particles

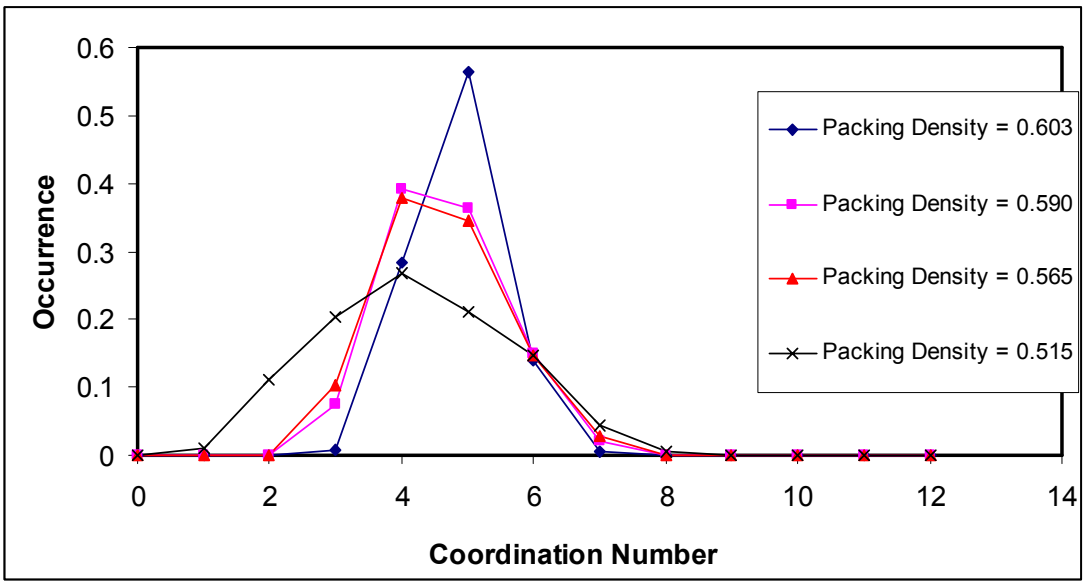

Figure 2-18 Coordination number distribution for uncaged particles

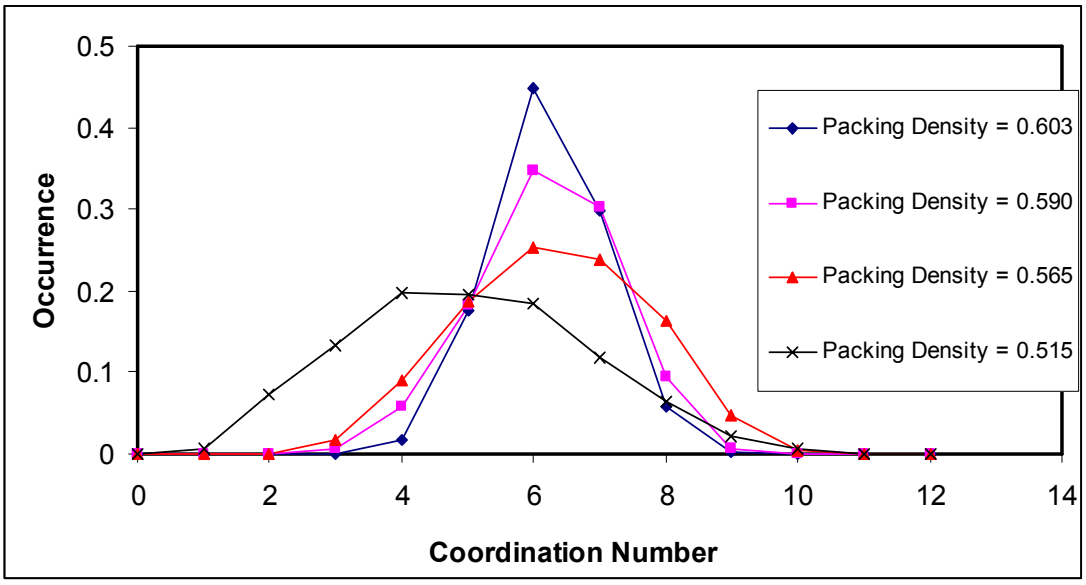

Figure 2-19 Coordination number distribution all particles

It is interesting to note that the distributions of coordination number for different packing densities remain Gaussian in nature (bell-shaped) but, as expected, they modify their shape generally shifting towards lower values of coordination number

for looser packings. Particular attention must be given to the average values of these distributions, which are plotted against packing density in Figure 2.20.

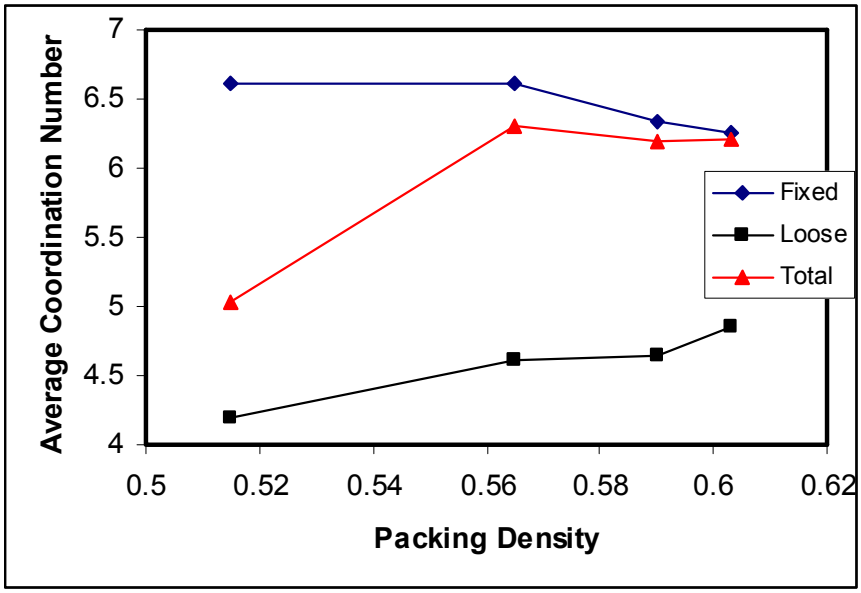

Figure 2-20 Average coordination numbers from To's simulation

The average coordination number for packing densities around 0.60 are within the expectations from previous works. The measures on loose (uncaged) and total spheres show the expected decrease of the average coordination number with decreasing values of packing densities, while the opposite behaviour is observed for the fixed (caged) spheres. This could be due to the definition itself of caged spheres, which implies the lower bound represented by the caging number. Nonetheless, further investigation would be needed in this sense to validate these results.

Liu et al. (1999) have studied spherical packings of spheres modelled under a field of centripetal forces by means of a spherical growth algorithm. The inhomogeneity of these structures implies that the mean coordination number varies through the

packing as a function of the distance from the packing centre R_p. Plotting the values of $\langle C \rangle$ against $1/R_p$ they extrapolate a limit mean coordination number of 6.213, which is in good agreement with those measured for packings under gravity and is consistent with the concept that, for a random close packing of monosized spheres to have mechanical stability, the mean coordination number should be 6 (Bennett's hypothesis).

Liu et al. (1999) observed that the generation of a packing is actually a dynamic process in which the various forces acting on particles at the time of placing are instrumental in the packing that is developed, thus a simulation made purely on a geometric bases cannot be expected to deliver a correct packing. However the DEM approach overcomes this limitation.

Using DEM techniques, Yang (2003), Yang, et al (2000a; 2003b) and Zou et al. (2003a; 2001b; 2003c) have extensively studied packings of fine particles simulating their response to real-life parameters such as van der Waals forces (Yang et al 2000a), moisture content (Yang 2003; Zou et al 2003a; Zou et al 2001b) and friction. In their analysis coordination number, for coarse particles, "varies from 3 to 10 and its frequency distribution is approximately symmetrical with its most probable value at 6". As considered earlier, packings of coarse particles are dominated by gravity and tend to be unaffected by light cohesive forces and friction. This result is, therefore, in perfect agreement with the experiments conducted by Aste et al (2004a; 2005b), the hypothesis of Bennett (1972) and Silbert et al (2002) and the simulations by Matheson (1996), To & Stachurski (2004) and Liu et al (1999).

Yang, Zou et al. also show how, as a consequence of the increasing importance of superficial interparticle forces, as particle size decreases the distribution of coordination number becomes narrower and the mean value lower. In this respect, a summary of their results is shown in Figure 2.21and 2.22 and Table 2.

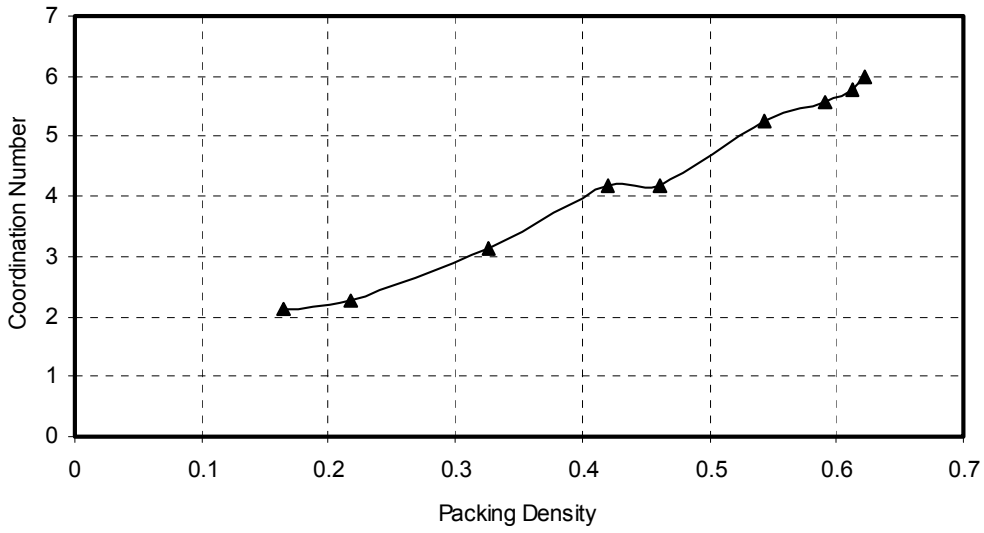

Figure 2-21 Yang et al. simulate very loose packings using frictional spheres

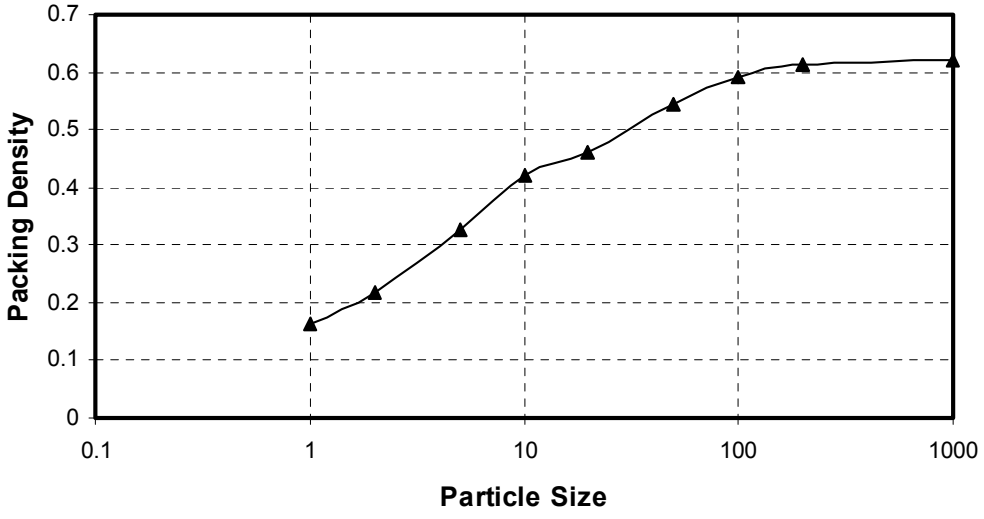

Figure 2-22 As an effect of superficial interparticle forces, the packing's density varies with particles size

Table 2 Different packing densities and coordination numbers for various particle sizes

Particle size (μm)	1	2	5	10	20	50	100	200	1000
Porosity ε	0.835	0.783	0.674	0.580	0.539	0.457	0.409	0.387	0.378
Mean coordination number	2.13	2.26	3.13	4.18	4.17	5.25	5.57	5.78	5.98
Packing density ρ	0.165	0.217	0.326	0.420	0.461	0.543	0.591	0.613	0.622

In Yang's simulation we can note that the mean coordination number reaches values as low as 2.13, which had not been observed before. These values can be explained considering that, to maintain the continuity in both structure and force, a minimum number of contacts equal to 2 is required, so that a particle can be supported by one particle and at the same time support another.

A very interesting study has been conducted by Yang et al. (2003b) to explore the possibility of a "quasiuniversality law" that uniquely links coordination number and packing density in random assemblies of monosized spheres. For this investigation, with a DEM method they have simulated four packings with different physical parameters: packings A and B have similar porosity of 0.550 and 0.555 but different particle density and sliding friction coefficient, while packings C and D have similar porosity of 0.726 and 0.721 but different van der Waals forces and rolling friction coefficient (see results in Figure 2.23).

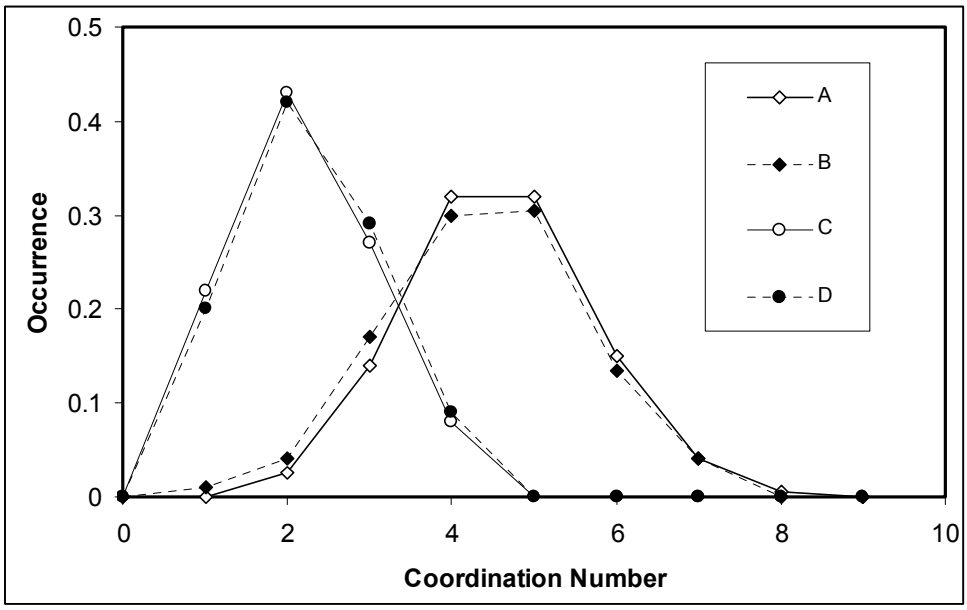

Figure 2-23 Yang et al. show that packing density is the major factor affecting coordination number

The results of Yang et al. (2003b)

> "confirm that there is a one-to-one relationship between porosity and microstructural properties so that the microstructural information of a packing can be mapped by the porosity of the packing, consistent with the finding of Jullien et al. for coarse particles. Therefore the quasiuniversality may exist for the packing of particles with porosity as high as 0.8. This finding provides a good explanation why, in engineering practice, porosity or its related parameter such as packing density can alone satisfactorily characterise a packing. The correlation between porosity and mean coordination number $\langle C_n \rangle$ is useful for many practical applications and it can be described by the following equation:

$$\langle C_n \rangle = \langle C_0 \rangle \frac{1 + m\rho^4}{1 + n\rho^4} \qquad (11)$$

where parameters $\langle C_0 \rangle$, m and n are respectively 2.02, 87.38 and 25.81." (Yang et al 2003b, p. 3032).

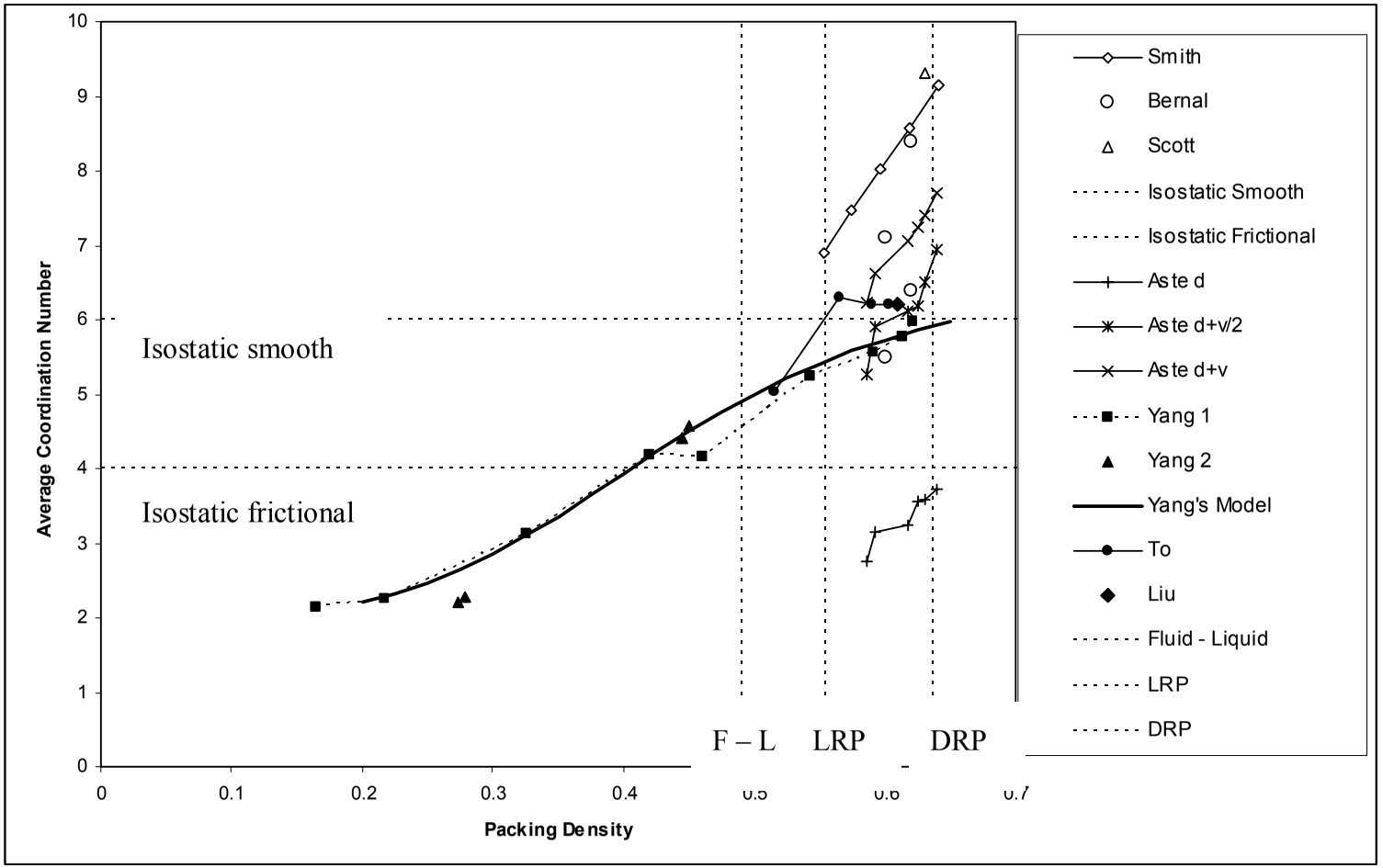

Figure 2-24 Summary plot of coordination number against packing density from the literature

2.8 Bidisperse Packings

Although many researches can be found in this area too, the literature about packings of spheres of two different sizes, i.e. bidisperse packings, is certainly less vast than for the monodisperse case. This is probably due to the slightly less numerous applications and, above all, to the much higher complexity of these systems. Nonetheless, the information available can give indications on the actual state of the art, the common point of views and the possible ways forward.

As for the monodisperse case, very often the attention is concentrated on the estimation of the packing density. Santiso & Muller (2002, p. 2461) have used a sequential addition algorithm, which can be considered within the Drop and Roll category, to study the density of binary sphere assemblies. They observed that these distributions "are denser than the equivalent monodisperse distribution and agree with the theoretical prediction for an infinite size ratio limit", where size ratio is the ratio between the radius of large and small spheres. This density limit, ρ, derived as a function of the packing density of the monodisperse system, ρ_m, and of the mass fraction of the larger particles, w_1, can be defined as:

$$\rho = \frac{\rho_m}{1 - w_1(1 - \rho_m)} \qquad \text{for } w_1 < \frac{1}{2 - \rho_m} \qquad (12)$$

$$\rho = \frac{\rho_m}{w_1} \qquad \text{for } w_1 \geq \frac{1}{2 - \rho_m} \qquad (13)$$

Figure 2.25 shows the packing densities obtained for different size ratios compared to the limit for infinite size ratio.

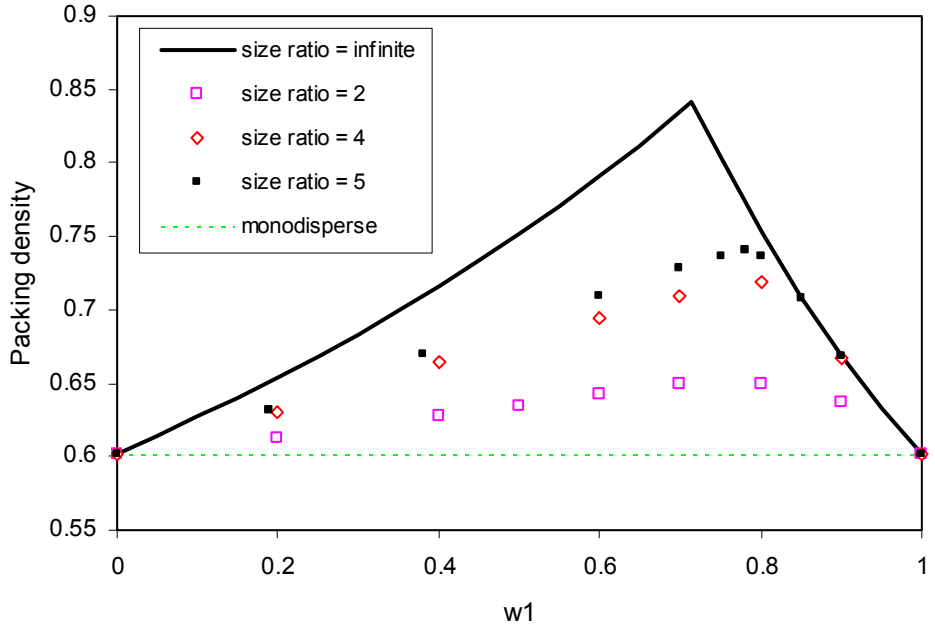

Figure 2-25 Theoretical packing densities in bidisperse packings

The peak at $w_1 = \frac{1}{2 - \rho_m}$ corresponds, as shown by Elliott et al (2002), to the densest possible packing of two components. These results, confirmed also by Okubo & Odakaki (2004) for random packings of binary hard disks generated by a Monte Carlo algorithm, indicate that when small particles are introduced in a uniform packing of larger ones their first effect is to fill the voids. When this phase ends, a maximum possible density for that particular size ratio is reached and any further addition of small spheres will correspond to a dilution of the original packing of large spheres, slowly transforming the bidisperse packing into a monodisperse packing of small spheres. Interestingly, it has to be noted that this effect can be observed even if the smaller spheres are actually larger than the initial

voids between the large spheres, therefore managing to fill the voids by disrupting the original organisation of the large spheres system.

Pinson et al. (1998, p. 457) affirm that "previous experimental studies do not provide complete information about coordination number. For example, a binary mixture gives three types of contacts (partial coordination numbers): large-to-large, large-to-small or small-to-large and small-to-small, and each type of contact should have its own distribution; but this information is not available in the literature". They also suggest that "few attempts have been made to develop mathematical tools for predicting the partial coordination numbers, **but none of them can predict distributed coordination numbers**. Further work is therefore necessary in order to properly describe coordination numbers and their distributions".

The lack of detailed information about these types of systems underlined by Pinson can still be found in more modern literature. For instance, Kristiansen et al. (2005) have recently investigated binary mixtures of spheres using a Mechanical Contraction algorithm and focusing on the relationship between coordination number and composition of the mixture (mass fraction of small spheres). They only differentiate between the average number of contacts on small spheres, $<C_{small}>$, and on large spheres, $<C_{large}>$, and report their change with the percentage of small spheres.

On the other hand, experimental studies by Zou (2001b; 2003c) and Oda (1977) and simulations by Beck & Volpert (2003), Gopalakrishnan &

Shashidhar (2003) and Troadec et al (1987b) report partial coordination numbers for different mixtures, but the relationship between these different parameters and a satisfactory description of their general behaviour can not be found.

2.9 Summary of the Literature Review

The main points from this literature review can be summarised as follows:

- Packing density is considered the most representative parameter to describe granular materials. Numerous studies have focused on relating packing density to the packing's structure and to its mechanical behaviour, using many different approaches such as theoretical, computational and experimental. Although different approaches can deliver slightly different results, it is generally agreed that particular values of packing density delimit different "states" of the assembly.

- The radial distribution function describes the average packing density that is found at a given radial distance from the centre of each particle. Therefore, while packing density is a general description of the packing, the radial distribution function is a description of the structure of the packing "from the point of view of a particle". Interestingly, it shows characteristics (peaks positions, peaks values) that seem to be strictly related to the structures formed by the particles but, at the same time, are independent from the packing method adopted. This makes it a very useful tool to compare packings obtained by different algorithms or by physical experiments.

- Kissing number, parking number and caging number seem to be well defined geometrical quantities for which a value is given in the literature, even for spheres of different size than the central one. In other words, they refer to exact geometrical problems that seem to have been solved.

- Coordination number, on the other hand, is not a well defined quantity because:
    - Its determination is very ambiguous for physical experiments, where the particles position is known with large approximation and therefore it is practically impossible to define a "contact".
    - Even in the case of numerical simulation, where the spatial position of the particles is known exactly and, therefore, it is possible to define real contacts, it has been shown that coordination number cannot be uniquely related to packing density as it is also dependent on the packing method.

- Bidisperse packings are much more complicated than monodisperse packings and have been much less studied. In particular:
    - The literature review showed only a very brief mention about the radial distribution function of these structures.

- Coordination number seems to have been treated in a very superficial way, often without differentiating between types of contact. The literature shows general trends of average coordination numbers for different size ratios and gradings, but a theoretical basis and a logic behind the numbers is still to be defined.

2.10 Conclusions from the Literature Review

There is a huge amount of work that has taken place on sphere packing and coordination number, only some of which has been reviewed here. However the key findings, summarised above, show that the following topics of particular importance could be studied:

- Coordination number in bidisperse packings distinguishing between different contact types, relating them to other geometrical parameters and trying to indicate the basis for a general fundamental theory about coordination number.

- Radial distribution function in bidisperse packings. Describing this parameter for these structures will allow to compare them to the existent literature about monodisperse packings and to possible future physical experiments, in a more reliable and complete way than could be done using only coordination number and packing density.

- Develop a parameter to describe the relative position/distribution of contact points on the particle's surface. This could, in future, be related to the particle's fracture probability and other concepts of the micromechanics of granular materials.

Therefore, these points are, broadly, the subjects of the following chapters of this thesis.

3 METHODOLOGY

3.1 Introduction

The literature review presented in Chapter 2 has shown that the topic of sphere packing is of great importance in many research fields. A very large number of studies have dealt with the multiple aspects related to this subject throughout the years,

a) some using complex mathematical tools;

b) others by physical or numerical experiments and critical observations.

As stated in the introductory chapter, the nature of the approach undertaken in this research could only be of this second type.

Most of the studies that were found in the literature about bidisperse packings revealed a lack of a robust interpretation of coordination number in these systems. For this reason the development of a relationship between packing and coordination number in bidisperse collections of spheres was, therefore, chosen as one of the main aims of this project. In order to assist in this development a preliminary task was to develop some basic concepts that could lead to a better understanding of the structure of bidisperse packings. These are now described.

3.2 Basic concepts

This study has, as its basis, two main concepts that differentiate it from previous literature that addresses this subject:

a. In bidisperse packings the differentiation between the type of contacts that can occur within the particles (namely large-large, large-small, small-large and small-small, see Figure 3.1) is of fundamental usefulness because, as will be shown later, each type of contact has a precise statistical and spatial distribution. Only some studies (see Chapter 2) have considered this aspect in any form and none have arrived at explaining the fundamental concepts that rule the statistical distribution of the various type of coordination number. As, in practical assemblages, the differences between the two kind of spheres might be mechanical and chemical apart from being geometrically different, the possibility of considering the different types of contact is of primary importance and this topic should be of great interest for many different disciplines.

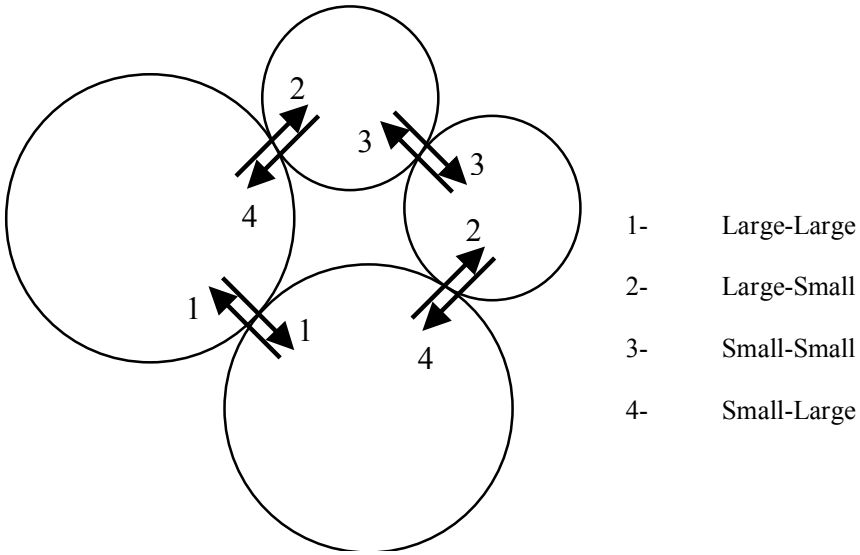

Figure 3-1 Different types of coordination number in bidisperse packings

b. Every particle that lies on a given surface will affect the distribution of all the other particles that are also on that surface. Despite its simplicity, the application of this concept can take the analysis of coordination number to a more advanced level that has previously been achieved.

3.3 Three Spheres Problem

The introduction of the original idea expressed in (3.1.b) represents an effort to try to relate the different types of coordination number to each other. In this case, the question to be answered could be formulated, for instance, as:

"What is likely to be the number of small spheres touching a large sphere if two other large spheres are also touching it?"

This question requires the estimation of the "disturbance" that a large sphere would cause on the surface of a large sphere that is covered with small spheres. In general terms, if $C_{a,b\ max}$ is the maximum possible number of "a-type" spheres on the surface of a "b-type" sphere, the presence of a number "n" of "c-type" spheres on that surface would decrease this number, which would become $C_{a,b}{}^{cn}{}_{max}$. This problem, approached at a very early stage of the research, was called "Three Spheres Problem" and was formulated in its general form as follows:

"What is the maximum number of a-type spheres that can stay on the surface of a b-type sphere if a c-type sphere is also on that surface?"

The determination of $C_{a,b\ max}$ is a well known geometrical problem for which some references could be found in the literature (Mansfield et al

1996). The basic solution idea is to consider the surface occupied by three a-type spheres touching each other on the surface of the b-type sphere, calculate the curved area of the triangle formed by these three spheres (non-Euclidean geometry) and count how many of these triangles can be placed on the b-type sphere's surface. This number corresponds to the number of faces of the theoretical convex solid that has the a-type spheres at its vertices. Applying Euler's theorem is then possible to calculate the number of these vertices knowing the number of faces of the solid. This procedure is explained more in detail in Appendix A, but it is important to note here that two checks of its reliability have been possible:

- If a-type and b-type spheres are of the same dimension, this procedure gives a value of $C_{a,b\ max}$ of 13.4, which is a value used until recent in the literature as an upper bound for the kissing number of equal spheres (Aste & Weaire 2000)

- With this procedure, the value of the ratio R_1/R_2 that reduces $C_{a,b\ max}$ to 4 is found to be 0.225, which corresponds to calculating the radius of the maximum sphere that can be fitted in the void inside a tetrahedron formed by 4 equal spheres of unit radius, and coincides to the Apollonian limit (Elliott et al 2002; Santiso & Muller 2002).

On the other hand, no examples could be found in the literature that refer to the solution of the Three Spheres Problem, $C_{a,b}{}^{cn}{}_{max}$. As a fundamental part

of the research, therefore, this number has been estimated as function of the spheres radii using non-Euclidean geometry and Euler's theorem. Extensive details of the procedure are given in Appendix A, together with the procedure to estimate $C_{a,b\ max}$. For the purpose of the analyses discussed in the later chapters, these numbers have been calculated using an Excel spreadsheet that contains this procedure.

3.4 Types of packings

Although the main subject of the study is the analysis of the structure of bidisperse packings, at different stages of the research and during the development of the algorithm for bidisperse packings other types of sphere assemblies have been encountered and, to some extent, analysed in order to acquire deeper knowledge on the subject and greater confidence in the adequacy of the algorithms developed. Moreover, the data collected in this variety of cases constitute an important source of information and a very solid basis by which it is possible to analyse, compare and discuss the ultimate bidisperse results. The diagram in Figure 3.2 shows the different types of packings encountered and how they relate to each other.

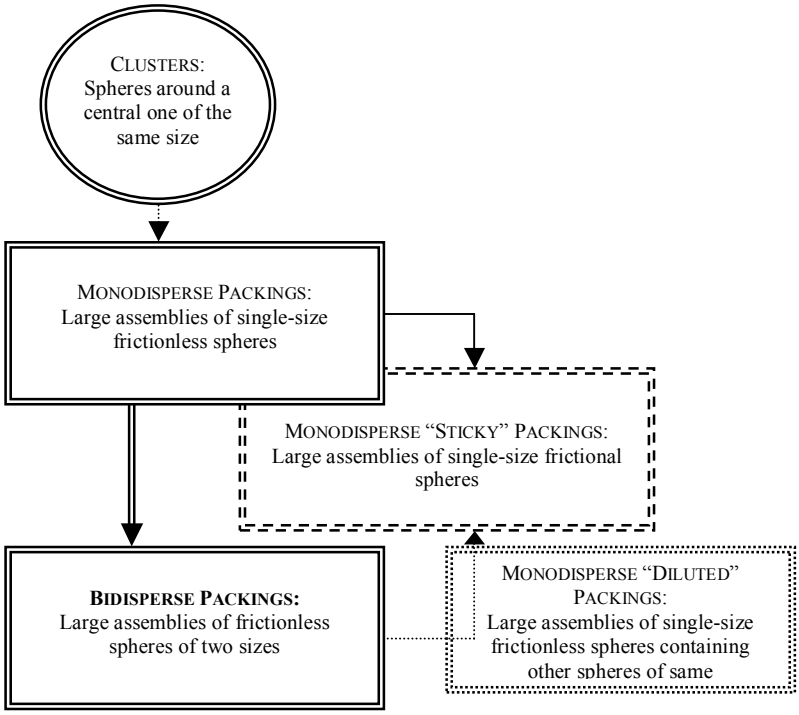

Figure 3-2 Types of packings studied in this research

3.5 Algorithms

A brief review of the main algorithms that are generally employed for the numerical simulations of sphere packings has been given in Chapter 2. Only two of them, the Drop and Roll and the Spherical Growth, have been employed in this research:

Although, as shown in the literature review, it cannot deliver densely packed assemblies, the Drop and Roll algorithm has the advantage of being relatively simple and requiring shorter computational times than the more complex previous ones. For this reasons, it has been used to simulate the large monodisperse and bidisperse packings that are the main subject of this study.

The Spherical Growth algorithm has, instead, been applied to generate clusters of spheres around a central one (seed) by limiting their "growth" to the first level of coverage of the inner particle.

Moreover, it must be said that a modified Drop and Roll algorithm has been used to simulate the packing of frictional single-size spheres. In this case, each sphere was allowed to roll only within a given distance from the dropping point. As can be imagined, varying this range would correspond to varying the "stickiness" of the particles.

In order to keep the focus on the main concepts of the research and on the analysis of the results, detailed descriptions of the different algorithms are only given in the correspondent Appendices B – E.

3.6 Main parameters studied

There are at least three aspects that need describing in order to give a complete picture of the position of the particles relatively to each other, therefore, for all the different types of sphere packings encountered in this study, the following parameters have been employed:

- Coordination Number: the number of contacts between a particle and its neighbours. The literature review has revealed the need for a better description of this parameter, particularly in bidisperse packings.

- Superficial Distribution: a parameter that is being introduced in this research to describe the relative position that the contact points have on the surface of the considered particle. Intuitively, this parameter could be related to the distribution of stresses within the particle under external load.

- Radial Distribution Function: describes the structure of the packing as a function of the distance from the considered particle. This parameter has been extensively studied by other researchers for monodisperse packings, while information about it in bidisperse ones is missing.

As can be seen, the study of each one of these parameters within this project can deliver an interesting and original contribution to the subject. Moreover, together they can supply a fairly complete picture of the sphere system, describing different areas of interest within packing:

Coordination Number (first degree neighbours)	-	Number of contacts
Superficial Distribution (first degree neighbours)	-	Position of contacts
Radial Distribution Function (further spheres)	-	Long-range organisation

4 COORDINATION NUMBER

4.1 Introduction

This chapter reports the analysis of the coordination number (number of contacts between particles) for the various structures simulated during this research. In the case of clusters the object of the study is, obviously, only the central sphere, of which are known the touching neighbours and their chronological order of deposition.

The basic case of monodisperse packing of frictionless spheres has been developed in two directions:

- Monodisperse frictional spheres ("sticky" packings);
- Bidisperse frictionless spheres.

The latter case is also used to produce packings of two types of spheres of same dimension, which have been called "diluted" packings, and their coordinance is compared to that of the monodisperse sticky packings in order to investigate the effect of variable packing density on coordination number. To the author's knowledge, there are two different ways to obtain a wide range of packing densities with single size hard spherical particles subjected to vertical attractive forces (gravity): variation in movement freedom and dilution. Although the algorithms used to simulate these two

cases differ, the main structure and concepts remain similar and are discussed hereafter and in appendices C, D and E.

Finally, bidisperse packings of spheres of two different dimensions are studied applying the concepts expressed in Chapter 3. The direct analysis of the results of these simulations are presented in this chapter, while further observations are discussed in Chapter 8.

4.2 Clusters

Using the Spherical Growth algorithm described briefly in Chapter 2 and more in detail in Appendix B, approximately 80000 configurations were computed. It must be noted that this kind of configuration does not consider all those situations where a sphere is not touching the central one but is close enough to influence its Voronoi cell (Figure 4.1a is considered while Figure 4.1b should have been).

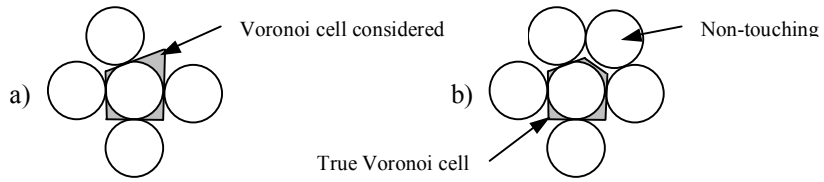

Figure 4-1 Voronoi cell in a cluster (a) and in a packing (b)

Investigating these configurations to find the link between the packing density and coordination number would be useless for the purpose of predicting the properties of a spheres' assembly.

As shown in Figure 4.2, all of these final configurations have a minimum coordination number of 6, which means that this is the minimum number of spheres that can be "parked" on the central sphere randomly occupying the whole available surface. Every random sphere generation has, therefore, reached at least 6 spheres placed around a central sphere, while only one of them was found to reach 12 (the maximum value as predicted by Kepler (Pfender & Ziegler 2004; Plus Magazine 2003; Aste & Weaire 2000).

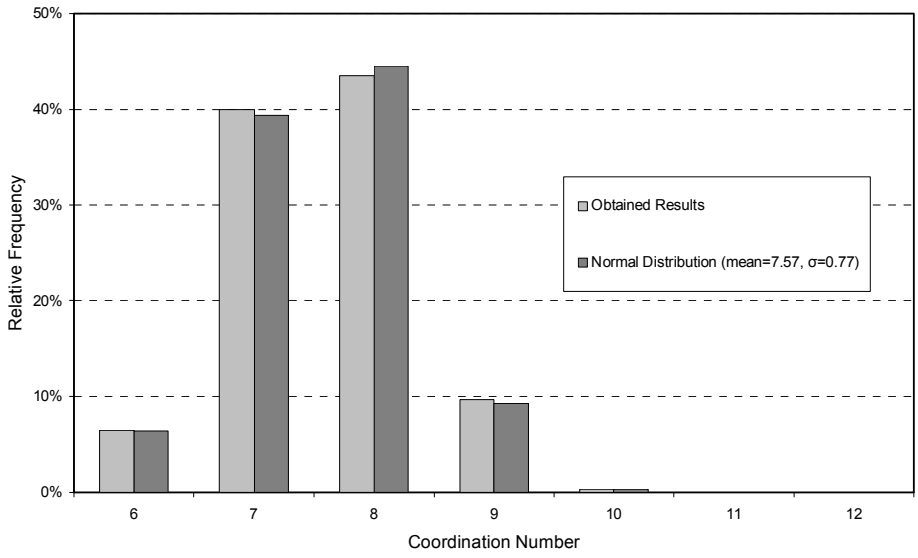

Figure 4-2 Statistical distribution of coordination number for clusters

It can be noted from Figure 4.2 that the relative frequency of the number of spheres needed to completely occupy the surface of an identical sized sphere can be expressed as a normal distribution with mean value of 7.57 and standard deviation of 0.77. It has been found that the relative frequency of coordination number also takes a normal distribution when the outer spheres are of different diameter to the central sphere but, even if considered by the authors an interesting point of discussion, this will not be referred to further in this thesis for reasons of clarity and brevity.

Of course, each final configuration of N spheres may also be considered as producing an intermediate configuration for each $n < N$ spheres group, consisting in the right number of spheres in chronological order of deposition. For analytical convenience (discussed later) only assemblages having 5 or more spheres (i.e. 4 or more placed around the central sphere) are considered. A 9-spheres configuration (coordination number = 8) will,

then, produce one interim configuration for each of the 5, 6, 7 and 8 spheres groups considering, respectively, the first 4, 5, 6 and 7 placed spheres. The total number of clusters that can be analysed is, thereby, approximately 370000. For each value of coordination number, the number of clusters produced is such that it is possible to derive a statistic of the outer spheres distribution on the central sphere's surface. Although this will be the subject of Chapter 5, some considerations can be useful at this stage too.

As will be shown more in detail later, the volume of the Voronoi cell created by the neighbours around the central particle of each cluster can be used as an indicator of the superficial distribution of the contact points. In particular, if this volume is infinite, i.e. the Voronoi cell is "open", the central particle is unstable (uncaged).

The analysis of all the clusters generated shows that approximately 52% and 10% of all the possible configurations of particles with coordination numbers respectively of 4 and 5 are unstable, which means that, in an assembly subjected to external forces, they would not take part in the global mechanism. These results allow us to estimate the Parking Number and the Caging Number for equal spheres, contributing to the ongoing discussion.

In Chapter 2 we defined the parking number P as "the maximum number of probe spheres that can be placed on the surface of a target sphere if

tentative sites for each succeeding sphere are selected entirely at random". The algorithm used hereby satisfies this randomness requirement, and the histogram in Figure 4.2 shows the relative frequency of the different "maximum numbers" obtained in the simulation. Having described these data by means of a normal distribution with mean value = 7.57 and standard deviation = 0.77, it is possible to check the statistical meaning of the value of P = 8.75 generally accepted for equal spheres in the literature (Figure 4.3):

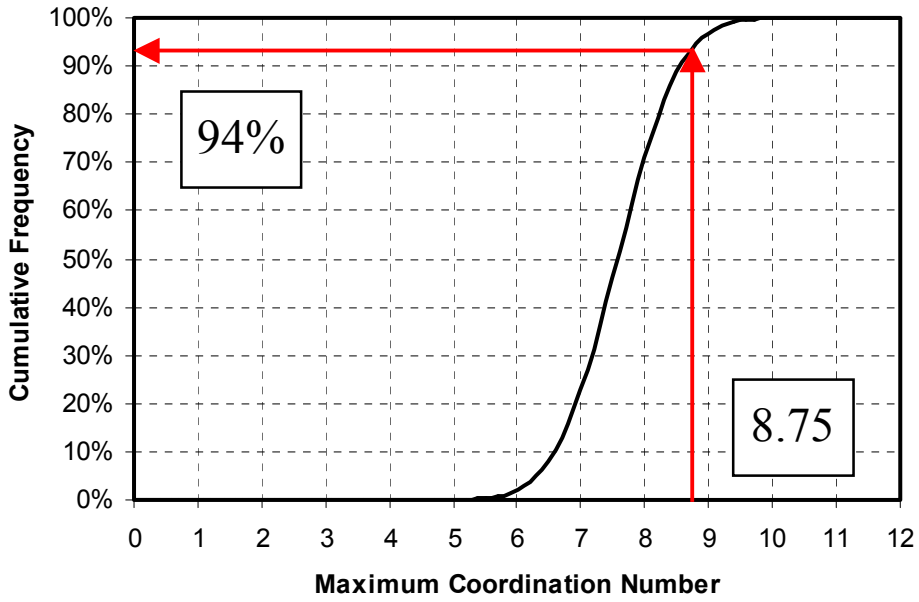

Figure 4-3 Statistical meaning of the parking number

From this analysis, we can conclude that the value of P = 8.75 corresponds to the 94 percentile of the distribution considered.

Moreover, always in Chapter 2 we defined the caging number as "the average minimum number of spheres (randomly placed on the surface of a central one) that blocks all the translational degrees of freedom" of the central sphere.

As will be discussed further in Chapter 5, this "caging problem" can be considered as a particular case of the more general "superficial distribution problem". The method illustrated in Chapter 2 used by Aste (2005) to evaluate the "escape probability" of a particle and, thus, to determine whether a particle is caged or not by its neighbours is fundamentally different from our approach: we consider a particle "unstable" or "uncaged" if the volume of the Voronoï cell constructed considering only its kissing neighbours is infinite.

The data obtained in this part of the study are, therefore, appropriate for calculating the caging number for equal spheres with the procedure shown in Table 3.

Table 3 Procedure for estimation of the caging number

A	B	C	D	E	F
Coordination number	Number of particles with this coordination number	Number of uncaged particles with this coordination number	Number of caged particles with this coordination number	Percentage of caged particles with this coordination number	Percentage of particles that became caged when reaching this coordination number
i	N(i)	U(i)	C(i) = N(i) – U(i)	PC(i) = C(i) / N(i)	PC'(i) = PC(i) – PC(i-1)
3	80270	80270	0	0.0%	0.0%
4	80270	41744	38526	48.0%	48.0%
5	80270	8317	71953	89.6%	41.6%
6	80270	313	79957	99.6%	10.0%
7	75094	1	75093	100.0%	0.4%
8	42973	0	42973	100.0%	0.0%
9	8027	0	8027	100.0%	0.0%
10	265	0	265	100.0%	0.0%
11	12	0	12	100.0%	0.0%
12	1	0	1	100.0%	0.0%

The values of PC'(i) in column F of Table 3 represent how often, in our simulation, a cluster has become caged when reaching a given coordination number, i.e. how often a coordination number has been found to be the minimum required to cage a cluster. These values of PC'(i) can then be used as weights in a weighted average of coordination numbers, the result of which is the caging number. This value has been found to be 4.63, very close to the 4.71 reported in the literature (Wouterse et al 2005).

4.3 Monodisperse 1: Packing sticky particles

The algorithm used to simulate frictional equal spheres in this part of the research is a modified version of the Drop and Roll algorithm and it's been briefly described in Chapter 3 and with more details in Appendix D. The parameter that simulates the degree of friction between particles is the distance *d* from the dropping point within which the lowest position for the new particle has to be found. Varying the value of d the number, Num, of spheres that is possible to fit in a given box varies too. Figure 4.4 shows how this number Num, normalised by the average number, Av. Nroll, of spheres that can be placed in the box in condition of perfect rolling, varies with the parameter d, normalised by the spheres size, for different pairs of box size and sphere radius (A – F).

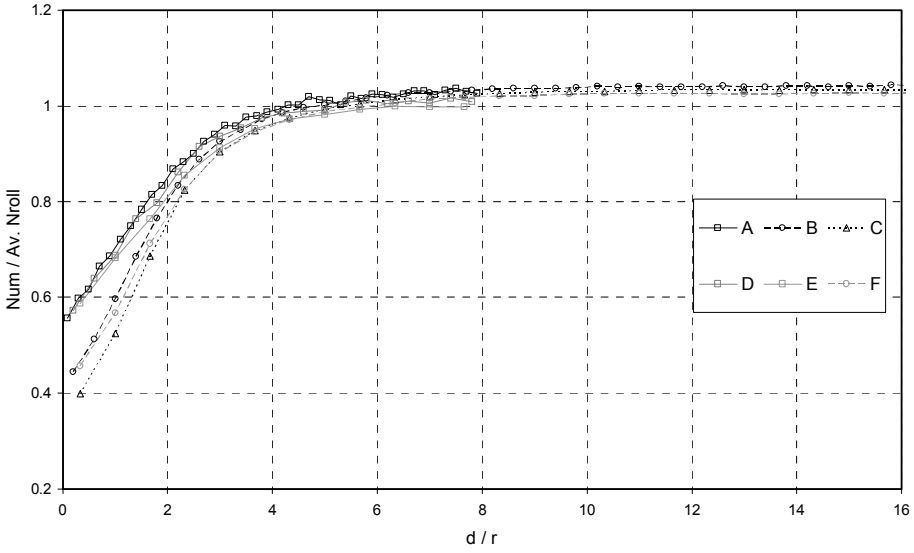

Figure 4-4 Effect of stickiness parameter d on packing density

After having studied its characteristics, which for reasons of brevity are discussed in Appendix D, this "stickiness" algorithm has been applied generating a number of packings with d/r values ranging from 0 to 10. In order to avoid the well-known wall effects that affect packings of this kind, only the particles more than 5r from the box's walls and bottom were included in the computation. The volume, V_i, belonging to each particle was calculated using the packings' Voronoi decomposition (see Section 2.2) and a packing density P_i was assigned to each sphere being

$$P_i = V_s / V_i \qquad (14)$$

where V_s is the sphere's volume. For each packing (i.e. for each value of d/r), coordination number and packing ratio were then averaged between all the particles. A difficulty with this algorithm is that the results do not have packing densities uniformly distributed throughout the whole range, with the dense packings being much more numerous than the loose ones (see again Figure 4.4). To overcome this and provide a graph with equally important points, the results were grouped according to packing density value in ranges R_n defined as

$$R_n = n*0.05 \pm 0.025 \quad n = 1, 2, \ldots \qquad (15)$$

Within each range the mean packing density is calculated and the mean coordination number for the results lying in that range. Those two values are then used to plot the data points as shown in Figure 4.5.

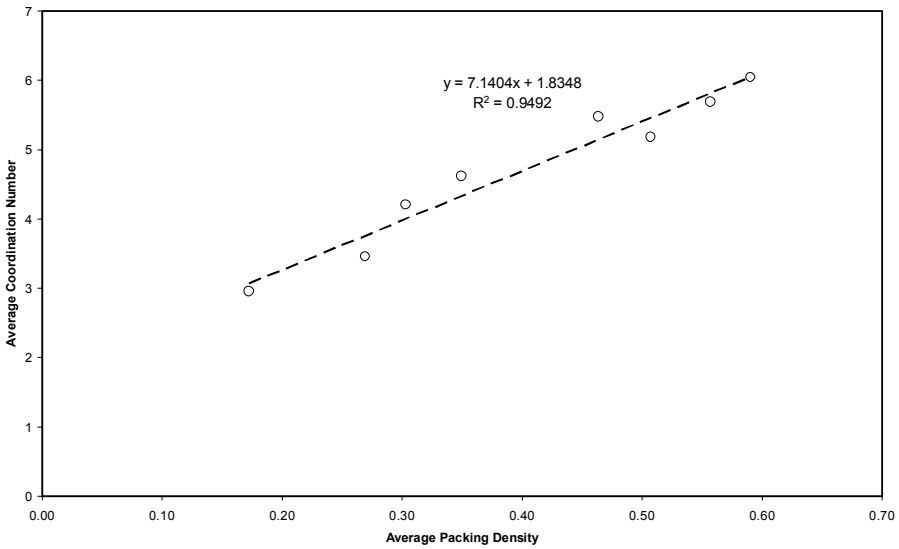

Figure 4-5 Relationship between coordination number and packing density for packings of sticky spheres

4.4 Monodisperse 2: Diluting a packing

Obviously, the dilution of the primary spheres by the addition of other spheres delivers, in general, a bidisperse (two-sized) packing, which is not the topic of this chapter. As will be shown later on, in this kind of packing the relationship between coordination number and packing density depends on the size ratio r_i/r_j between the two types of particles (where r is the sphere radius) (Beck & Volpert 2003; Pinson et al 1998), as is qualitatively shown in Figure 4.6 which represents a typical analysis of the coordination number between particles of the same size (C_{ii}) in bidisperse packings.

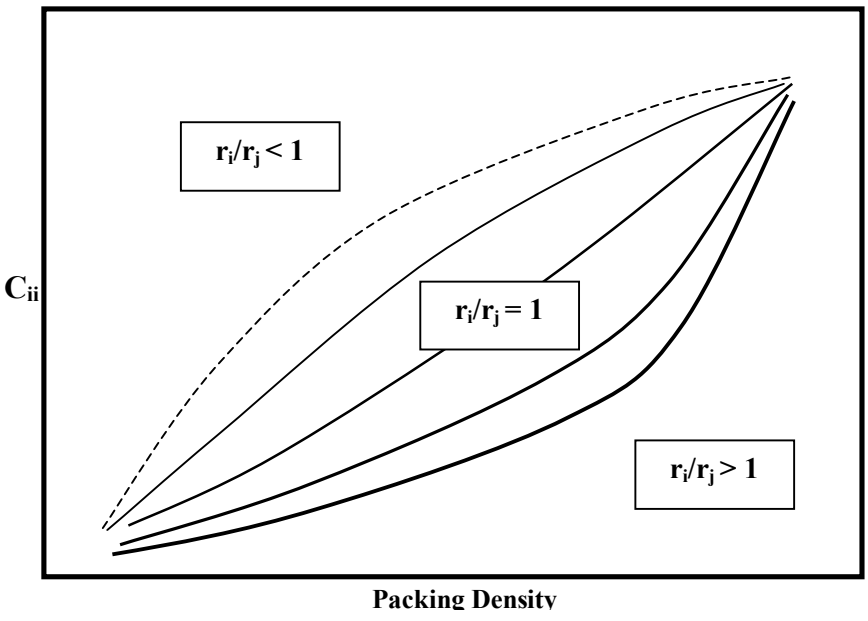

Figure 4-6 General dependence of coordination number from packing density for bidisperse packings as described in Beck & Volpert 2003 and Pinson et al 1998

We can relate this to the single size problem if the extra spheres are of the same dimension of the original ones, i.e. $r_i/r_j = 1$. Although being identical in size, for the purpose of this approach we still have to differentiate between the two types of spheres that form the packing in order to focus on the behaviour of the original ones. For this reason they will be referred to as "black" and "white" respectively for the original and the added spheres (this approach is similar to the one used by Beck and Volpert (2003) to produce gapped gapless packings). In this case, the Drop and Roll algorithm is modified including a procedure to randomly decide whether the incoming sphere should be white or black in order to achieve the requested relative quantities (see Appendix E).

As the spheres are always being placed in the lowest pocket, the volume occupancy is optimised and the packings produced are the densest possible when no rearrangements (due to gravitationally induced horizontal movements or compaction) are considered (Santiso & Muller 2002).

The volume of white spheres was varied from 0% to 90% of the total solid volume. 10 different mixtures were, therefore, considered with the compositions listed in Table 4.

Table 4 Composition of the diluted mixtures with variable stickiness

Black	100%	90%	80%	70%	60%	50%	40%	30%	20%	10%
White	0%	10%	20%	30%	40%	50%	60%	70%	80%	90%

As our interest is in the behaviour of the black spheres, the white spheres may, in effect, be considered as voids. All the 10 mixtures become, then, packings of black spheres with various packing densities. As before, only the particles within the packings' nucleus were considered in the analysis. Performing, for the black spheres, a Voronoi decomposition of the packings and averaging coordination number and packing ratio within each packing, the points on the chart in Figure 4.7 were produced.

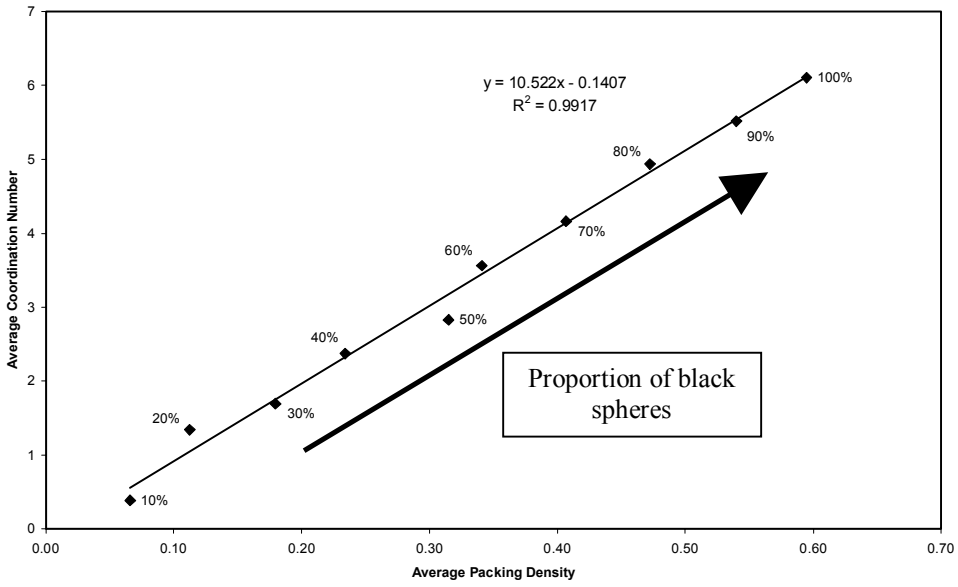

Figure 4-7 Relationship between coordination number and packing density for diluted packings

4.5 Comparing the two types of packings

Some important considerations can be made from a comparison of the results obtained from the two methods presented earlier (Figure 4.8). First of all, it must be noted that in both cases the average coordination number can be expressed as a linear function of the average packing density for the range of results that were produced, this fact being in accordance with the numerical and practical results of the existing literature (Beck & Volpert 2003; Oda 1977). Moreover, as expected, the two algorithms delivered the same results for dense packings. For this region, with an average packing density of 0.60 an average coordination number of 6 was measured, this fact too being in accordance with the existing literature (see Chapter 2). Apart from the area of maximum packing density, the average coordination number measured when using the second algorithm is always larger than that measured when using the first algorithm, for similar packing ratios.

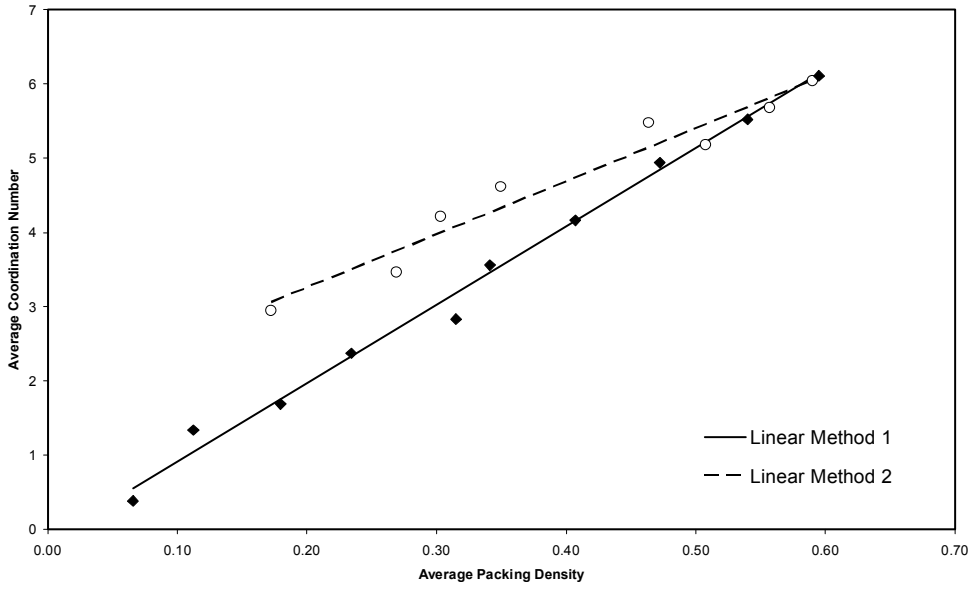

Figure 4-8 Comparison of the two methods

This fact was anticipated as a result of the two different processes used to obtain loose packings. While in the first one every sphere must touch at least one other sphere to stop moving vertically, in the second one the black spheres could, as their concentration decreases, be in contact with only white spheres.

This observation can give some indication about what to expect from packings of real spherical particles: in reality, their packing ratio will be influenced by a number of factors like friction between surfaces, interlocking, cohesion, etc. If they are all of the same type they should behave in accordance with the results of the second method because, no matter what the cause is, if a looser packing is achieved without diluting the mixture it means that the particles have been prevented from rolling perfectly and, therefore, the lower packing ratio must have been achieved as a consequence of some influence on their freedom of movement.

4.6 Hybrid method: Diluting a monodisperse packing of sticky particles

After having studied where these two different approaches lead to, it is interesting to see how their results combine in order to get one step closer to real packings. The mixtures of "black" and "white" spheres listed in Table were then modelled using the first algorithm, i.e. performing on each mixture the same procedure that had already been performed for the 100% "black" spheres mixture bringing the results of Figure 4.7. The resulting packing densities and coordination numbers of "black" spheres were then determined and analysed as before, plotting the relevant results in Figure 4.9.

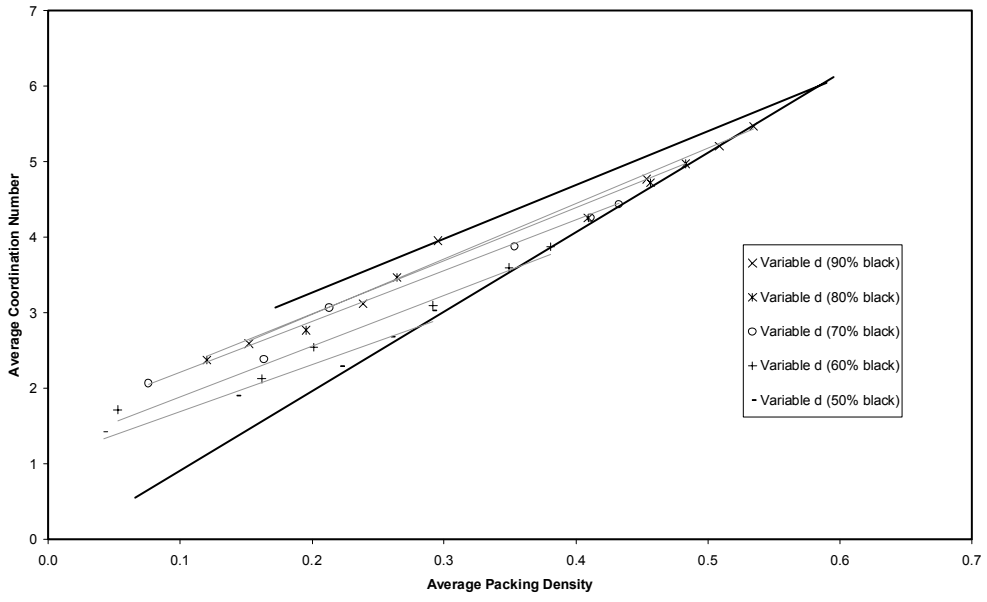

Figure 4-9 Results from the hybrid method

The packings with a percentage of "black" spheres less than 50 are not represented in Figure 4.9 as they were considered unsuitable for a statistical analysis due to the low number of "black" spheres counted. As can be seen, all the light lines meet the bold line with their densest packings confirming the fact that the two algorithms coincide when the parameter *d* is large. The information obtained from this analysis has been re-elaborated and summarised to produce the chart in Figure 4.10.

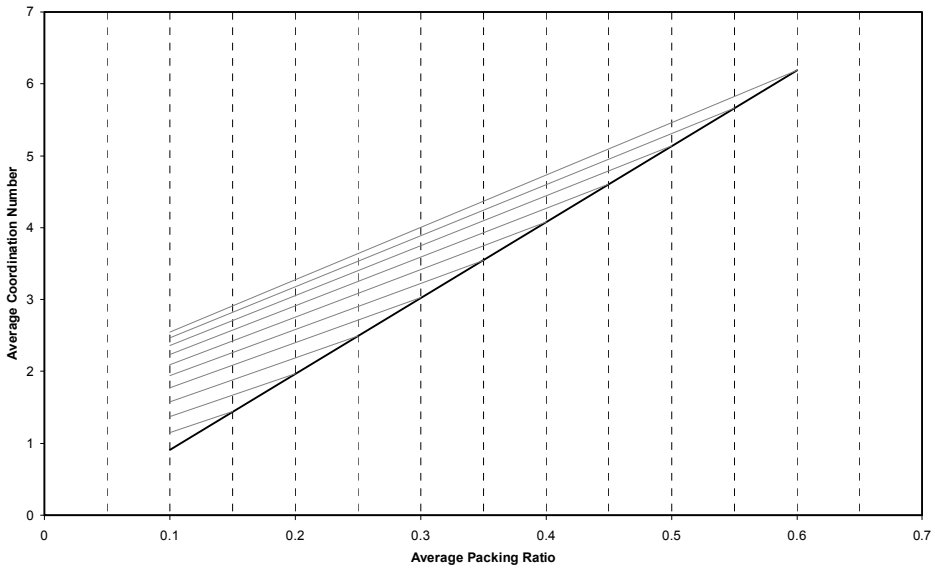

Figure 4-10 Model derived from hybrid method

The light lines in Figure 4.10 represent the grid that resembles the results of the combination of the two algorithms. In this chart, the average coordination number (C) of a certain packing of equal spheres of two types is identified by two parameters: the ultimate packing ratio (Q), which is the expected packing ratio in case of perfect rolling, and their measured average packing ratio (P). The following equation (16) can be used as equivalent to the chart:

$$C = (P - Q)(aQ + b) + aQ - d \qquad (16)$$

where

a = 3.3075;

b = 5.2881;

c = 10.522;

d = 0.1407.

The use of the equation and the chart in Figure 4.10 is clarified by the following example:

Imagine filling a box with 150 black spheres of radius R = 1 cm and 50 white spheres of radius R = 1 cm and to find that they have filled a volume of 1650 cm^3. To evaluate the average number of contact points that the black balls have with other black balls we can use the equation with the parameters

*Q_{bb} = (150 / (150 + 50)) * 0.60 = 0.45*

(as 0.60 is found to be the maximum packing density achievable with this type of algorithms, see also Plus Magazine 2003)

*P_{bb} = 150 * Vs / 1650 = 0.38*

(where Vs is the volume of one sphere)

Hence

$C_{bb} = 4.05$

Alternatively, we can use Figure 4.10 starting from an average packing ratio (Q_{bb}) of 0.45 that yields an average coordination number, C_{bb}', of 4.60 (See Figure 4.11).

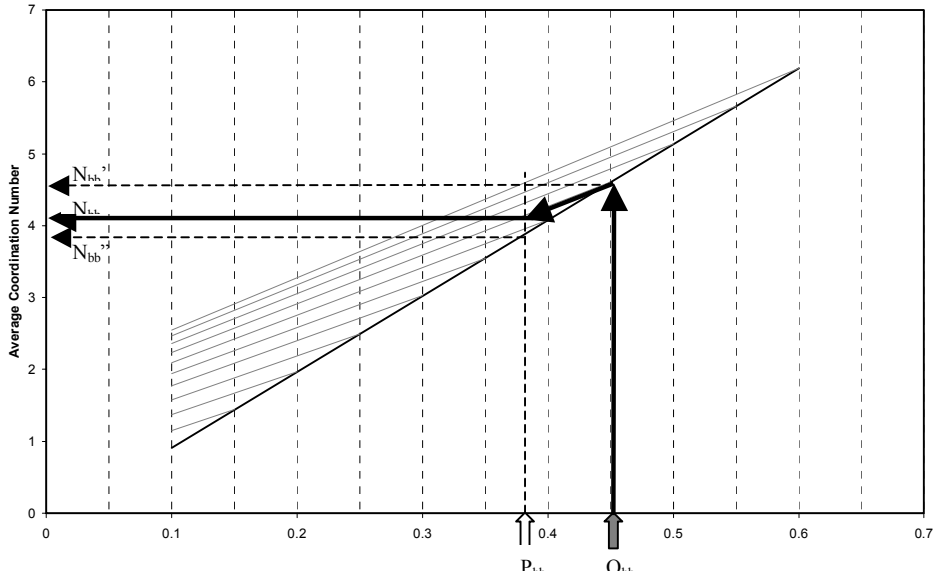

Figure 4-11 Application of the graphical method

However, this overestimates C_{bb} because we have not considered the loosening effect due to friction (etc.) that are not evidenced under "perfect rolling":

$Q_{bb} = 0.45 > 0.38 \rightarrow C_{bb}' = 4.60 > 4.05$

Therefore, it is necessary to track down the light line until the true, looser, packing density, P_{bb}, is reached, yielding an actual mean coordination

number of 4.05. The use of the parameter P_{bb} by itself would bring to an underestimation of C_{bb} (C_{bb}") because the packing is looser not because it is more diluted but because, for some reason, it has had less freedom of movement:

$P_{bb} = 0.38 \rightarrow C_{bb}" = 3.86 < 4.05$

Moreover, inverting the role of black and white spheres we can focus on the white ones and repeat the procedure to calculate the average coordination number between white spheres C_{ww}:

$Q_{ww} = (50 / (150 + 50)) * 0.60 = 0.15$

$P_{ww} = 50 * Vs / 1650 = 0.13$

Hence

$C_{ww} = 1.30$

Since the two types of spheres are geometrically identical, it can be shown (see Appendix K) that when the number of black and white spheres in the packing is much larger than 1, as it normally should be for a statistical approach to be valid, the average number of white spheres in contact with a white sphere, C_{ww}, is the same of white spheres in contact with a black one, C_{bw}. Therefore the total average coordination number of a black sphere is:

$C_b = C_{bb} + C_{bw} = 4.05 + 1.30 =$ ***5.35***

We could have calculated this number acting as if all the spheres were black. In that case the parameters would have been:

$Q_b = (200 / 200) * 0.60 = 0.60$

$P_b = 200 * Vs / 1650 = 0.51$

Hence

$C_b =$ ***5.37***

The fact that the two values of C_b calculated in different ways are found to be almost coincident is proof of a certain solidity of this procedure.

4.7 Bidisperse

At an early stage of this research, the original intention was to simulate the experiments conducted by Oda (1977). For the reasons of time consumption and required precision explained in the introduction to this chapter and in Appendix F, some limitations had to be taken into account in this simulation in order to achieve suitable results in a reasonable amount of time. Therefore, the number of size ratios considered was reduced to 2, respectively 1/2 and 1/4 (which are both larger than the Apollonian ratio), and the gradings being considered as summarised in Table 5.

Table 5 Composition of the bidisperse packings simulated

Size Ratio R_1/R_2	% of the Total Solid Volume ($\%V_1 - \%V_2$)				
(A) 1 / 2	(1) 10 - 90	(2) 30 - 70	(3) 50 - 50	(4) 70 - 30	(5) 90 - 10
(B) 1 / 4	(1) 10 - 90	(2) 30 - 70	(3) 50 - 50	(4) 70 - 30	(5) 90 - 10

The number of particles of the two sizes that form the various packings is summarised in Table 6.

Table 6 Number of small and large particles in the packings

Size Ratio R_1/R_2	Number of Particles ($N_1 - N_2$)				
(A) 1 / 2	(1) 1454 - 1636	(2) 3692 - 1076	(3) 5333 - 666	(4) 6688 - 352	(5) 7578 - 105
(B) 1 / 4	(1) 11636 - 1636	(2) 29538 - 1076	(3) 42666 - 666	(4) 52705 - 352	(5) 60631 - 105

Measurement of the Packing Density

Before analysing the packings from the point of view of the coordination number, their packing density had to be calculated. As explained earlier in Chapter 2, it is not possible to use a Voronoi decomposition in packings of spheres of different sizes as it does not consider the real dimension of the spheres but only the spatial position of their centres. In this case, the examples that can be found in the literature suggest employing variations such as the Radical Tessellation and the Navigation Map.

Although these are both tools suitable to calculate the amount of space belonging to each particle, the type of information that is derived from them may not be of interest at this stage of the study, as what is needed now is an evaluation of the total space occupancy of the two types of spheres (i.e. the amount of volume that, in each packing, the two types are occupying). From an engineering point of view, this is the parameter needed when trying to reproduce these packings in practice: knowing the volume of the container, we can use it to calculate the amount of spheres of each type that have to fill it.

On this purpose, we have chosen to apply the following procedure (Figure 4.12):

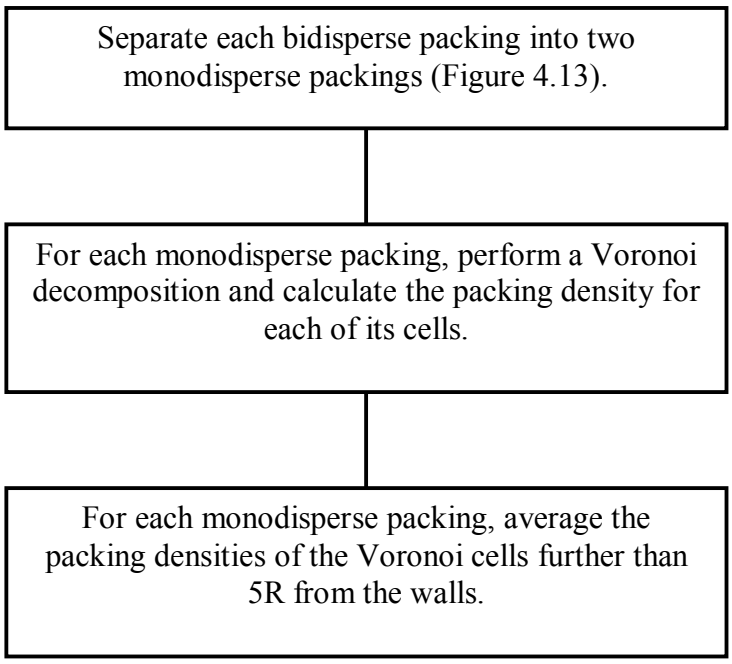

Figure 4-12 Calculation of the packing density of the two sphere fractions

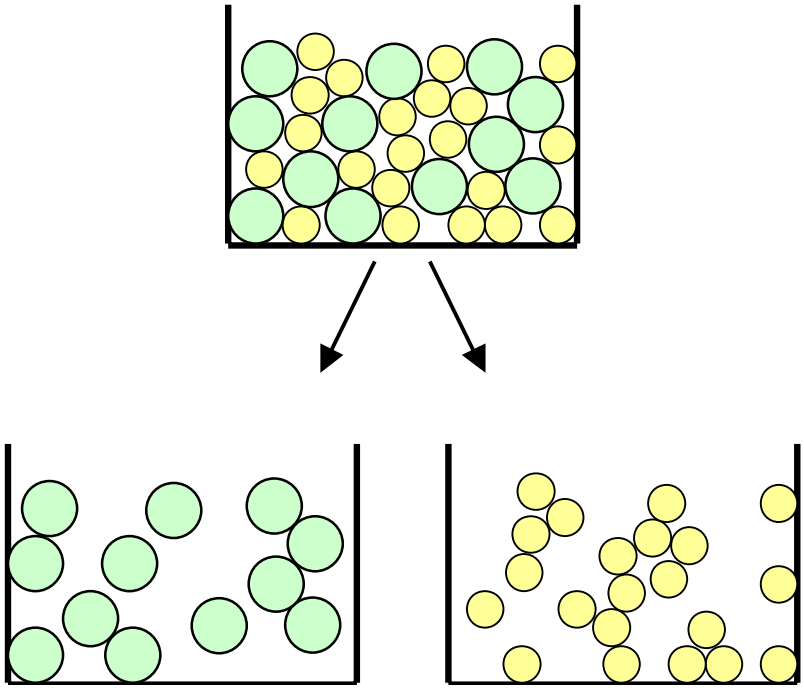

Figure 4-13 Separation of a bidisperse packing into two monodisperse ones

This way, for each bidisperse packing we obtained the average packing densities of the two components and, adding the two of them, the packing's total packing density (Table 7).

Table 7 Packing densities of the small and large spheres fractions

Size Ratio R_1/R_2	Packing density ($SR_1 - SR_2 - SR_{TOT}$)				
(A) 1 / 2	(1) 0.1039 0.5888 0.6927	(2) 0.1702 0.4730 0.6432	(3) 0.2893 0.3428 0.6321	(4) 0.4020 0.2047 0.6117	(5) 0.5321 0.1044 0.6365
(B) 1 / 4	(1) 0.1433 0.6052 0.7485	(2) 0.1993 0.5282 0.7275	(3) 0.3159 0.3663 0.6822	(4) 0.4330 0.22662 0.6596	(5) 0.5438 0.1090 0.6528

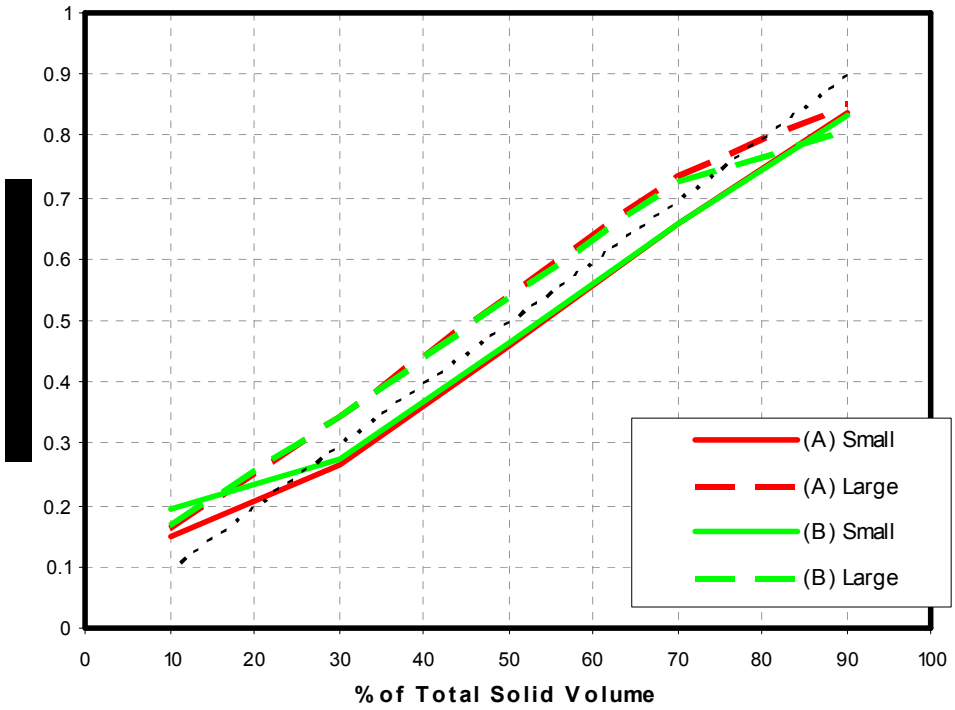

Figure 4-14 Percentage of total solid ratio against percentage of total solid volume

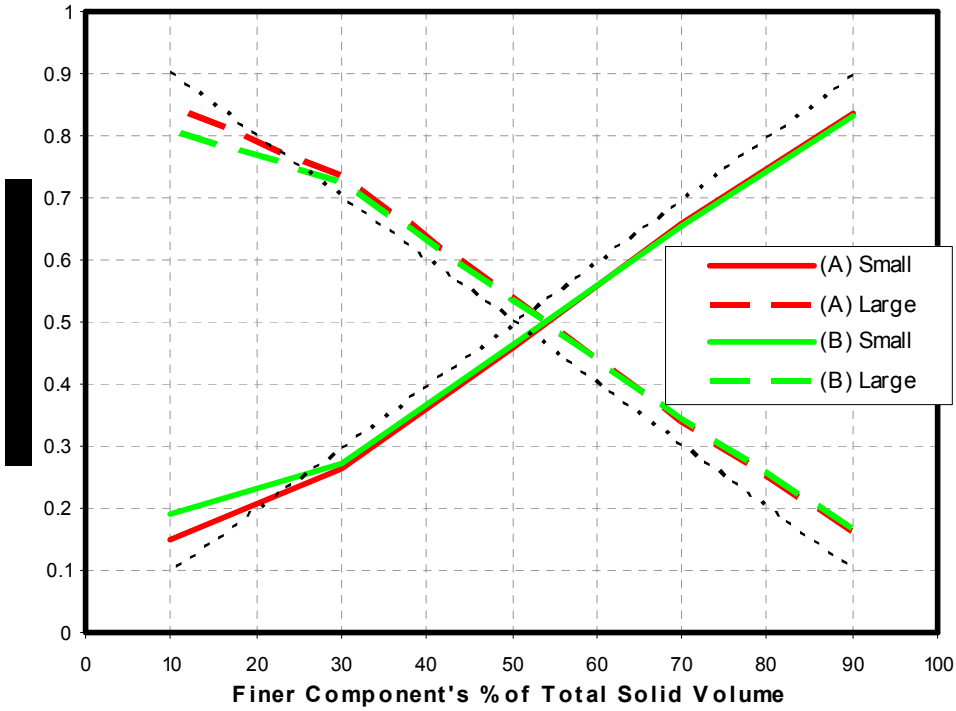

Figure 4-15 Percentage of total solid ratio against percentage of finer component over total vsolid volume

Figures 4.14 and 4.15 show an interesting feature that is typical of these packings. When the finer component's volume is less than 30% of the total solid volume, a given increment in its percentage does not correspond to an equal increment in its influence over the total packing density (i.e. the slope of the lines (A) Small and (B) Small in Figures 4.14 is < 1). This means that in this region the finer component is using only a small part of its solid volume to substitute larger particles, while dedicating most of it to fill the voids between the larger particles. As expected, this is more evident for the (B) packings (i.e. for the packings with smaller size ratio), as their finer component can fill the voids more efficiently. Therefore we can say that, in this region, the packing is fundamentally dominated by the larger component.

When the finer component's volume exceeds 30% of the total solid volume we observe a slope very close to 1. This shows that the two components are now equally important for the determination of the packing's total packing density: a given variation of the quantity of any of the two components results in an equal variation of its contribute to the total packing density.

It has to be noted that for the monodisperse case we would have expected a slope of 1 in every region.

Introduction to the Analysis of Coordination Number in Bidisperse Packings

The analysis of the coordinance of the packings obtained has been done distinguishing between the different types of contact, also known as "partial coordination numbers", which have been named as follows:

- Cll - number of contact points that a large sphere has with large spheres (self-same contact);
- Cls - number of contact points that a large sphere has with small spheres (self-different contact);
- Csl - number of contact points that a small sphere has with large spheres (self-different contact);
- Css - number of contact points that a small sphere has with small spheres (self-same contact).

This differentiation is of fundamental usefulness when trying to evaluate the characteristics of these packings because, as will be shown later in this work, each type of contact has a precise distribution that must be considered for itself. Moreover, as this topic is of high interest for many different disciplines, the differences between the two kinds of spheres might be mechanical and chemical apart from geometrical: the possibility to consider the different types of contact is, therefore, of primary importance in this study. Aiming for maximum clarity, for every packing

we have counted the spheres (further than 4R from the walls) of the two types according to their self-same and self-different coordination number, obtaining tables such as, for instance, Table 8.

Table 8 Example of organisation of the coordination number data for small spheres

A – 4 – S		Total Csl	Css									
			0	1	2	3	4	5	6	7	8	9
Total Css		3507	2	26	144	392	806	1017	740	319	56	5
Csl	0	1388			4	19	127	383	511	286	53	5
	1	1497			28	171	466	573	223	33	3	
	2	514		4	74	163	206	61	6			
	3	104	2	20	36	39	7					
	4	4		2	2							

Table 8 refers to the coordination number of the small spheres in the packing "A – 4" formed by 70% small spheres and 30% large spheres and a size ratio of ½ and supplies a type of information that can not be found in the existent literature. Apart from showing the general distribution of Csl (column "Total Csl") and Css (row "Total Css") in this packing, it also differentiates between the different distributions of Css for different values of Csl (rows) or the different distributions of Csl for different values of Css (columns). For instance, we know that 36 small spheres in this packing had Csl=3 and Css=2, while 466 were those with Csl=1 and Css=4. This type of differentiation represents a level of accuracy in the description of coordination number within a packing much higher than before.

Self-same coordination numbers – General analysis

The analysis of the average number of the two self-same contact types Cll and Css (more generally Ckk) has confirmed the results of some the previous studies (Beck & Volpert 2003; Oda 1977; Pinson et al 1998). Its dependence on size ratio and packing fraction is shown in Figures 4.16 and 4.17. The existent literature has focused mainly on this type of graph, which is describing the average value of Ckk but is not giving any information about its statistical distribution.

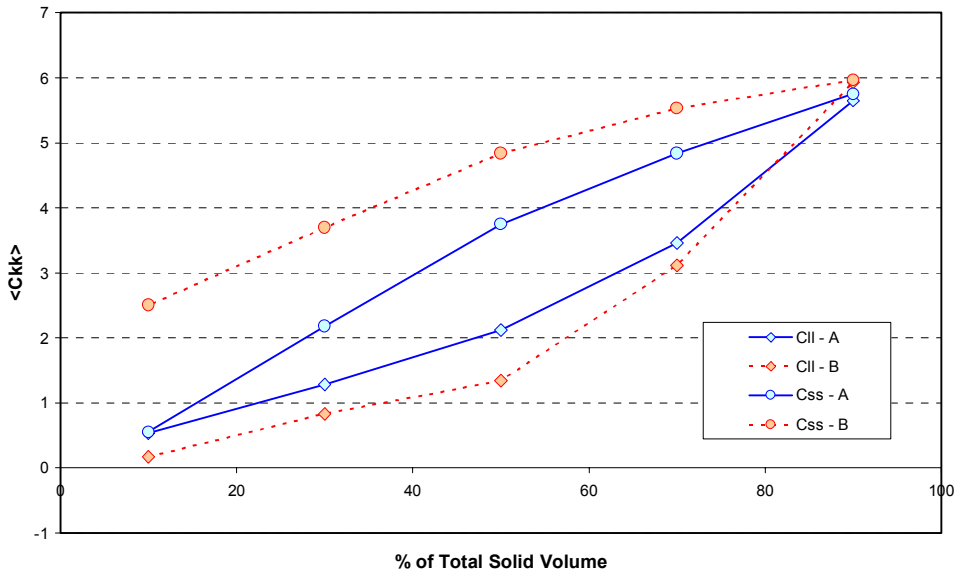

Figure 4-16 Average Ckk against percentage of total solid volume

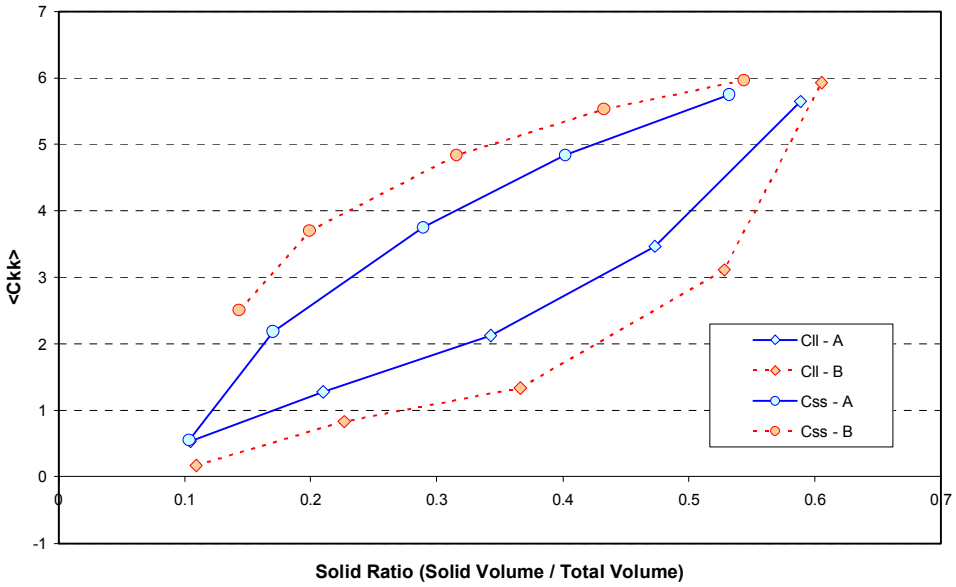

Figure 4-17 Average Ckk against fraction solid ratio

We, instead, believe that these two parameters must be given equal importance if the purpose of the study is to provide a complete evaluation of coordination number.

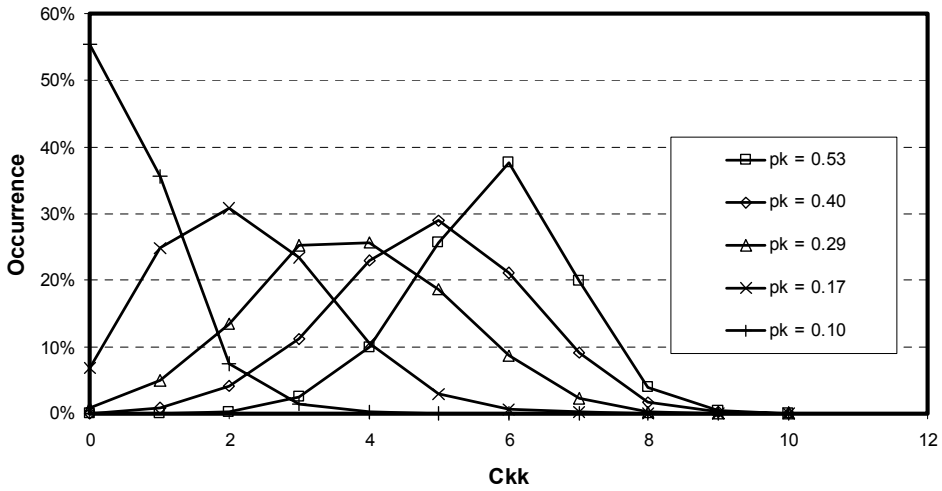

Figure 4-18 Example of distribution of Ckk for different packings

Figure 4.18 shows a typical example of distributions of Ckk resulting from this study. As can be seen, the coordination number follows a normal distribution when the packing density pk is relatively high. The effect of decreasing the packing density, pk, of the fraction considered is a shifting of this distribution towards the lower classes of Ckk, with some variation of the standard deviation. As pk decreases further the distributions are no longer normal, but, as shown in Figure 4.19, they still can be considered as the "non-negative" part of normal distributions that extend to negative classes.

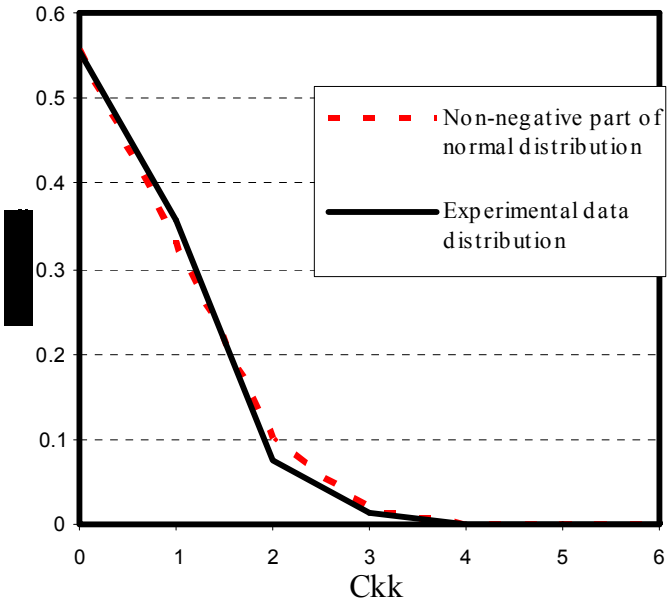

Figure 4-19 The experimental data can be fitted with the non-negative part of a normal distribution

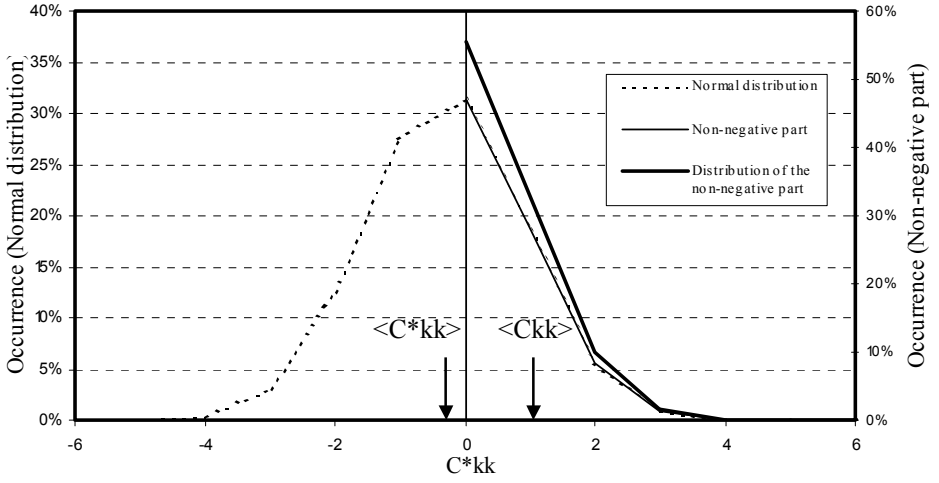

Figure 4-20 Difference between average and average of the correspondent normal distribution

To state it another way, it is possible to find a value of mean (<C*kk>) and standard deviation (SD) of a normal distribution whose non-negative part's distribution best fits the experimental distribution of Ckk. Obviously, the average values <C*kk> of these normal distributions do not coincide anymore with the real average values of Ckk (Figure 4.20).

Doing this way it is possible to plot, for each distribution, the mean value <C*kk> and the standard deviation SD of the best fitting normal distribution, producing the graphs in Figures 4.21 – 4.24. Figures 4.21 and 4.22 are similar to Figures 4.16 and 4.17 (the only ones used in the literature) but provides the elements to know both average and distribution of coordination number at a given packing ratio, provided the standard deviations of the correspondent normal distributions are supplied too.

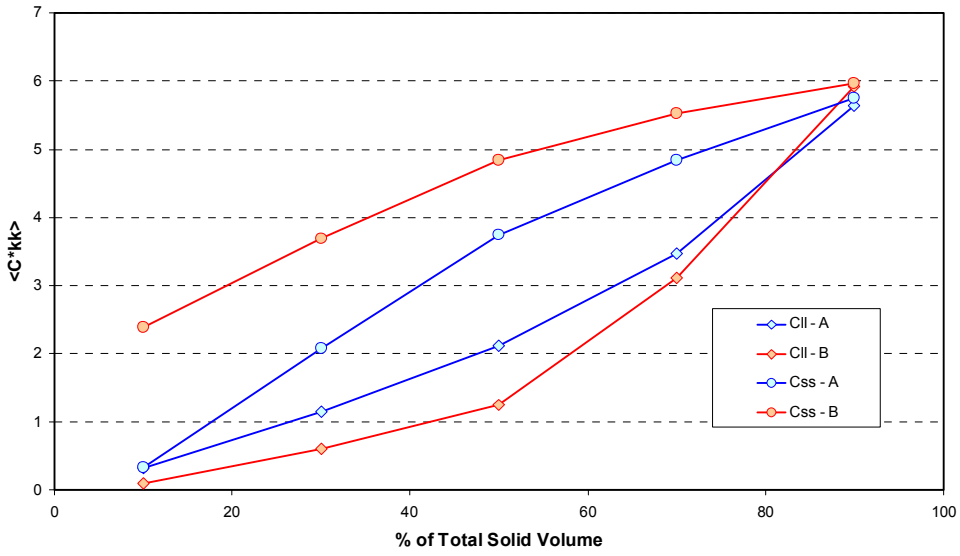

Figure 4-21 Average of correspondent normal distribution against percentage of total solid volume

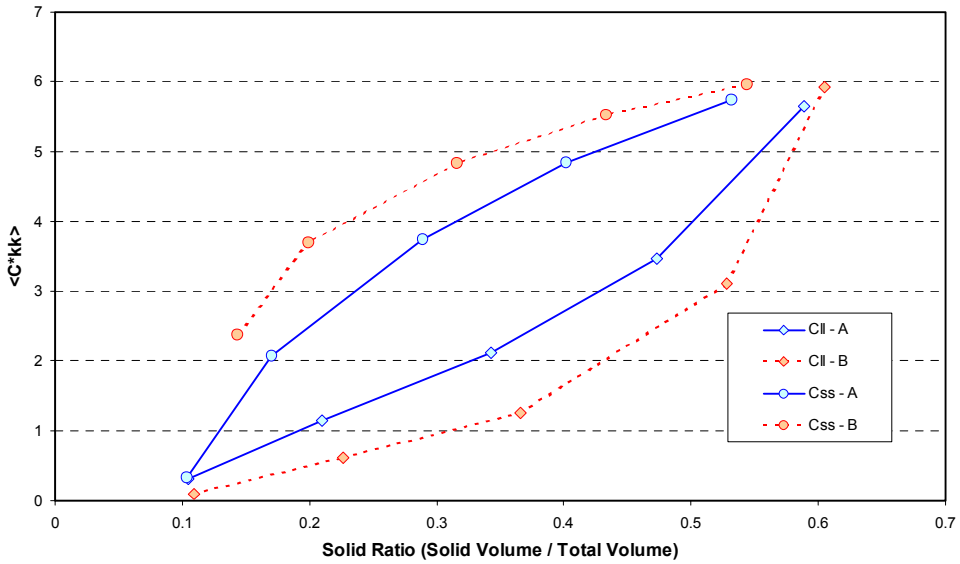

Figure 4-22 Average of correspondent normal distribution against solid ratio

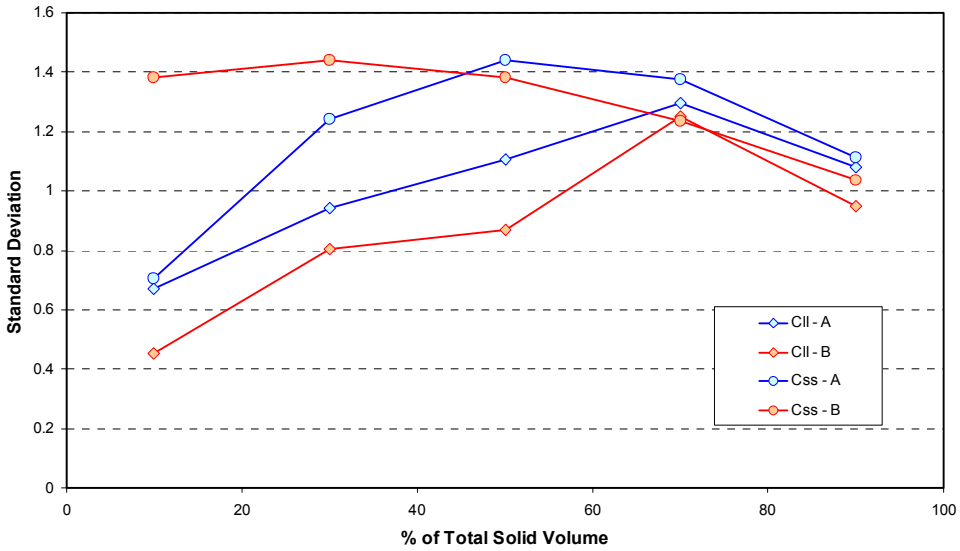

Figure 4-23 Standard deviation of correspondent normal distribution against percentage of total solid volume

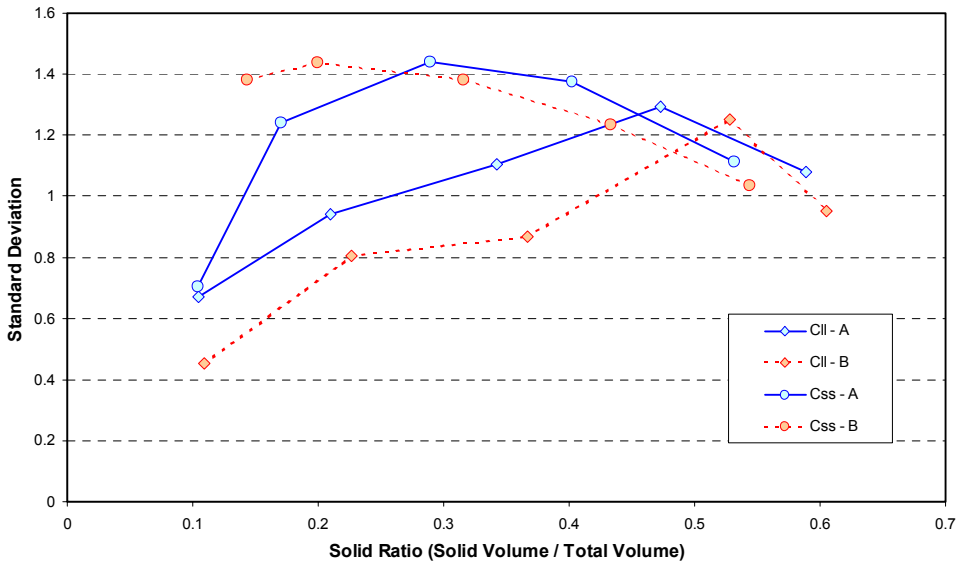

Figure 4-24 Standard deviation of correspondent normal distribution against solid ratio

Self-same coordination numbers – Detailed analysis

In the previous section we have looked at the properties of the coordination number between spheres of the same size. In this part of the analysis we study how it distributes in relationship with the self-different coordination number measured for the same spheres. As said before, the data relative to each packing are presented in the form of Table 8 for each of the two sizes.

The analysis of the previous section was done considering the data, for instance, from row "Total Css", which in each cell contains the total number of spheres with a certain self-same coordination number, while now we want to consider this distribution more in detail looking at the distribution of Css for the various values of Csl, therefore considering the rows from "Csl = 0" to "Csl = 4". As shown in Figure 4.25, for the different values of Csl we have different distributions of Css. We can call these "Relative Distributions of Partial Coordination Numbers" and indicate them as a function of Css and Csl, $f(Css, Csl)$. As an example, $f(Css, 2)$ represents the distribution of the number of small spheres in contact with a small sphere if 2 large spheres are also touching it. We can also use the notation introduced during the discussion of the Three Spheres Problem and indicate these partial coordination numbers as Cij^{kn}, where "i" is the type of the central sphere, "j" is the type of the touching spheres considered, "k" is the type of touching spheres disturbing the j-type spheres and "n" is the number of k-type spheres touching the central sphere (please note that the indices i and j can assume the value of "small" or "large"

independently from each other, while k ≠ j). The sum of these relative distributions of the partial coordination numbers delivers the total distribution of the partial coordination numbers (see Figure 4.25), for example:

$$\sum_{i=0}^{Csl\,\max} F(i)\cdot f(Css,i) = F(Css)$$

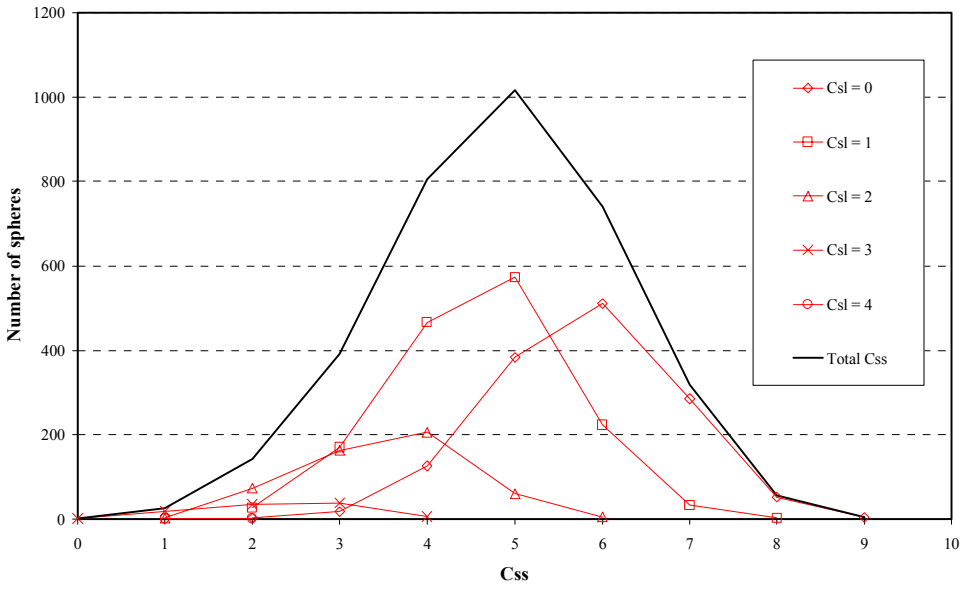

Figure 4-25 Example of relative distributions of partial coordination number Css

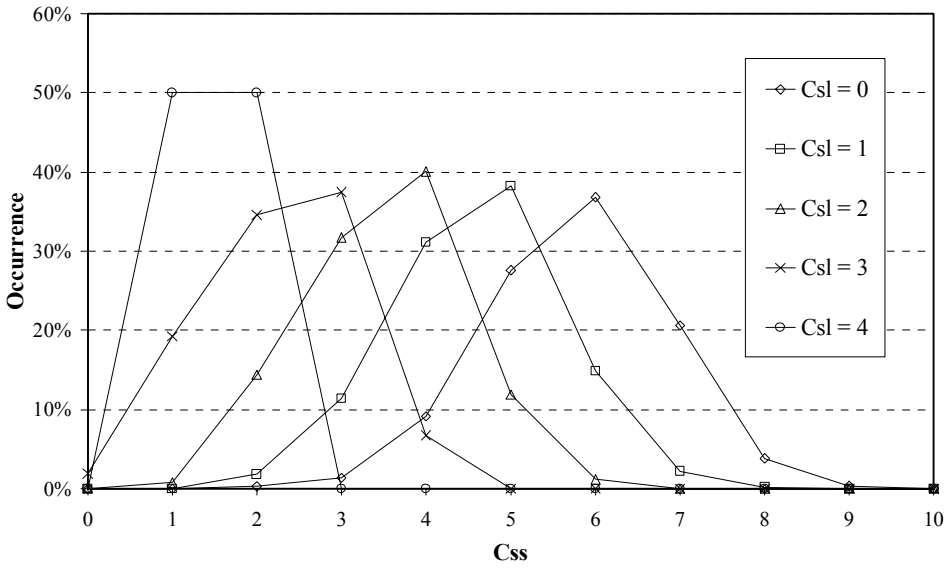

Figure 4-26 Normalised relative distributions of partial coordination number Css

As can be noted from Figure 4.26, the relative distributions of Css look very similar to each other but shifted towards lower values for higher Csl. This was expected as more contacts with large spheres (i.e. larger Csl) means less surface left available to make contact with small spheres (see Chapter 3 and Appendix A). Moreover, all these distributions can be accurately approximated by a normal distribution of variable mean and standard deviation.

These normal distributions, for the packing considered in Table, are shown in Figure 4.27 in their cumulative form.

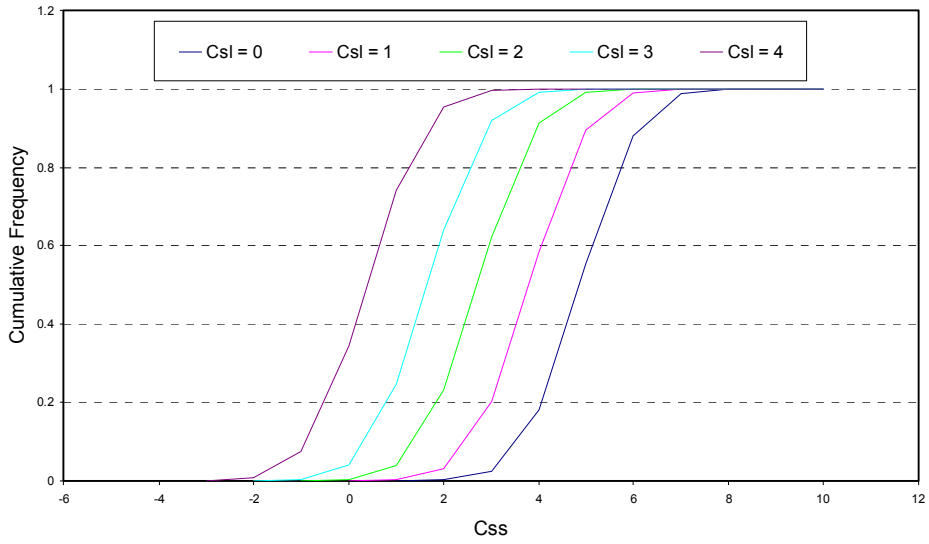

Figure 4-27 Cumulative form of relative distributions of partial coordination number Css

Applying the concept of space consumption and normalising, it is interesting to try to re-conduct these different normal distributions to a single general behaviour. Various attempts are listed in Table 9.

Table 9 Definition of the attempted transformations and of the parameters needed

Variable	Definition
Cssmax	Maximum possible number of small spheres on the surface of a small one. Cssmax = 13.4
$Css^{L1}max$	Maximum possible number of small spheres on the surface of a small one if Csl = 1, i.e. Cssmax when there is a large sphere disturbing the small spheres.
Pss	Parking Number of small spheres on the surface of a small one. Pss = 8.75
Psl	Parking Number of large spheres on the surface of a small one.
Css'	Normalised coordination number correspondent to Css after transformation.
Transformation	Definition
A1	$Css' = \frac{Css}{Css\max - Csl \cdot (Css\max - Css^{L1}\max)}$
A2	$Css' = \frac{Css}{Pss - Csl \cdot (Css\max - Css^{L1}\max) \cdot (\frac{Pss}{Css\max})}$
A3	$Css' = \frac{Css}{Pss \cdot (1 - \frac{Csl}{Psl})}$
B1	$Css' = \frac{Css + Csl \cdot (Css\max - Css^{L1}\max)}{Css\max}$
B2	$Css' = \frac{Css + Csl \cdot (Css\max - Css^{L1}\max) \cdot (\frac{Pss}{Css\max})}{Pss}$

The effect of these transformations on the data of Table 8 is shown in Figures 4.28 – 4.32.

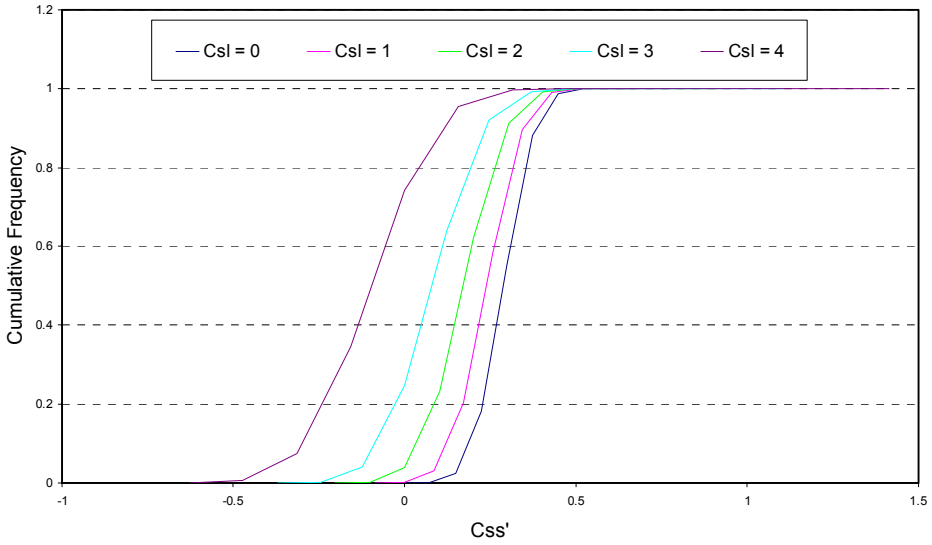

Figure 4-28 Effect of transformation A1 on the distributions in Figure 4.27

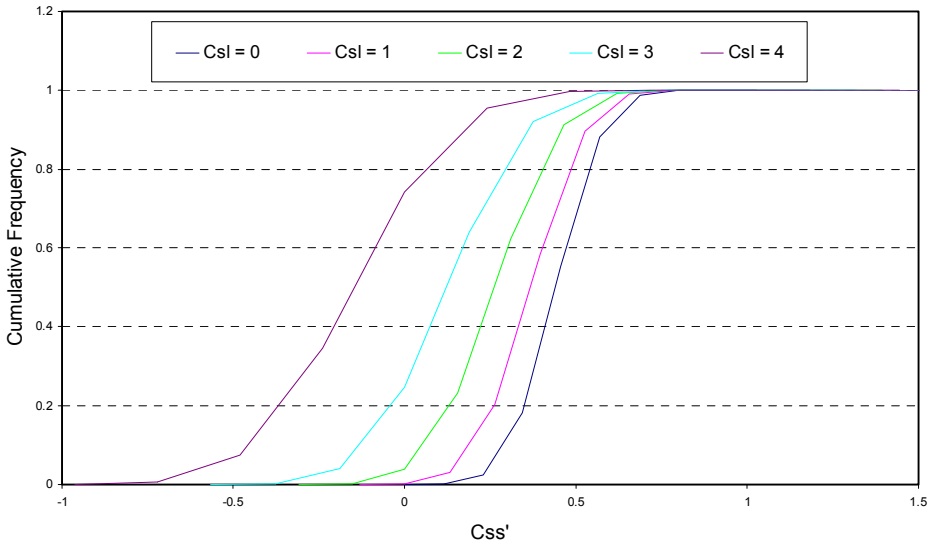

Figure 4-29 Effect of transformation A2 on the distributions in Figure 4.27

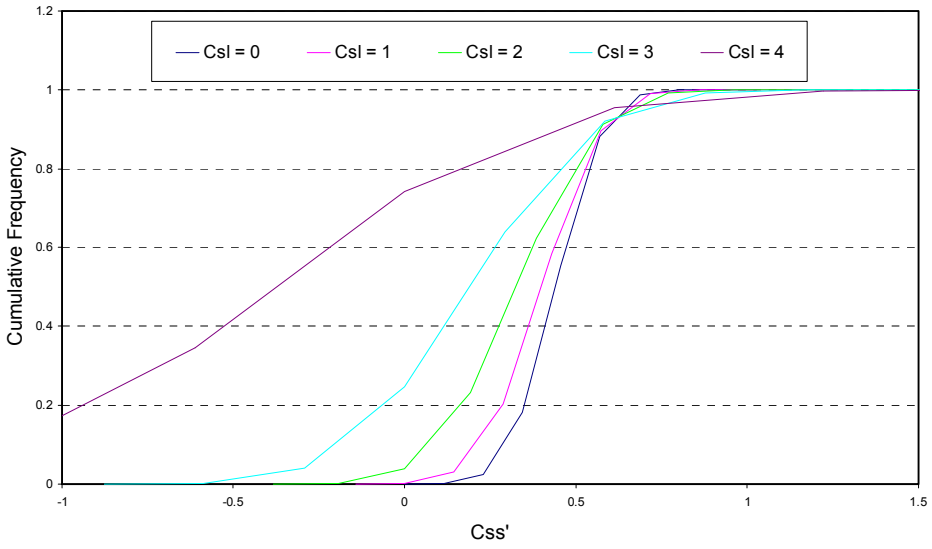

Figure 4-30 Effect of transformation A3 on the distributions in Figure 4.27

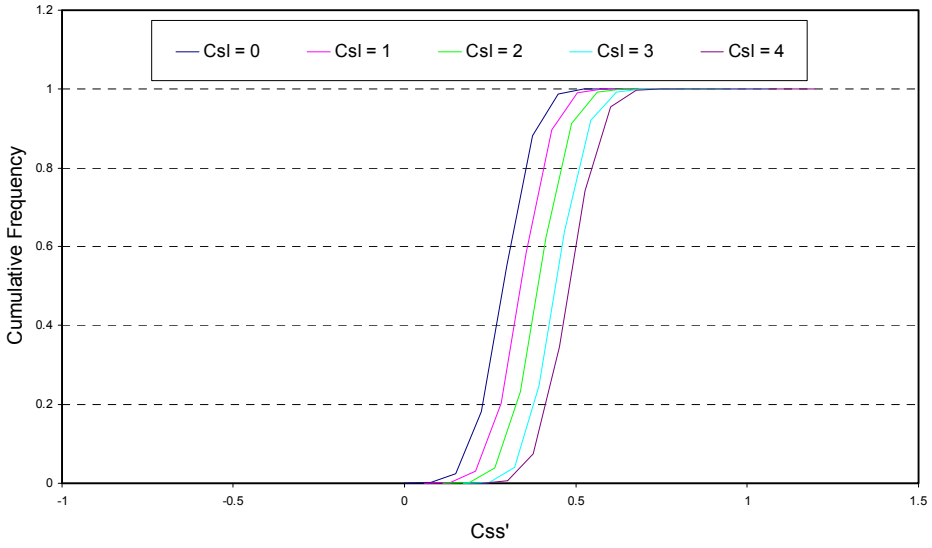

Figure 4-31 Effect of transformation B1 on the distributions in Figure 4.27

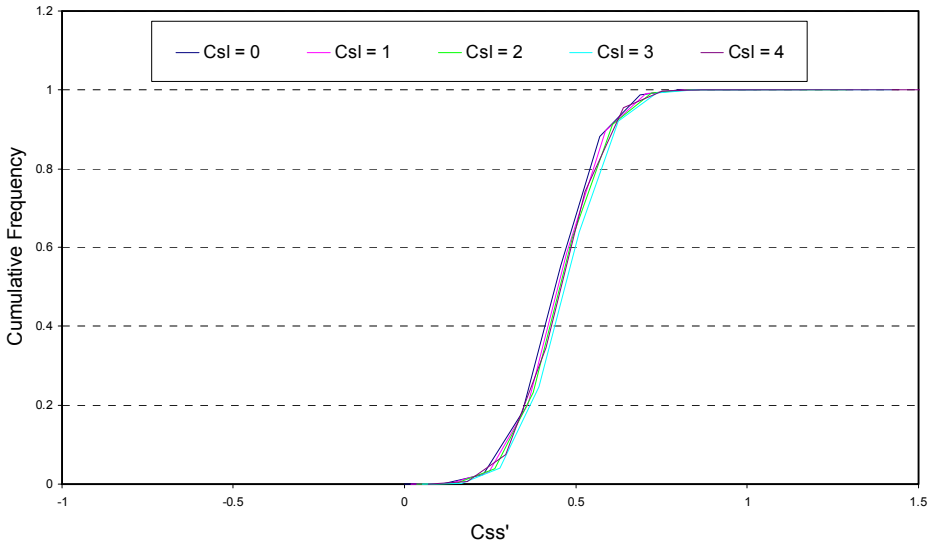

Figure 4-32 Effect of transformation B2 on the distributions in Figure 4.27

The transformations belonging to the "A" type aim to normalise the data modifying (decreasing) the maximum number of contacts to which the real number of contacts (Css) must be related for the normalisation. This results in a change of the shape and slope of the lines of Figure 4.27, which is not what we seek.

The "B" type transformations seem to have a more useful effect: they act on the data adding to the real Css some kind of compensation for the contemporary presence of a certain value of Csl. The graphic result is a shifting of the lines of the relative distributions of Css. As can be seen, a very satisfying result is achieved applying transformation B2: the relative distributions of Css are now coinciding.

This means that all the different relative distributions of Css can be described by the same function if Css is transformed in Css' through the transformation B2 (Figure 4.33).

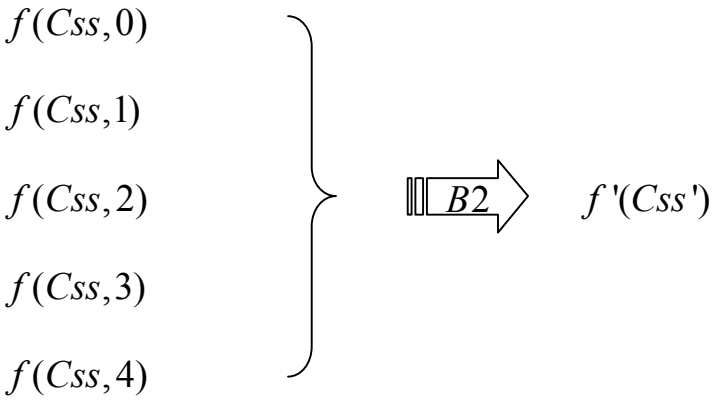

Figure 4-33 Unifying the relative distributions

The main principle of this normalisation is that to each value of Cij we have to add the theoretical number Cij(eq) of j-type spheres that are supposed to have been removed from the surface of the i-type sphere as a consequence of the presence of n (i.e. Cik) spheres of type k. Then, we normalise this total value dividing it by the parking number Pij.

$$Cij' = \frac{Cij + Cij(eq)}{Pij} \qquad (17)$$

Calculating Cij(eq) means, therefore, transforming the measured value of Cik in an equivalent value of Cij.

$$Cij(eq) = Cik \cdot Dijk \cdot \frac{Pij}{Cij\max}$$

where

Cik is the measured number of k-type spheres touching the i-type one;

Dijk is the theoretical "disturbance" caused by placing a k-type sphere on the surface of an i-type sphere covered with the theoretical maximum number of j-type spheres:

$$Dijk = Cij\max - Cij^{k1}\max \qquad (18)$$

where **Cij^{k1}max** is the theoretical maximum number of j-type spheres on the surface of an i-type one if one k-type sphere is already on that surface (see "Three Spheres Problem" in Chapter 3 and Appendix A);

Pij is the parking number (practical maximum coordination number for random packings, see Chapter 2 for definition and earlier in this chapter for a practical description) for j-type spheres on an i-type one;

Cijmax is the theoretical maximum number of j-type spheres on the surface of an i-type one (see Chapter 2 and 3 and Appendix A).

As can be seen, the term $Dijk \cdot \frac{Pij}{Cij\max}$ corresponds to the practical "disturbance" caused by placing a k-type sphere on the surface of an i-type sphere covered with the practical maximum number of j-type spheres. It

represents the number of j-type spheres that would realistically occupy the place of each single k-type sphere on the given surface. Multiplying this by the measured number of k-type spheres, Cik, we obtain the desired Cij(eq).

Finally, we can express the general form of this normalisation as

$$Cij' = \frac{Cij + Cik \cdot (Cij\max - Cij^{k1}\max) \cdot (\frac{Pij}{Cij\max})}{Pij} \qquad (19)$$

Moreover, as shown in Figure 4.34, it is possible to optimise the transformation substituting the Parking Number Pij with a modified value Pij'. For the example in Figure 4.34 it has been calculated Pij' = 7.90 instead of the usual Pij = 8.75.

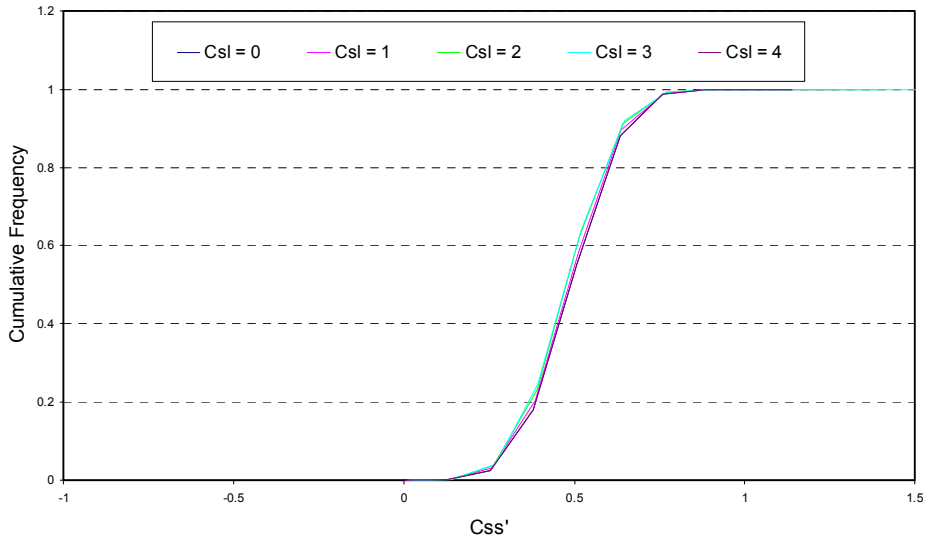

Figure 4-34 Optimisation of transformation B2 by the modified parking number

Repeating this procedure we find that, for all the different packings with more than 30% of the solid volume occupied by small spheres, $f'(Css')$

is independent from size ratio and composition and can always be described by a cumulative normal distribution with Mean = 0.635 and Standard Deviation of 0.12 (see Figures 4.35 and 4.36).

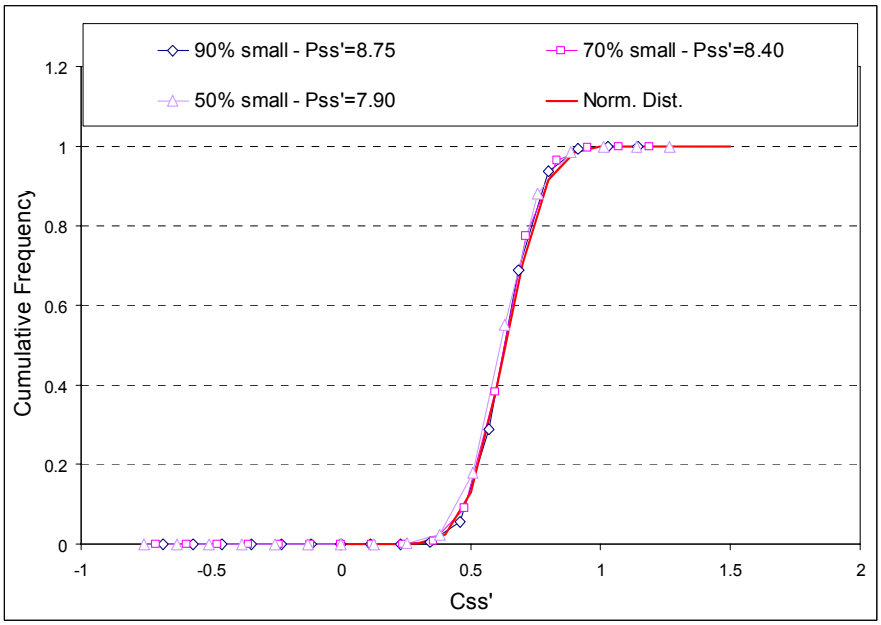

Figure 4-35 Same distribution for different packing densities – packings A

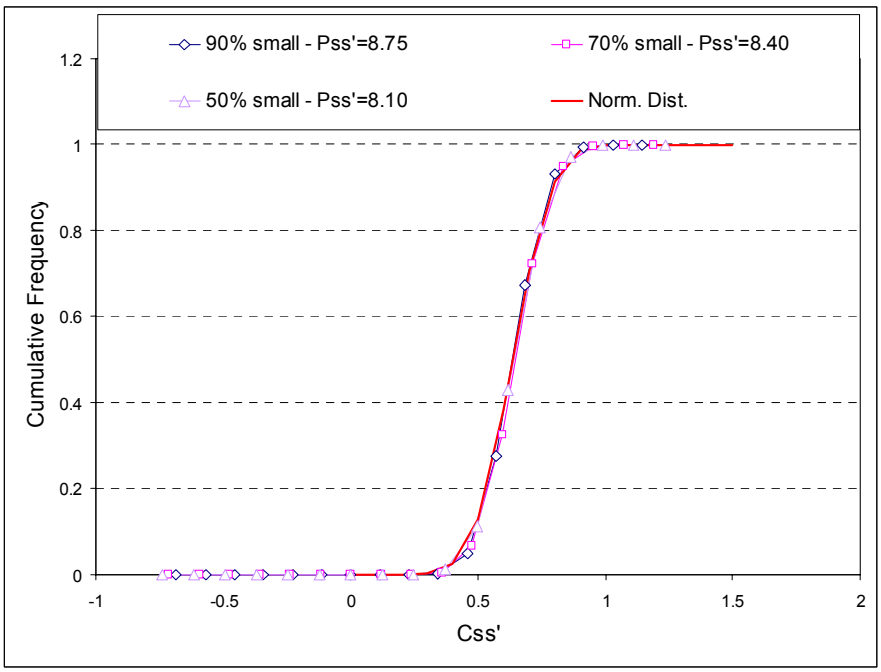

Figure 4-36 Same distribution for different packing densities - packings B

Self-different coordination numbers

An approach similar to the one used to analyse the distributions of relative self-same coordination numbers can be taken to study the relative self-different ones. As in the previous section we analysed the example of Css for the packing named "A-4", now we can analyse Cls (number of small spheres touching a large one) for the same packing.

Table 10 summarises the raw data collected for the large spheres of this packing.

Table 10 Example of organisation of coordination number data for large spheres

A – 4 – L		Total Cll	Cls										
			8	9	10	11	12	13	14	15	16	17	18
Total Cls		109	6	5	17	16	27	11	13	9	4	0	1
Cll	0	22	0	0	1	2	4	3	4	5	2	0	1
	1	49	0	2	3	6	17	6	9	4	2	0	0
	2	29	4	2	11	6	4	2	0	0	0	0	0
	3	9	2	1	2	2	2	0	0	0	0	0	0

Due to the small number of particle and the larger range of possible values, this part of the analysis is subject to a much larger variability than experienced in the previous section, as shown in Figures 4.37 - 4.39.

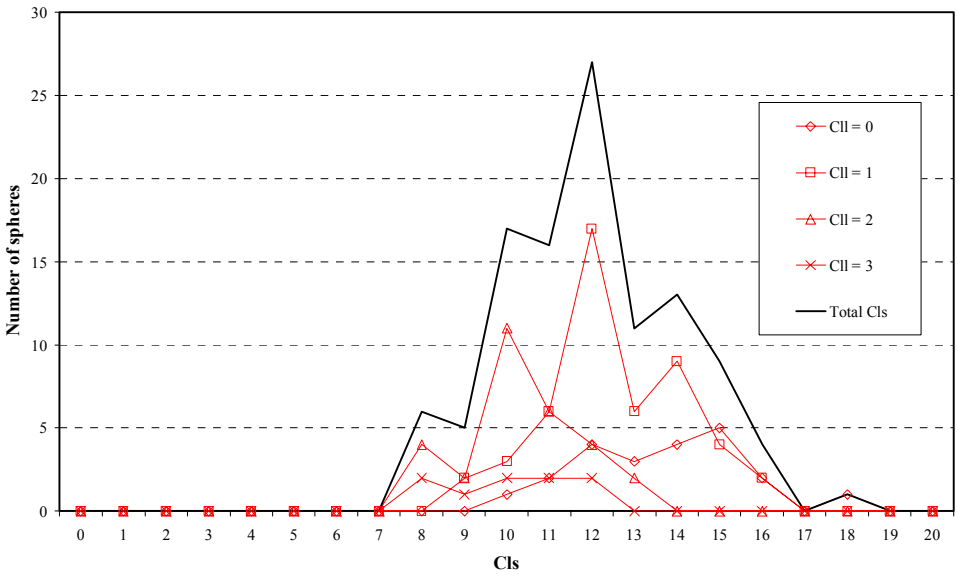

Figure 4-37 Example of relative distributions of partial coordination number Cls

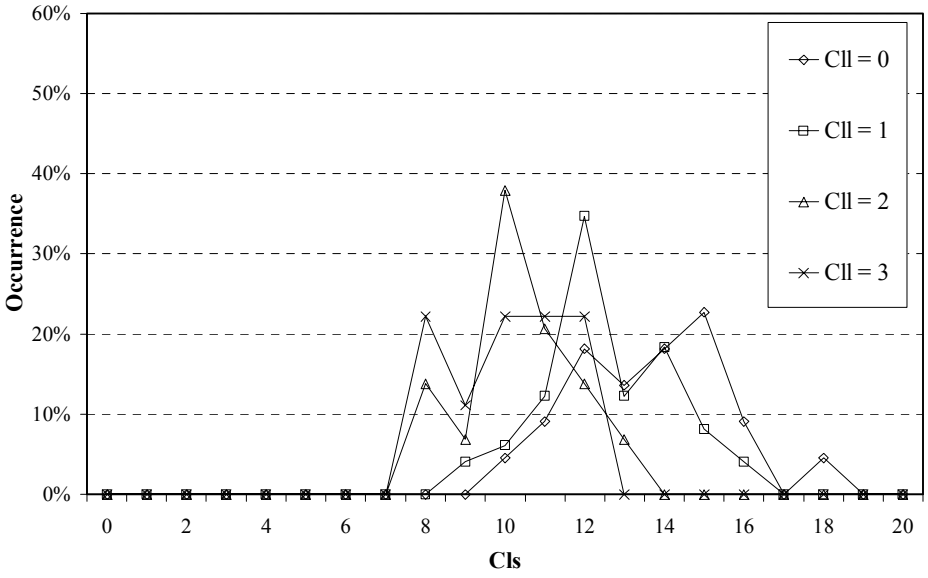

Figure 4-38 Normalised relative distributions of partial coordination number Cls

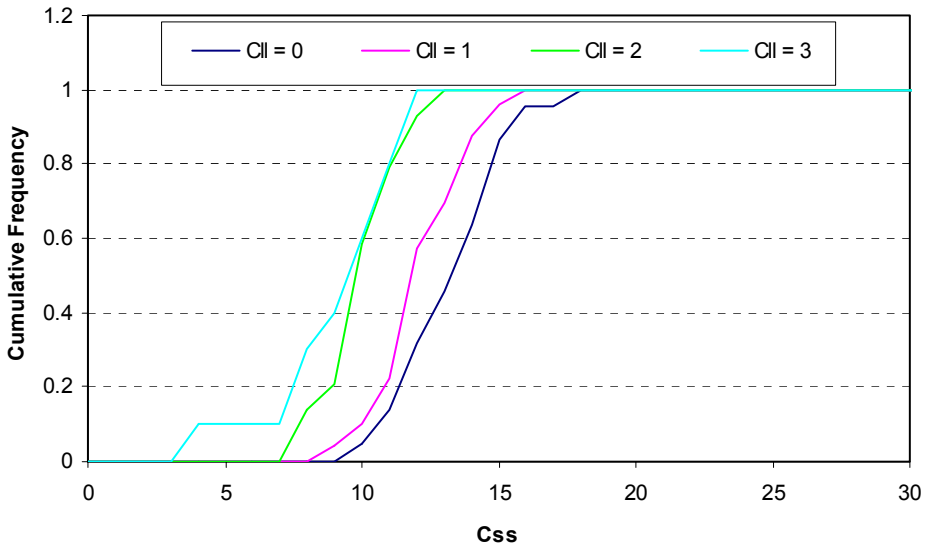

Figure 4-39 Cumulative form of partial coordination number Cls

In this situation is particularly evident the advantage of using a cumulative representation of the occurrence such as in Figure 4.39. This allows focusing the attention on the general behaviour of the data as a whole rather than on the singular values. Applying the normalisation introduced in the previous section, Figure 4.39 is transformed in Figure 4.40.

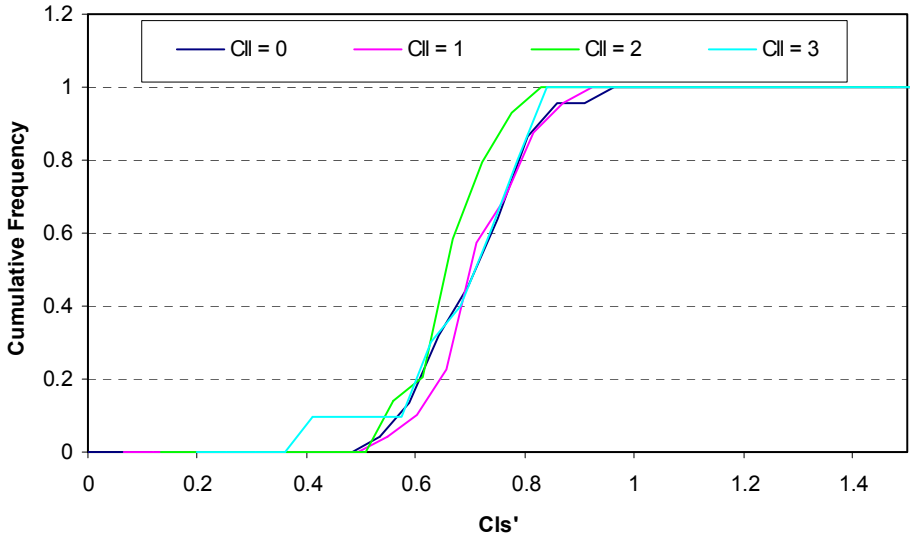

Figure 4-40 Effect of transformation B2 on the distributions in Figure 4.39

As can be seen, Cls can be transformed in Cls' delivering a unique normal distribution that describes all the different relative distributions from Figure 4.39. All the observations made for Css are still valid for Cls, but the values of Mean and Standard Deviation change for the two size ratios as summarised in Table 11.

Table 11 Average value and standard deviation of the normal distributions obtained with transformation B2 for different size ratios

Parameter	Size ratio between central and touching spheres	Average	St. Dev.
Css A,B	1	0.635	0.120
Cls A	0.5	0.710	0.100
Cls B	0.25	0.780	0.055

Interestingly, we observe a well defined trend behaviour of the Average and Standard Deviation values of this distribution as a function of the size ratio between the considered spheres and the central one, i.e. of the curvature of the surface on which the probe spheres are being distributed (see Figure 4.41).

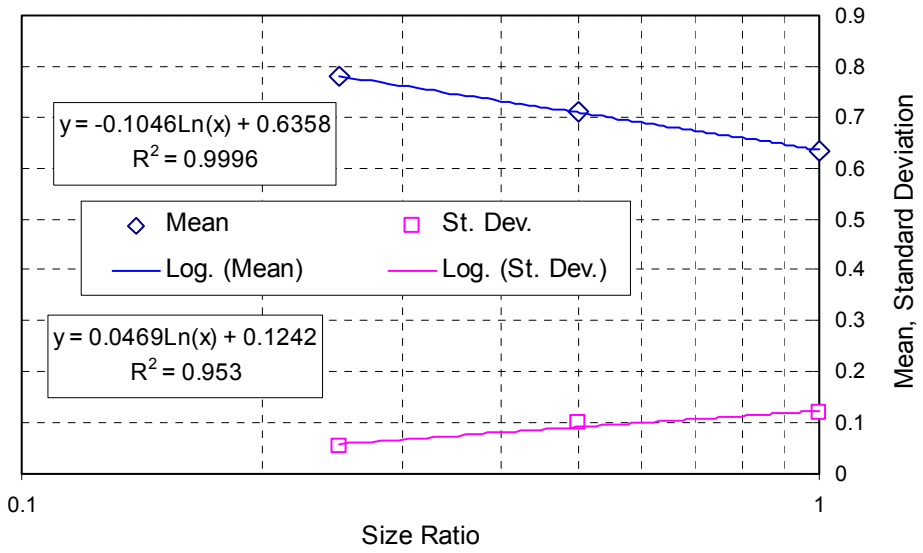

Figure 4-41 Dependence of average and standard deviation on size ratio

The two equations in Figure 4.41 are of extreme importance as they allow us to describe the general distribution of spheres of a given dimension on the surface of another sphere of another different dimension, independently from other spheres of a third dimension that might also be on that surface. We can call this the "Characteristic Distribution" of A-type spheres on a B-type one. Transformation B2 can then deliver the particular relative distribution for any number of disturbing spheres.

Limitations

As shown in Figure 4.42, also the distribution of Csl can be represented as a normal distribution or its non-negative part.

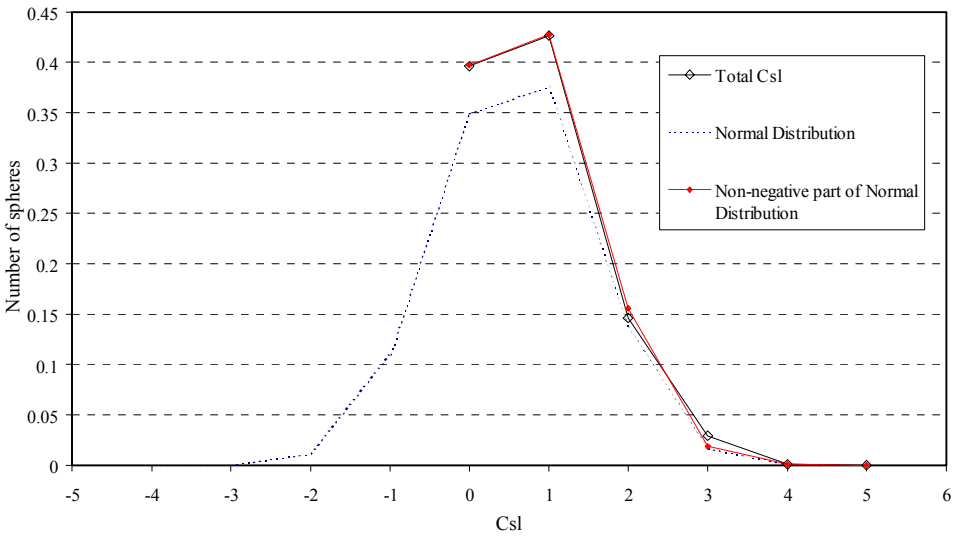

Figure 4-42 Distribution of Csl as non-negative part of a normal distribution

Problems arise when defining and using Cll' and Csl' (arrangements of large spheres on a large and on a small one). Transformation B2 is based on the concept of the disturbance caused by a k-type particle on a superficial arrangement of j-type ones. This disturbance is well defined when the disturbing particle is larger than the disturbed ones (Figure 4.43), while if it is smaller its definition is more uncertain.

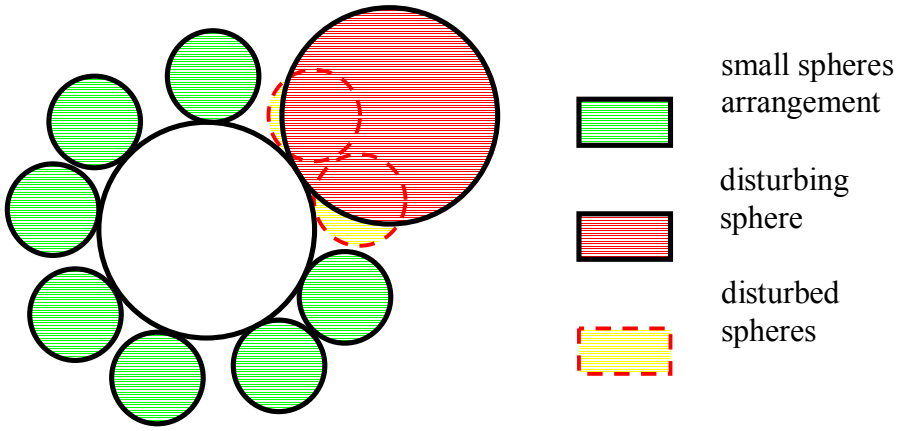

Figure 4-43 Disturbance of a large sphere on the superficial distribution of small spheres

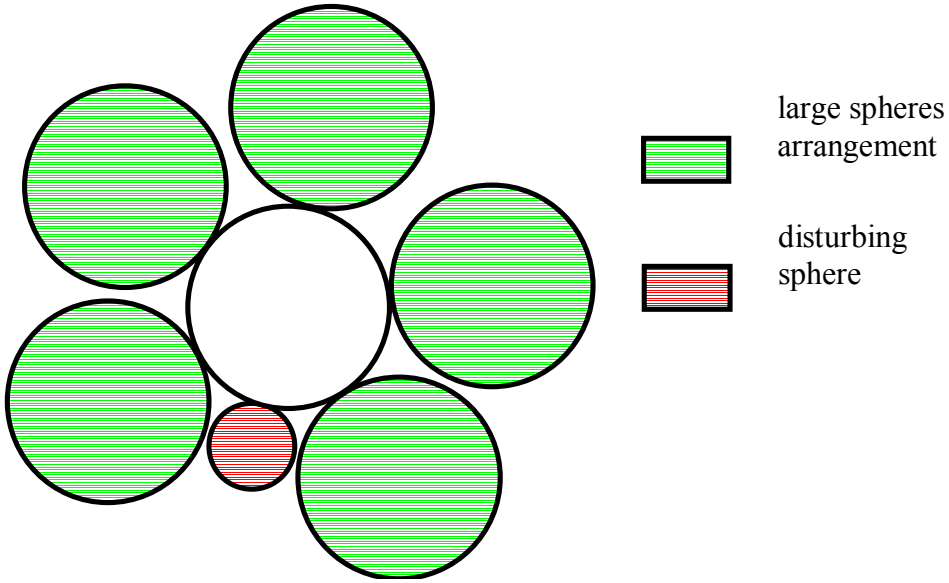

Figure 4-44 Disturbance of a small sphere on a superficial distribution of large spheres

As can be seen from Figure 4.44, the smaller particle can even fit between the larger particles without disturbing them. This seems to affect the applicability of the procedure developed earlier, therefore further investigation is required to allow the generalisation of the concept of mutual disturbance.

Moreover, we can observe from Figure 4.45 that the modified Parking Number Pij', introduced to optimise the modelling of the relative distributions of the partial coordination numbers Css and Cls, follows a very distinctive trend with Packing Density.

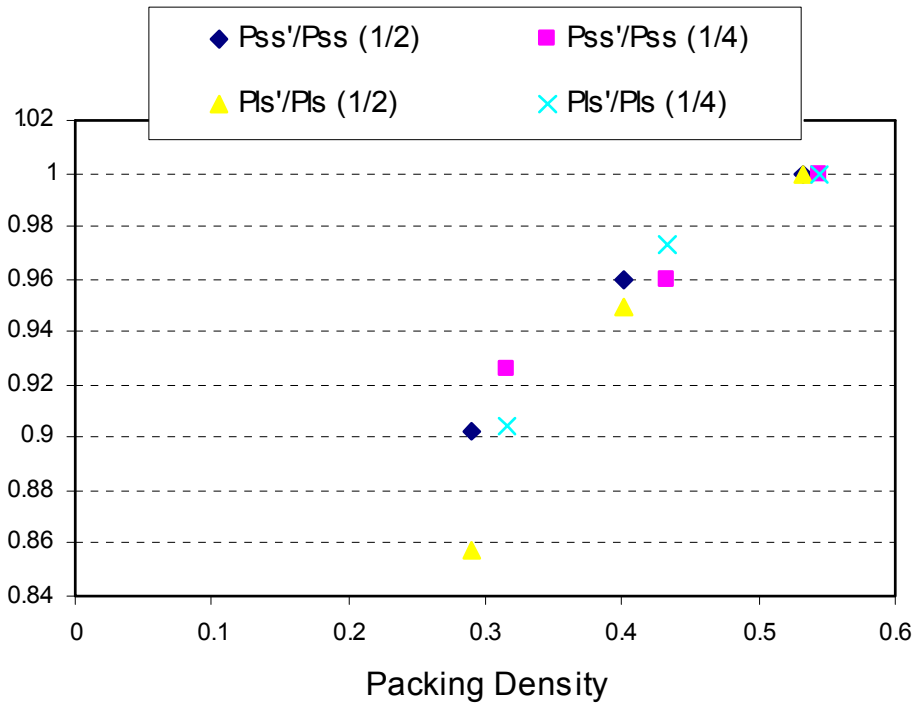

Figure 4-45 Dependence of modified parking number on packing density

The physical meaning of this parameter that, given the originality of this analysis, has not been observed in previous studies will need further investigation than what is possible at this stage.

5 SUPERFICIAL DISTRIBUTION

5.1 Introduction

This chapter introduces a parameter, called Superficial Distribution, that has been developed in this research to describe the arrangement of the contact points on the surface of each given particle. The "evenness" of the distribution of these points can be expressed as a function of the Voronoi cell they create, and might be directly related to the stress distribution within the particle.

The study of this parameter has been conducted on clusters of equal spheres, generated by a "Spherical Growth" algorithm (see Appendix B), and on large packings of spheres of two sizes (bidisperse), generated with a "Drop and Roll" algorithm (see Appendix F). The clusters are supposed to have been formed under isotropic conditions, while the bidisperse packings were obviously subject to vertical attractive forces, therefore with a privileged direction of movement. Nonetheless, as will be shown later, for the purpose of the analysis the particles within the bidisperse packings will have to be treated as part of isolated clusters.

5.2 Clusters

The clusters that were presented in the previous chapter, where their coordination number was studied, will now be analysed focusing on the distribution of the outer spheres on the central sphere's surface. The volume of the Voronoï cell, Vv, (see Chapter 2) formed can represent a measure of this distribution: a uniform configuration will have a lower Vv than a less uniform one. In particular, unstable (or uncaged) configurations (that is where the Voronoï cell is open-ended – see Figure 5.1) will have $Vv = \infty$.

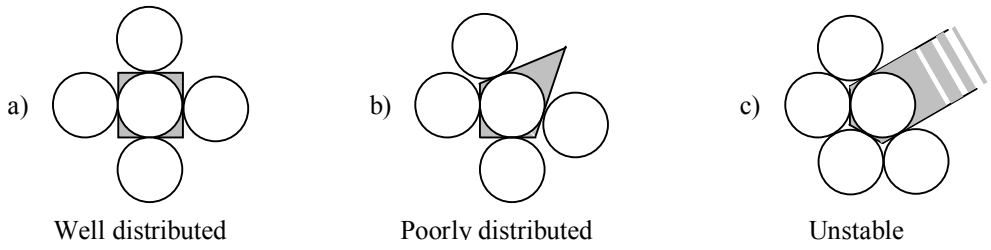

Figure 5-1 Effect of particle's superficial distribution on the Voronoi cell's volume

Figure 5.1 shows the variation, in a 2 dimensional sketch, of the Voronoï cell volume when four spheres are poorly distributed around the central sphere. For example, with a coordination number of 6 the best distribution corresponds to the situation where the Voronoï cell is a cube. The volume of this cube is also the minimum volume (Vvmin) that a Voronoï cell can have if formed by only 6 spheres. Any distribution of the 6 spheres that differs from this one will present a larger value of Vv, and this value will increase as the distribution gets less uniform.

Based on these considerations, the concept of "superficial distribution" (D) of the contacts on a particle can be introduced by the following definition (20):

$$D = Vvmin/Vv \quad (20)$$

Such that its values are comprised between 0 and 1, where lower values indicate a poor superficial distribution and higher values a more even distribution. Obviously, Vvmin is a function of coordination number. The normalization of Vv by Vvmin makes this concept independent of a sphere's radius (as this also affects the Voronoï cell volume) and from coordination number: a configuration of 4 spheres (or 4 contacts) uniformly distributed is, therefore, considered as well distributed as a configuration of 12 spheres uniformly distributed, being in both cases D = 1.

Note that Vvmin for a coordination number of 3 is always ∞ (as there can not be any solid with less than 4 faces) and it is for this reason, therefore, that only coordination numbers greater than 3 have been considered in this part of the work. Table 12 shows the values of Vvmin that were found for the different coordination numbers and that were used for the subsequent analysis.

Table 12 Minimum volumes of Voronoi cells for clusters

Coordination number	Obtained Vvmin
4	13.91
5	10.50
6	8.12
7	7.33
8	6.75
9	6.30
10	6.02
11	5.85
12	5.56

An analytical value of Vvmin can be found for those coordination numbers whose minimum Voronoï cell is a regular polyhedron, i.e. 4 (tetrahedron),

6 (cube) and 12 (dodecahedron). These analytical values can be calculated by equations (21), (22) and (23) and are given in Table 13 (Whister Alley 2004).

Table 13 Available analytical minimum values of the volume of Voronoi cells

Coordination number	Analytical Vvmin
4	13.86
6	8.00
12	5.55

$$\theta = acos[(cos\alpha - cos^2\alpha) / sin^2\alpha] \quad (21)$$

$$s = r_i * 2 * tan(\pi/n) / [(1-cos\theta)/(1+cos\theta)]^{1/2} \quad (22)$$

	Tetrahedron	**Cube**	**Dodecahedron**	
Volume =	$2^{1/2} * s^3 / 12$	s^3	$(15+7*5^{1/2}) * s^3 / 4$	(23)

where α is the plane angle between two consecutive sides, θ is the dihedral angle between two faces, n is the number of sides in each face, r_i is the radius ($r_i = 1$ in our case) and s is the side length.

As can be seen comparing the data from Table 12 and Table 13, the minimum Voronoï cell volumes obtained are entirely consistent with the analytical results. In particular, they provide upper bound values of the analytical solutions, showing that all the configurations generated respect these minima. Therefore, it is reasonable to assume that this method is also indicating reliable values of the minimum Voronoï cell sizes when no analytical solution is available.

Figure 5.2 shows the cumulative frequency of D (Equation 20) for each coordination number.

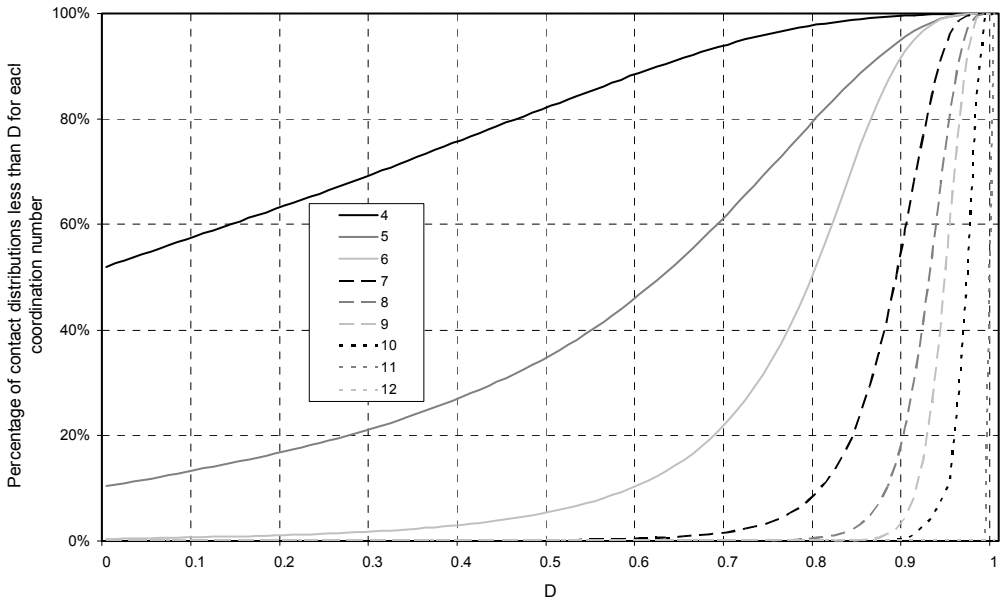

Figure 5-2 Cumulative frequency of D for different coordination numbers

For a given value of D, say D*, this chart shows the percentage of spheres with a given coordination number that were found to have D<D*.

Interestingly, as shown in Figure 5.3, the cumulative plots of D from Figure 5.2 follow quite well an exponential law:

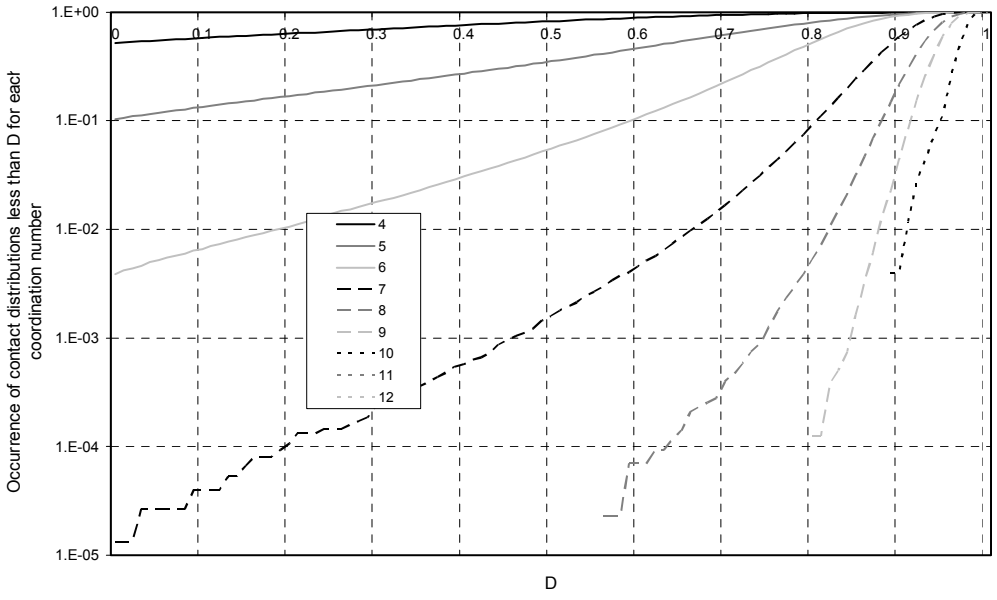

Figure 5-3 Cumulative frequency of D in exponential form

In particular, the lines referring to 4, 5, 6 and 7 contact points can be described as exponential functions of D with great precision within the range $0 \leq D \leq 0.6$ (see Figure 5.4).

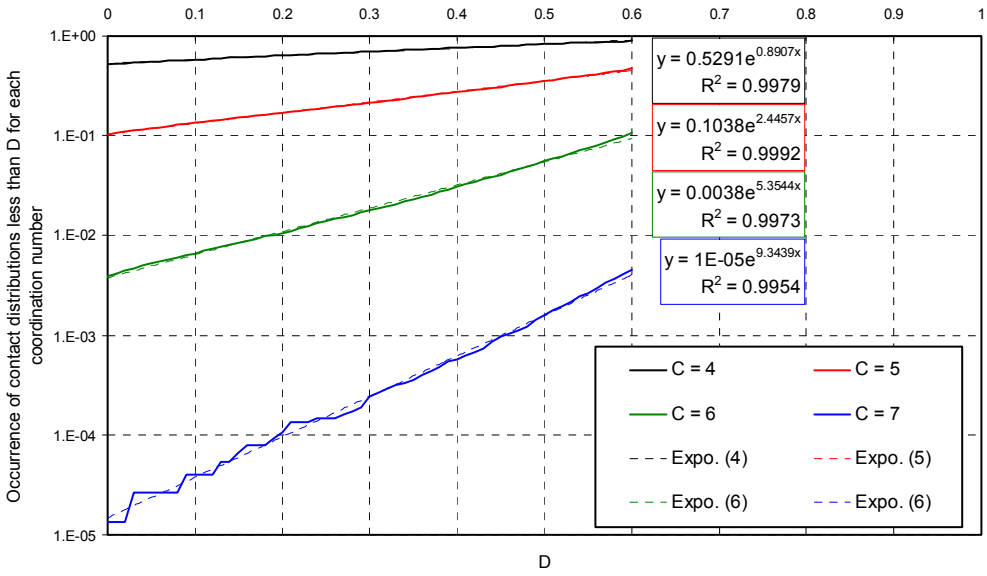

Figure 5-4 Exponential trend lines of the cumulative frequency of D for a coordination number of 4, 5, 6 and 7

In theory, the maximum coordination number for an unstable particle (i.e. Vv = ∞ → D = 0) is 9. Consider a configuration such as the face-centred cubic, which has 6 spheres along an equator of the central sphere and 3 at the top and bottom (for a total coordination number of 12), it is possible to see that an open-ended Voronoï cell is obtained subtracting the 3 top or bottom spheres, leaving a coordination number of 9. However, it can be seen from Figure 5.4 that, in reality, unstable spheres are very unlikely to be generated with a coordination number higher than 6. This is anticipated as, according to Kepler's conjecture, 12 is the maximum possible coordination number for same sized spheres placed around a central one. Thus, 6 is the expected maximum number of spheres that can be randomly placed in one hemisphere yet leave the other open-ended such that Vv = ∞. The 7th sphere would be expected to be placed in the opposite hemisphere and thus to stabilize the particle.

The likelihood of an unstable arrangement with 7, 8 or 9 spheres around a central one can be evaluated noting that it represents a very narrow subgroup of the 11, 12 and 13-sphere groups. Intuitively, we can say that the situation of placing the first 7, 8 or 9 spheres in the same hemisphere is much more likely to have happened for the 13-sphere group (coordination number = 12) than for the 11-sphere group (coordination number = 10) because with lower final coordination numbers the spheres are less well packed, therefore we can deduce that the probability of an unstable Voronoi cell with coordination number of 7, 8 or 9 is highest for a final coordination number of 12, which, on the other hand, has the lowest frequency occurrence. The probability of the first 9 outer spheres of a 13-sphere assembly forming an unstable configuration can be calculated as follows.

Given a group of 12 outer spheres, we are selecting 9 of them. The total number of ordered combinations of 9 elements out of 12 is

$$N(9/12\ \text{ordered}) = 12! / (12-9)! \quad (24)$$

Therefore each 9-element group has a probability of

$$P(9/12\ \text{ordered}) = (12-9)! / 12! \quad (25)$$

The acceptable combinations are those comprising the first 9 elements placed, although they may be selected in any order. Their number is

$$N(9/9\ \text{ordered}) = 9! \quad (26)$$

Therefore the probability for the first 9 spheres to be the ones we choose from a final placing of 12 around a central sphere is

$$N(9/9\ \text{ordered}) * P(9/12\ \text{ordered}) = 9! * (12-9)! / 12! = 3! / (12*11*10) \approx 0.0045 = 0.45\% \quad (27)$$

Finally, considering that we can choose the 9 spheres in 8 different ways so that they are all on one side of an equator, the indicated probability is then

$$P(\text{unstable}) = 8 * 9! * (12-9)! / 12! = 8 * 3! / (12*11*10) \approx 0.0364 = 3.64\% \quad (28)$$

Thus, this is the probability for a final 13-sphere group to produce an interim unstable 10-sphere group. For the reasons explained before, we can expect this percentage to be much lower when the final coordination number could be 11 and 10. Considering that these percentages must also be multiplied by the respective coordination number's relative frequency, these observations fully explain the randomly generated results shown in Table 14.

Table 14 Probability of configurations of clusters with different coordination numbers to be unstable

Total number of spheres	Coordination number	Inspected Clusters	Unstable Clusters	%	Instability
4	3	80270	80270	100	Certain
5	4	80270	41744	52	Possible
6	5	80270	8317	10.36	Possible
7	6	80270	313	0.39	Unlikely
8	7	75094	1	0.00	Very unlikely
9	8	42973	0	0.00	Very unlikely
10	9	8027	0	0.00	Very unlikely
11	10	265	0	0.00	Impossible
12	11	12	0	0.00	Impossible
13	12	1	0	0.00	Impossible
TOTAL		367182			

Stated another way, it is reasonable to assume that an 8-sphere arrangement (a central sphere plus 7 added) or a 9, 10, 11, 12 or 13-sphere arrangement is inherently stable. On the other hand, 52% and 10% of all the possible configurations of particles with coordination numbers respectively of 4 and 5 are unstable, which means that, in an assembly subjected to external forces, they would not take part in the global mechanism. As shown in the previous chapter, in Section 4.2 dedicated to the analysis of the coordination number of these clusters, the analysis of the particular case of superficial distribution when D = 0 can also be used to describe an important parameter such as the Caging Number, leading to results that are in good agreement with existing literature.

5.3 Bidisperse

The definition of Superficial Distribution given in the previous section of this chapter is based on the possibility, in the case of clusters and monodisperse packings, of defining and calculating the volume of the Voronoi cell generated by the touching neighbours around the central sphere. As was discussed in Chapters 2 and 4, this Voronoi decomposition is not directly applicable to packings of spheres of two dimensions, as it does not consider the real dimension of the spheres but only the spatial position of their centres. In this case, the examples that can be found in the literature suggest employing variations such as the Radical Tessellation and the Navigation Map (see Chapters 2 and 4).

Nonetheless, it is still possible to use the concept introduced in this chapter to describe the Superficial Distribution of the self-same contact points on the central sphere's surface within bidisperse packings, studying the volume of the Voronoi cell constructed using only the touching neighbours that have same dimension as the central sphere.

It has to be noted that this process is fundamentally different from the one described in Chapter 4 for the determination of the packing density relative to each sphere type. In that case the bidisperse packing was divided into two monodisperse packings on which the Voronoi decomposition could be applied, while in this case each particle has to be "extracted" from the

packing together with its same-sized touching neighbours and then the Voronoi cell of this cluster is calculated (Figures 5.5 and 5.6).

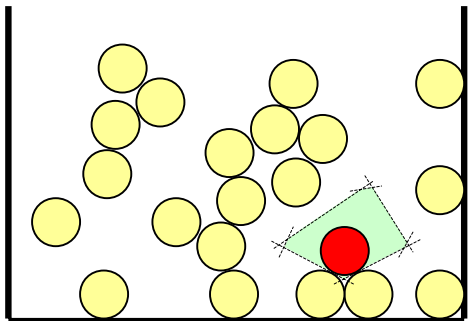

Figure 5-5 Voronoi cell within a packing

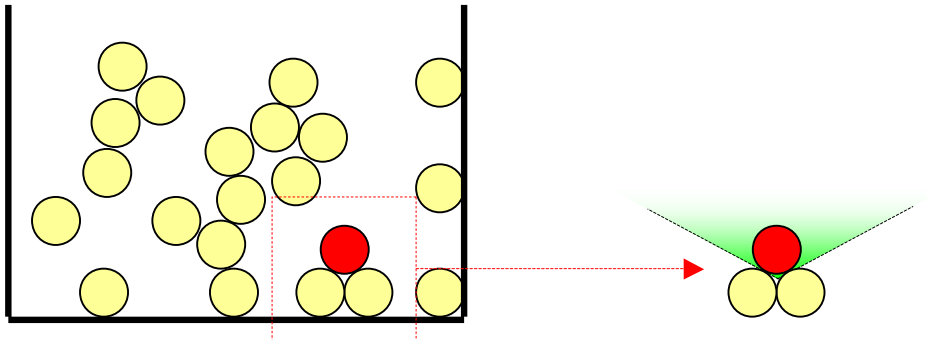

Figure 5-6 Voronoi cell of the extracted cluster

As can be seen in Figure 5.5, it is not possible for a sphere within a packing to have an open Voronoi cell even if this sphere is uncaged, because its Voronoi cell will always be determined also by the distant spheres. To focus on the effect of the position of the touching neighbours, therefore, the cluster has to be extracted from the packing and treated separately (Figure 5.6).

This analysis has been applied to the bidisperse packings generated in this study, whose composition was presented earlier in Chapter 4 and is going to be recalled here in Table 15 for greater clarity.

Table 15 Composition of the bidisperse packings simulated - Copy of Table 5

Size Ratio R_1/R_2	% of the Total Solid Volume (%V_1 – %V_2)				
(A) 1 / 2	(1) 10 - 90	(2) 30 - 70	(3) 50 - 50	(4) 70 - 30	(5) 90 - 10
(B) 1 / 4	(1) 10 - 90	(2) 30 - 70	(3) 50 - 50	(4) 70 - 30	(5) 90 - 10

The results, as shown in Figure 5.7, are substantially similar to what observed in the case of clusters.

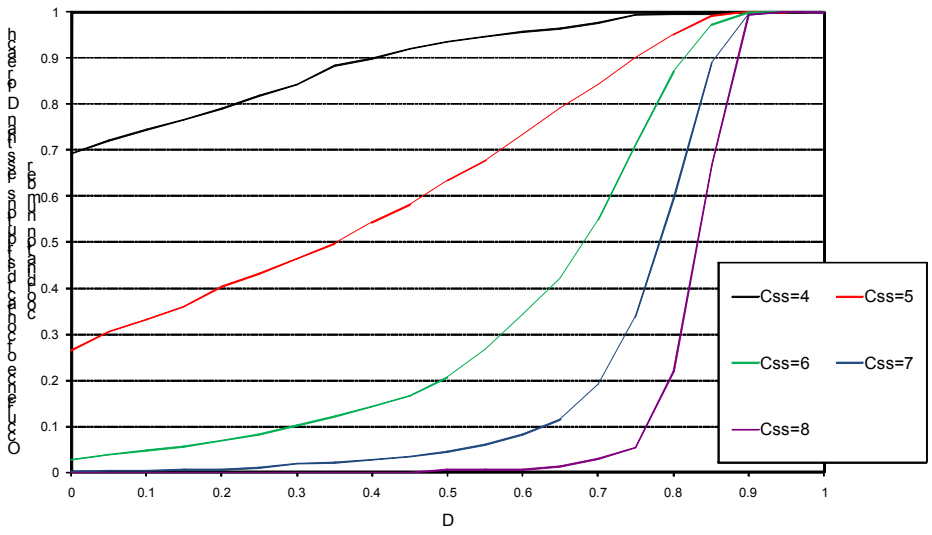

Figure 5 7 Cumulative frequencies of D for small spheres in bidisperse packings

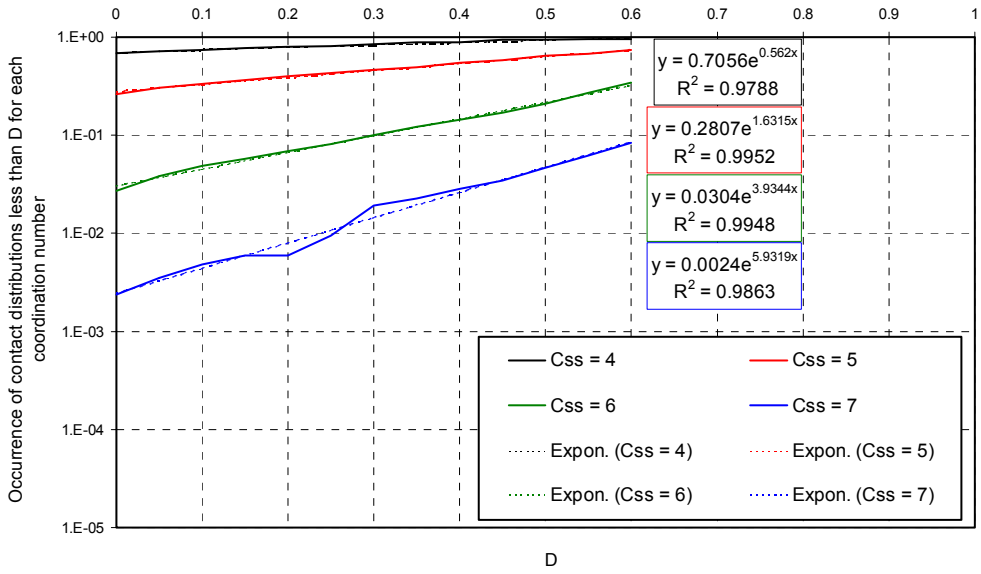

Figure 5-8 Cumulative frequencies of D for small spheres in bidisperse packings in logarithmic scale

As in the case of clusters, the cumulative frequency of D can be expressed with high accuracy for each value of coordination number as an exponential function of D:

$$CF(D) = \alpha \cdot e^{\beta D} \qquad (29)$$

where the two coefficients α and β vary for the different coordination number considered. In particular, as $CF(D=0) = \alpha$, we can see that the coefficient α represents the percentage of uncaged particles with a given coordination number, i.e. the percentage of spheres that were found not to be caged by a given number of spheres of the same dimension.

Although, for reasons of brevity, the results for all the different bidisperse packings will be reported in Appendix I, we can now observe from Figures 5.8 and 5.9 how α varies with grading and size ratio.

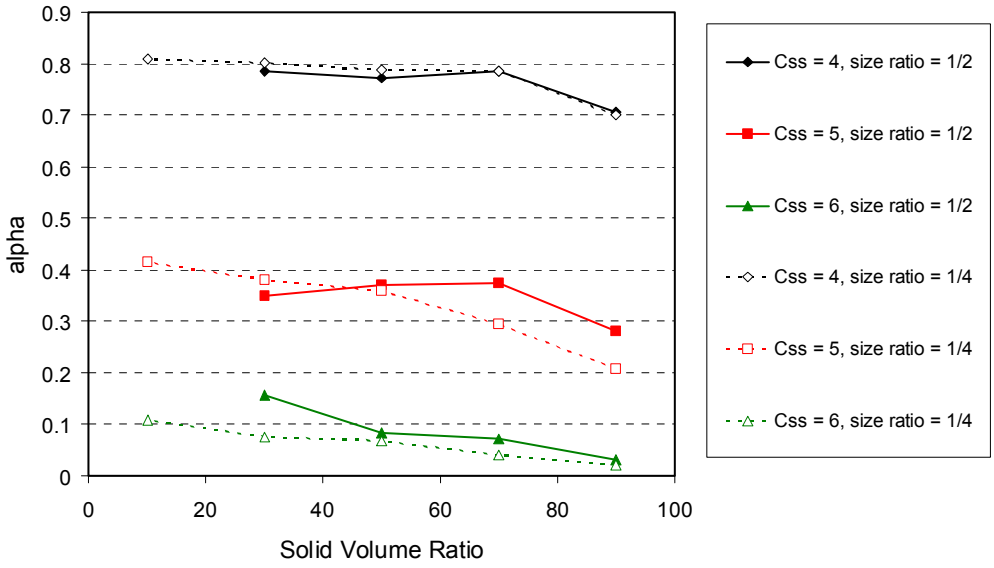

Figure 5-9 Fraction of small spheres that are not caged only by small spheres

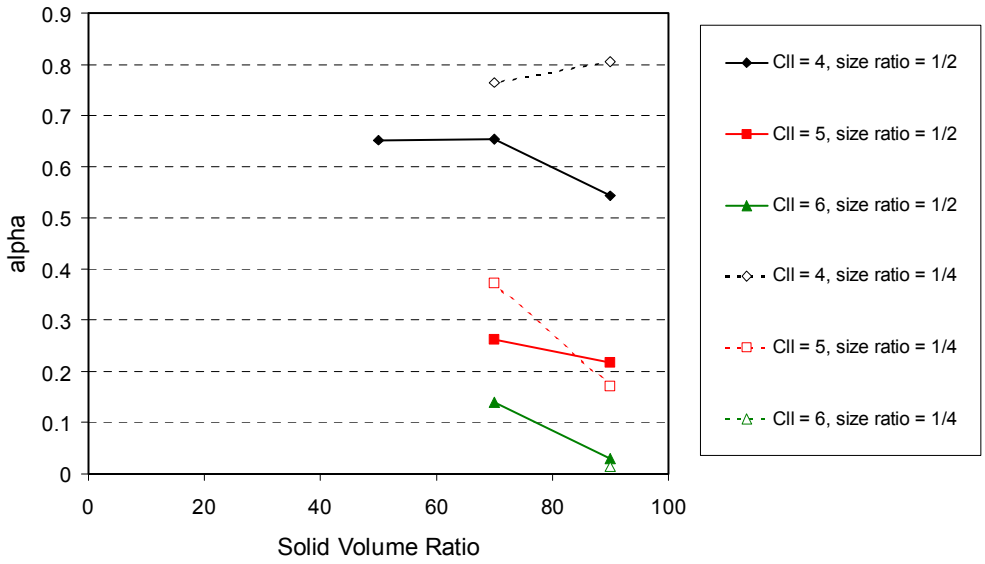

Figure 5-10 Fraction of large spheres that are not caged only by large spheres

In some cases, such as for the small spheres when size ratio = ½ and their packing fraction = 10% or for almost all the cases of large spheres when their packing fraction < 70%, the number of clusters extracted from each packing was not large enough to obtain meaningful results. Nonetheless, the analysis of the remaining cases can give useful information.

Interestingly, it can be noted that the percentage of uncaged configurations, α, always increases when the amount of considered spheres (small or large) decreases in the packing. This is observed as a general trend for every value of coordination number and for both small and large spheres.

It is important to point out that this behaviour is not an obvious consequence of diminishing the quantity of considered spheres, as that is supposed to be already reflected by the decreased coordination numbers. To state it another way with an example, what we observe here is that not only a configuration of 5 small spheres around a small sphere becomes less likely to happen when the quantity of small spheres in the packing decreases (effect on coordination number), but these 5 small spheres will also be more poorly distributed on the surface (effect on superficial distribution), being more likely to leave the central sphere uncaged. Moreover, as these clusters are actually embedded in larger packings, the fact that a particle can not be caged by only those touching neighbours that have its same size means that it has to rely on the particles of the other size to be caged and to be able to transfer any external load.

Finally, considering that, as discussed before, uncaged configurations are likely to be formed only with coordination numbers lower than 7, we can conclude that there are two different factors that increase the probability of an A-type particle having to rely on B-type particles to ensure that it remains caged when the quantity of A-type particles in the packing decreases:

- The coordination number between A-type particles decreases, increasing the quantity of configurations of A-type spheres (those with coordination number < 7) that are more likely to be uncaged;
- The likelihood of each type of configuration to be uncaged increases too.

6 RADIAL DISTRIBUTION FUNCTION

6.1 RDF in Monodisperse Packings

As shown in Chapter 2, previous authors have extensively treated the study of the Radial Distribution Function in monodisperse packings, therefore it will only be referred to briefly here to show that the results obtained in this study are in line with the earlier works.

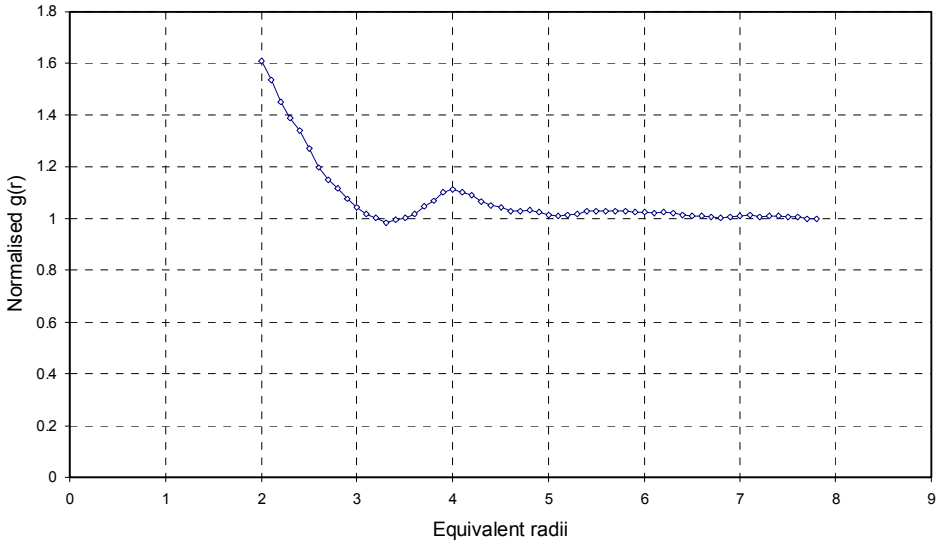

Figure 6-1 Normalised radial distribution function for a monodisperse packing simulated by a drop-and-roll algorithm

In Figure 6.1 we can clearly see that the monodisperse packings generated with the Drop and Roll algorithm used for this research can show the characteristics that were summarised in the Literature Review:

- Clear first peak at a radial distance of $r = 2d$ equivalent diameters;
- Not possible to distinguish the sub-peak at $r = \sqrt{3}d$ due to the low density of the packing;
- Visible second peak at $r \approx 3d$;
- Radial Distribution Function equal to Packing Density for large r.

Given the good agreement between the results of our analysis and the literature, we can now extend the study of the Radial Distribution Function to the bidisperse packings that are the main subject of this research.

6.2 RDF in Bidisperse Packings

The radial distribution function $g(r)$ was introduced in Chapter 2. No example was found in the literature about the application of $g(r)$ to bidisperse packings, therefore, in order for our results to be comparable to existing research findings, an approach similar to that discussed in the last section was chosen. Each bidisperse packing has been divided into two monodisperse packings (as was done in the previous chapters for coordination number and superficial distribution), which have then been treated separately.

Nonetheless, as will be shown, the study of this type of analysis can supply interesting information about the original bidisperse structures.

6.3 Radial distribution function of large spheres in bidisperse packings

Each bidisperse packing analysed in the previous chapters with regard to coordination number and superficial distribution has been split in two separate monodisperse packings, namely of large and of small spheres. Figures 6.2 and 6.3 show the behaviour of $g(r)$ for large spheres in the two cases of size ratio ½ and ¼ :

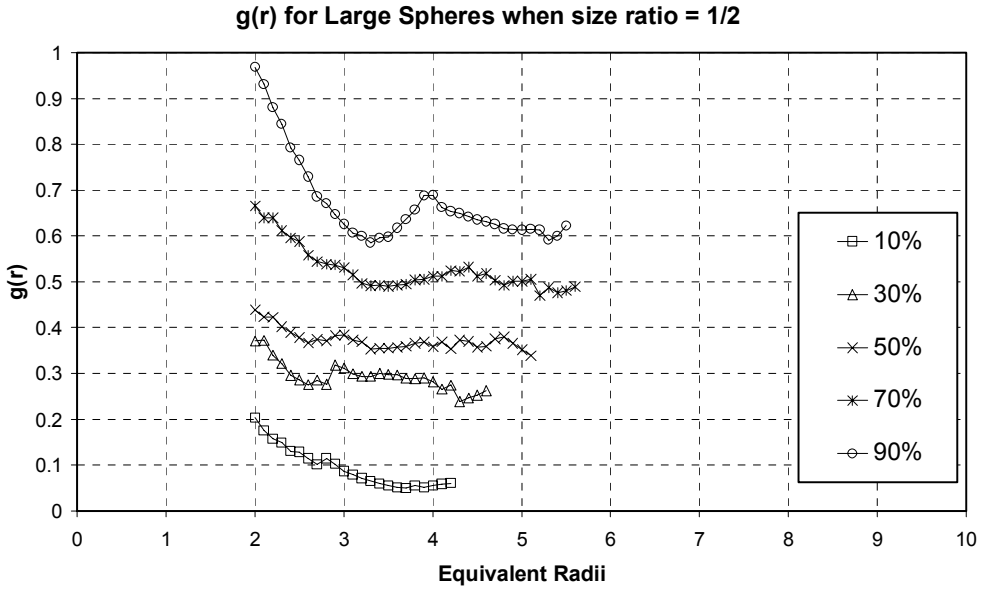

Figure 6-2 RDF plots for large spheres, size ratio = 0.5

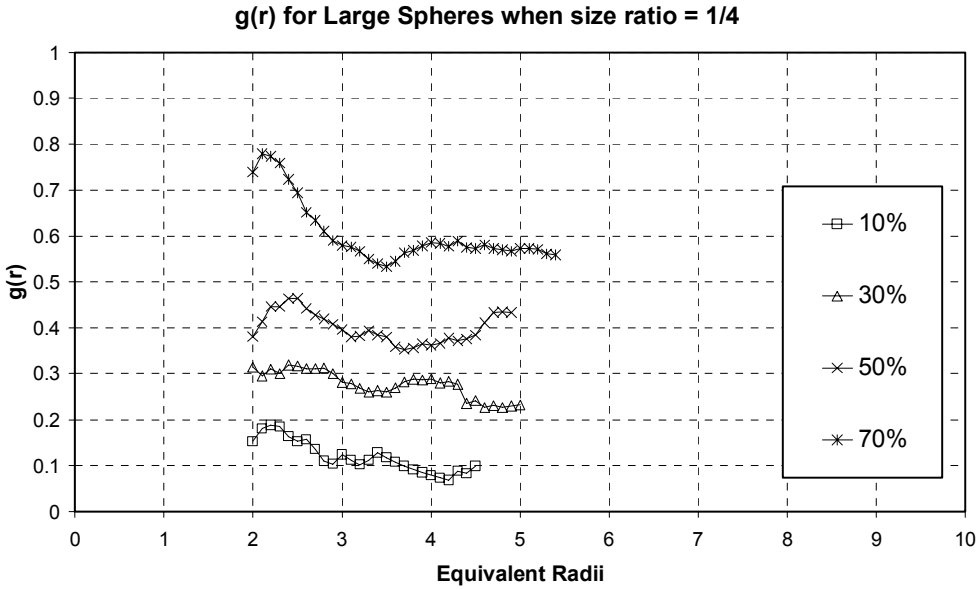

Figure 6-3 RDF plots for large spheres, size ratio = 0.25

The same functions $g(r)$ can be normalised dividing them by the respective solid ratio of large particles, obtaining the plots of $g(r)$ in Figures 6.4 and 6.5:

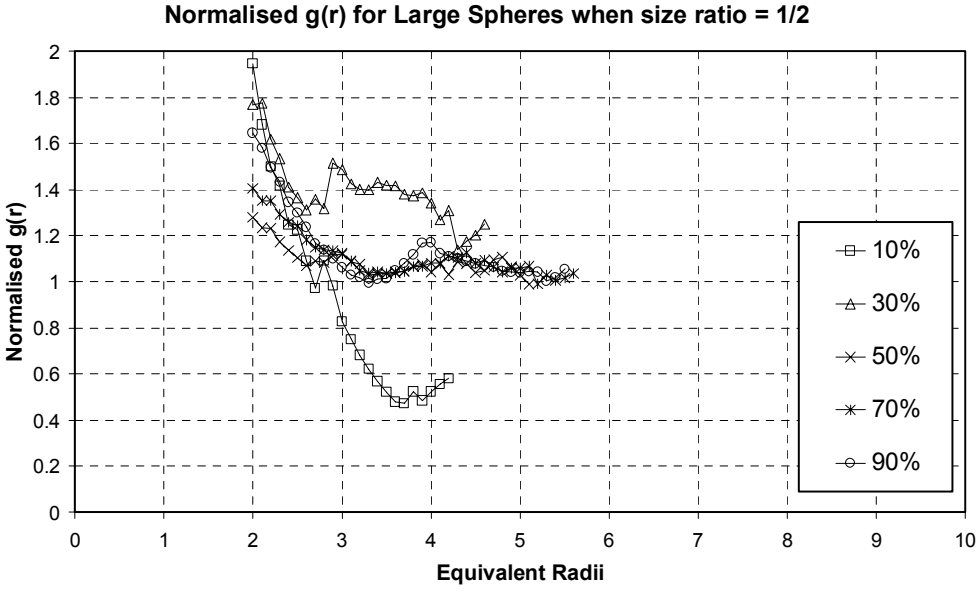

Figure 6-4 Normalised RDF plots for large spheres, size ratio = 0.5

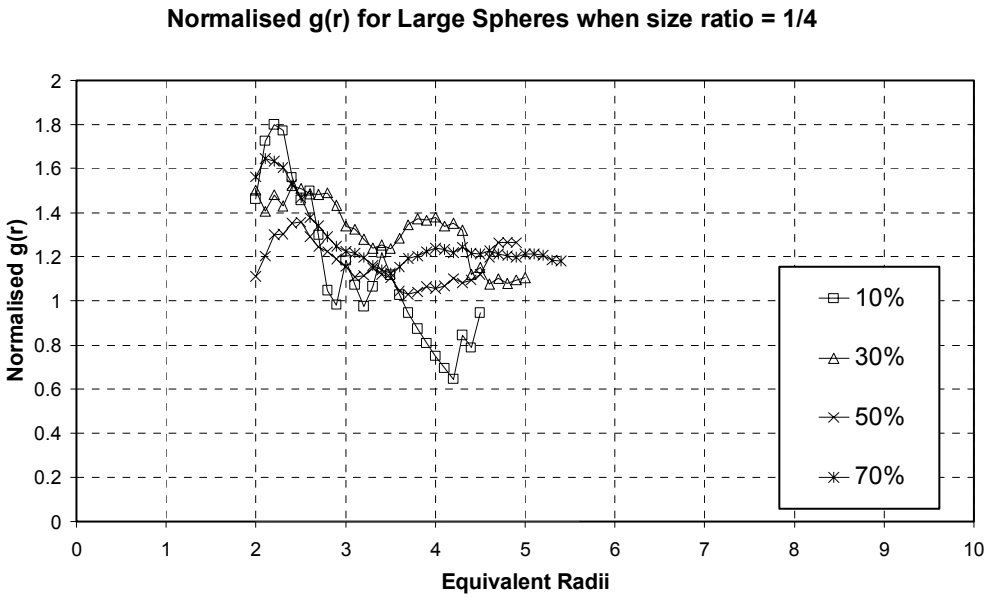

Figure 6-5 Normalised RDF plots for large spheres, size ratio = 0.25

Several considerations can be made of these results:

1. Due to the very small number of large particles considered, the packings with only 10% large spheres are showing very large fluctuations and will not be examined further.

2. The packings with 30% and 50% large spheres show the dominance of the small spheres' structure over the large spheres one. The peak for $r \approx 4R_l$ starts to be visible, but the influence of the presence of numerous small spheres is more evident: when the radius of the small spheres, Rs, is ½ of the radius of the large ones, Rl, $g(r)$ presents a peak at $r \approx 3R_l$, while, quite similarly, in the case of Rs =

¼ Rl we observe a clear peak at $r \approx 2.5R_l$. These newly observed peaks could be interpreted as the result of structures such as those shown in Figures 6.6 and 6.7.

1. It has to be noted that in these packings the peak at $r \approx 4R_l$ does not necessarily have the same topological meaning as in the monodisperse case (i.e. three large spheres on a straight line). For both the size ratios studied here a number of configurations involving small spheres can be found that deliver a radial distance r

between large spheres of approximately $4R_l$ which, therefore, can not be assumed to be representative of an organisation between only large spheres. Moreover, given the numerical prevalence of small spheres in these packings, it could be suggested that these other configurations are probably the ones contributing the most to the formation of this peak.

2. The quantity of 70% large spheres had already been identified, reasoning on the solid ratios in this and other researches (see packing density in Chapter 2), as an interesting threshold for the structure of bidisperse packings. The study of $g(r)$ in this situation seems to reinforce that concept. The radial distribution function of the packings containing a fraction of large spheres $> 70\%$ of the total solid volume shows how, only at this stage, the large spheres can then form a considerable number of the organised structures that are typical of the monodisperse case (e.g. with a peak in the $g(r)$ curve at 2r and 4r). In particular, the packing containing 90% large spheres seems fundamentally unaffected by the presence of 10% small spheres. This is to be expected if the void space between the coarse particles is large enough to contain small particles without upsetting the layout of the large ones.

6.4 Radial distribution function of small spheres in bidisperse packings

The plots of $g(r)$ obtained for the small spheres of bidisperse packings with size ratios of ½ and ¼ are presented in Figures 6.8 and 6.9, together with the monodisperse case that can be considered as a packing of 100% small spheres. The data and calculations are as before.

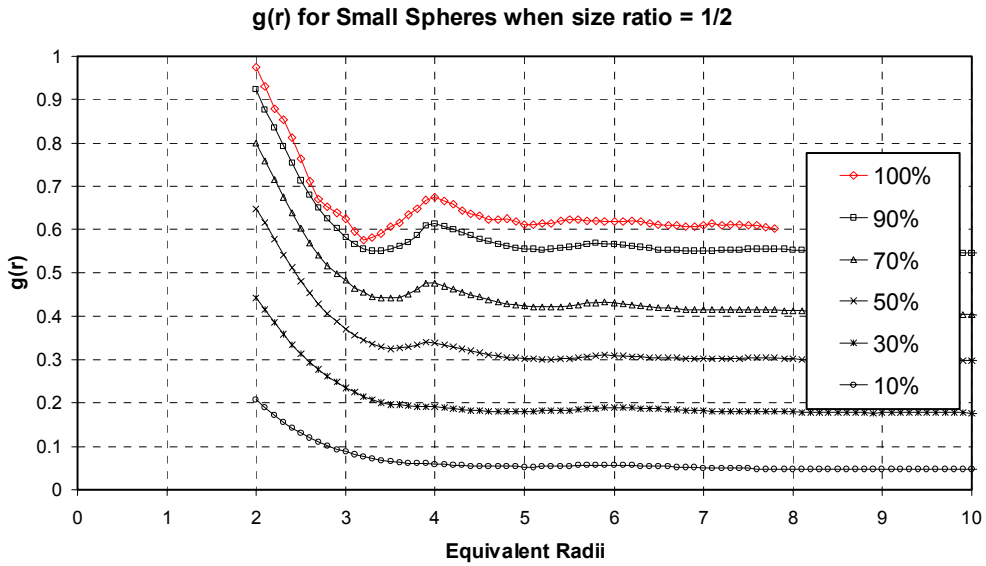

Figure 6-8 RDF plots for small spheres, size ratio = 0.5

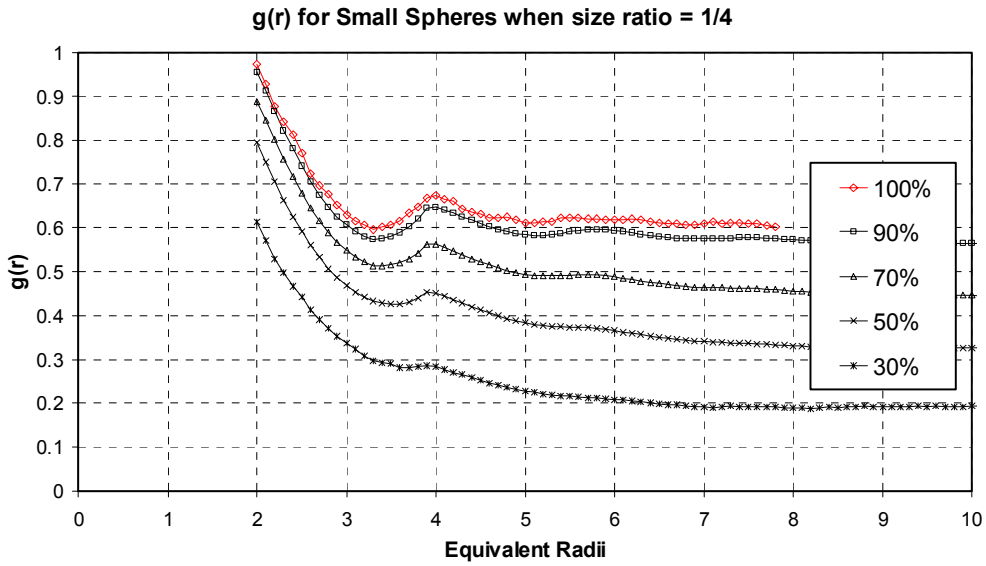

Figure 6-9 RDF plots for small spheres, size ratio = 0.25

Figures 6.10 and 6.11 show the plots of $g(r)$, the radial distribution function normalised by the packing's solid ratio.

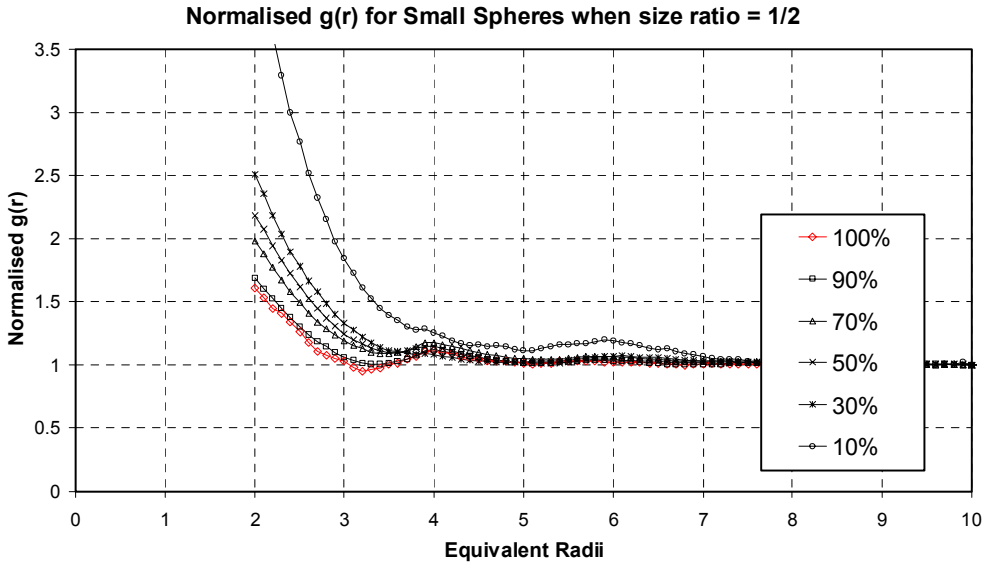

Figure 6-10 Normalised RDF plots for small spheres, size ratio = 0.5

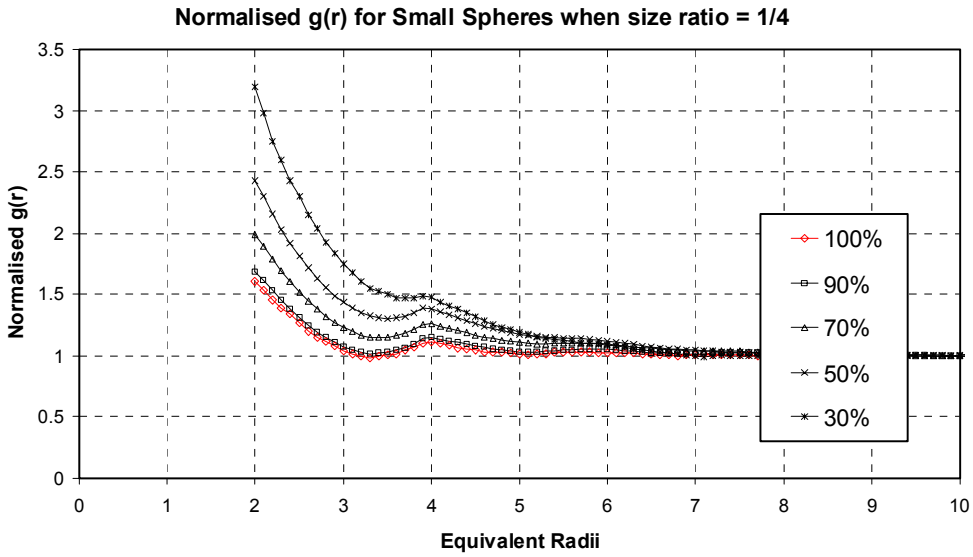

Figure 6-11 Normalised RDF plots for small spheres, size ratio = 0.25

The radial distribution function of the small spheres in bidisperse packings is very different from that of the large spheres of the same packings. For each different percentage of small spheres, the general shape of $g(r)$ seems unaltered, always showing very clear second and third peaks at $r \approx 4R_s$ and $r \approx 6R_s$.

As already observed by other authors (see Chapter 2 for literature review), a reduction of solid ratio under 0.60 (due to particle properties or packing algorithm) results in the disappearance of the first sub-peak at $r = 2\sqrt{3}R$ of the second peak, which is also the case for this study.

To simplify the notation, we will refer, hereafter, to the radial distribution function of small spheres of a bidisperse packing with, for instance, 90% small spheres as $g_{s90}(r)$.

Figure 6.12 shows how, for a size ratio of ½, the normalised $g(r)$ of small spheres for values of $r \geq 4R_s$ is essentially coincident for the different small sphere quantities. This fact is even more evident if we consider $g_{s100}(r)$ as a reference for the other distributions (see Figure 6.12).

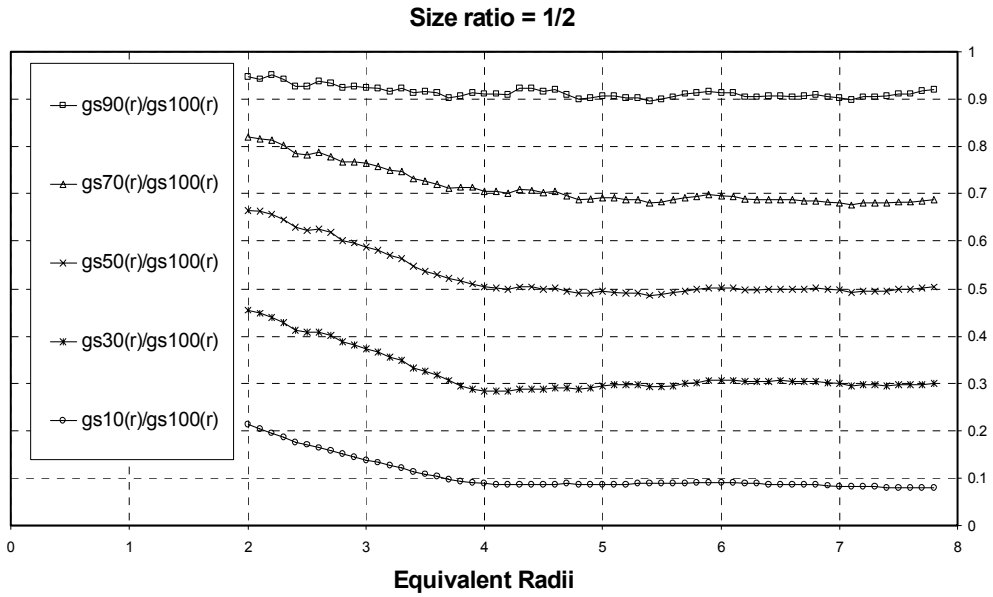

Figure 6-12 RDF plots for small spheres normalised by the monodisperse case, size ratio = 0.5

Surprisingly, we observe a very sudden change in the behaviours of these functions before and after the value $r \approx 4R_s$. For $r \geq 4R_s$ the different $g(r)$ result to be an almost perfect reproduction of the monodisperse case, scaled accordingly to the respective solid ratios. This does not happen in the region $2R_s \leq r \leq 4R_s$, where the proportion factor increases linearly decreasing the distance r.

This observation is of great importance as it allows us to say that, in a packing of single-sized spheres, the addition of a given quantity of spheres of size double the original ones will affect the original structure by distorting it on a "local" level, i.e. very close to the original spheres, yet decreasing $g(r)$ less than what would be expected on the basis of the respective solid ratios. On the other hand, the "long distance" relationships between the original spheres will not be distorted but only "scaled" proportionally to the reduced quantity of small spheres relative to the total solid volume.

It must be noted that if the added spheres were of the same dimension as the original ones we would expect this perfect scaling over the whole range of r. Therefore we deduce that, (from a structural point of view) for each sphere of radius 1, any sphere of radius 2 placed at a distance larger than 4 from the first sphere's centre will have the same effect as an equivalent volume of spheres of radius 1 (i.e. 8 spheres of radius 1 if the size ratio is ½).

A similar behaviour can be noted also in the case of size ratio of ¼, where the structural threshold can be placed at $r \approx 8R_s$ (see Figure 6.13), suggesting that the size of the zone of "distorted" $g(r)$ is somehow proportional to the large sphere's size (see also Table 16).

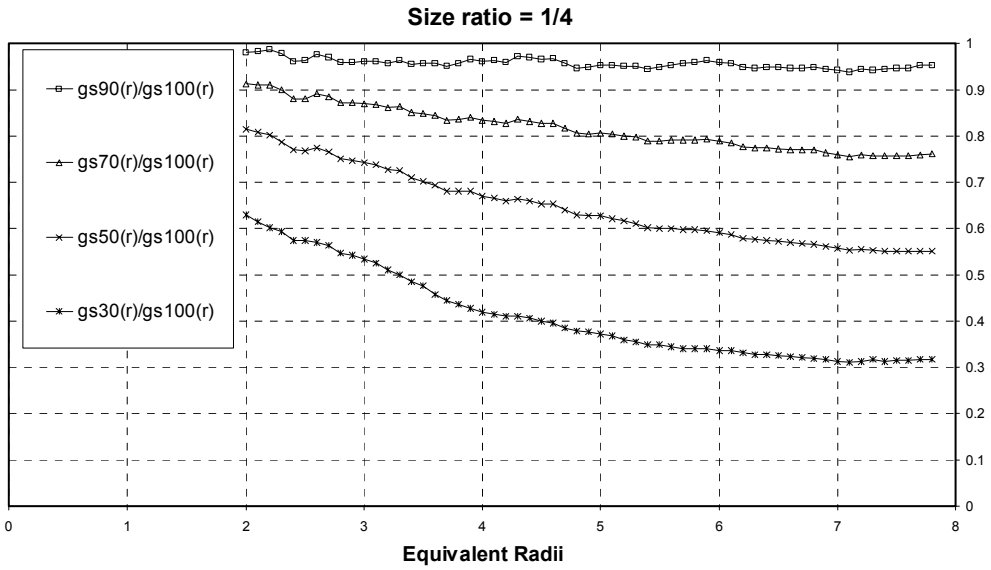

Figure 6-13 RDF plots for small spheres normalised by the monodisperse case, size ratio = 0.25

From a geometrical point of view, these observations can be seen as in Figure 6.14:

Table 16 Distorted and scaled RDF zones

Figure 6.14.	Rs/Rl	Distorted $g(r)$ Zone	Scaled $g(r)$ Zone
a)	1/2	$2R_s \le r \le 4R_s$	$r \ge 4R_s$
b)	1/4	$2R_s \le r \le 8R_s$	$r \ge 8R_s$

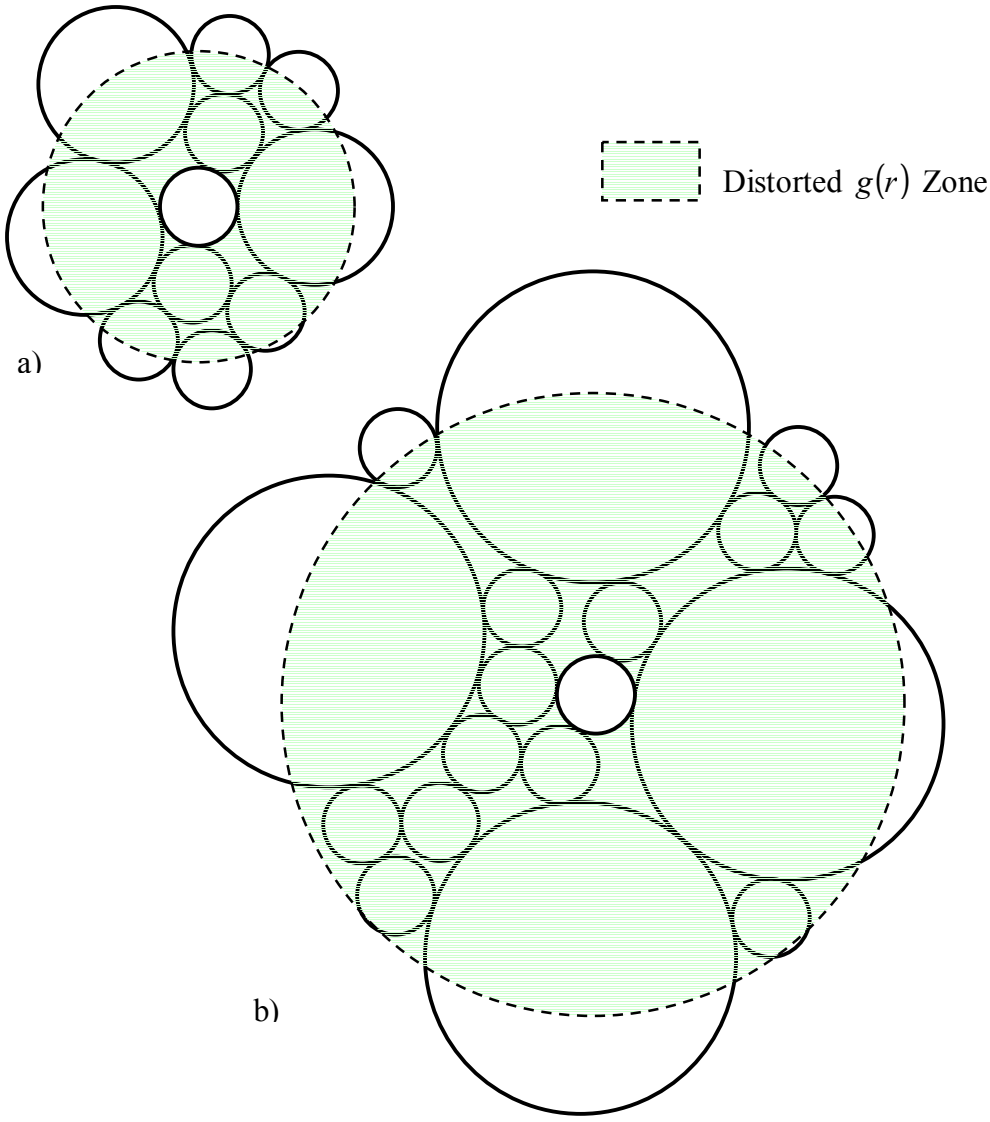

Figure 6-14 Zones of RDG distorsion around particles

7 X-RAY EXPERIMENT

7.1 Introduction

During the last period of the research the School of Civil Engineering at the University of Nottingham acquired the X-Tek 2D-3D CT X-ray equipment, and it was envisaged that a direct application of this new facility could be to deliver an insight into the structure of granular materials.

Computed Tomography is a non-destructive method of investigating a specimen's microstructure, obtaining digital information without disturbing it in order to leave it capable of being, eventually, subject to mechanical testing. This technique consists in the acquisition, using ionising radiation (X-rays), of a series of projection images or radiographs through specific sections of a target object (specimen). This object is first scanned using a complete set of different angular positions and then reconstructed as a function of its X-ray attenuating property, delivering a 2D slice (planar fan beam configuration in Figure 7.1) or, in the case of this particular equipment, also a 3D solid volume (cone beam configuration in Figure 7.1) representing the specimen in a 16-bit grey scale.

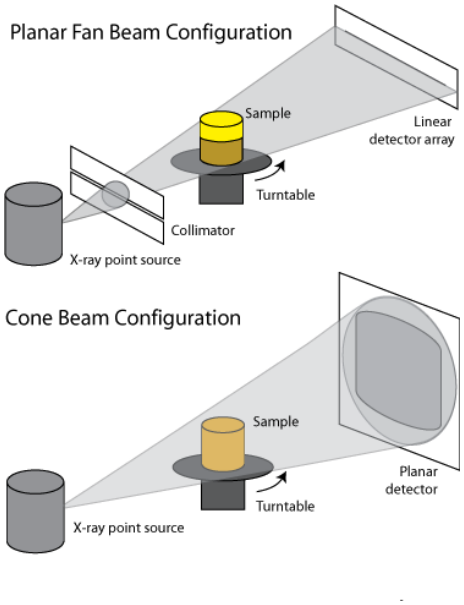

Figure 7-1 Common beam configurations

For the purposes of this research, only the apparatus for 2D image acquisition has been used, which has the following specifications (see Townsend 2006):

2D X-ray System

X-Tek 350kV 900W Mini-Focus X-Ray Source, Focal Spot 1.0mm (0.6mm x 0.8mm) to EN 122543. 1kW Generator, RS232 control, Oil Cooler.

2D High Resolution Line Array Detector

Industrial 6" dual-field Image Intensifier, low burn scintillator, 768 x 572 pixel 8-bit Firewire camera.

The final resolution used for the experiments is of 20 pixels per millimetre.

Manipulator

Venlo 5 Axis manipulator, with high precision turntable.

In the case of this particular research, although its use had to be restricted due to time limits, even a simple application of this technology can be useful to:

- explore the potential of this new equipment for the study of these packings;

- provide practical measurements of some sort to support the results from the numerical simulations and verify the performance of the algorithms, in particular to evaluate the possibility to estimate coordination number and radial distribution function for real packings;

- suggest future developments of the research.

The use of this equipment could only play a marginal role in the final part of this research, therefore the following section will briefly describe the details of the experiment and of the analysis process and the results obtained. Townend (2006) provides more detailed information about the equipment and previous studies that employed X-ray CT.

Experiment.

Into a plastic cylinder, of diameter 90mm, were poured, without shaking or compaction, glass beads having the following specifications:

POTTERS BALLOTINI - A-Series Technical Quality Solid Glass Spheres

Stock Number	Size (mm)	% Round
Premium 1.5MM	1.3-1.7	90

Density g/cc 2.50

Refractive Index 1.51 - 1.52

Crush Resistance psi 14,000 - 36,000

Hardness, MOH 5 - 6

Hardness, Knoop 100g load 515 Kg/mm2

Coefficient of Friction, Static 0.9 - 1.0

The X-ray CT machine scanned the central part of this specimen, which was approximately 20mm high, at a rate of 4 sections per millimetre. Therefore, each sphere is supposed to have been sliced, on average, approximately 5.8 times.

The built-in software then analysed the scan to find the horizontal position of ellipsoid particles. This results in a list of the x and y coordinates and the maximum and minimum radius of the ellipses that best overlap each

particle seen in the given image. The procedure approximated the particles' sections with good precision in the central area of each slice, while many particles closer to the border of the scan, that were visible by eye, were not isolated by the software (Figure 7.2).

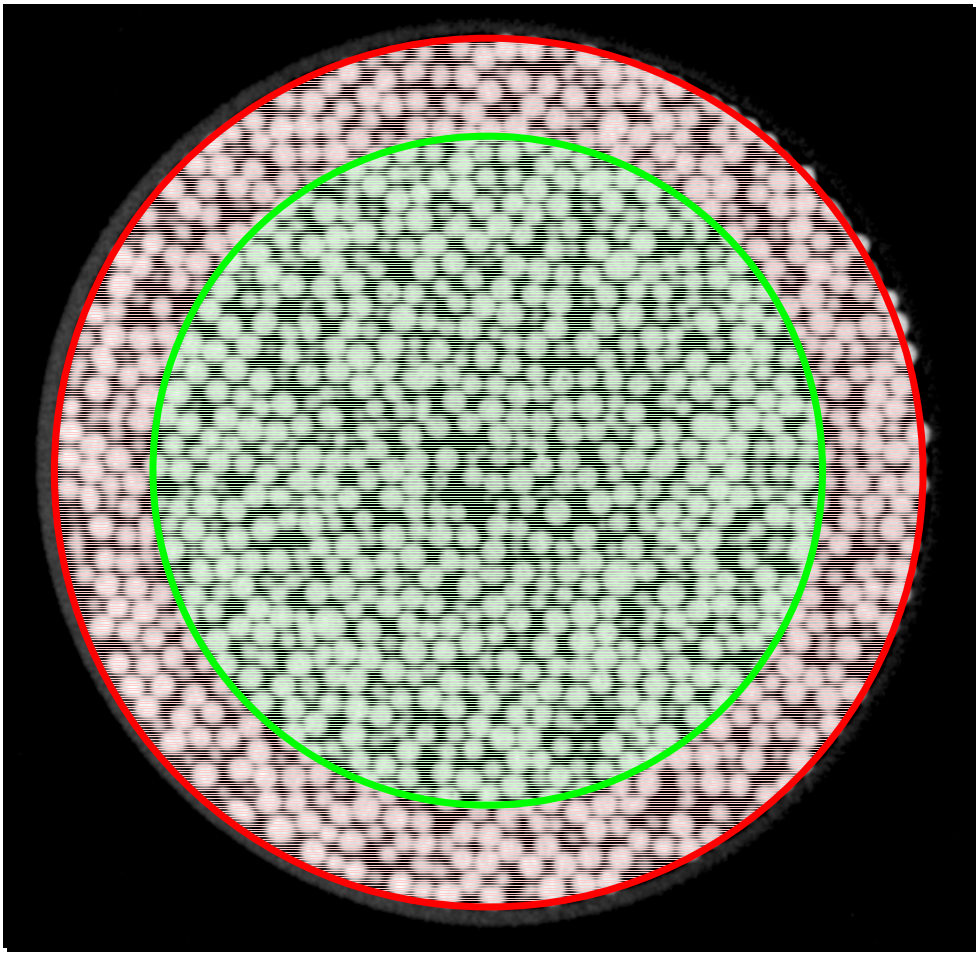

Figure 7-2 The image analysis accuracy decreases towards the specimen's border

Size thresholds must be set for the ellipses that can be isolated by the software. If a large limit is set, there is a danger that clusters of small particles will be interpreted as single large particles, such as in Figure 7.3.

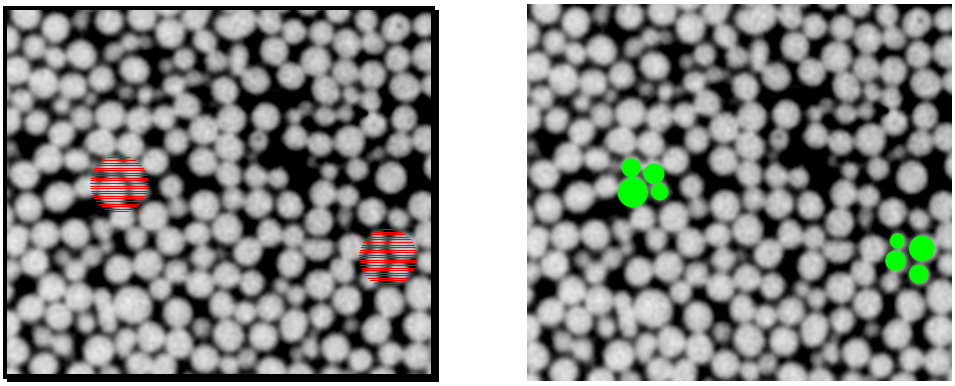

Figure 7-3 Maximum size threshold to distinguish clusters of small particles

To take into account the wall effect and the imprecision of the image analysis, for each section only the ellipses with centres further than 6 sphere radii from the wall of the specimen were analysed.

7.2 Three dimensional Re-construction.

The process of reconstructing the three dimensional assemblage corresponds to finding the vertical position of each particle by stacking the various images one on top of the other. In this process each particle will be approximated with a sphere, therefore the ellipses found during the image analysis will be approximated with circles of radius equal to the average radius of the ellipses. It is possible to calculate their vertical position using only the sections that cut a particle in a region close to its centre (see Figure 7.4 and 7.5), therefore a minimum threshold, R_{min}, for the circle radii can be set.

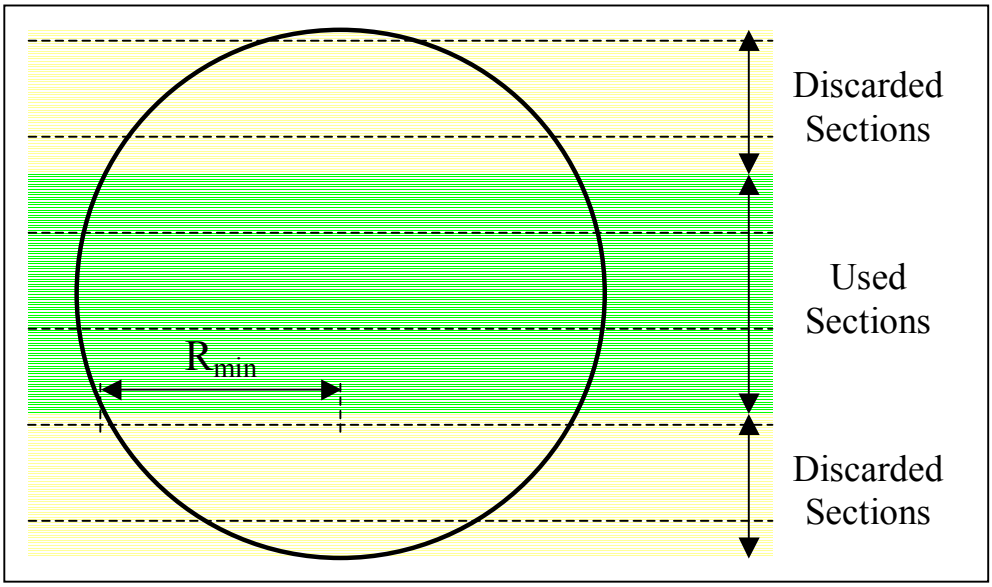

Figure 7-4 Section used to determine the sphere's centre

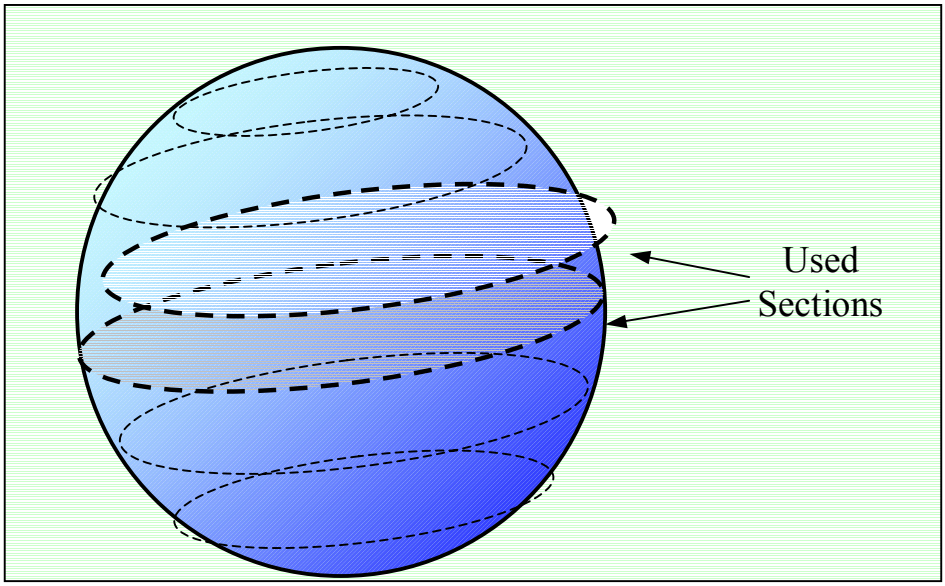

Figure 7-4 The sections used are not necessarily aligned

The x, y and z coordinates of the centre of the sphere are then calculated as weighted average of the x, y and z coordinates of the centres of the circles that were found to have radii larger than R_{min}, where the weights are the circles radii (this way, in the average we give more importance to the larger circles, as they more likely to be close to the sphere's equator).

This process identified approximately 7000 particles in the core considered, for a calculated packing density of about 0.60.

7.3 Results.

During the process of numerical reconstruction of the sample, a number of approximations contribute to the final level of accuracy of the analysis. The main ones can be summarised as:

- **Sphericity.** We consider the particles to be perfect spheres while in reality most of them are slightly ellipsoidal (Figure 7.6a).

- **Size.** We consider the particles to be all of the same dimension, but in reality this might not be the case:
    - Some particles might be larger or smaller than the nominal size, but we have to consider them to have the nominal size (Figure 7.6b);
    - A very few particles might even be smaller than R_{min} and so they might be lost during the re-construction process;
    - Some particles might not be of the size that the image shows due to inaccuracies of the image re-construction process performed by the equipment.

- **Position.** Even if the particles were all perfect spheres of the same size, we would still introduce an error in the estimation of the position of their centres due to approximations in our re-construction process (Figure 7.6c):

- Circles that represent successive sections of the same particle do not necessarily have same centre x and y coordinates, as represented in Figure 7.5;
- Averaging the x, y and z coordinates of the centres of the circles is obviously not the most accurate way to calculate the sphere's centre, especially in presence of all the previously cited sources of errors.

Figure 7.6 represents in two dimensions these inaccuracies and what could be their combined effect (Figure 7.6d).

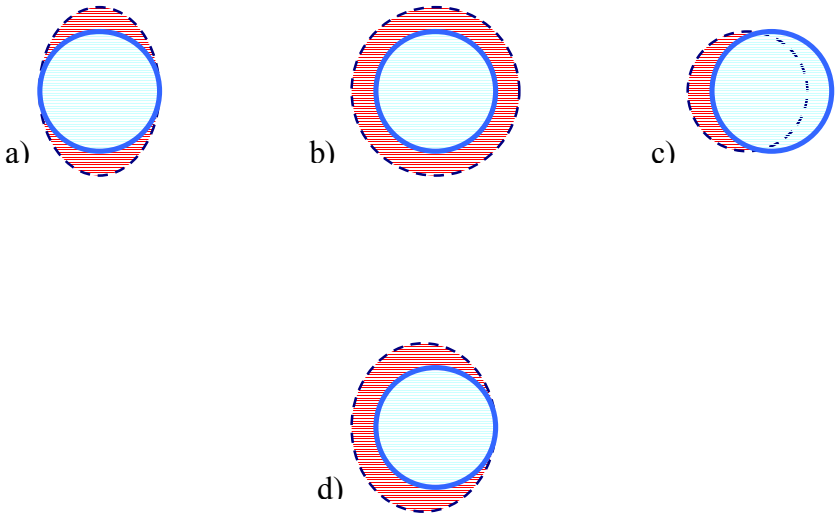

Figure 7-5 Different type of inaccuracies in the process of particle's numerical reconstruction

Figure 7.7 shows examples of evident errors of sphericity and size observable directly from one of the scans used for the re-construction.

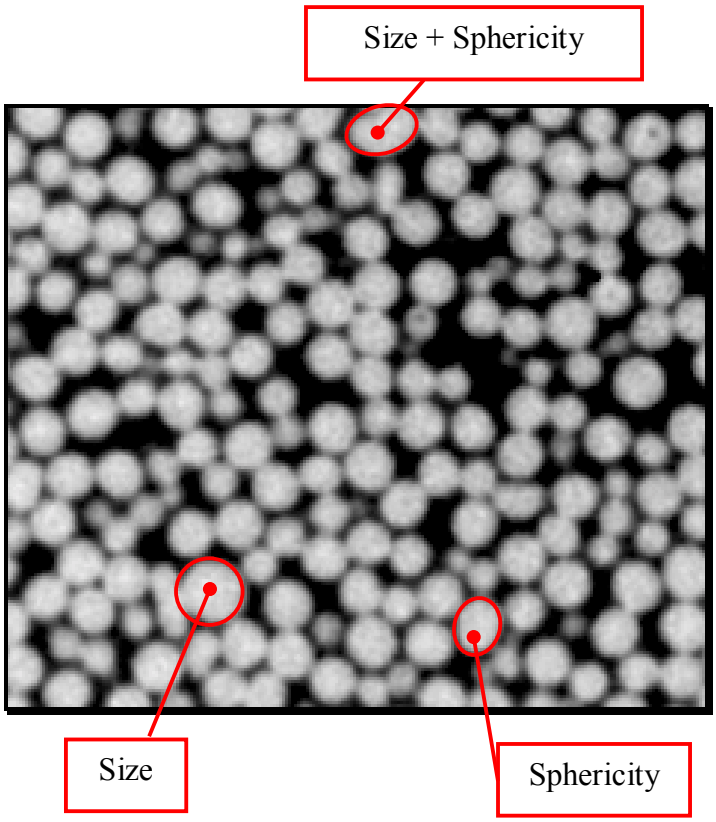

Figure 7-7 Examples of sources of inaccuracy

Due to these various inaccuracies discussed above, it would be difficult to define with confidence whether or not a particle is in contact with another. As was discussed in the literature review presented in Chapter 2, the contact between two particles and, therefore, coordination number are, in practice, "ill defined" parameters that depend on the threshold set for the distance between the centres of the considered particles. Defining this threshold requires greater accuracy than could be achieved in this preliminary study in a reasonable timescale.

A parameter that is supposed to be less affected by these errors is the Radial Distribution Function, $g(r)$. It still relies on the estimation of the

relative distances between particles to give information about the packing structure, but in a more continuous way than coordination number. The analysis of $g(r)$ for the re-constructed sample is shown in Figure 7.8.

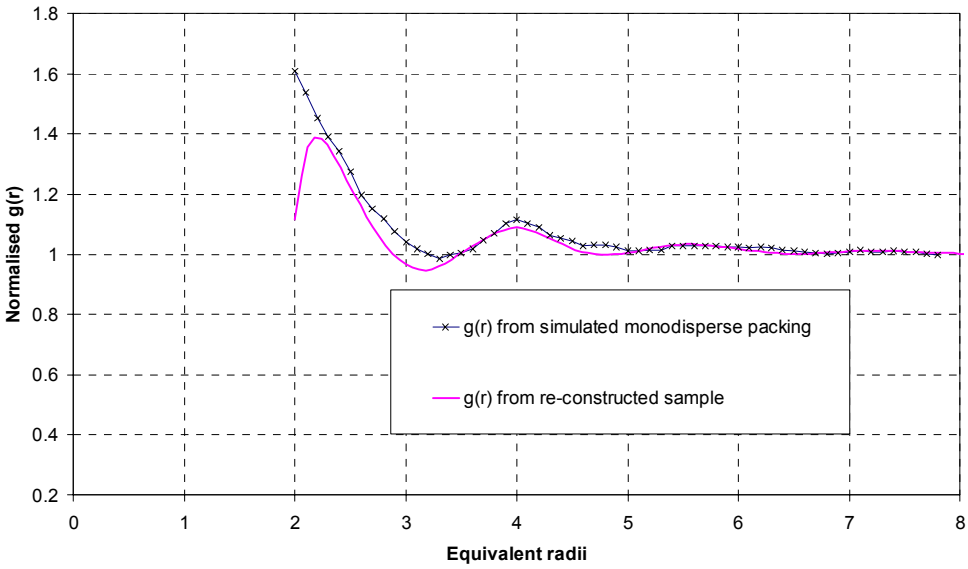

Figure 7-8 Comparison between normalised RDF of a simulated monodisperse packing and of a numerically reconstructed real packing of spherical particles

It can be seen that this method, even with the limitations and approximations discussed earlier, works remarkably well, showing very clear peaks of $g(r)$ at a radial distance of about 2, 4 and 6 radii. The comparison with the result from the simulated monodisperse packing (see Figure 7.8) shows very good agreement between the two.

Nonetheless, Figure 7.8 also exposes the well-known problems of this type of technique when dealing with coordination number: while in the simulation the distance between the centres of two spheres is always

strictly larger than or equal to two radii, in the physical experiment this threshold is not so sharp.

This can be observed noting that:

1. The first peak that is supposed to be at $r = 2R$ (and that represents the spheres in contact with the central one) is instead found at a slightly larger distance. This indicates that the structure of two contacting spheres is found when the distance between the centres is larger than expected, meaning that probably the spheres radii are often larger than the assumed nominal value (at least in the direction of the contact).

2. The value of $g(r)$ at the first and second peaks is a little lower than in the simulation, meaning that a smaller number of particles were found at that particular distance. This indicates that the structures associated with the first and second peaks are not as "fixed" as in the simulation, having the possibility to appear at radial distances slightly different than expected. Again, this supports the hypothesis of variable spheres radii.

3. Few particles were found to have centres at a reciprocal distance lower than $r = 2R$, in which case their radii have to be smaller than the assumed nominal value. This explains why there is not a sharp cut-off in the X-ray derived data at $r = 2R$ as is the case for the simulation.

8 DISCUSSION

8.1 Introduction

The previous chapters have presented results obtained by the various algorithms and how these were used to study Coordination Number, Superficial Distribution of contact points and Radial Distribution Function. This chapter's aim is to further discuss the concepts that were elaborated during the previous analysis to develop a better understanding of their possible implications.

For this purpose, it can be useful to summarise the main concepts and observations in order to have a clear overview of what has been shown so far (see Table 17).

Table 17 Summary of findings and notes

Parameter	Case Description	Analysis Results	Location	Notes from Literature
Parking Number Maximum number of probe spheres that can be placed on the surface of a target sphere if tentative sites for each succeeding sphere are selected entirely at random (P_{ij}).	Clusters. Parking number of equal spheres on a sphere of same size (P_i).	The value of 8.75 suggested in the literature for equal spheres is found to correspond to the 94th percentile of the population considered.	Section 4.2 Page 90	Estimation of parking number P_{ij} as a function of the size ratio r_i/r_j between target and probe spheres radius: $P_{ij} = 2.187 \cdot \left(\frac{r_i}{r_j} + 1 \right)^2$
	Bidisperse packings. Parking number of small spheres on a small sphere (P_{ss}).	Our model for coordination number in bidisperse packings (see point e) can only be optimised if the parking number is considered to be variable with packing density. The ratio between variable parking number, P_{ij}', and traditional parking number, P_{ij}, decreases with the packing density of the j-type spheres in the same way for every size ratio investigated.	Section 4.7 Page 140	
	Bidisperse packings. Parking number of small spheres on a large sphere (P_{ls}).		Section 4.7 Page 140	
Caging Number Average minimum number of spheres (randomly placed on the surface of a central one) that blocks all the translational degrees of freedom.	b.1 Clusters. Caging number of equal spheres on a sphere of same size.	Calculated value of 4.63.	Section 4.2 Page 92	A formula is given in the literature that describes caging number as a function of the size ratio r_i/r_j between central and outer spheres radius. For equal spheres a value of 4.71 is suggested.
Packing Density Ratio between solid volume of particles and total volume occupied.	c.1 Clusters. The Voronoi cell generated by its touching neighbours is supposed to be the portion of space belonging to each central sphere.	These data can be used to describe the superficial distribution of the contact points on the surface of the central sphere (see point f).	Section 4.2 Page 87	Definition of Voronoi cell.

Parameter	**Case Description**	**Analysis Results**	**Location**	**Notes from Literature**
	c.2 Monodisperse Sticky Packings. Affecting the freedom of movement of the particles by means of a "stickiness" parameter it is possible to obtain monodisperse packings with packing density that varies over a wide range.	A linear increment of the stickiness parameter d generates more dense packings than loose ones. In order to give equal importance to the analysis for each packing density, the results were grouped in ranges according to packing density value and averaged within each range.	Section 4.3 Page 93	Researchers have obtained packings of various packing densities simulating the effect of real-life parameters such as Van der Waals forces, moisture content and friction on particles of variable size. Packings of coarse particles are dominated by gravity while the importance of superficial interparticle forces increases as particle size decreases.
	c.3 Monodisperse Diluted Packings. The packing density of a monodisperse packing can be varied by adding to the original packing a variable quantity of secondary particles. These added particles will then effectively be considered as voids.	If the secondary (diluting) particles are chosen of the same size of the original ones, a linear increment of their quantity brings a proportional decrement of the packing density of the original particles.	Section 4.4 Page 98	Not mentioned.

Parameter	**Case Description**	**Analysis Results**	**Location**	**Notes from Literature**
	c.4 Bidisperse Packings. We study how the partials (for the two components) and the total packing densities vary with the packing composition (proportion of solid volume of small spheres over total solid volume).	It is observed that when the finer component's volume is less than 30% of the total solid volume only a small part is used to substitute larger particles, while most of it is dedicated to fill the voids between the larger particles. Therefore we can say that, in this region, the packing is fundamentally dominated by the larger component. Only when the finer component's volume exceeds 30% of the total solid volume the two components become equally important for the determination of the packing's total packing density.	Section 4.7 Page 111	Analytical and numerical results indicate that an important transition takes place when the volume of the smaller fraction increases over 30% of the total solid volume of the mixture. The role of the smaller spheres changes from filling the voids between large particles to surrounding and displacing the larger particles, forming the main matrix of the mixture.
Self-same Coordination Number Number of contacts between a particle and particles of the same type (i.e. dimension) (C_{ii}). Self-same and self-different coordination numbers are called Partial Coordination Numbers.	d.1 Clusters. We counted the number of particles that it is possible to fit around a central one in case of perfect randomness and with no readjustments.	Every cluster has reached at least C_{ii} = 6, while only one of them was found to reach C_{ii} = 12. The distribution of C_{ii} can be expressed as a normal distribution with mean value of 7.57 and standard deviation of 0.77. These results can be used to estimate the physical meaning of the value of parking number for equal spheres reported in the literature (see point a.1).	Section 4.2 Page 88	The maximum number of spheres of same dimension that is possible to place on the surface of another sphere is the so-called Kissing Number. If the central sphere has the same size as the outer ones its value has been proved to be 12.

Parameter	**Case Description**	**Analysis Results**	**Location**	**Notes from Literature**
	d.2 Monodisperse Sticky Packings. The average C_{ii} was calculated within each range R_n of packing density defined as $R_n = n*0.05 \pm 0.025$ With n = 1, 2, ….	The average Cii measured for sticky packings is always larger than that measured for diluted ones, at similar packing densities. Combining the two algorithms we produce a model that can deliver information about C_{ii} in real packings of same-size particles, where dilution and friction might take place at the same time.	Section 4.3 Page 95	Some researchers have studied coordination number of packings of fine particles simulating their response to real-life parameters such as Van der Waals forces, moisture content and friction. These are superficial forces and, therefore, their importance compared to gravity is a function of particles size.
	d.3 Monodisperse Diluted Packings. The average C_{ii} was calculated for each packing.		Section 4.4 Page 98	Particular case of bidisperse packings. See further.
	d.4 Bidisperse Packings. C_{ss} – Number of contacts between a small sphere and other small spheres.	General behaviour similar to what described in literature. A representation is proposed that describes the average and standard deviation of normal distributions whose non-negative part approximates the distribution of C_{ss} and C_{ll} for different values of packing density.	Section 4.7 Pages 119 - 120	C_{ss} and C_{ll} are both said to decrease when decreasing the quantity of respectively small or large spheres, but following different lines. The value of C_{ss} stays large at first and then drops at lower densities, while the value of C_{ll} drops quickly and stays low. This behaviour becomes more marked for larger size differences.
	d.5 Bidisperse Packings. C_{ll} – Number of contacts between a large sphere and other large spheres.			

Parameter	**Case Description**	**Analysis Results**	**Location**	**Notes from Literature**
Relative Distribution of Partial Coordination Numbers Distribution $f(C_{ij},C_{ik})$ of the values of C_{ij} for a given value of C_{ik}, where: i = small, large, j = small, large, k ≠ j.	e.1 Relative distribution of small spheres on a small one. Can be indicated as a function of C_{ss} and C_{sl}, $f(C_{ss},C_{sl})$. For instance, $f(C_{ss},2)$ is the distribution of the number of small spheres in contact with a small sphere if 2 large spheres are also touching it.	It can be shown that all the different $f(C_{ij},C_{ik})$ can be described by the same function if C_{ij} is transformed in $C_{ij}'(C_{ik})$: $f(C_{ij},C_{ik})\rightarrow f'(C_{ij}')$ The transformation $C_{ij} \rightarrow C_{ij}'$ is based on the concept of disturbance caused by a large sphere on an arrangement of small ones. $f'(C_{ij}')$ is a normal distribution whose mean and standard deviation are found to be a logarithmic function of the size ratio between the considered spheres and the central one. We call $f'(C_{ij}')$ "Characteristic Distribution" of j-type spheres on an i-type one.	Section 4.7 Page 128	Not mentioned.
	e.2 Relative distribution of small spheres on a large one. Can be indicated as a function of C_{ls} and C_{ll}, $f(C_{ls},C_{ll})$. For instance, $f(C_{ls},2)$ is the distribution of the number of small spheres in contact with a large sphere if 2 large spheres are also touching it.		Section 4.7 Page 135	Not mentioned.
Superficial Distribution of Contact Points A measure of the evenness of the distribution of the contacts on the surface of the central sphere: $D=V_{vmin}/V_v$ where	f.1 Clusters. Cumulative distribution of D calculated for each value of coordination number larger than 3.	In this condition of perfect randomness, the analysis of the particular case of superficial distribution when D = 0 (uncaged particles) was used to estimate the value of the caging number for equal spheres (see point b.1). The cumulative distributions of D referring to 4, 5, 6 and 7 contact points can be described as exponential functions of D.	Section 5.2 Page 146	Not mentioned.

Parameter	**Case Description**	**Analysis Results**	**Location**	**Notes from Literature**
V_v is the volume of the Voronoi cell generated by the touching neighbours; V_{vmin} is the minimum V_v.	f.2 Bidisperse. Each particle is extracted from the packing together with its same-sized touching neighbours and then the volume of the Voronoi cell of this cluster is calculated.	In all cases, the cumulative frequency of D can be expressed with good accuracy for each value of coordination number as an exponential function of D. The percentage of uncaged configurations found for each given coordination number always increases when the amount of considered spheres (small or large) decreases in the packing.	Section5.3 Page 154	Not mentioned.
Radial Distribution Function Probability distribution $g(r)$ of finding the centre of a particle in a given position at distance r from a reference one.	g.1 Monodisperse (simulated). Brief analysis of $g(r)$ for the simulated monodisperse packings to verify the procedure against the literature examples.	The result agrees with the literature.	Section 6.1 Page 157	$g(r)$ presents peaks at $r = d, 2d, 3d \ldots$. These peaks suggest the presence of determinate structures between the particles.
	g.1 Monodisperse (real). By means of the x-ray CT equipment a monodisperse packing of glass beads has been studied. The specimen has been reconstructed numerically and $g(r)$ was calculated. packings to verify the procedure against the literature examples.	Despite the various inaccuracies that have affected this part of the research in the phase of data acquisition and during the sample numerical reconstruction, the resulting $g(r)$ was found to be in extremely good agreement with the simulated one (g.1).	Section 7.3 Page 183	

Parameter	**Case Description**	**Analysis Results**	**Location**	**Notes from Literature**
	g.3 Bidisperse. In order for the results to be comparable to the existent researches, each bidisperse packing has been divided in two monodisperse packings, which have then been treated separately.	The new functions display features that clearly suggest the formation of structures between the two types of spheres. The analysis of $g(r)$ for the small spheres packings with different densities allows us to say that, in a packing of single-sized spheres, the inclusion of a given quantity of larger spheres will affect the original structure by distorting it on a "local" level, i.e. very close to the original spheres, yet decreasing $g(r)$ less than what would be expected on the basis of the respective packing densities. On the other hand, the "long distance" relationships between the original spheres will not be distorted but only "scaled" proportionally to the reduced quantity of small spheres relative to the total solid volume.	Sections 6.2 – 6.3	Not mentioned.

As can be seen from Table 17, so far were presented a large number of findings, some of which are probably more important and interesting than others. In particular, the following section shows how some of those results regarding the coordination number in bidisperse packings can be used to fill the gaps of knowledge that have remained after the first analysis discussed in the previous chapters. The ultimate aim of this part of the research is to provide a way to estimate the distribution of partial coordination numbers in a packing of spheres of two different sizes for which are given the respective quantities and the size ratio. **This aim will be identified as the MAIN TASK.**

8.2 Estimation of partial coordination numbers in bidisperse packings.

Although Chapter 4 concluded that it has not been possible to describe relative distributions of large spheres due to the problem of defining the disturbance created by the addition of a small sphere (see Chapter 4, section), using the results collected so far we can now show how to overcome this problem and close this gap of knowledge.

Considering points d.4, d.5, e.1 and e.2 from Table 17, the known aspects of the MAIN TASK are:

1. Total distribution of self-same partial coordination numbers of small spheres on a small one (Css) as a function of packing density and size ratio, $F(Css)$.

2. Total distribution of self same partial coordination numbers of large spheres on a large one (Cll) as a function of packing density and size ratio, $F(Cll)$.

3. Relative distribution of partial coordination numbers of small spheres on a small one (Css) as a function of size ratio and number of large spheres on the same small one (Csl), $f(Css, Csl)$.

4. Relative distribution of partial coordination numbers of small spheres on a large one (Cls) as a function and size ratio and number of large spheres on the same large one (Cll), $f(Cls, Cll)$.

To achieve a complete view of all the partial coordination numbers within the packing, we also need to know the self-different ones:

- MAIN TASK .a - Distribution of partial coordination numbers of small spheres on a large one (Cls), $F(Cls)$.
- MAIN TASK .b - Distribution of partial coordination numbers of large spheres on a small one (Csl), $F(Css)$.

MAIN TASK .a and MAIN TASK .b can be calculated from the previously defined distributions (1-4) considering the initial definition of relative distribution of partial coordination numbers. In both cases the process has the form of a weighted average of the relative distributions: in the first case we know the relative distributions and their weights and we just have to perform the weighted average; in the second case we know the relative distributions and the result of their weighted average, therefore we need to calculate the correct weights.

Case MAIN TASK .a.

In this first case, the unknown **total distribution of Cls** is a linear combination of the known **relative distributions of Cls for each value of Cll**, where the coefficients of the linear combination are the known **occurrences of each value of Cll**, i.e. the distribution of large spheres on a large one, Cll.

There are, therefore, as many equations as there are values of Cls, i.e. Clsmax.

$$\sum_{i=0}^{Cll\max} F(i) \cdot f(Cls, i) = F(Cls) \qquad (30)$$

for $Cls = 1, 2, \ldots, Cls\max$

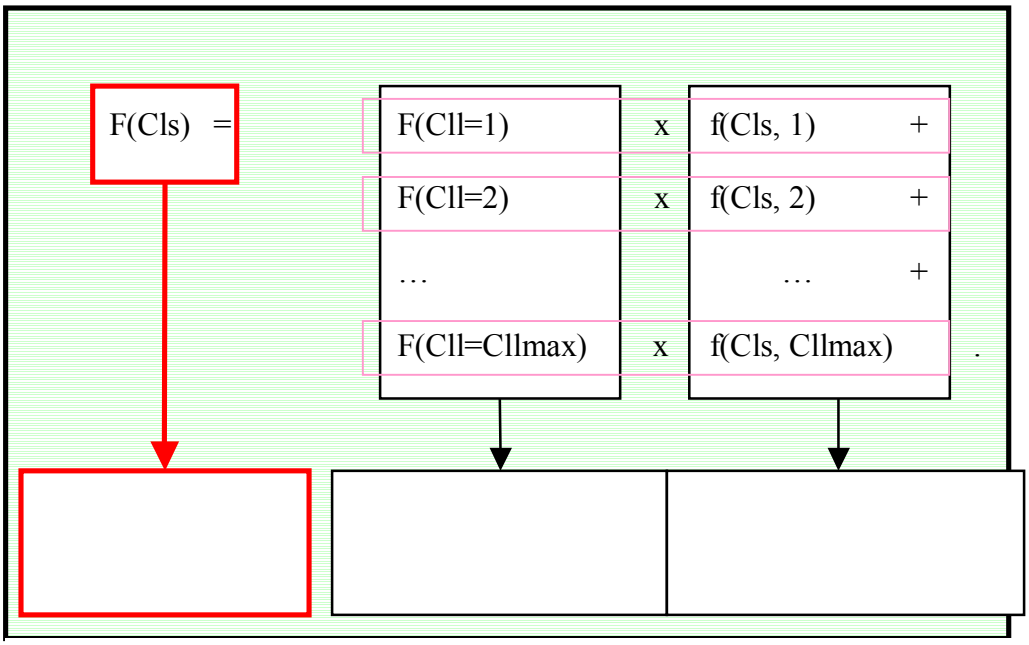

Figure 8-1 MAIN TASK .a - Estimating the distribution of Cls

Figure 8.1 shows one of the equations, delivering the value of F(Cls) for a particular Cls. To obtain the full distribution of F(Cls) we have to solve one equation (30) for each value of Cls.

Case MAIN TASK .b.

In this second case, the known **total distribution of Css** is a linear combination of the known **relative distributions of Css for each value of Csl**, where the coefficients of the linear combination are the unknown **occurrences of each value of Csl**, i.e. the distribution of large spheres on a small one, Csl.

There are, therefore, as many equations as there are values of Css, i.e. 12.

$$\sum_{i=0}^{Csl\max} F(i)\cdot f(Css,i) = F(Css) \qquad (31)$$

for $Css = 1,2,\ldots,12$

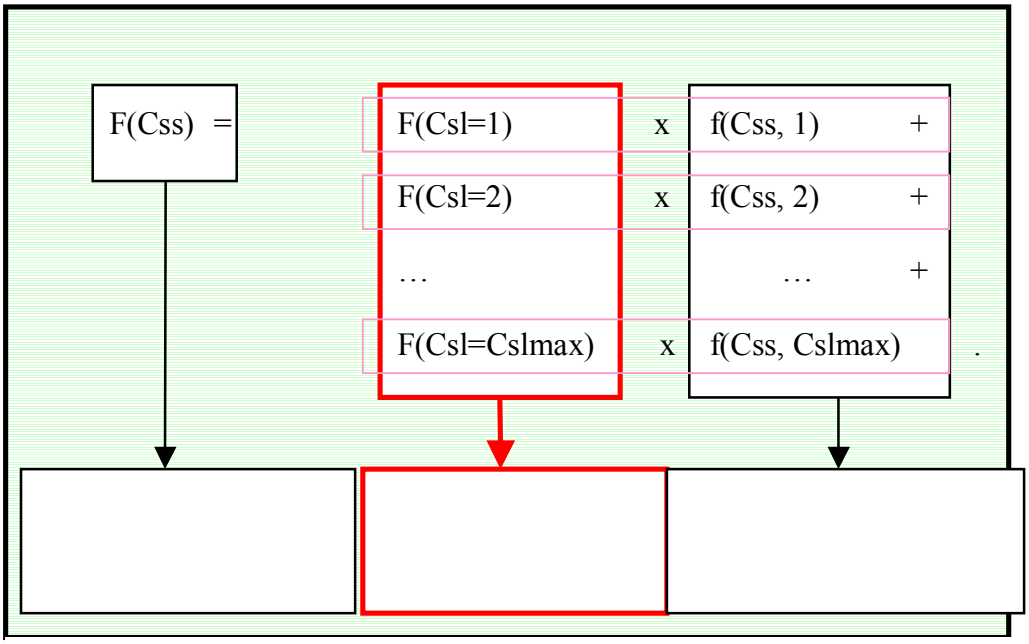

Figure 8-1 MAIN TASK .a - Estimating the distribution of Cls

Figure 8.2 shows one of the 12 equations. In this case we have 12 equations and Cslmax unknowns. Considering that a corollary of Kepler's conjecture is that Cslmax (maximum number of large spheres around a small one) is necessarily less than (or equal to) 12, it is possible to conclude that MAIN TASK .b will have $\infty^{12-Csl\max}$ sets of solutions. This can be narrowed down considering that the correct set of solutions is supposed to follow a normal distribution (or at least its non-negative part), therefore, amongst all the possible solutions, will be chosen the set that follows a normal distribution and best fits the system of 12 equations.

Figures 8.3 – 8.6 represent this process. In the first case explained earlier the problem is to find the weights in Figure 8.4 to transform Figure 8.3 in Figure 8.5 so that the total of the distributions in Figure 8.5 corresponds to known distribution in Figure 8.6, while in the second case considered the aim is to calculate the total distribution in Figure 8.6 adding together the relative distributions in Figure 8.5 obtained multiplying the distributions in Figure 8.2 by the weights in Figure 8.4.

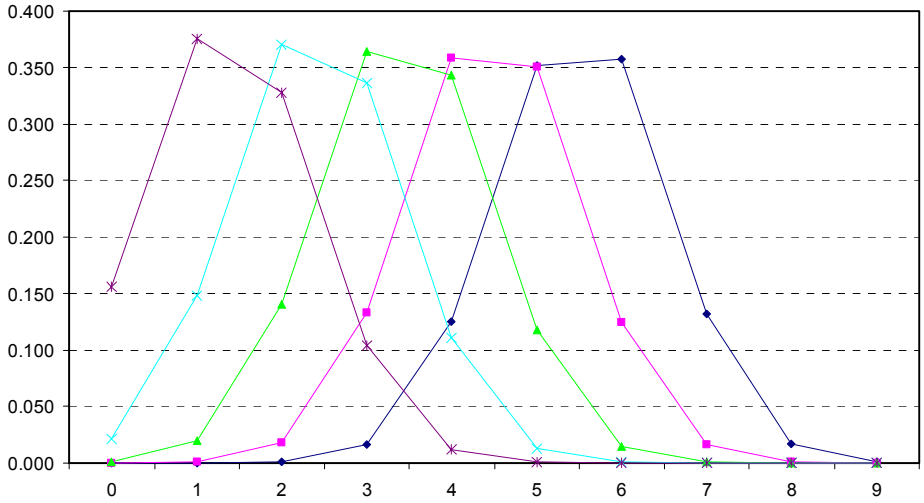

Figure 8-3 Normalised relative distributions

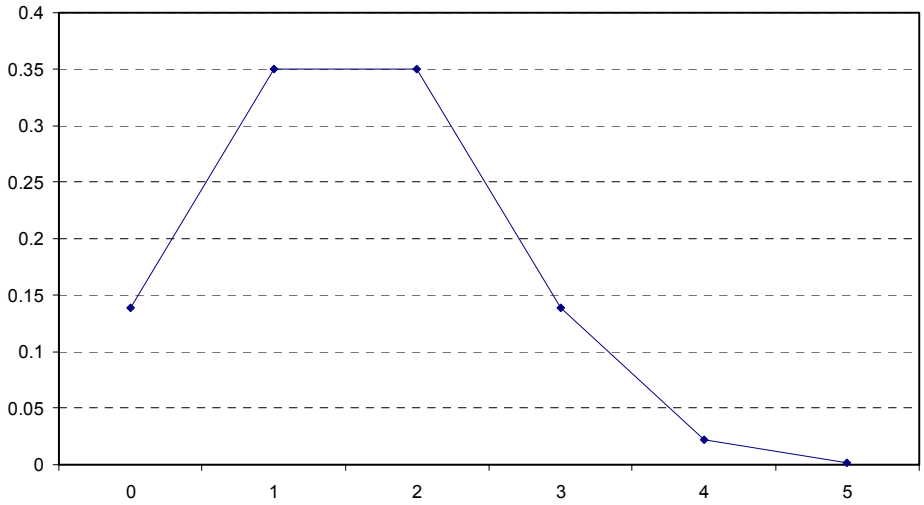

Figure 8-4 Weights of the normalised relative distributions

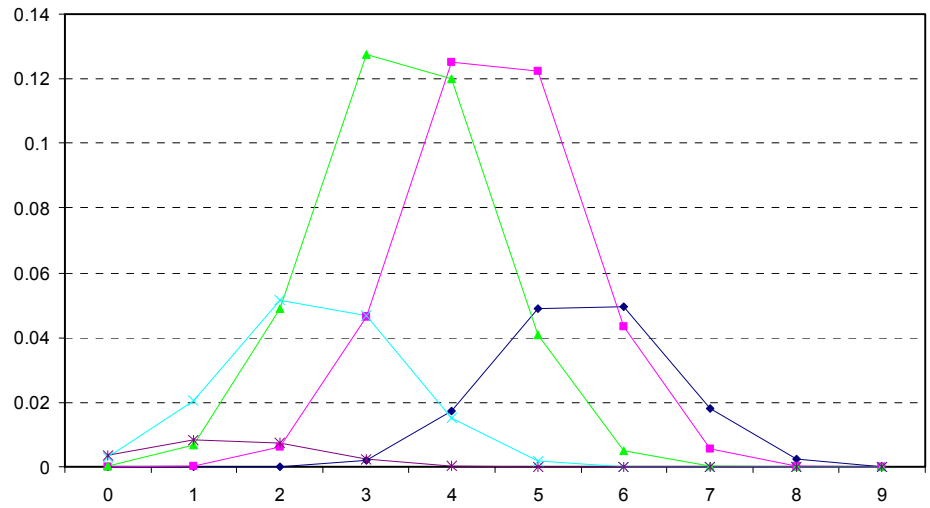

Figure 8-5 Weighted relative distributions

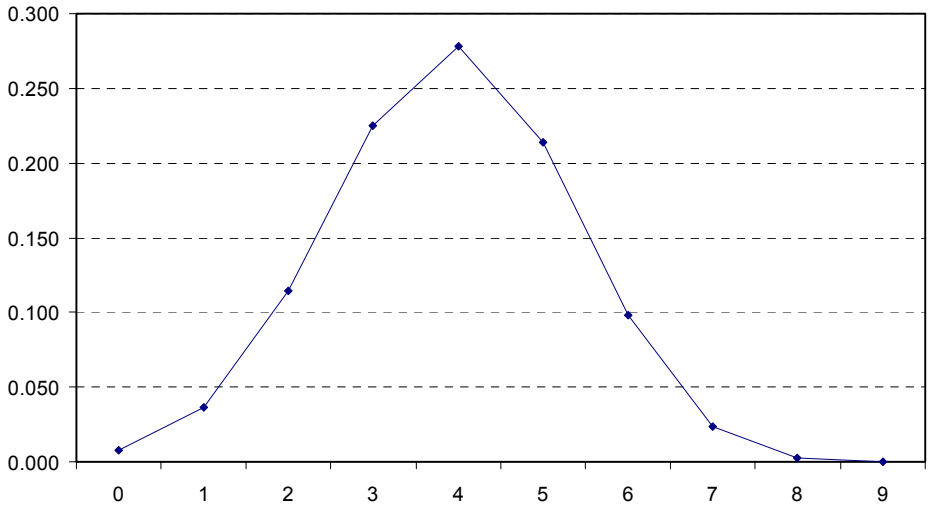

Figure 8-6 Total distribution, sum of the weighted relative distributions

A numerical example in Appendix J shows how to apply these concepts in practice.

9 CONCLUSIONS

9.1 Introduction

The granular form is one of the most common structures that materials of any type can assume in nature, therefore it is not surprising to find that they have been studied for centuries in many different topic areas. In general, they are usually treated as spheres (since many natural materials are, approximately, spheres and this shape is easier to analyse than others) and their properties are derived from observations on large packings of particles. Moreover, the recent introduction of Discrete Element Modelling (DEM) has brought even more interest on this subject, showing that packings of spheres are a general tool that can be used, with the right assumptions, to model almost any other physical structure (see Chapters 1 and 2).

In recent years, the development of techniques of computer modelling and constantly increasing analytical capacity have opened new frontiers for these studies, allowing researchers to simulate large quantities of these particles (sometimes millions of spheres) and to describe their behaviour with a much greater level of detail. This has helped overcome (or has reduced) some problems related to physical experiments, such as the

limited sample size and the elusive definition of "contact" between two particles.

From an engineering point of view, the most basic geometrical parameters that are generally used to describe these packings are coordination number and packing density, the latter being also represented at a more local level by the Radial Distribution Function (see Section 2.3 and Chapter 6). The literature review presented earlier (Chapter 2) shows that these parameters have been widely investigated for monodisperse packings, while the extent of knowledge concerning packings formed by two (bidisperse) or more (polydisperse) types of spheres is surprisingly limited.

Diversity between particles within a granular material can be for reasons of geometry, physical characteristics, chemistry or any other possible type of property. For this reason, it would be extremely useful to be able to describe how the parameters of engineering interest, such as packing density and coordination number, are affected by the interaction between particles of different types.

An apparently simple and fundamental question such as "how many contacts will a sphere of type A have with spheres of type B in a given packing" could not be satisfactorily answered by the literature reviewed, which seemed to contain fragmentary and, in many cases, superficial pieces of information. Therefore, contributing to this subject was set as the main aim of this PhD research, keeping in mind that delivering a better

insight into the topic would constitute an important base for future developments.

9.2 Investigation

Several different algorithms have been employed to simulate four different types of packing:

- Clusters of equal spheres;
- Monodisperse packings;
- Monodisperse "sticky" packings;
- Bidisperse packings.

In addition, the bidisperse packings algorithm can be used for polydisperse ones. Although the main subject area of this research is the investigation of bidisperse packings, some interesting observations have been made on the results from the other algorithms that, in the Author's opinion, reinforce and extend the knowledge in the area, and help to consolidate and develop the approach adopted for the main subject.

In relation to the various packings encountered, the parameters that we focused on are:

- Packing density;
- Coordination number;
- Superficial distribution;
- Radial Distribution Function.

Finally, it has been considered of interest to try to relate, to some extent, the simulated packings to a real one by means of X-ray tomography equipment in order to investigate the potential of the new analytical approaches described in this thesis and the new X-ray technique.

9.3 Results

This research has delivered a large number of notable points, as listed in Table 17 in Chapter 8. Some of them can be considered minor observations that do not need further attention, others are more significant and on which some final comments are warranted.

As shown in the discussion in Chapter 8, the results obtained allow us to draw a complete picture of coordination number in bidisperse packings. The introduction of the relative distributions of partial coordination numbers, and their normalisation by the concept of "disturbance" caused by a large sphere on a superficial distribution of small spheres, has shown that, underlying the various distributions of partial coordination numbers there always lies the same concept, here called "Characteristic Distribution". This is a normal distribution whose mean and standard deviation are found to be logarithmic functions of the size ratio between outer and central spheres.

The characteristic distribution seems to be a geometrical property of spheres and is almost (though see below) independent of the packing considered. In other words, it describes at the same time all the different *relative* distributions of partial coordination numbers of B-spheres on an A-sphere, independently from other spheres that may also be on the same A-sphere. The actual *total* distribution of partial coordination numbers will

then depend on the distribution of the number of disturbing spheres, that may differ for the various packings (this is when the packing composition plays a role in defining the distributions of *total* partial coordination numbers).

If we compare the level of detail and understanding provided by this concept and what has been found in the studies reviewed in Chapter 2 (that, at best, went as far as describing the general behaviour of the *total* distributions of partial coordination numbers) then the importance of the contribution of this research is evident. The characteristic distributions of small spheres on the surface of a small and of a large sphere represent the missing link between self-same and self-different partial coordination numbers, showing how the four of them (C_{ss}, C_{sl}, C_{ls} and C_{ll}) influence each other. Without the identification of a characteristic distribution and without the estimation of spheres' mutual disturbance (referred in this document as the "Three Spheres Problem") these different coordination numbers would appear to behave according to their own patterns, whereas it is now clear that a more general and unifying concept rules the complex structure of bidisperse packings.

The characteristic distributions have been obtained applying transformation B2, which was introduced in Chapter 4. All the components of this formula are functions only of spheres sizes, except for the modified parking number Pij', which was used to optimise the model and seems to be a function of the packing's composition. This is the only parameter that can not be

calculated from the sphere sizes alone, but which needs the actual packing composition to be specified.

The physical meaning and the significance of this parameter would need to be investigated further before reaching any conclusion about it, but some considerations can be made here to stimulate future investigation. Parking number has been found during this research to correspond, for the monodisperse case in isotropic conditions, to the 94th percentile of all the possible values of coordination number or, according to its definition, to the maximum coordination number that is likely to be reached. It would seem that the optimisation of transformation B2 requires this parameter, in the case of small spheres within a bidisperse packing, to decrease with packing density, therefore indicating that the number of small spheres that are likely to be placed on a central one is, for some reason, decreasing, even if the central small sphere is not touched by any large one. One explanation could be an effect of some "long distance" disruption caused by the presence of some large spheres within the small spheres' structure but at some distance from the sphere being considered. Thus, this observation would suggest the connection in Figure 9.1.

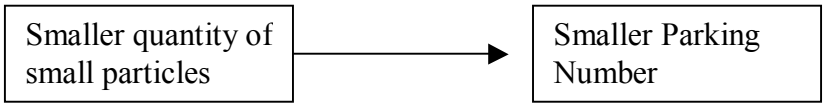

Figure 9-1 Connection between parking number of small particles and quantity of small particles suggested by the analysis of coordination number in bidisperse packings

Nonetheless, this reasoning would seem to contradict the observations concerning the superficial distribution of contact points (Chapter 5). The analysis of the superficial distribution of contact points has shown quite clearly that for each value of coordination number the proportion of small particles that can not be caged solely by other small particles tends to increase when decreasing the percentage of small particles in the packing. As discussed earlier in this thesis (Section 4.2 and Chapter 5), uncaged configurations of small particles on a small one happen when the outer particles are not evenly distributed. Intuitively, one could argue that the less evenly distributed are the outer spheres, the more likely they are to be in an arrangement that leaves space for more small spheres to be placed. This would, therefore, correspond to a superficial configuration that, if it wasn't for the presence of the large spheres, would tend to reach larger coordination numbers (Figure 9.2).

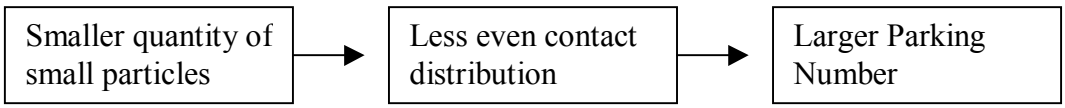

Figure 9-1 Connection between parking number of small particles and quantity of small particles suggested by the analysis of superficial distribution of contact points in bidisperse packings

The results about superficial distribution of contact points also supplied interesting information about the degree of interaction between the two types of particles in the packing. As observed earlier, the fact that a particle can not be caged by its same-size neighbours (self-uncaged) means that it has to rely on one or more particles of the other type to be stabilised and to,

eventually, transmit contact forces. The total percentage of number of self-uncaged particles of a given type could be taken as a measure of the "dependence" of this type of sphere on the spheres of the other type. In this sense, it could be interesting for future research to study the stress distribution within the packing for different degrees of interdependence between sphere types, or to investigate the effects of maximising this interdependence by varying the packing composition.

Another finding of interest arises from the analysis of the radial distribution function relative to each sphere type in bidisperse packings. This analysis has shown that large spheres affect the structure of the small ones mainly at a long range, while at a shorter range the presence of a large sphere is, in average, less "invasive". This is due to the fact that, although for this research the used size ratios of ½ and ¼ are both larger than the Apollonian limit, the small particles tend to form monodisperse "colonies" occupying the voids within the large particles. The particles that are in the inner part of these colonies are, effectively, within a monodisperse packing influenced by the "wall effect" caused by the large particles. For geometrical reasons, the inner particles tend to be much more numerous than the particles that are at the colony's border, which are the only ones actually in contact with large particles. As an average, therefore, if we consider a small particle it is very likely that it will be positioned somewhere inside the colony rather than at its border. At a short radial distance from this considered particle there will be mostly other small particles, but as the distance increases it becomes more likely that a large

sphere will be found within this distance. When the radial distance is such that even the very central particles of the colony are being related with particles outside the colony, i.e. this radial distance is larger than the "size" of the colony, the radial distribution function, which is a local measure of density, will be perfectly scaled according to the average packing density, because between the particles of one colony and the particles of other colonies there will be the space occupied by a representative number of both small and large spheres. This effect becomes even more evident as the size ratio decreases, because the colonies of small spheres become more populous for a given zone between large spheres.

Since the radial distribution function represents the average density at a given distance from each particle, this study can be particularly useful when the parameters or properties of interest are directly related to local density values, as it would possible to infer that they should follow a behaviour similar to that of the radial distribution function. As a practical example, if the small spheres were magnets and the large spheres were not, the radial distribution function of the small spheres as defined in this study would allow us to calculate the average magnetic field to which each small sphere would be subject, as it defines the probability of finding the centre of another small sphere (in this case, a magnet) at each radial distance from the original (probe) one. In a similar way, the same concepts could be applied to study problems of gravitational fields, electric conductivity, heat transfer etc.

Finally, although in this research the main effort has been directed to the simulation and analysis of bidisperse packings, it has been recognised that it is important from an engineering point of view to try to relate, even at this early stage, the modelling to the real world. This has been achieved in two ways: simulating monodisperse packings of frictional spheres and studying a real monodisperse packing of approximately spherical particles.

In the first case, both friction and dilution were shown to affect the coordination number of the particles of a monodisperse packing, and a procedure was developed to allow their combined effects to be separated and taken into account to better estimate the coordination number of real particles. As a point for future research, it would be extremely interesting to calibrate and verify this procedure by means of accurate measurements of coordination number in real packings and to extend this approach to bidisperse packings, although in this case some modifications might be needed in the algorithms developed in this study so far.

The second case involved x-ray tomography equipment to scan a reasonably large sample of spherical particles of constant nominal size. The assemblage was numerically re-constructed to determine the three-dimensional position of the centre of each particle. Due to the various types of approximations that have been shown to affect the different stages of this technique, it was decided, for this experiment, to focus on the analysis of the radial distribution function rather than coordination number. The comparison between radial distribution function for the re-constructed

sample and for a monodisperse packing simulated with the new algorithm of Chapter 4 shows a very high level of agreement. This gives confidence in the reliability of the numerical procedures on which this research has been built. Moreover, although it was not possible to apply this technique to real bidisperse packings due to time limits, the observed consistency of the behaviour of the radial distribution function between simulated monodisperse and bidisperse packings and the common concepts behind the various algorithms suggest that a similar level of reliability can be expected of the analyses performed on the more complex structures. Therefore, the results reported in this thesis on the basis of numerical models should, to a large degree, be representative of what really happens in nature.

Although the algorithms employed in this research have delivered values of coordination numbers that are in good agreement with the previous literature for the monodisperse and bidisperse cases, it should be kept in mind that different algorithms can, and are expected to, deliver slightly different values, depending on the final packing density reached and the packing process adopted. The comparison made between "sticky" and "diluted" monodisperse packings (see Chapter 4) is a clear and extreme example of how packings with the same densities can have very different average coordination numbers because they were created with different algorithms. The results presented in the previous chapters should, therefore, be considered from a conceptual point of view rather than a strictly numerical one. The fact that a reasonable theoretical basis could be

provided for all the major findings reported is a symptom that these observations could be extended to other packings (i.e. different size ratios, polydispersity, different packing densities, different algorithms and, maybe, slightly different particle shapes), but a large amount of research (at least as much as has already been done) would be needed for this further validation.

9.4 Summary of Findings

In summary, therefore, this research study has delivered:

1) A procedure for the estimation of the disturbance caused by a c-type sphere on a distribution of b-type spheres on the surface of an a-type sphere;

2) Algorithms for the simulation, in Excel and Matlab, of clusters of spheres of same size, large monodisperse packings of frictionless and frictional spheres under gravity, large bidisperse and polydisperse packings of frictionless spheres under gravity;

3) A parameter that describes the superficial distribution of contact points on a particle;

4) A procedure for the estimation of coordination number in real assemblies of spherical particles of same size;

5) Understanding of the general physical relationships between the four partial coordination numbers (C_{ss}, C_{sl}, C_{ls} and C_{ll}) through the introduction of original concepts such as:
    a. Disturbance between particles as reported in 1);
    b. Relative distributions of partial coordination numbers;

c. Characteristic distribution of partial coordination numbers;

6) A model that estimates the statistical distribution of the partial coordination numbers as a function of size ratio and grading applying the novel concepts reported in 5);

7) A study of the long-distance relationships between particles in bidisperse packings showing how the space around small particles is affected by the presence of large particles;

8) A simple procedure for the numerical re-construction of a packing of spherical particles scanned with an X-Ray CT equipment for comparison between simulated and real data.

9.5 Recommendations for future work

The research presented in this PhD thesis has touched some of the main points of interest in this subject, delivering observations that could not have been foreseen *a priori*. The topic area involved is so wide that future work can be undertaken on a large number of subjects, some of which would extend this work to a wider range of cases, others have been indicated in the earlier part of this chapter and derive from the conclusions.

Future research that falls into the first group would aim to validate some of the concepts expressed here considering, for instance, a wider range of size ratios, sticky bidisperse packings, polydisperse packings and refined use of x-ray tomography techniques. Most of these studies would certainly be time-consuming but, on the other hand, would have the advantage of re-using most of the algorithms developed in this PhD.

The second group of possible future works would, instead, try to push the analysis more in depth into the subject, aiming to clarify some of the aspects that could not be taken any further in this research. In this sense, some points of great interest that derive from this study would be:

- Understanding the role of the modified parking number and its relationship with the change in superficial contact distribution observed for different packing compositions;

- Investigating the effect of different values of superficial contact distribution on the internal stress distribution within a particle, which might be related to the fracture probability of a particle;

- Investigating the importance of interdependence between sphere types in the stress distribution within a bidisperse packing for various packing composition, size ratios, material properties etc.

- Simulate the behaviour of porous materials using bidisperse packings where one sphere type is considered as voids;

- Study the probability of fracture of particles in bidisperse packings as a function of their coordination number and their superficial contact distribution.

A THREE SPHERES PROBLEM

In order to evaluate how a particle affects the position of the others on the surface of an inner one (Figure 3.8) and to estimate how much its presence disturbs their distribution we can identify two tasks:

TASK 1. Calculate the maximum possible number of spheres of type b and radius R2 that can be placed on the surface of the central sphere of type a and radius R1, $C_{a,b\,max}$.

TASK 2. Calculate how this number decreases due to the presence of a sphere of type c and radius R3 on the central sphere of type a and radius R1, $C_{a,b}{}^{c1}{}_{max}$.

A.1 Task 1

As one can see, the problem of kissing number for equal spheres is just a particular case of this wider concept.

The basic solution idea is the following: considering three spheres on the surface of a bigger one (Figure A.1a) and wanting them to be as close as possible to each other, obviously they will form an equilateral triangle each one of them touching the others. Thinking of the centres (Figure A.1b), we can see a tetrahedron formed by the three centres of the small spheres (base) and the centre of the big central sphere (vertex) as in Figure A.1c.

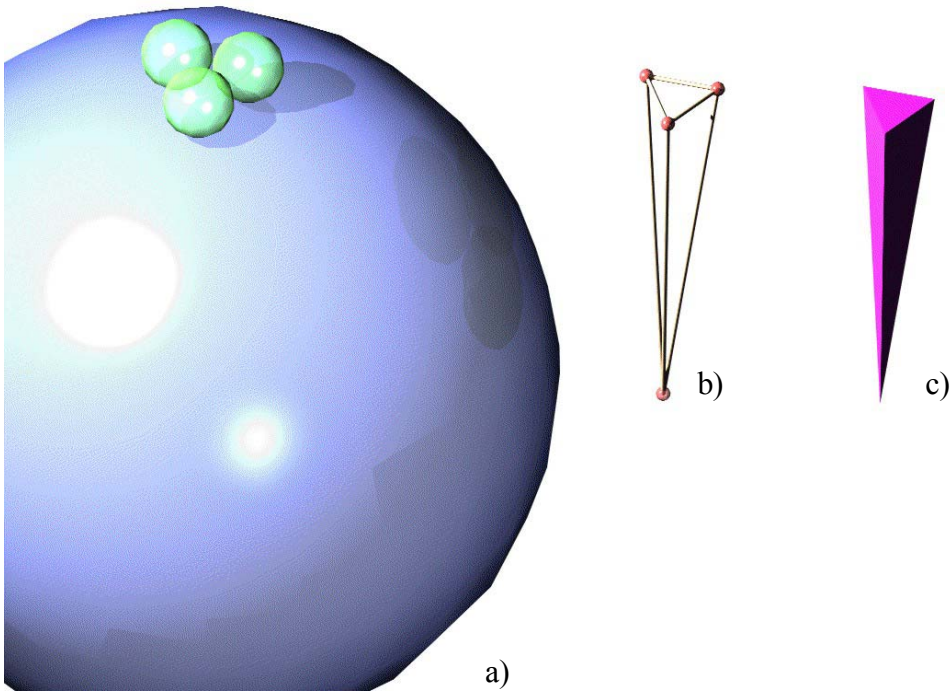

Figure A-1 Densest packing of three spheres around a central one

If this is the densest configuration for those three, we are looking for how many of these tetrahedrons it is possible to form around the central sphere. Thus, we have two different points to reach:

- given the radius of the central (R1) and outer (R2) spheres, number the triangles that can cover the sphere of radius R = R1 + R2 or, to state it another way, the tetrahedrons that can fill, with their upper vertex, a solid angle of 4π steradians;
- given the number of triangles/tetrahedrons, calculate the number of outer spheres that can generate it.

Counting the triangles

The first thing to do is to calculate the curved area of one triangle (Figure A.2a) as a function of the two radii R1 and R2, thus we need to use the non-Euclidean geometry.

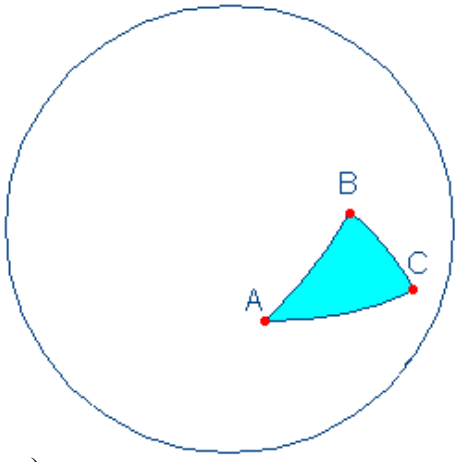

a)

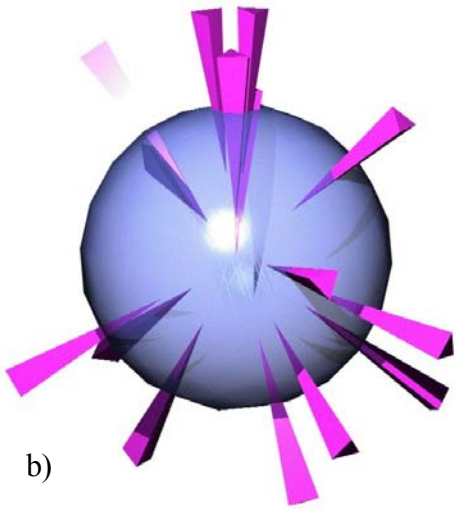

b)

Figure A.2 a) Curved area of the triangle; b) Volume of the tetrahedron

Once we know this area, we just have to divide the total area of the sphere by this to calculate the theoretical number N of allowable triangles. The procedure is exactly the same if we calculate the solid angle of the tetrahedron's vertex and then divide 4π steradiants by it as in Figure A.2b.

Counting the balls

For the second point of this section, we have to introduce the Euler's Theorem: it expresses the relationship between number of vertices (V), number of edges (E) and number of faces (F) of a regular solid:

$$V - E + F = 2 \tag{32}$$

Given that the solid having as vertices the outer spheres' centres can be considered "regular" as its faces are all identical equilateral triangles, we can use this theorem to calculate the number of vertices, V, it has just noting that its faces, F, must be N and its edges must be N*3/2 (each face has 3 edges, but each edge is in common between 2 faces), hence

$$V - \frac{3}{2}N + N = 2 \tag{33}$$

Verifying the algorithm for $C_{a,b\ max}$.

It has been possible to find two different checks for the suitability of this algorithm.

Proof N.1

If R1/R2 = 1 this algorithm indicates the availability of space for 13.4 spheres on the surface of the central one, and this leads to a theoretical maximum solid ratio of 0,78 (corresponding to the solid ratio of each tetrahedron). This number had already been found in 1958 by Rogers (in Aste & Weaire 2000) and has been used until recently as an upper bound for the kissing number of equal spheres: that is a good proof of the reliability of the general method, which is then able to produce an upper bound for each pair of dimensions in which we might be interested.

Moreover, it can be noted that this algorithm calculates the number of tetrahedrons needed to fill the given surface considering them as if they could really find a convenient geometrical arrangement. Therefore, given that as the ratio R1/R2 increases (i.e. as the outer spheres become smaller compared with the inner one) the configuration moves towards the plane state where the equilateral triangles are actually able to perfectly fit the surface, it could be reasonable to associate

the overestimation of the coordination number to the surface's curvature and assume that it rapidly loses significance increasing R1/R2 (see Figure A.3).

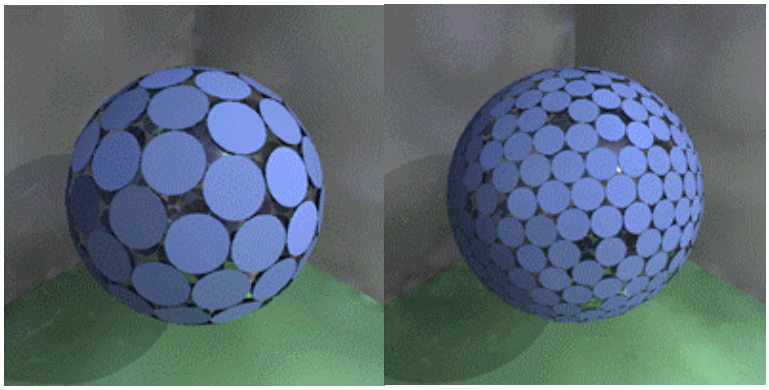

Figure A.3 Surfaces of larger curvature allow better superficial arrangements

Proof N.2

With this algorithm has also been possible to find the value of the ratio R1/R2 that reduces the kissing number to 4. This is the same as calculating the radius of the maximum sphere that can be fitted in the void inside a tetrahedron formed by 4 equal spheres of unit radius (Figure A.4). The result, 0.225, is confirmed by a geometrical construction:

$$R_1 = \frac{\sqrt{6}}{2} - 1 \approx 0.225 \tag{34}$$

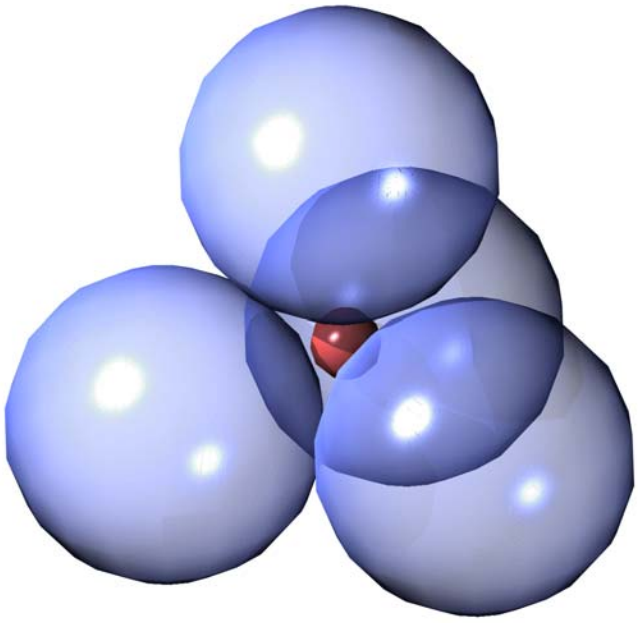

Figure A.4 Representation of the Apollonian limit

A.2 Task 2

After estimating the maximum possible number ($C_{a,b\ max}$) of spheres of radius R2 on the surface of a sphere of radius R1, this further algorithm calculates how this number decreases if another different sphere of radius R3 already lies on the central sphere (Figure A.5).

This has been done in the following steps:

1) Knowing $C_{a,b\ max}$, calculate the superficial density of b-type spheres on the a-type sphere's surface, D.
2) Calculate the curved area delimited by the b-type spheres around the c-type sphere on the a-type sphere's surface, A.
3) Calculate the number N_1 of b-type spheres that would fit in that area.
4) Calculate the number N_2 of b-type spheres that would delimit the Area A.
5) The number of b-type spheres that would remain can be calculated subtracting from the total the number of spheres that would have occupied the unavailable surface (Figure A.6a – A.6b) but considering that half of each spheres surrounding that area is actually still inside that area (Figure A.6c):

$$C_{a,b}{}^{c1}{}_{\max} = C_{a,b\max} - N_1 + N_2/2 \qquad (33)$$

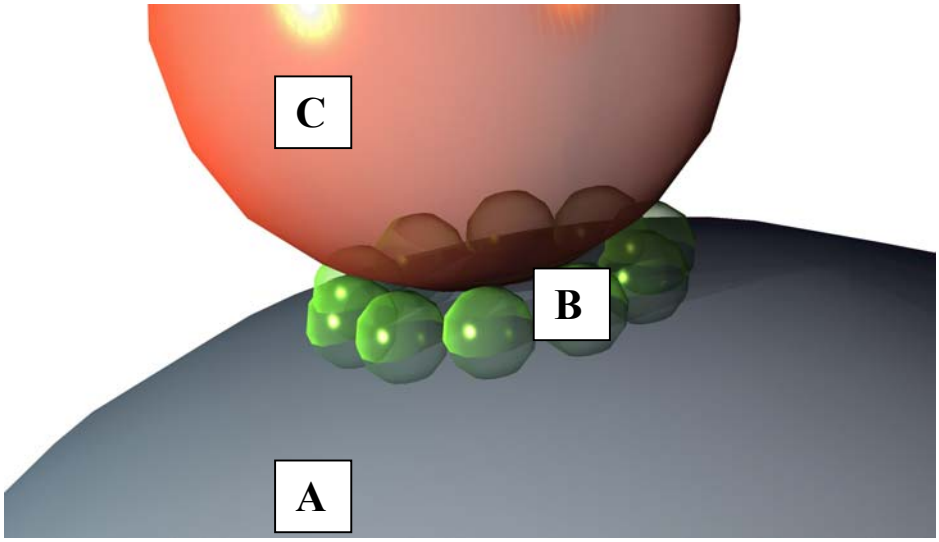

Figure A.5 Disturbance caused by the c-type sphere

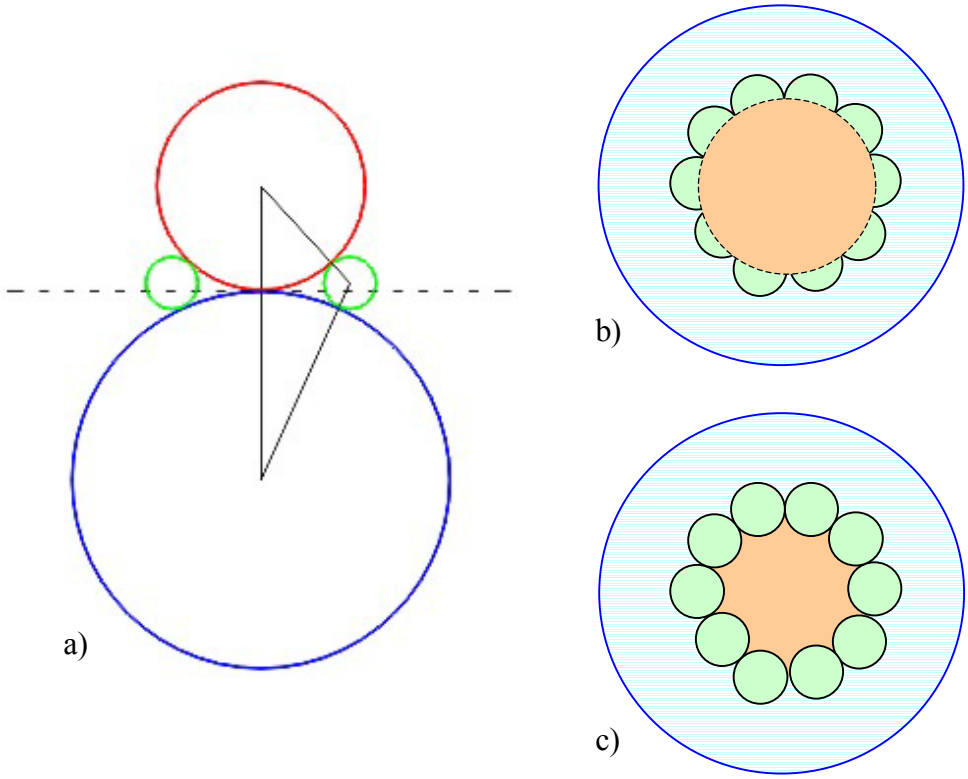

Figure A.6 Estimation of $C_{ab}^{C1}{}_{max}$

Although no references could be found in the existing literature about this particular topic, a good proof of the reliability of this algorithm is in this simple and intuitive observation: if R3 = R2, then it must be:

$$C_{a,b^{c1}\max} = C_{a,b\max} - 1 \qquad (34)$$

because one c-type sphere would subtract exactly the space of one b-type sphere. This algorithm reflects exactly this result therefore, subject to further confirmation, it is reasonable to think that is working properly.

B SPHERICAL GROWTH ALGORITHM

B.1 Introduction

The algorithm presented in this section represents an attempt to generate all the possible configurations of spheres around a central one of the same radius (clusters) in conditions of randomness and anisotropy. Each outer sphere is identified by its contact point with the inner one, expressed in a spherical coordinate system centred on the inner sphere by the angles θ (longitude) and φ (latitude). To randomly generate the position of an outer sphere, relative to the central one, means to produce a couple (θ; φ) indicating a kissing point on the surface of the central sphere. It is possible to demonstrate (Wolfram 2002) that a statistically uniform distribution for these points can be achieved with θ and φ being taken as follows:

$$\theta = 2\pi u \qquad (35)$$

$$\cos\varphi = 2v - 1$$

with u and v being random real numbers that vary between 0 and 1. It would be incorrect to select directly the spherical coordinates from the uniform distributions θ = [0, 2π] and φ = [0, π] because the points would be

weighted towards the "poles" of the inner sphere (relatively to the coordinate system).

In order for the configuration to be geometrically acceptable, the chosen contact point for the second (and subsequent) outer sphere must not permit the new outer sphere to overlap a previous outer sphere. The easiest way to check this condition is to impose that the chord distance between each pair of kissing points must not be less than one radius length (Figure B.1).

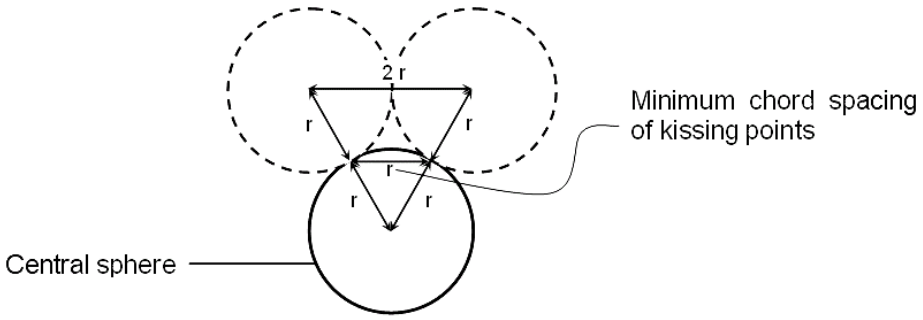

Figure B.1 Non-overlapping condition

There are, basically, two different algorithms to deal with this aspect, which are presented hereafter.

B.2 1st Spherical Growth Algorithm

Intuitively, the most direct way is to:

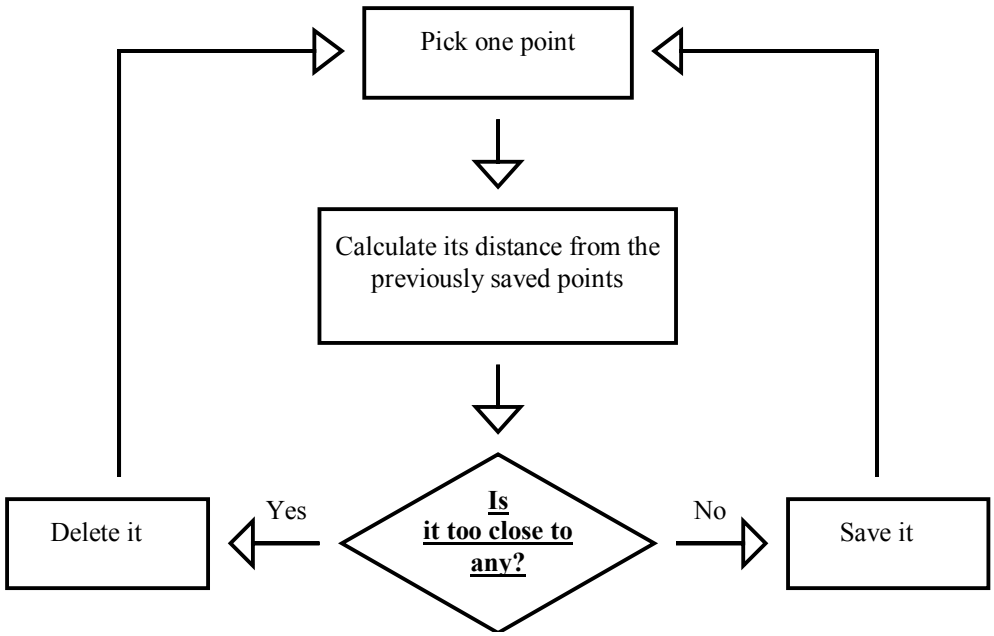

Figure B.2 First spherical growth algorithm

The simple algorithm in Figure B.2 has two weak points that make it unsuitable for this study. First: it does not know when to stop. As discussed in Section 2.4, the maximum possible number of spheres that may be placed (the "Kissing Number") is 12 (an observation often referred to as the "Kepler Conjecture" since it was first observed by Kepler (Pfender & Ziegler 2004; Sloane 1998; Plus Magazine 2003; University of Pittsburgh 1998). However, this number belongs to a situation when all the spheres are very well packed all together. Therefore, it is possible (and, as will be shown later, it is very likely to happen) that after having placed 8-9 spheres

randomly there is actually no physical way to place the 10th one, and this is perfectly acceptable. This first algorithm is not able to check this condition, thus it would go on forever trying to reach 12. Second: as the number of saved points increases, the number of attempts and the time to find the next acceptable coordination point increases greatly. This way, it was found that a normal computer would take a day for 8 points and a month for 9! Considering that the main target is to produce many thousands of configurations, this work would have taken centuries!

B.3 2nd Spherical Growth Algorithm

Instead of going on picking the points in the whole surface of the inner sphere as in Section B.2, it is much better to randomly pick each n^{th} contact point only in the surface which remains available after having placed the previous n-1 points (Figure B.3):

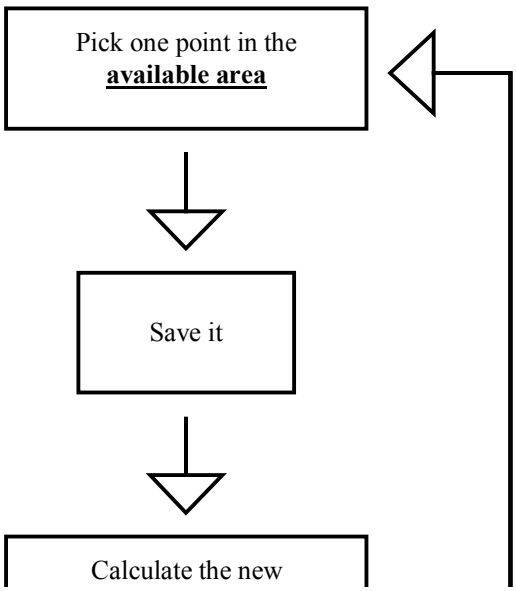

Figure B.3 Second spherical growth algorithm

In this way both the problems of the previous algorithm are solved. First: the program will run as long as there is still any available area on the sphere's surface, no matter what the number of placed spheres is. Of course, the maximum possible number is still 12, but we don't need to define this. Second: the algorithm doesn't need to make many attempts to pick a point, because it is just choosing it among the acceptable ones. Thus,

with this new algorithm the required time to produce a full configuration is always a fraction of a second.

Each placed sphere thus reduces the available area for subsequent coordination points (as shown in Figure B.4 for a 2 dimensional representation). Each new sphere placed will subtract (in the 2-D example) an angle equal to $1/3^{rd}$ of the total (i.e. $2\pi/3$ radians) from the available places where subsequent kissing may occur. The new angle subtracted is allowed to overlap as much as $1/6^{th}$ of the total (i.e. $\pi/3$ radians) with the angle subtracted by previously placed spheres (see Figure B.4c).

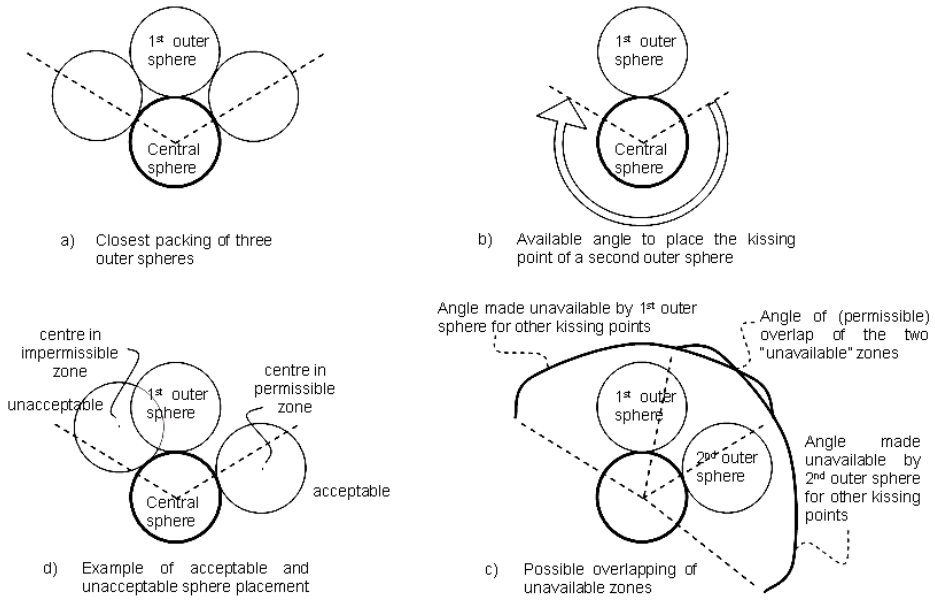

Figure B.4 Available surface for next spheres

Due to the transformation (1) introduced before, a relationship is established which uniquely links each polar pair (θ; φ) to the correct value

of the transformed pair (u; v). The sphere's surface can then be exactly represented in a u-v space as a square of unit side as shown in Figure B.5, where the shaded area is unavailable for the kissing point of the 4th outer sphere.

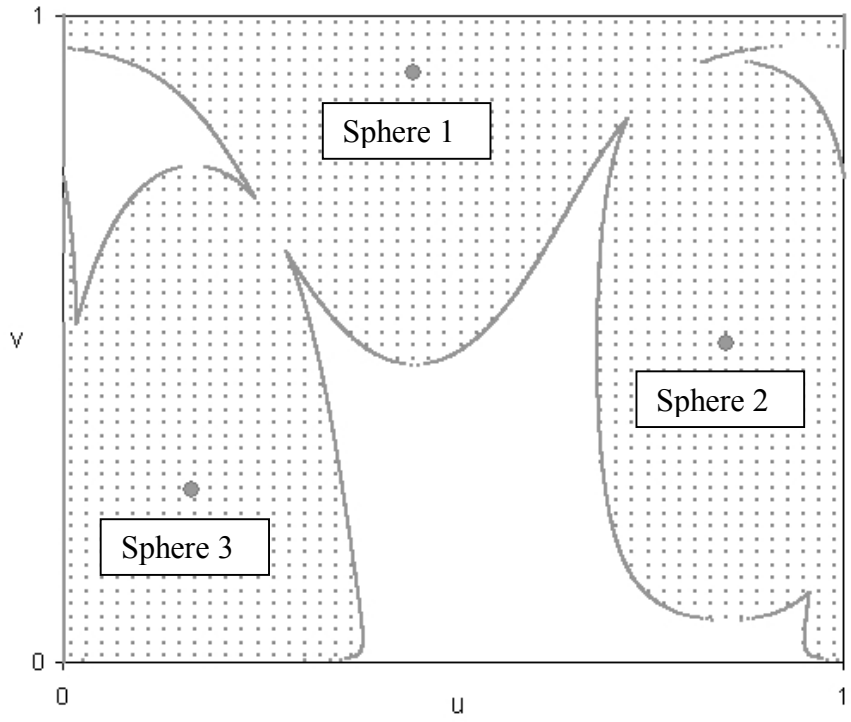

Figure B.5 Representation of the area occupied by three spheres on the surface of a central one on the u-v space

Moving from 2-D to 3-D the concept of available area does not change much: the angle becomes a cone around each ball and subtracts an area equal to 1/4th of the total but, of course, still allows overlapping (see sphere 2 and sphere 3 in Figure B.5). Having already taken into account all the necessary restrictions, every single white zone that remains, even the smallest one, is suitable for a further kissing point.

B.4 Development of a Cluster

In this section is given one result of this algorithm, graphically presented in the u-v space in Figures B.6 – B.10.

Table 18 Positions of subsequently placed spheres

No of spheres placed	1	2	3	4	5
φ	0,605882	1,586797	2,055561	2,896027	0,944683
θ	2,824826	5,338029	1,041890	2,775142	0,089266
X	0,541154	0,585541	0,446453	0,226964	0,807085
Y	0,177393	0,810485	0,763887	0,087105	0,072237
Z	-0,822	0,016	0,466	0,970	-0,586
SPACE	750,483	501,248	260,273	129,189	80,147

In this example 5 spheres are positioned. The first two lines in Table 18 give the values of the angles φ and θ for each contact point, which have also been transformed in the Cartesian coordinates X, Y, Z in the following three lines relatively to the centre of the central sphere with coordinates (0, 0, 0). The last line represents a measure of the remaining surface after placing each ball, having the "clean" surface a SPACE value of 1000. It is important to note how this number decreases adding the spheres: due to the increasing overlapping of the forbidden areas, the occupation rate slows down allowing 5 balls to fit. As the space number hasn't reach 0 yet, we also know that is possible to go on.

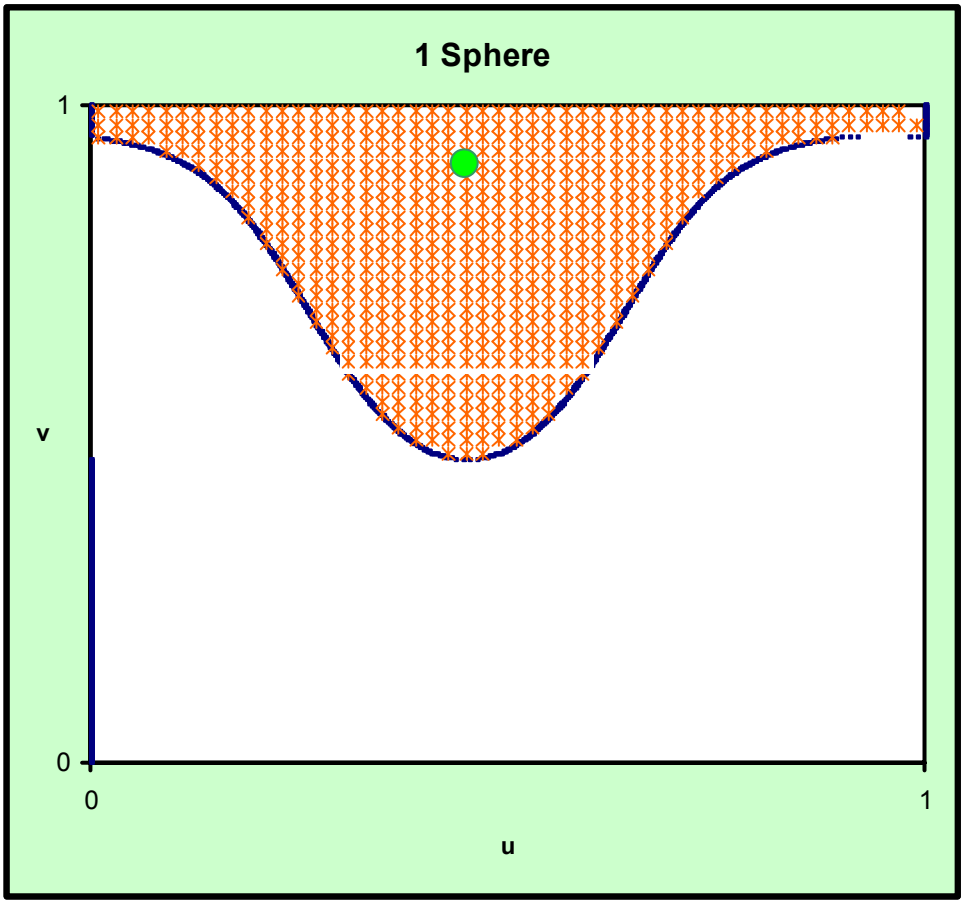

Figure B.6 Position of sphere 1

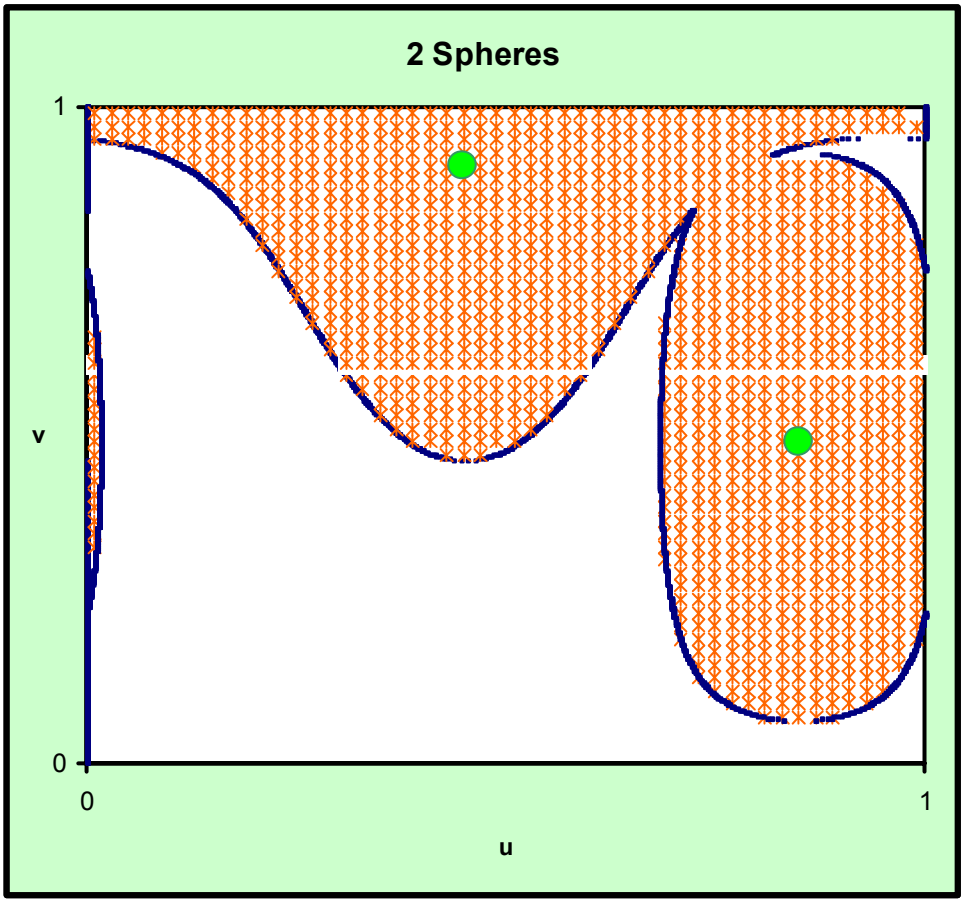

Figure B.7 Position of sphere 2

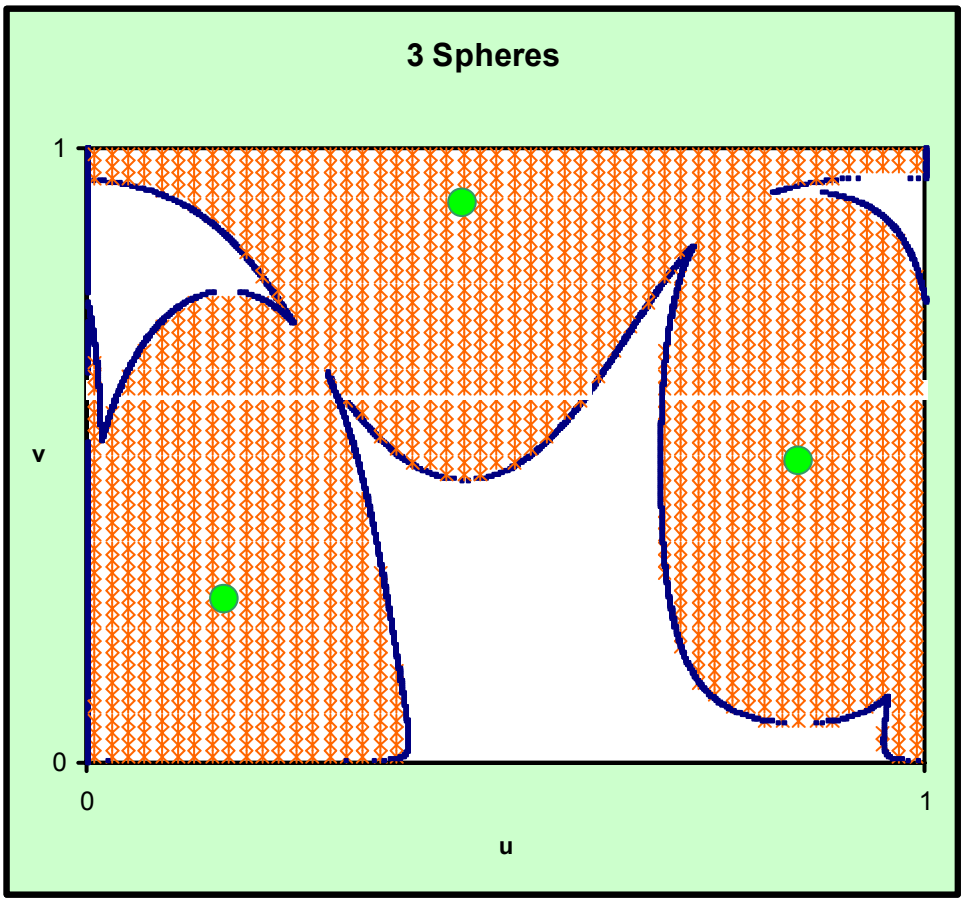

Figure B.8 Position of sphere 3

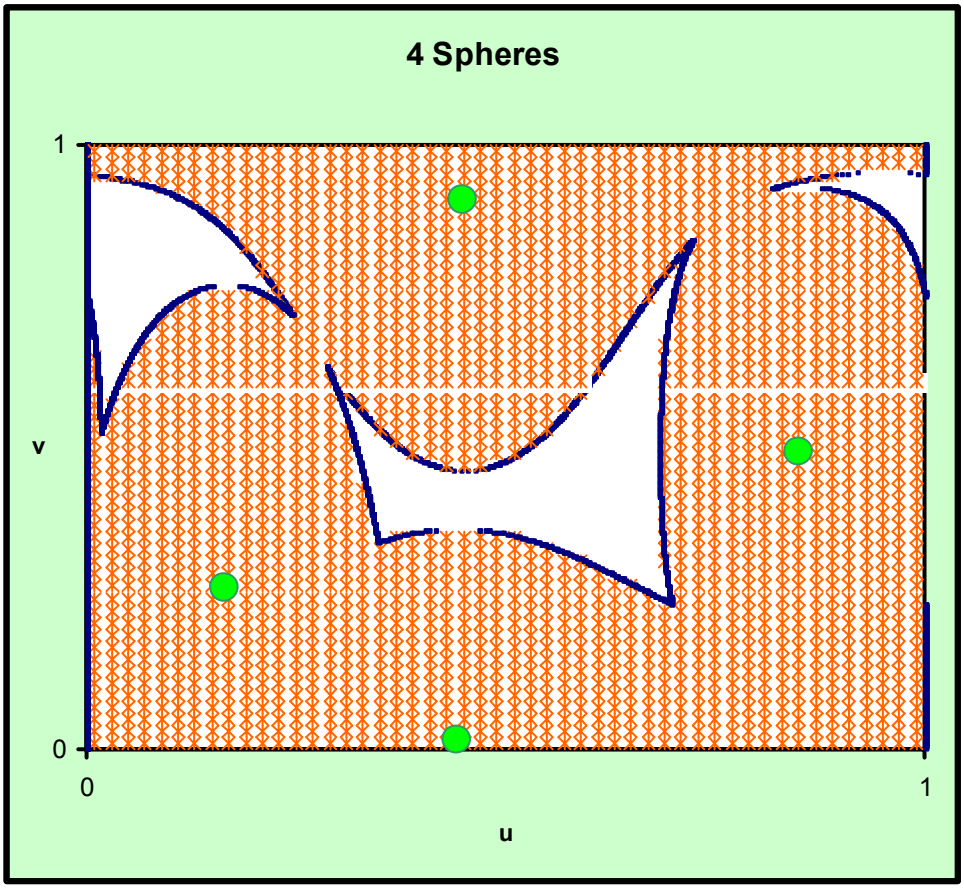

Figure B.9 Position of sphere 4

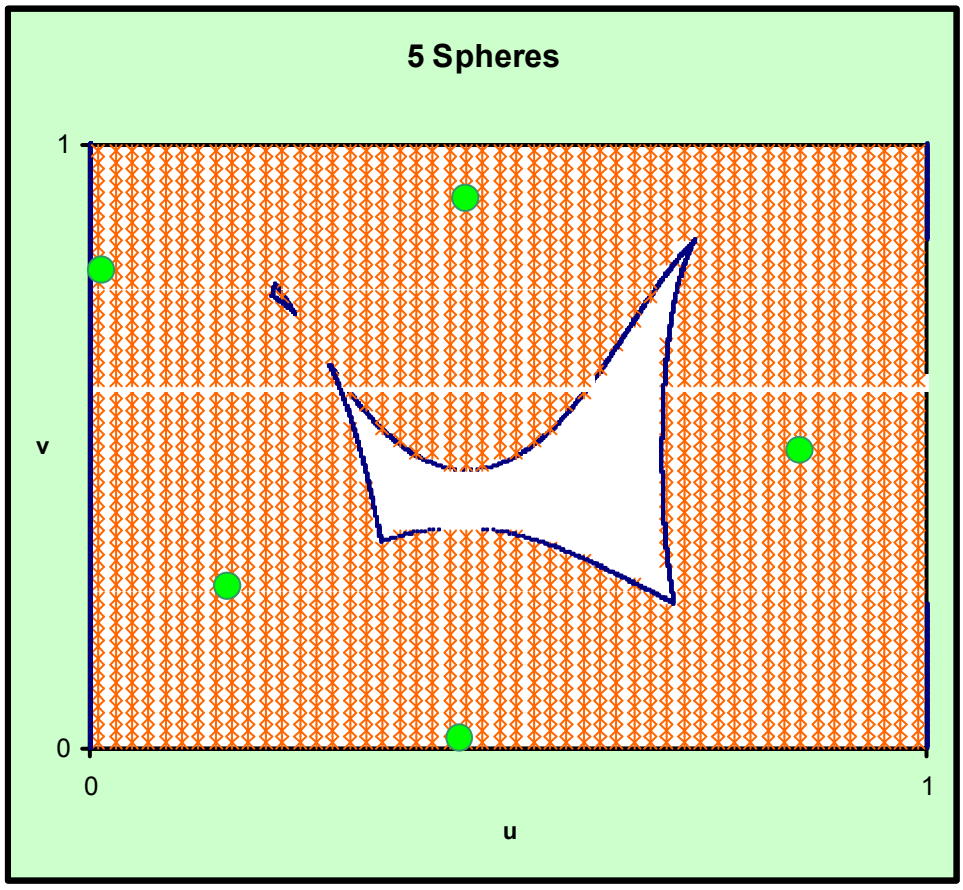

Figure B.10 Position of sphere 5

C DROP-AND-ROLL ALGORITHM FOR MONODISPERSE PACKINGS

C.1 General algorithm

In this section are presented the flow chart and the general concepts of the algorithm that was used in this research to model monodisperse packings of hard spheres. This algorithm (Figure C.1) simulates the packing that can be obtained dropping one sphere at the time inside a box of given dimensions.

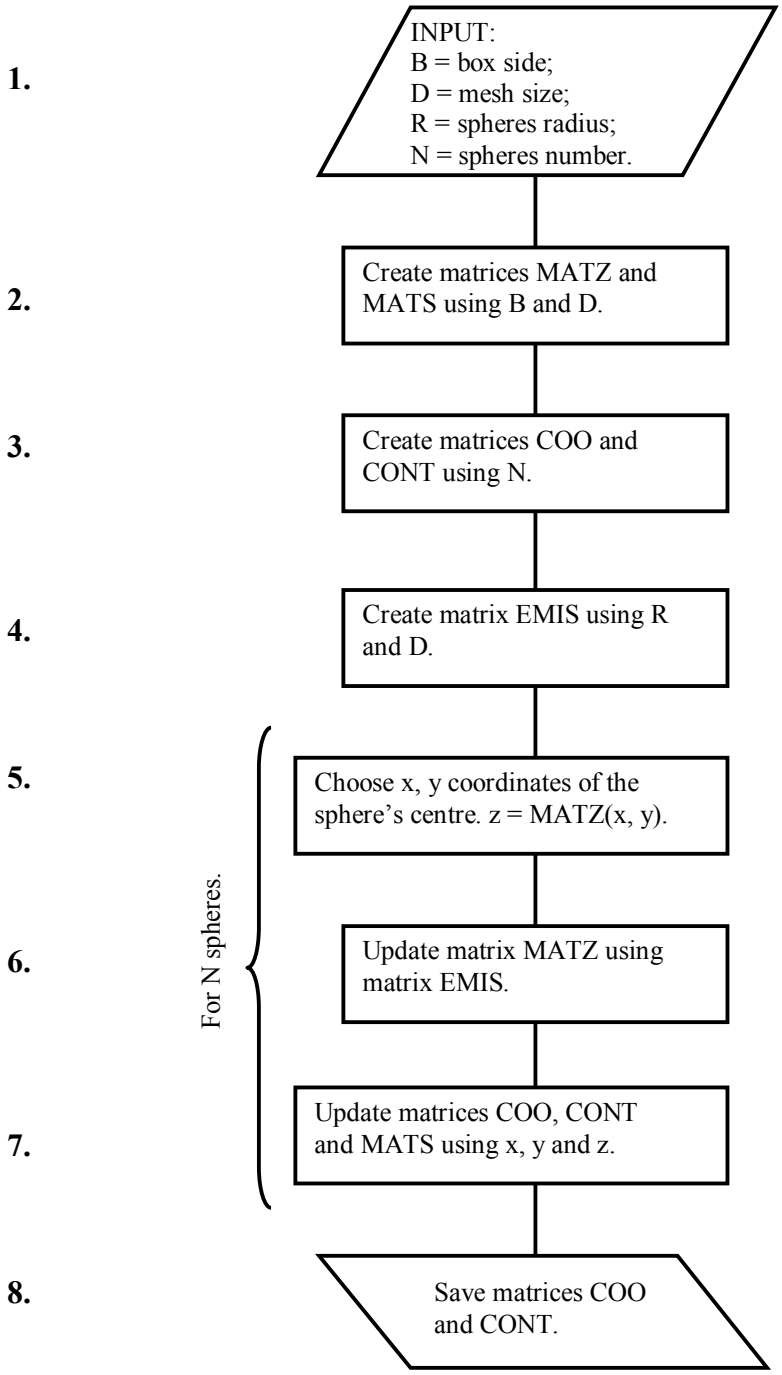

Figure C.1 General flow chart of the drop-and-roll algorithm for monodisperse packings

Step 1.

Input phase. The user assigns a value to the parameters B, D, R and N.

Step 2.

The algorithm divides the bottom of the box according to the indicated mesh size and creates a matrix MATZ where the indices i and j (respectively for rows and columns) represent the coordinates x and y of a point of the mesh inside the box. The value that will be stored inside each cell of MATZ will be the z coordinate, for each given (x, y) pair, of the surface where the centre of the next incoming sphere can lie. Similarly, matrix MATS is created, where each cell will contain the identifying number of the sphere that is generating the MATZ surface in that particular (x, y) pair. Therefore, before placing any sphere it will be:

MATZ (i, j) = R;

MATS (i, j) = 0.

Step 3.

Matrix COO will contain the x, y and z coordinates of the centre of each placed sphere in chronological order of deposition. Matrix CONT is a matrix where the i^{th} row will contain the identifying numbers of the spheres that are in contact with the i^{th} sphere.

Step 4.

The objects that the algorithm deals with are not spheres of radius R but hemispheres of radius 2R, which represent the possible laying surface for

the centre of the next vertically incoming spheres. This concept is explained in Figure C.2 and can be sometimes referred to as "cherrypit" model (Sanstiso & Muller 2003): each sphere can be considered as formed by a hard core surrounded by an interpenetrable shell, which corresponds to the surface where the centre of an outer touching sphere can stay without penetrating the inner one.

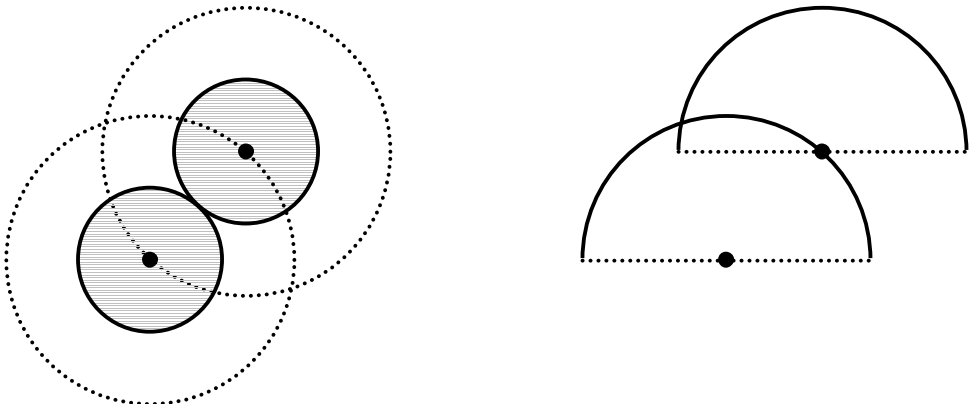

Figure C.2 Equivalence between spheres of radius R and hemispheres of radius 2R

Matrix EMIS is the 4R x 4R matrix that contains the z values of this hemisphere and it is calculated as a function of R and of the mesh size D. Figure C.3 is an example of three-dimensional plot of EMIS.

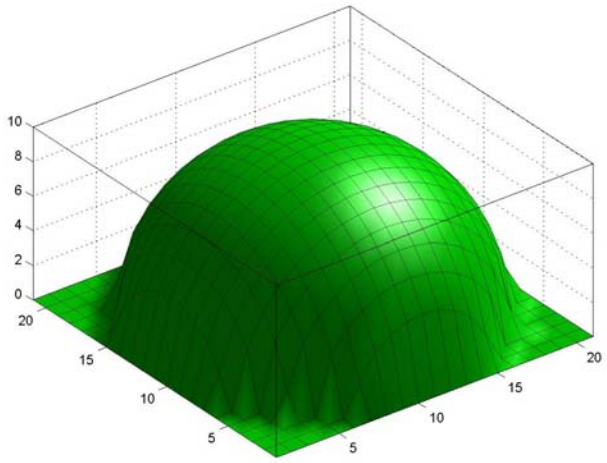

Figure C.3 Representation of matrix EMIS

Step 5.

The horizontal position of each sphere can be chosen in different ways according to the purpose of the simulation. Within monodisperse packings, this is the step that differentiates the various algorithms, therefore its variations will be described in detail in the next Appendices for the different cases that may occur.

Step 6.

When the position for the new i^{th} sphere is chosen, the surface MATZ for the centre of the next sphere must be updated adding the new hemisphere in the chosen position.

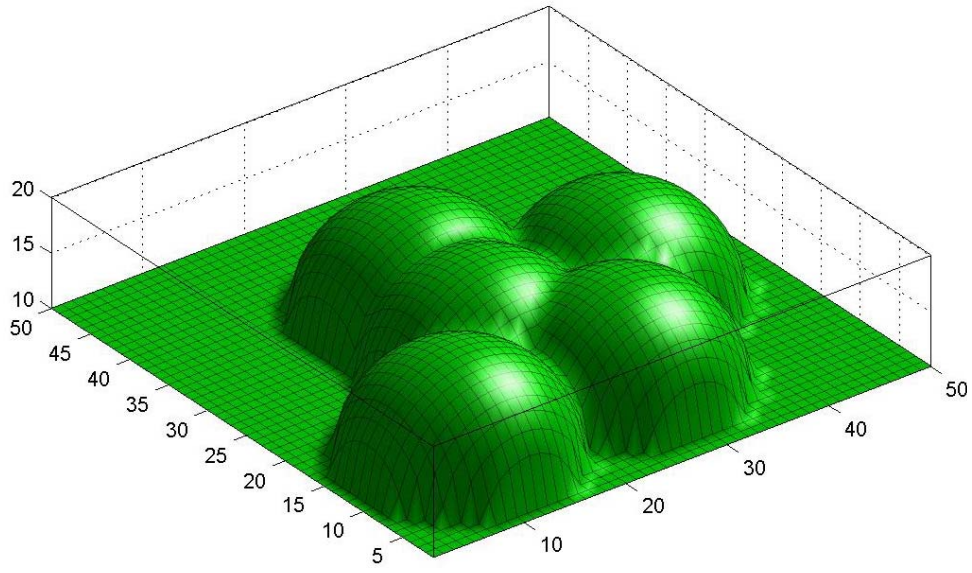

Figure C.4 Representation of matrix MATZ with the first 5 hemispheres

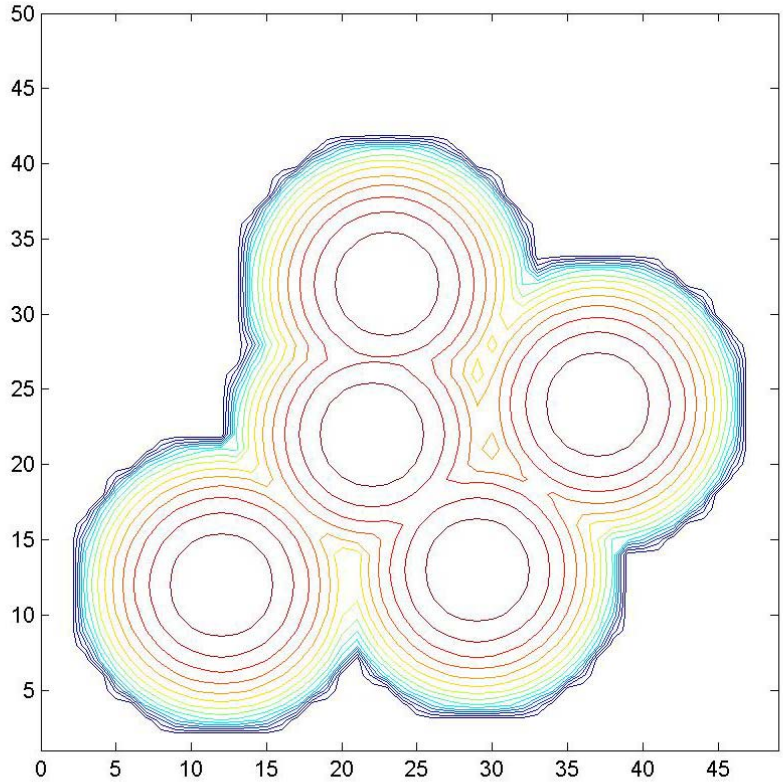

Figure C.5 Top view of matrix MATZ with the first 5 hemispheres

As can be seen, the hemispheres are allowed to overlap up to a certain extent as they don't represent the real volume of the spheres. Figure shows the surface where the centre of the sixth sphere will lie. Once its position is chosen, its correspondent hemisphere will be placed in order to form the new surface (Figures C.4 – C.7).

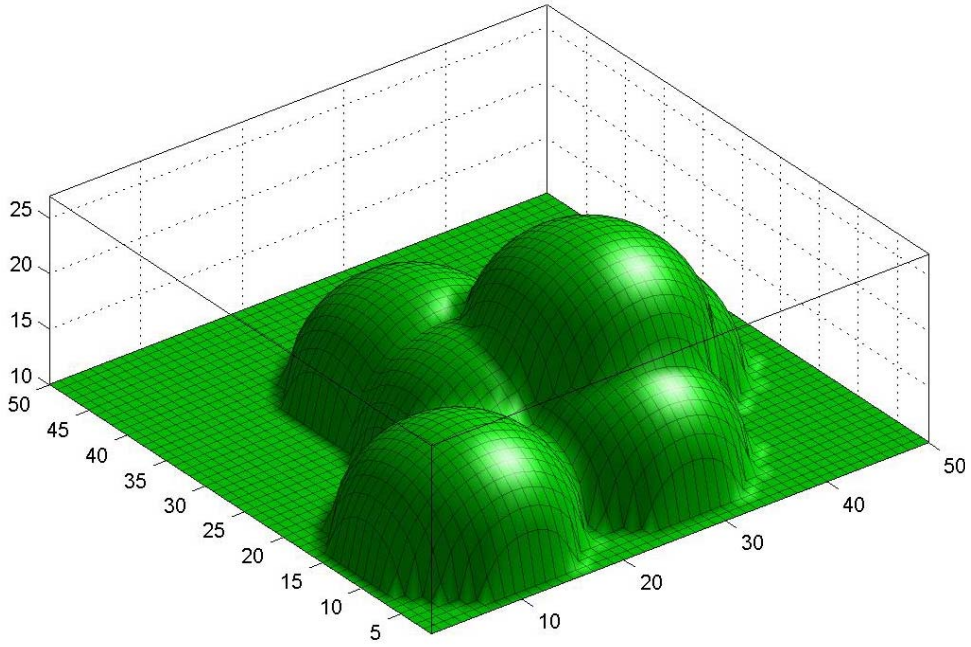

Figure C.6 Representation of matrix MATZ with the first 5 hemispheres

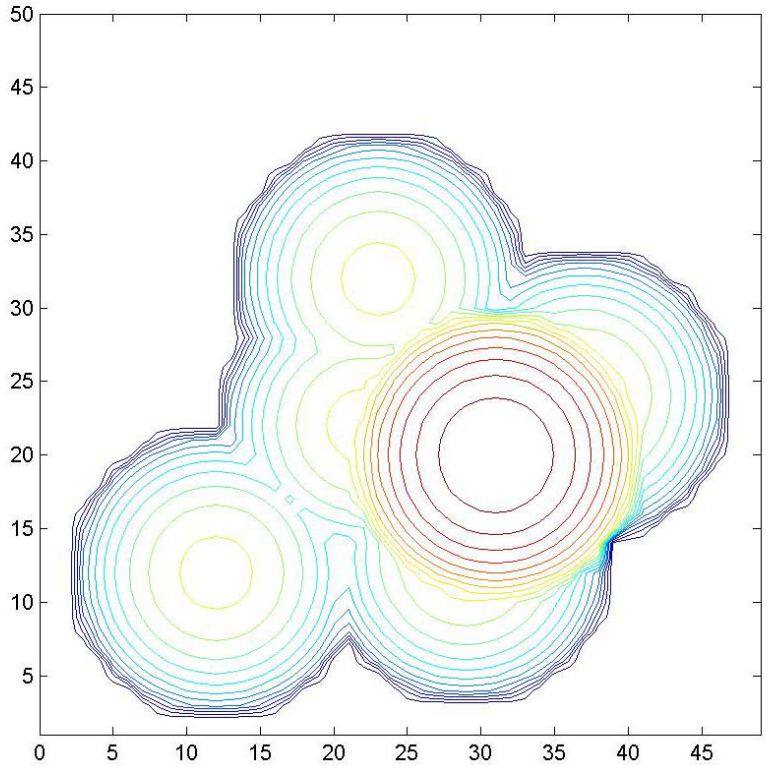

Figure C.7 Top view of matrix MATZ with the first 5 hemispheres

Step 7.

After placing the i^{th} sphere, matrix COO is updated storing in the i^{th} row the x, y and z coordinates of the i^{th} centre. To determine which spheres the new i^{th} one is touching the algorithm reads the cells of MATS that surround the chosen x and y coordinates of the new centre and stores their value (say j, k and w) in the ith row of CONT matrix. At the same time, the identifier "i" is added at the list of touching spheres of each touched sphere (i.e. number "i" will be stored in the j^{th}, k^{th} and w^{th} row of CONT).

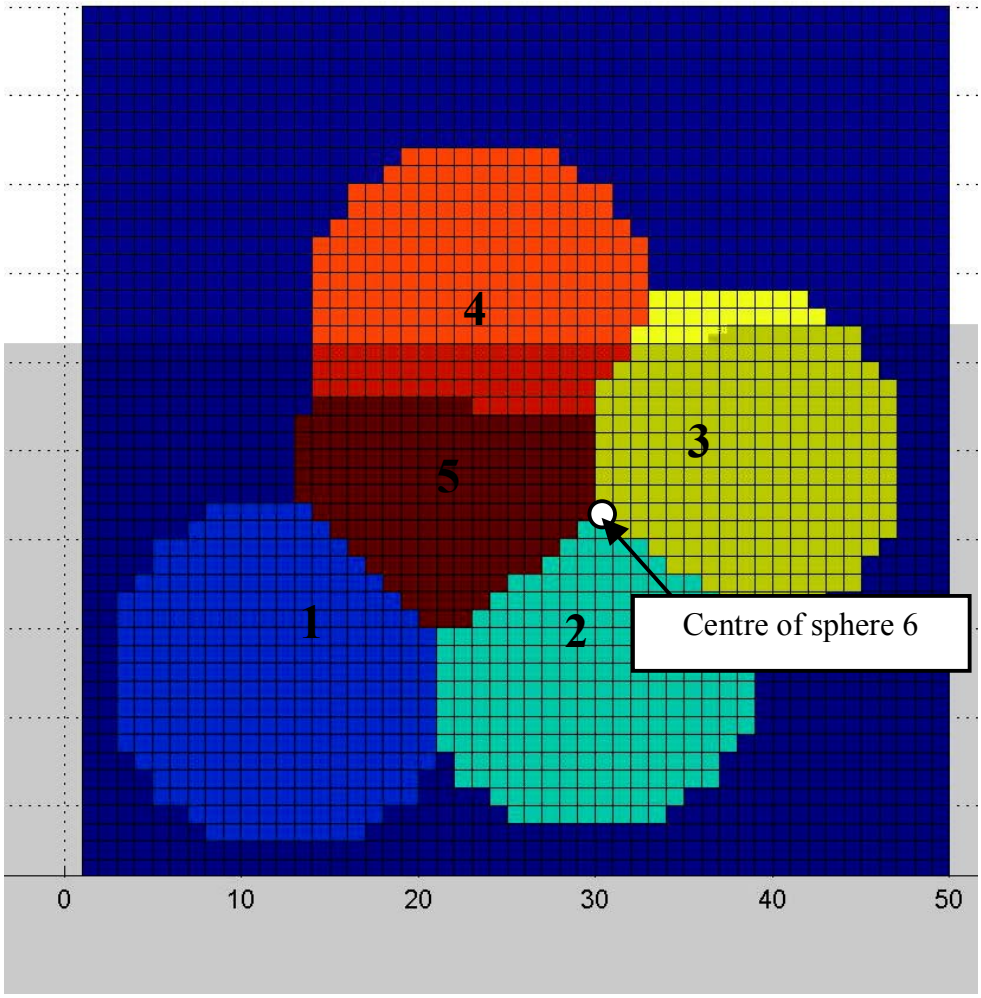

Figure C.8 Representation of matrix MATS for determination of coordination number

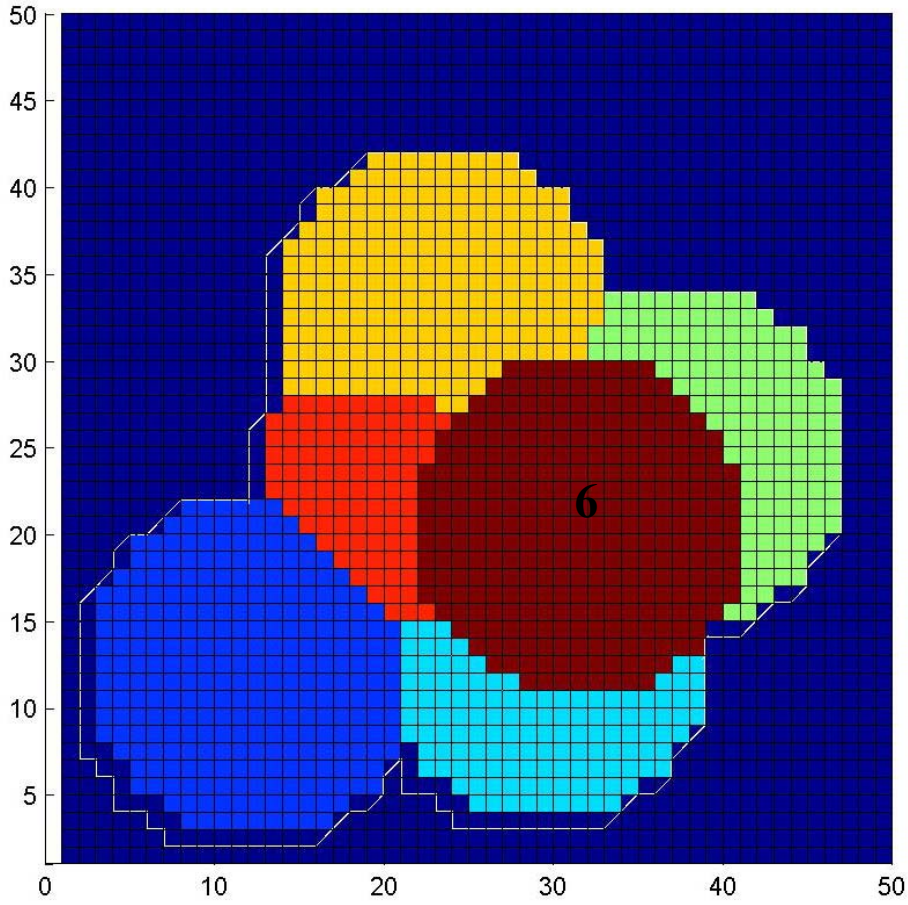

Figure C.9 Updated matrix MATS after the placement of the 6th sphere

For the situation shown in Figures C.8 and C.9, it can be seen that the cells of MATS that surround the chosen centre of the 6th sphere belong to the spheres number 2, 3 and 5. These numbers will be stored in the 6th row of matrix CONT, while the number 6 will be added to the 2nd, 3rd and 5th row of matrix CONT.

Matrix MATS is then updated adding the 6th sphere as for matrix MATZ.

Step 8.

Once the process has been repeated for the desired number of spheres, the output consists in the two matrices COO and CONT.

C.2 Free Rolling

When there are no particular requirements concerning the horizontal position of the spheres, trial Step 5 usually consists in the general "free rolling" algorithm (Step 5.1) explained hereafter in Figure C.10.

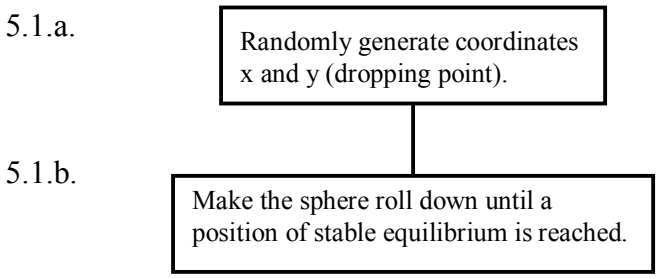

Figure C.10 Step 5 in case of free rolling

D MONODISPERSE "STICKY" PACKINGS

D.1 Introduction

It is well known that if identical spheres are allowed to arrange themselves in a container by rolling freely to a stable position they will always deliver similar packings with rather constant packing ratios. This is shown in Table 3.1 where the results obtained using the "free rolling" version of Santiso's Drop-and-Roll algorithm (explained in the previous Appendix where it is referred to as "Step 5.1") are presented.

Table 19 Preliminary assessment of the independence of results from B and R

Analysis	Box side (B)	Spheres' radius (R)	B/R	Av. Nroll	P. Density
A	100	10	10	107	0.448
B	100	5	20	941	0.493
C	100	3	33	4417	0.500
D	50	5	10	105	0.440
E	30	3	10	101	0.423
F	60	3	20	915	0.479

Column "Av. Nroll" of Table 19 refers to the average number (Nroll) of spheres that can be placed inside the box using the free-rolling algorithm. By this number we can calculate the overall packing densities, column "P.

Density", which show similar values for constant B/R. For increasing B/R values we have registered increasing packing densities as the wall effect of the box sides and base becomes less important. Considering these factors, it is immediate to see that the free-rolling algorithm delivers, in any case, very similar packings and is unsuitable for investigating the relationship between packing density and coordination number.

D.2 Stickiness Algorithm for Monodisperse Packings

As discussed in Section 4.3, affecting the particles' freedom of movement (i.e. preventing them to roll freely) is a way to obtain different packings. Step 5 of the general algorithm for monodisperse packings presented in Appendix C must, then, be enunciated in Figure D.1 in a different way than in Step 5.1 (Step 5.2):

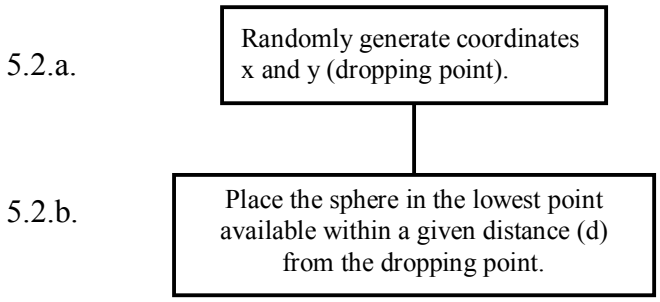

Figure D.1 Step 5 for sticky particles

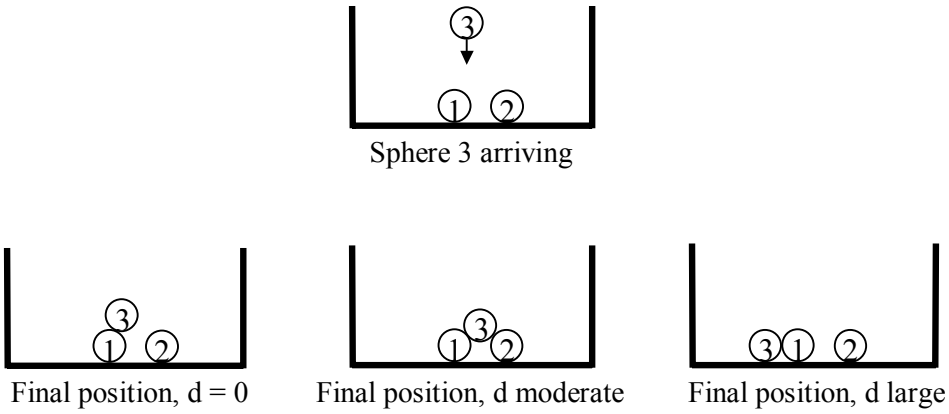

Figure D.2 Different packings obtained varying parameter d when placing the 3rd sphere

This way, it is easy to see (Figure D.2) that the densest configurations will be those produced with the largest d, because each sphere has been placed at the lowest possible point and, therefore, it is possible to fill the box with a larger number of spheres, while when $d \rightarrow 0$ the spheres just "stick" where they fall, resulting in a looser packing.

D.3 Preliminary Results

The packings obtained are, therefore, a function of *d* alone, while box size and sphere radius do not influence them. This concept is clearly shown in Figure D.3 where this algorithm is applied to the 6 different pairs of box size and sphere radius that were already introduced in Table 19.

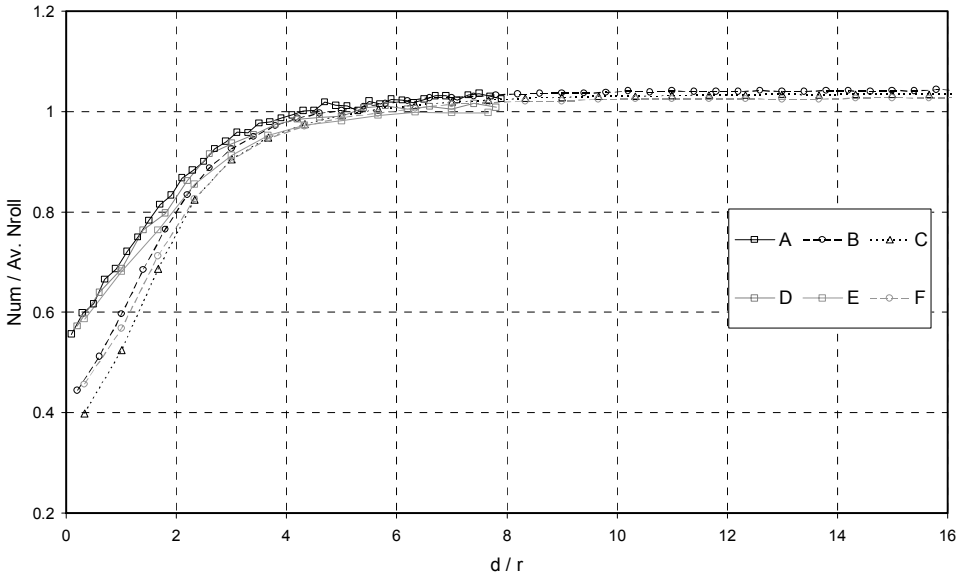

Figure D.3 Dependence of the number of placed spheres (Num) on d

As discussed earlier, the number Av. Nroll is a function only of the ratio B/R, therefore it is suitable to normalise the data as presented in Figure D.3.

Figure D.3 shows that, after making the normalisations, the relationship between number of placed spheres (which is also directly related to packing density) and *d* is the same for all 6 analysis, provided d/r is large.

However, we can note that the "free rolling" algorithm (that provides Av. Nroll) gives a slightly looser packing than the algorithm of Figure D.1 with large *d*. Considering Figure D.2, the "free rolling" algorithm would give the central result and not the right-hand one. Thus the maximum ratio resulting from this algorithm with large *d* is slightly greater than 1 (as shown in Figure D.3), while a ratio of 1 is observed for d/r = 5 ± 1.

The variability presented in Figure D.3 for low d/r values is due to the first layer of placed spheres, i.e. the bottom of each packing. In this algorithm, all the packings must start with a similar first layer which, for low values of d/r, is denser than subsequent layers of spheres placed. This denser region affects the mean result in different proportions as the total number of spheres in the assembly changes. A, D and E, which have similar Av. Nroll values, are affected more than B and F that, again, are affected more than C. This imprecision will disappear from the real tests results when the bottom, top and side spheres are discounted as atypical and only the internal ones will be considered.

E MONODISPERSE DILUTED PACKINGS

E.1 Introduction

It is possible to investigate the relationship between packing density and coordination number in bidisperse packings diluting the considered spheres by adding spheres of a second type. In, general, this process would produce bidisperse packings whose behaviour has been shown to be extremely complex and dependent on the size ratios between the two types of sphere, but we can relate this to the single size problem if the extra spheres are of the same dimension of the original ones. Although being identical in size, for the purpose of this approach we still have to differentiate between the two types of spheres that form the packing in order to focus on the behaviour of the original ones. For this reason they will be referred to as "black" and "white" respectively for the original and the added spheres (this approach is similar to the one used by Beck and Volpert (2003) to produce gapped gapless packings).

E.2 Dilution Algorithm for Monodisperse Packings

In this case, the procedure used during Step 5 of the drop and roll algorithm introduced in Appendix C is different from any previous one (see Figure E.1), and will therefore be referred to as "Step 5.3".

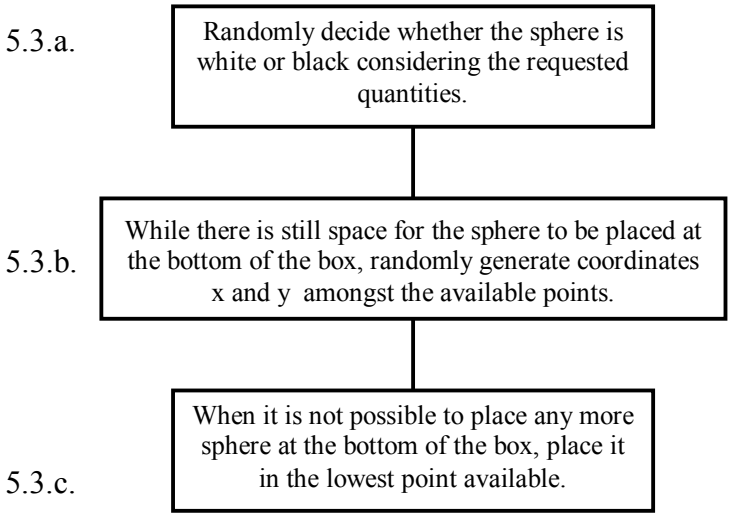

Figure E.1 Step 5 for diluted packings

As the spheres are always being placed in the lowest pocket, the volume occupancy is optimised and the packings produced are the densest possible when no rearrangements (due to gravitationally induced horizontal movements or compaction) are considered (see Appendix D).

F DROP-AND-ROLL ALGORITHM FOR BIDISPERSE PACKINGS

F.1 The Cherrypit Model for Bidisperse Packings

For each packing, given the packing ratio of the two components (large and small) and fixing the number of large spheres, the numbers Nl and Ns of large and small spheres is known and a random order of deposition is then elaborated.

As explained in Figure F.1, for binary mixtures there can be four different spheres according to the possible combinations of inner and outer sphere's size (Table 20).

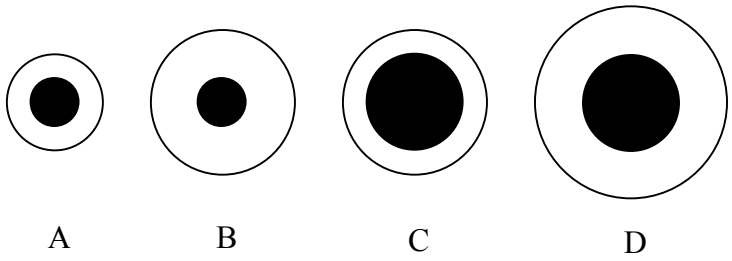

Figure F.1 Possible interpenetrable spheres in the "cherrypit" model for binary mixtures

Table 20 4 types of possible interpenetrable spheres

		Outer Sphere	
Inner Sphere		R1	R2
	R1	A	B
	R2	C	D

This approach was already used for the monodisperse case (see Appendix C) as it allows the algorithm to quickly deliver the surface formed by all the points available for the incoming sphere's centre. Moreover, as in this case this surface is a function not only of the radii of the spheres already placed but also of the radius of the incoming sphere, the algorithm comprises two different surfaces (i.e. two different "possible" boxes): one in case the incoming sphere is large and one if small. The sphere is then placed on the appropriate surface and both the boxes are updated.

This procedure is well explained in Figures F.2 – F.5 for the 2-dimensional case.

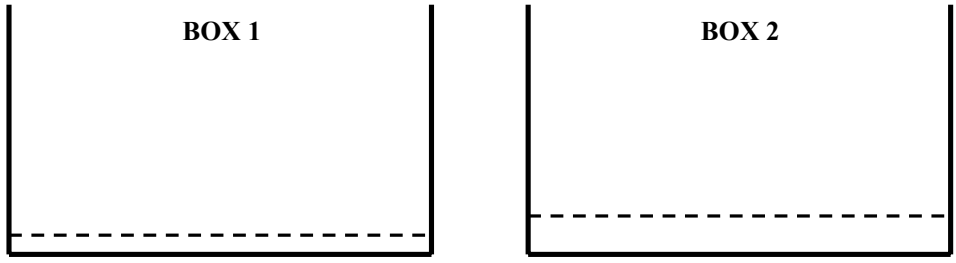

Figure F.2 Box 1 and Box 2 are empty. Box 1 contains the surface for centres of small spheres, Box 2 for large

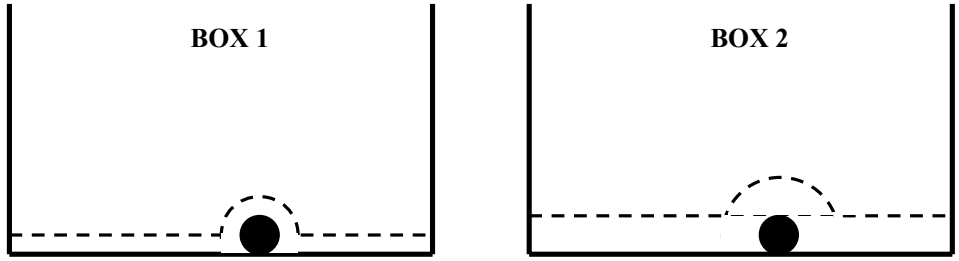

Figure F.3 Sphere 1 incoming. As it is a small one, the position of its centre must be found in Box 1. The surfaces in Box 1 and Box 2 are updated adding respectively an "A" and a "B" sphere in the chosen position

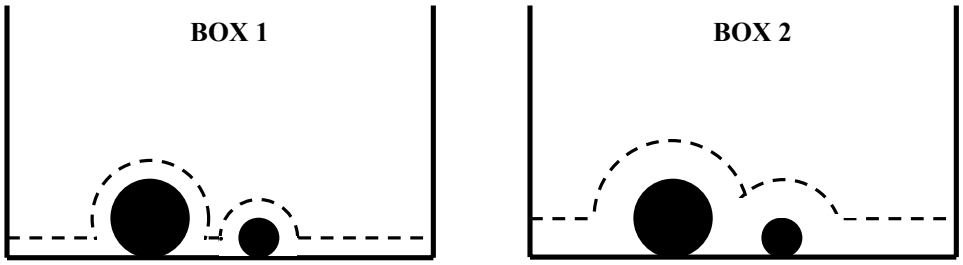

Figure F.4 Sphere 2 incoming. As it is a large one, the position of its centre must be found in Box 2. The surfaces in Box 1 and Box 2 are updated adding respectively a "C" and a "D" sphere in the chosen position

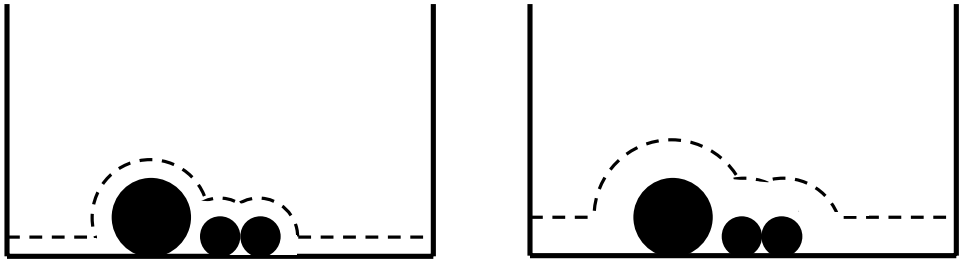

Figure F.5 Sphere 3 incoming. As it is a small one, the procedure is the same as in Figure 3.18b

The need of a different landing surface for the centre of the two (or more) types of spheres is not the only major change that had to be done on the single-size algorithm to allow the simulation of bidisperse (or polydisperse) packings. When there is more than one size of spheres, the small ones must be allowed to occupy positions underneath the larger ones as shown in Figure F.6. For this reason, the top hemispheres (i.e. matrix MATZ) are no more sufficient to define the allowable regions for incoming centres and two auxiliary surfaces are needed to complete the definition of each "Box" ("Aux T" and "Aux B").

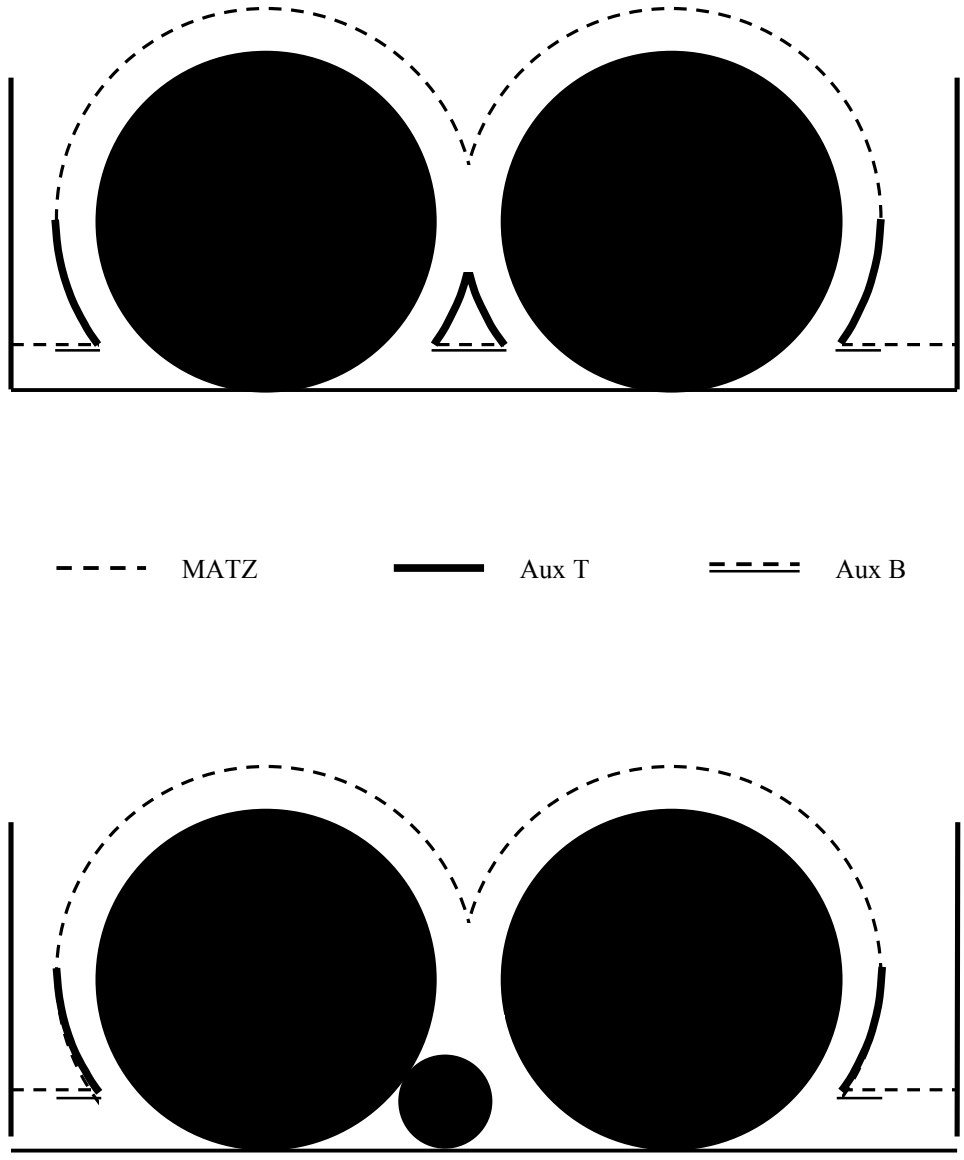

Figure F.6 Gap available for a small sphere underneath the large ones

G GENERAL LIMITATIONS

G.1 Drop-and-Roll Algorithm's Precision

The size of the side of the box, B, and of the mesh, D, relatively to the spheres radius, R, generally do affect the precision of the results of the various types of drop-and-roll algorithm developed and employed in this research. The wall effect affects the spatial arrangement of the particles of this type of packing in a measure that is inversely proportional to the distance of the particles from the walls, gradually decreasing the density achieved in these regions. In order to get rid of this disturbance, it is normal practice to consider for the real analysis only the particles that are positioned inside a certain nucleus of the packing, therefore discounting all the particles that lie within a given distance from the walls (usually expressed in sphere's radii). Thus, it is easy to see that a larger B/R ratio would deliver a larger nucleus of suitable particles to analyse.

On the other hand, it has been noted during preliminary tests that increasing B slows down some basic procedures of the algorithms inducing, then, a limit for the packing's horizontal extension.

Moreover, the mesh size D determines the precision by which each hemisphere is defined and, therefore, the number of points that are used to represent the surface available for the incoming spheres centres. The horizontal position of the spheres has to be found in one of the cells of this mesh and, therefore, the values of their x and y coordinates vary discontinuously. This leads to an approximation of what the real packings would actually be, and its accuracy is inversely proportional to the ratio D/R.

In the particular case of these algorithms, the imprecision of this approximation leads to an overestimation of coordination number during Step 7 (see Appendix C). Evaluating this error is of great importance in this phase since the value of D/R has a major effect on the time needed to place each sphere: the number of points by which each sphere is represented increases with the square of D/R, and so does the time needed for the calculation. To understand the effect of D/R on the measurement of coordination number, a preliminary trial was made applying the algorithm with various D/R ratios obtaining the results shown in Figure G.1.

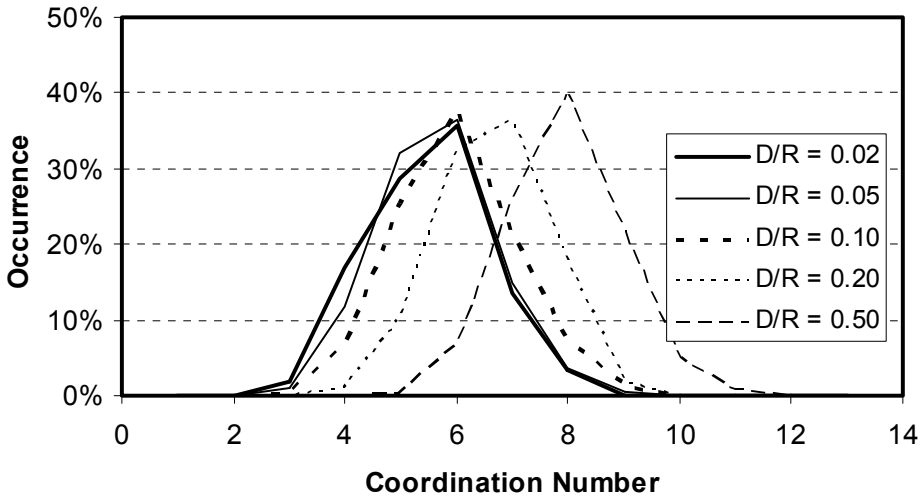

Figure G.1 Coordination number's distribution for different mesh sizes

Plotting the average coordination number of each packing against the respective D/R ratio it is possible to estimate their level of approximation (Figure G.2).

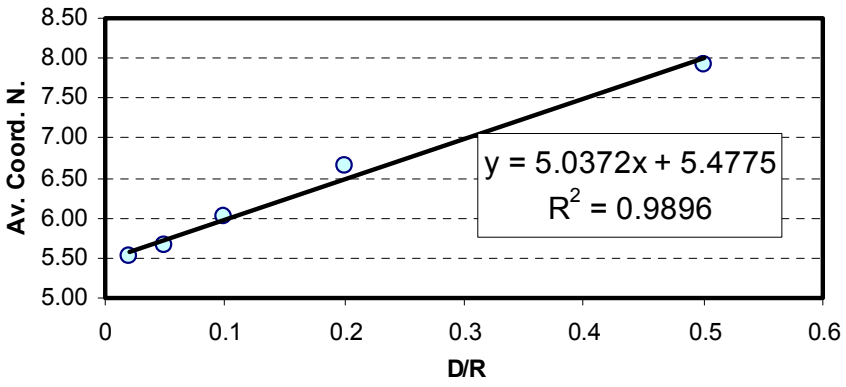

Figure G.2 Average coordination number as a function of mesh sizes

The trend line clearly shows how the measured average coordination number increases when the mesh becomes coarser. This does not mean that there are actually more contacts between the particles, but that the method used to measure them is committing a bigger error.

Being aware of the effect that this parameter has on the algorithm's precision and time consumption, the researcher will have to use a mesh size that ensures to achieve the desired level of accuracy in a reasonable time.

In the case of this research it was decided to always use a mesh size equal to $1/20^{th}$ of the radius of the smallest spheres in the packing, i.e. $D/R=0.05$ for the monodisperse packings and $D/R_{small}=0.05$ for the bidisperse ones.

G.2 Time Consumption for Bidisperse Packings and Apollonian Limit

As shown in Appendix F, the algorithm for bidisperse packings is considerably more complicated than for the monodisperse case. The amount of time needed to produce this type of packings increases greatly due to two main factors:

- Since updating the top surface of each box represents the most time-consuming process of the whole algorithm, the fact of processing each sphere twice for the reasons discussed earlier has the effect of almost doubling the total time needed.

- When modelling spheres of two sizes, the spheres of smaller size will inevitably have to be much more numerous than the larger ones (according to size ratio and packing grading). Therefore, bidisperse packings generally need a much larger number of particles than monodisperse ones.

As seen before, the count of coordination number for each particle is affected by the parameter ratio between mesh size and spheres radius. If in the packing there are spheres of different sizes they will, therefore, be affected in different measures. While it may be possible to correct the measured self-same coordination numbers with the linear relationship

obtained in Section G.1, this is not so simple for the self-different ones, as in this case the error that affects them is probably a function of both radii.

The study of this combined error could be particularly laborious, therefore its determination has not been approached in the present work. In order to minimize this imprecision, a D/R limit value for the smaller size has been fixed equal to 0.05 (i.e. $D = 0.05*R_{small}$). For the larger spheres, this parameter will obviously be even smaller and result in a more precise analysis. Moreover, as shown in Figure G.2, for these very small values of D/R the difference in error on the coordination number for the two radii is quite small (i.e. the error does not change much for the two sizes), but it tends to increase when increasing the difference in size between the spheres.

These considerations bring to the conclusion that, for reasons of time consumption and accuracy of the analysis, the size ratio between the particles has to be limited. For this purpose, it is reasonable to assume the Apollonian ratio as a lower threshold for the analysis, as it already represents a critical reference value for packings of spheres. Therefore, for the simulations we have assumed $R_{small} / R_{large} > \sqrt{6}/2 - 1 \approx 0.225$ and chosen to simulate bidisperse packings with size ratios ½ and ¼.

H COORDINATION NUMBER IN BIDISPERSE PACKINGS – ALL RESULTS

The tables presented in this Appendix contain the coordination numbers observed in the bidisperse packings generated by the drop-and-roll algorithm presented in Appendix F.

The various size ratios and gradings are summarised in Table 5 from Section 4.7, which is being reported hereafter as Table 21.

Table 21 Composition of the bidisperse packings simulated – Copy of Table 5

Size Ratio R_1/R_2	% of the Total Solid Volume ($\%V_1 - \%V_2$)				
(A) 1 / 2	(1) 10 - 90	(2) 30 - 70	(3) 50 - 50	(4) 70 - 30	(5) 90 - 10
(B) 1 / 4	(1) 10 - 90	(2) 30 - 70	(3) 50 - 50	(4) 70 - 30	(5) 90 - 10

A – 1 – S		Total Csl	Css									
			0	1	2	3	4	5	6	7	8	9
Total Css		668	370	238	50	9	1	0	0	0	0	0
Csl	0	1				1						
	1	16		8	6	2						
	2	170	72	70	23	4	1					
	3	294	147	126	19	2						
	4	165	130	33	2							

A – 2 – S		Total Csl	Css									
			0	1	2	3	4	5	6	7	8	9
Total Css		1923	132	476	593	450	201	57	11	3	0	0
Csl	0	40			2	8	13	11	5	1		
	1	294		10	43	92	103	38	6	2		
	2	721	13	93	263	266	78	8				
	3	646	37	263	257	82	7					
	4	213	76	107	28	2						

A – 3 – S		Total Csl	Css									
			0	1	2	3	4	5	6	7	8	9
Total Css		2875	21	141	389	724	737	538	249	68	8	0
Csl	0	417			1	16	76	126	136	55	7	
	1	1058		4	37	195	366	334	108	13	1	
	2	981	1	33	185	402	277	78	5			
	3	370	5	79	157	111	18					
	4	49	15	25	9							

A – 4 – S		Total Csl	Css									
			0	1	2	3	4	5	6	7	8	9
Total Css		3507	2	26	144	392	806	1017	740	319	56	5
Csl	0	1388			4	19	127	383	511	286	53	5
	1	1497			28	171	466	573	223	33	3	
	2	514		4	74	163	206	61	6			
	3	104	2	20	36	39	7					
	4	4		2	2							

A – 5 – S		Total Csl	Css									
			0	1	2	3	4	5	6	7	8	9
Total Css		4248	0	0	10	108	419	1086	1599	847	165	14
Csl	0	3339			1	13	155	742	1426	823	165	14
	1	830			3	63	235	332	173	24		
	2	77			5	31	29	12				
	3	2			1	1						
	4											

A – 1 – L		Total Cll	Cls																	
			0	1	2	3	4	5	6	7	8	9	10	11	12	13	14	15	16	17	18
Total Cls		523	76	141	141	101	47	11	6	0	0	0	0	0	0	0	0	0	0	0	0
Cll	0	0																			
	1	0																			
	2	1				1															
	3	12	1	1	3	2	3	1	1												
	4	62	5	12	19	15	8	2	1												
	5	151	11	35	46	36	15	4	4												
	6	180	29	50	49	32	16	4													
	7	105	26	36	23	15	5														
	8	12	4	7	1																

A – 2 – L		Total Cll	Cls																		
			0	1	2	3	4	5	6	7	8	9	10	11	12	13	14	15	16	17	18
Total Cls		335	0	3	6	11	26	48	61	54	42	54	20	7	3	0	0	0	0	0	0
Cll	0	0																			
	1	14							1			5	2	4	2						
	2	64						3	7	10	12	20	8	3	1						
	3	108				2	4	12	18	23	15	25	9								
	4	81				3	5	14	28	14	12	4	1								
	5	43			2	3	11	14	5	5	3										
	6	20		2	4	2	5	4	1	2											
	7	5		1		1	1	1	1												
	8	0																			

A – 3 – L		Total Cll	Cls																	
			0	1	2	3	4	5	6	7	8	9	10	11	12	13	14	15	16	17	18
Total Cls		208	0	0	0	0	0	3	9	16	23	33	43	32	16	18	10	3	2	0	0
Cll	0	12											1	2	4	3	1	1			
	1	48									1	8	6	7	4	11	7	2	2		
	2	80							3	3	5	11	25	21	6	4	2				
	3	42							2	7	9	10	11	1	2						
	4	23						2	3	5	8	4		1							
	5	3						1	1	1											
	6	0																			
	7	0																			
	8	0																			

A – 4 – L		Total Cll	Cls																	
			0	1	2	3	4	5	6	7	8	9	10	11	12	13	14	15	16	17	18
Total Cls		111	0	0	0	0	1	0	1	0	6	5	17	16	27	11	13	9	4	0	1
Cll	0	22											1	2	4	3	4	5	2		1
	1	49										2	3	6	17	6	9	4	2		
	2	29									4	2	11	6	4	2					
	3	10					1				2	1	2	2	2						
	4	0																			
	5	1							1												
	6	0																			
	7	0																			
	8	0																			

A – 5 – L		Total Cll	Cls																	
			0	1	2	3	4	5	6	7	8	9	10	11	12	13	14	15	16	17	18
Total Cls		30	0	0	0	0	0	0	0	0	0	0	2	3	5	5	8	2	1	2	2
Cll	0	17												1	2	2	6	2		2	2
	1	10											1	1	2	3	2		1		
	2	3											1	1	1						
	3	0																			
	4	0																			
	5	0																			
	6	0																			
	7	0																			
	8	0																			

B – 1 – S		Total Csl	Css									
			0	1	2	3	4	5	6	7	8	9
Total Css		7041	411	1354	1898	1764	1059	410	122	20	3	0
Csl	0	418			11	91	122	117	57	17	3	
	1	2434	10	165	556	769	614	257	60	3		
	2	2680	166	624	856	703	293	34	4			
	3	1306	185	482	412	194	30	2	1			
	4	191	45	79	60	7						
	5	12	5	4	3							

B – 2 – S		Total Csl	Css									
			0	1	2	3	4	5	6	7	8	9
Total Css		19446	119	1019	2942	4706	5052	3518	1636	401	51	2
Csl	0	3462			24	230	732	1125	976	328	45	2
	1	9058		102	760	2151	3143	2170	653	73	6	
	2	6147	63	597	1827	2257	1173	223	7			
	3	769	47	320	330	68	4					
	4	10	9		1							
	5	0										

B – 3 – S		Total Csl	Css									
			0	1	2	3	4	5	6	7	8	9
Total Css		29727	16	225	1234	3531	6615	8277	6689	2683	427	30
Csl	0	13425			20	316	1505	3764	4917	2455	418	30
	1	13214		33	441	2009	4388	4339	1767	228	9	
	2	2943	10	125	715	1193	721	174	5			
	3	142	4	66	58	13	1					
	4	3	2	1								
	5	0										

B – 4 – S		Total Csl	Css									
			0	1	2	3	4	5	6	7	8	9
Total Css		38234	2	37	402	1818	5073	10228	12548	6762	1291	73
Csl	0	27490			13	256	1801	6651	10906	6504	1286	73
	1	9925		14	198	1216	3065	3529	1640	258	5	
	2	807	1	18	186	345	207	48	2			
	3	12	1	5	5	1						
	4	0										
	5	0										

B – 5 – S		Total Csl	Css									
			0	1	2	3	4	5	6	7	8	9	10
Total Css		45690	0	2	59	549	2864	10365	18235	11251	2227	135	3
Csl	0	42029			2	163	1819	9011	17539	11134	2223	135	3
	1	3596		1	48	355	1028	1347	696	117	4		
	2	65		1	9	31	17	7					
	3	0											
	4	0											
	5	0											

B – 1 – L		Total Cll	Cls																													
			0	1	2	3	4	5	6	7	8	9	10	11	12	13	14	15	16	17	18	19	20	21	22	23	24	25	26	27	28	29
Total Cls		499	22	46	49	64	37	24	22	20	9	8	18	12	16	7	20	11	15	16	15	15	9	9	5	6	3	8	3	4	4	2
Cll	1	0																														
	2	0																														
	3	1															1															
	4	4			1		1					1						1														
	5	24	2	1	6	2	1	1	1	3			1		2				2	2												
	6	121	3	13	8	15	11	4	6	4	1		6	3	3	2	3	6	1	7	5	6	4	2		2		1	2		3	
	7	219	9	15	20	29	16	11	10	8	5	6	4	4	8	3	9	3	8	5	9	7	3	4	2	4	2	7	1	4	1	2
	8	112	6	14	12	18	7	7	5	4	3	1	4	4	2	1	6	1	4	2	1	2	2	3	2		1					
	9	18	2	3	2		1	1		1			3	1	1	1	1								1							

B – 2 – L		Total Cll	Cls																												
			16	17	18	19	20	21	22	23	24	25	26	27	28	29	30	31	32	33	34	35	36	37	38	39	40	41	42	43	44	45
Total Cls		321	1	3	3	0	0	4	10	27	15	29	25	28	32	20	35	29	16	14	13	8	4	1	3	1	0	0	0	0	0	0
Cll	1	6								1								1		2			1			1						
	2	27										1	3	1	3	2	1	5	1	3	3	1	2		1							
	3	56							1		2	1	4	4	7	1	11	5	6	3	6	1	1	1	2							
	4	116		1	1					8	4	10	8	9	12	12	16	13	7	6	3	6										
	5	79						1	5	12	6	12	8	9	9	5	6	3	2		1											
	6	29	1	1	1			2	3	4	3	5	2	4			1	2														
	7	5		1					1	1				1	1																	
	8	3			1			1		1																						
	9	0																														

B – 3 – L		Total Cll	Cls																													
			24	25	26	27	28	29	30	31	32	33	34	35	36	37	38	39	40	41	42	43	44	45	46	47	48	49	50	51	52	53
Total Cls		196	1	2	1	2	3	2	5	4	8	9	19	22	19	20	22	16	12	9	11	4	4	1	0	0	0	0	0	0	0	0
Cll	1	30										1	2	4	1	2	6	1	4	2	3	1	2	1								
	2	89						1		1	4	2	10	11	7	11	8	13	6	3	8	3	1									
	3	61		1	1			1	5	3	3	6	4	7	9	7	6	2	2	3			1									
	4	13	1	1		1	2				1		3		2		1			1												
	5	3				1	1										1															
	6	0																														
	7	0																														
	8	0																														
	9	0																														

B – 4 – L		Total Cll	Cls																													
			30	31	32	33	34	35	36	37	38	39	40	41	42	43	44	45	46	47	48	49	50	51	52	53	54	55	56	57	58	59
Total Cls		102	1	0	2	4	6	3	8	5	8	13	15	5	9	8	7	2	3	1	2	0	0	0	0	0	0	0	0	0	0	0
Cll	1	39				1	2		1			5	5	3	7	3	4	2	3	1	2											
	2	45			1		2	1	5	4	6	7	7	2	2	5	3															
	3	14				2	2	2	2		2	1	3																			
	4	4	1		1	1				1																						
	5	0																														
	6	0																														
	7	0																														
	8	0																														
	9	0																														

B – 5 – L		Total Cll	Cls																													
			35	36	37	38	39	40	41	42	43	44	45	46	47	48	49	50	51	52	53	54	55	56	57	58	59	60	61	62	63	64
Total Cls		30	1	1	1	1	0	3	6	5	4	0	2	2	2	2	0	0	0	0	0	0	0	0	0	0	0	0	0	0	0	0
Cll	1	26			1	1		2	6	4	4		2	2	2	2																
	2	3	1					1		1																						
	3	1		1																												
	4	0																														
	5	0																														
	6	0																														
	7	0																														
	8	0																														
	9	0																														

I SUPERFICIAL DISTRIBUTION OF CONTACT POINTS IN BIDISPERSE PACKINGS – ALL RESULTS

In Section 5.3 was presented a summary of the analysis of the superficial distribution of contact points for large and small spheres in bidisperse packings, in which the focus was mainly on the percentage of uncaged particles observed. As discussed in that section, this is only one aspect of this subject corresponding to the particular case when $D = 0$.

This section, instead, presents the plots of the full sets of results for $0 \leq D \leq 1$.

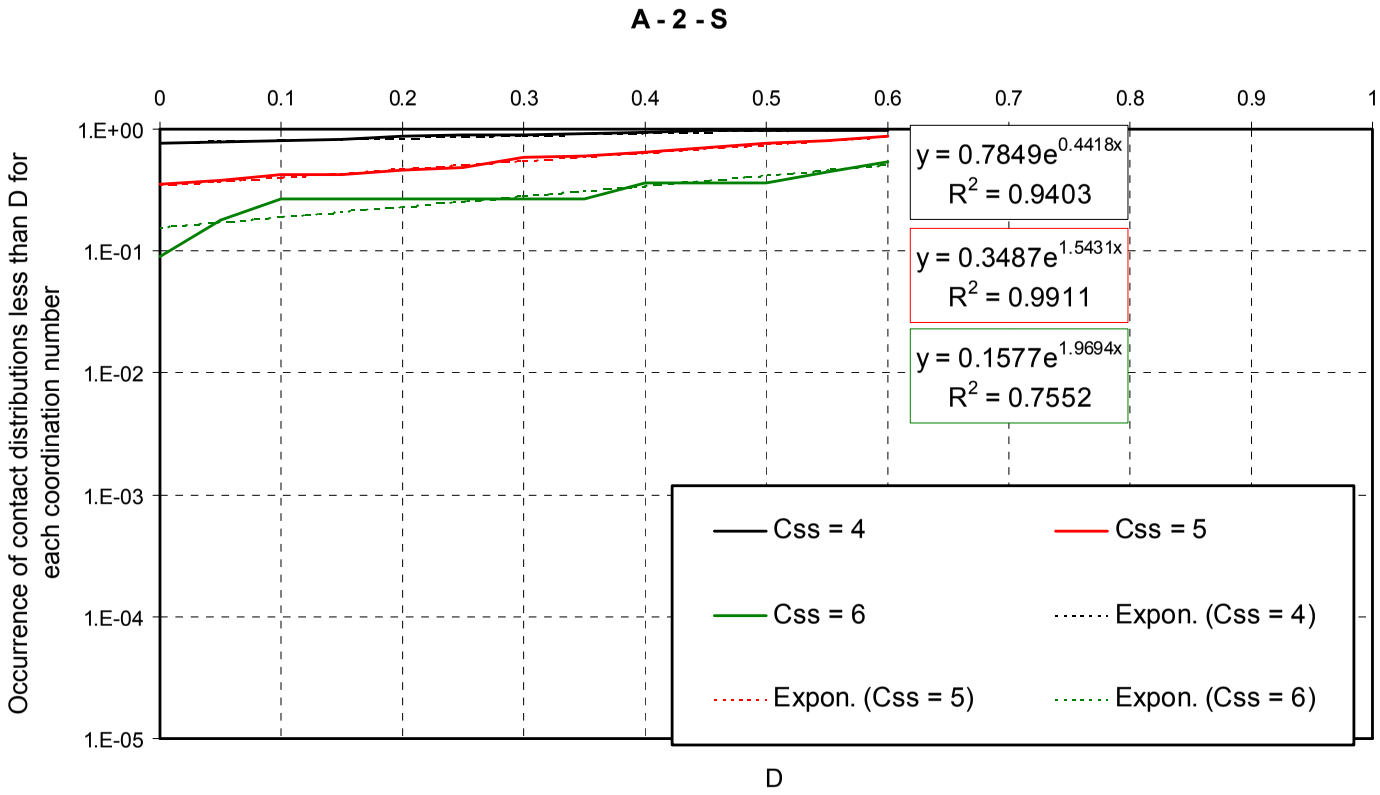
A - 2 - S
0
0.1
0.2
0.3
0.4
0.5
0.6
0.7
0.8
0.9
1
1.E+00
1.E-01
1.E-02
1.E-03
1.E-04
1.E-05
Occurrence of contact distributions less than D for each coordination number
D
y = 0.7849e^0.4418x
R^2 = 0.9403
y = 0.3487e^1.5431x
R^2 = 0.9911
y = 0.1577e^1.9694x
R^2 = 0.7552
Css = 4
Css = 5
Css = 6
Expon. (Css = 4)
Expon. (Css = 5)
Expon. (Css = 6)

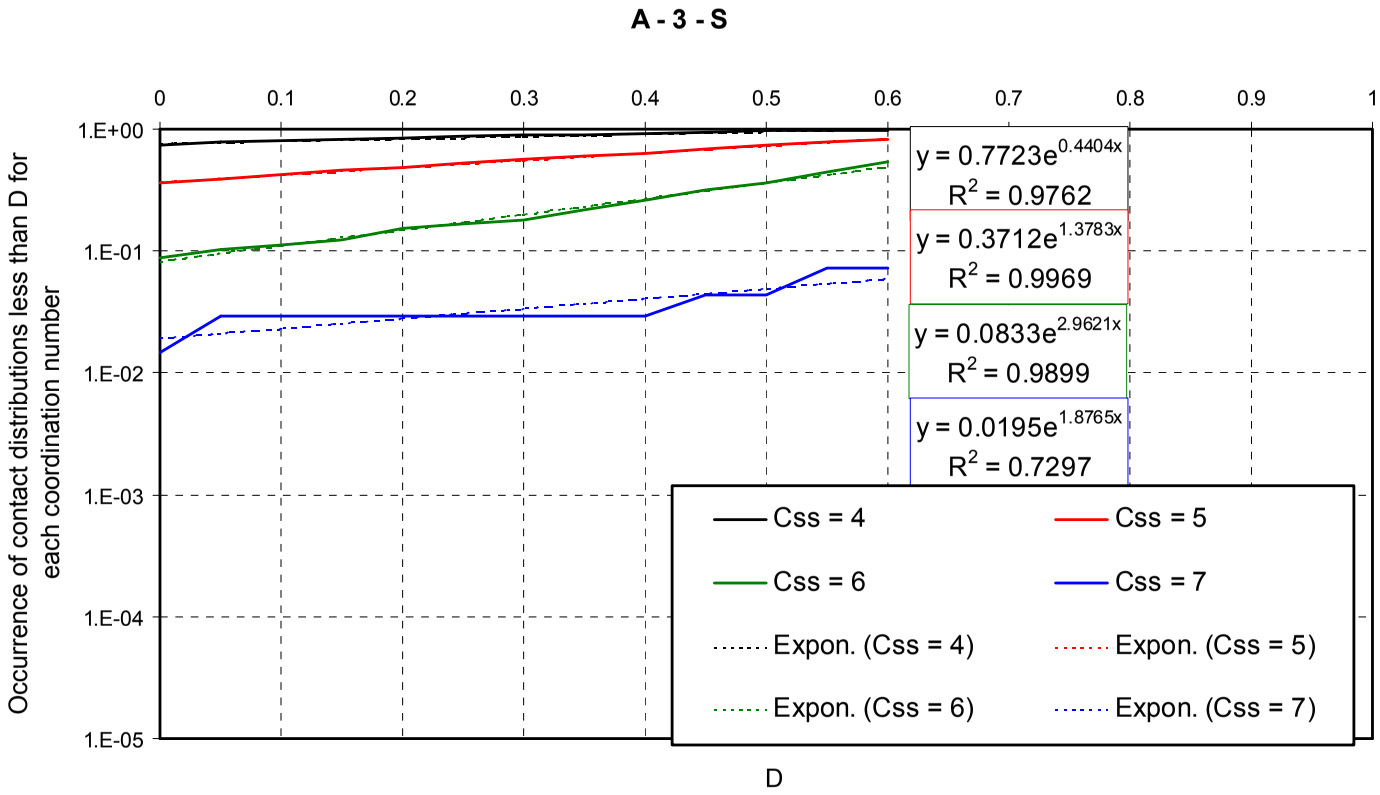
A - 3 - S
0
0.1
0.2
0.3
0.4
0.5
0.6
0.7
0.8
0.9
1
1.E+00
1.E-01
1.E-02
1.E-03
1.E-04
1.E-05
Occurrence of contact distributions less than D for each coordination number
D
y = 0.7723e^0.4404x
R^2 = 0.9762
y = 0.3712e^1.3783x
R^2 = 0.9969
y = 0.0833e^2.9621x
R^2 = 0.9899
y = 0.0195e^1.8765x
R^2 = 0.7297
Css = 4
Css = 5
Css = 6
Css = 7
Expon. (Css = 4)
Expon. (Css = 5)
Expon. (Css = 6)
Expon. (Css = 7)

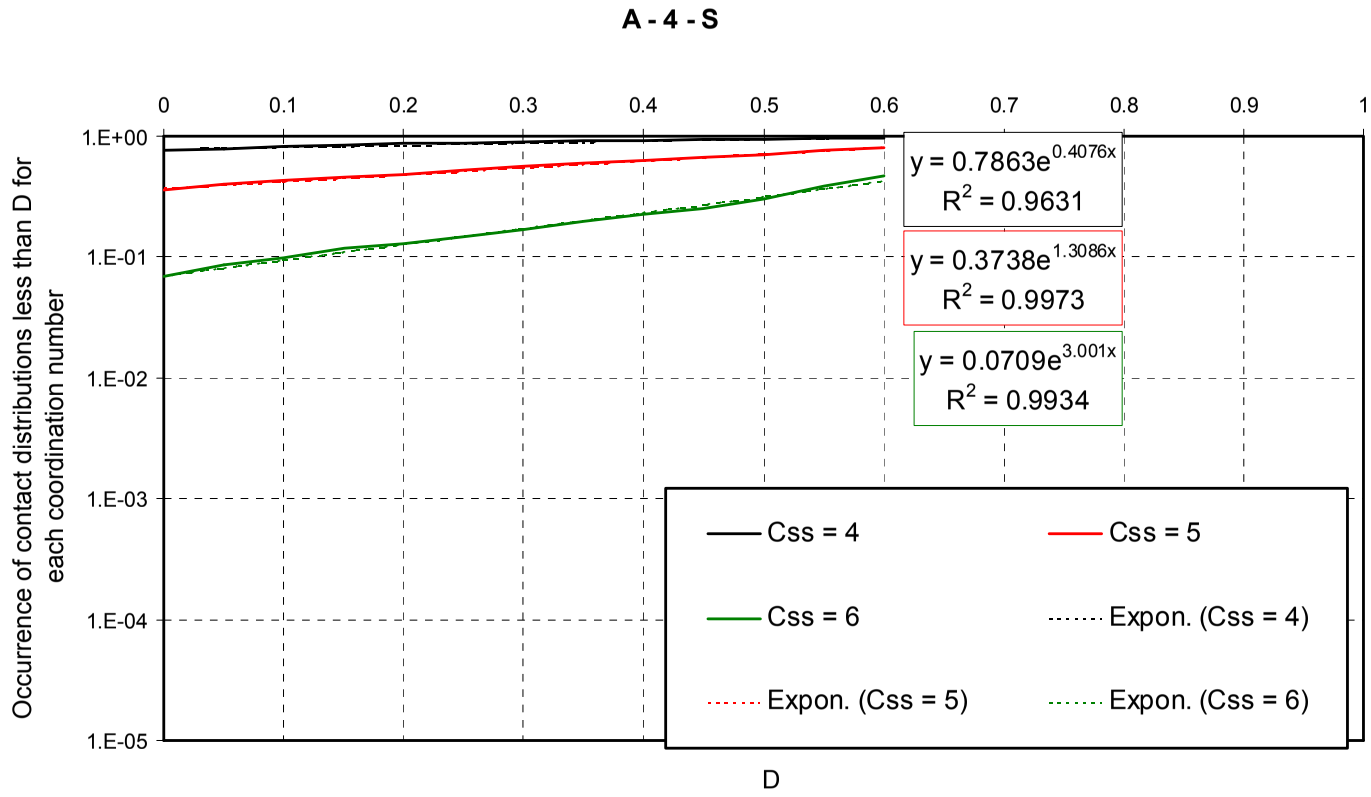
A - 4 - S
0
0.1
0.2
0.3
0.4
0.5
0.6
0.7
0.8
0.9
1
1.E+00
1.E-01
1.E-02
1.E-03
1.E-04
1.E-05
Occurrence of contact distributions less than D for each coordination number
D
y = 0.7863e^0.4076x
R^2 = 0.9631
y = 0.3738e^1.3086x
R^2 = 0.9973
y = 0.0709e^3.001x
R^2 = 0.9934
Css = 4
Css = 5
Css = 6
Expon. (Css = 4)
Expon. (Css = 5)
Expon. (Css = 6)

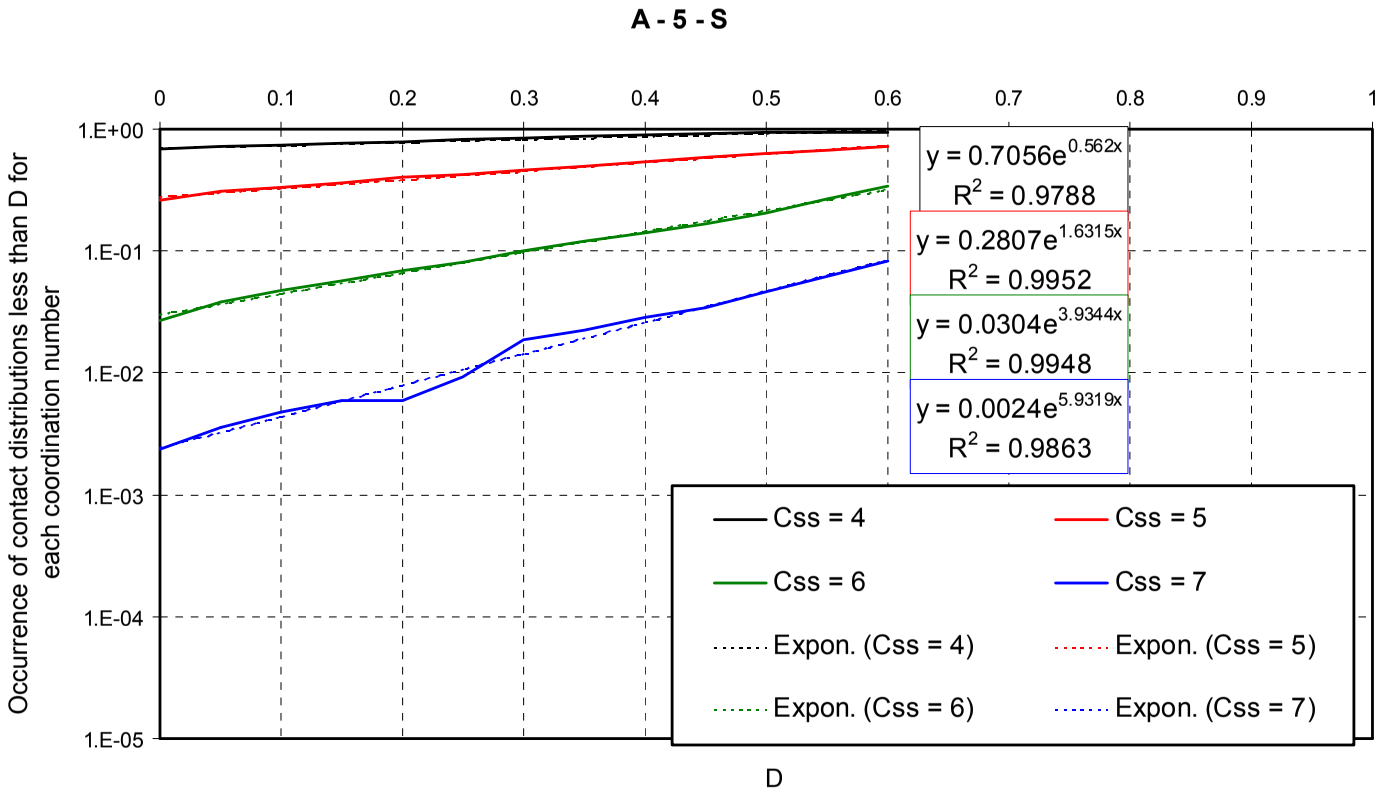
A - 5 - S
0
0.1
0.2
0.3
0.4
0.5
0.6
0.7
0.8
0.9
1
1.E+00
1.E-01
1.E-02
1.E-03
1.E-04
1.E-05
Occurrence of contact distributions less than D for each coordination number
D
y = 0.7056e^0.562x
R^2 = 0.9788
y = 0.2807e^1.6315x
R^2 = 0.9952
y = 0.0304e^3.9344x
R^2 = 0.9948
y = 0.0024e^5.9319x
R^2 = 0.9863
Css = 4
Css = 5
Css = 6
Css = 7
Expon. (Css = 4)
Expon. (Css = 5)
Expon. (Css = 6)
Expon. (Css = 7)

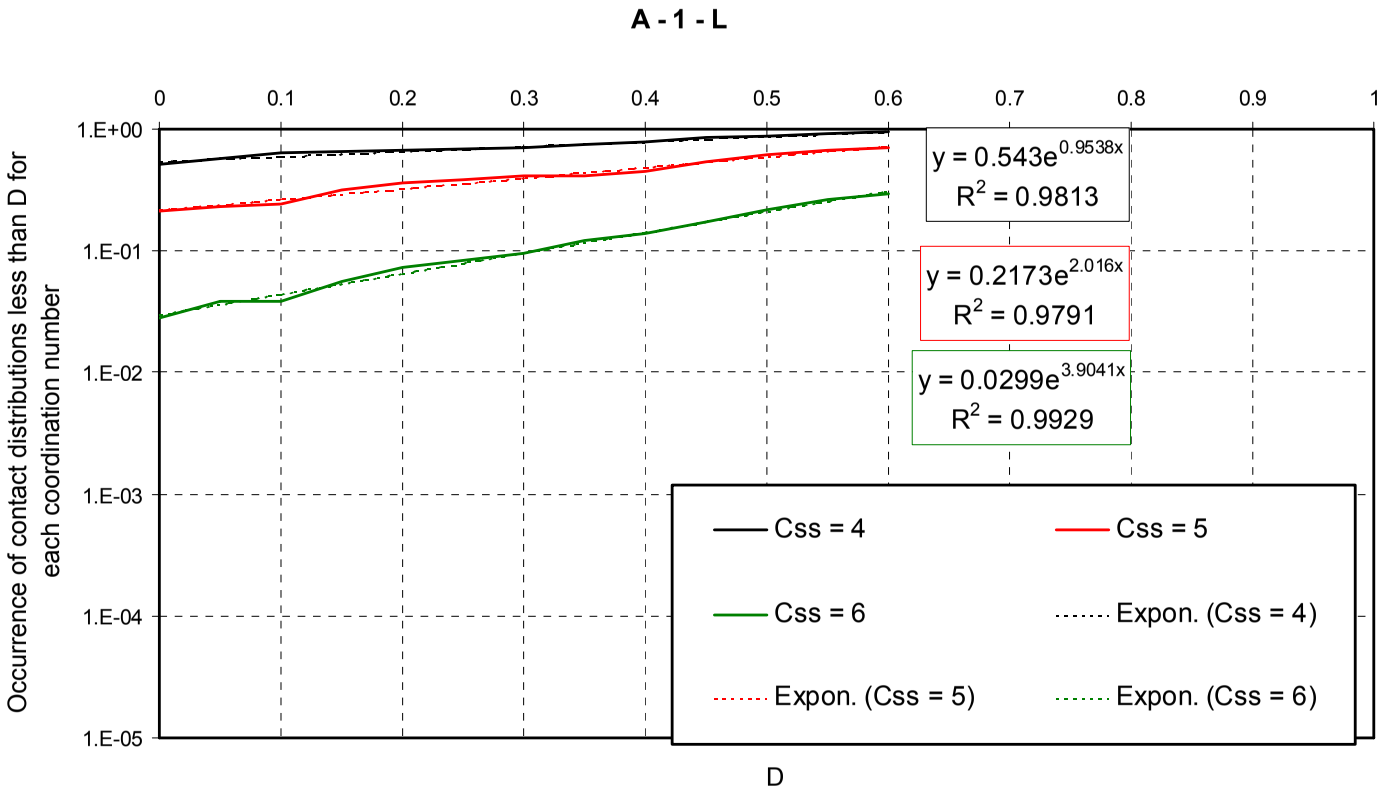
A - 1 - L
0
0.1
0.2
0.3
0.4
0.5
0.6
0.7
0.8
0.9
1
1.E+00
1.E-01
1.E-02
1.E-03
1.E-04
1.E-05
Occurrence of contact distributions less than D for each coordination number
D
y = 0.543e^0.9538x
R^2 = 0.9813
y = 0.2173e^2.016x
R^2 = 0.9791
y = 0.0299e^3.9041x
R^2 = 0.9929
Css = 4
Css = 5
Css = 6
Expon. (Css = 4)
Expon. (Css = 5)
Expon. (Css = 6)

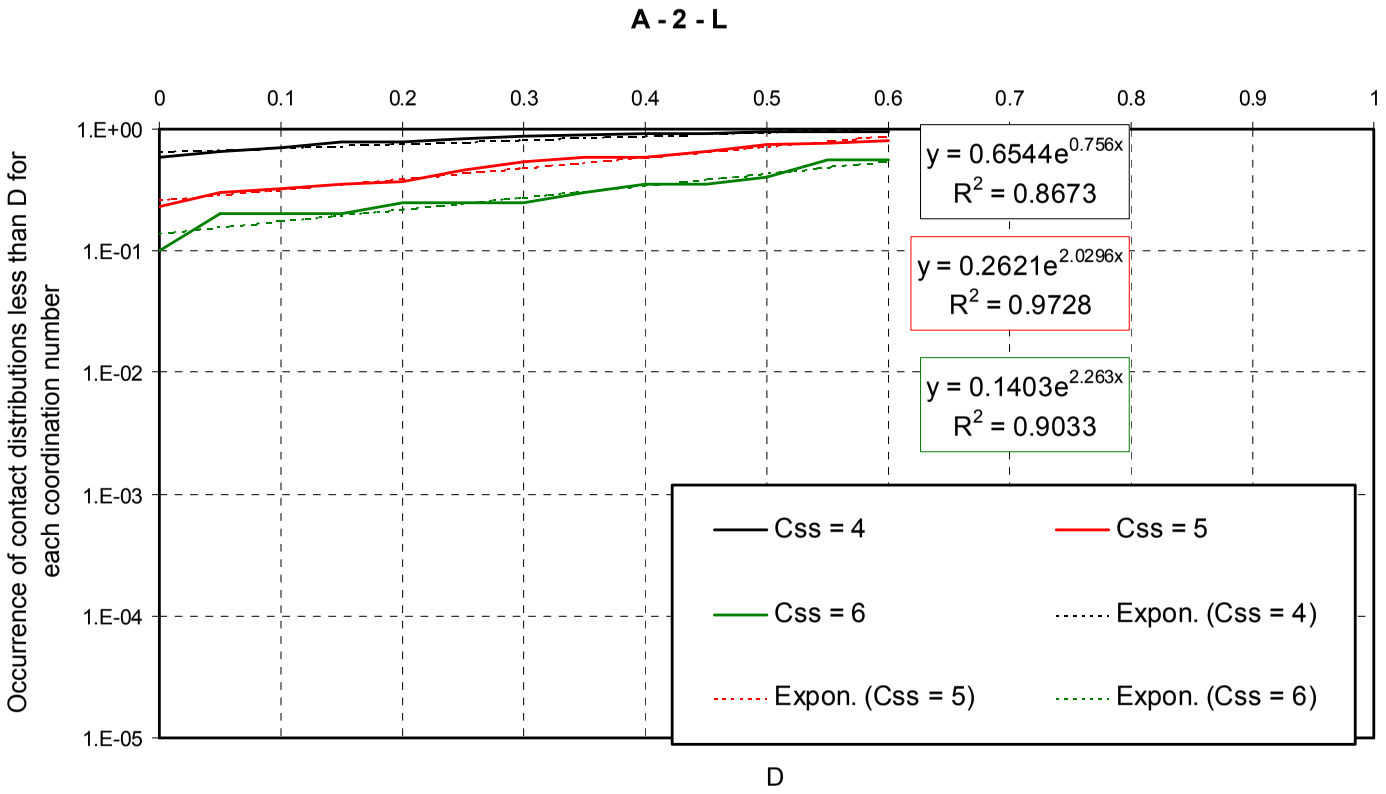
A - 2 - L
0
0.1
0.2
0.3
0.4
0.5
0.6
0.7
0.8
0.9
1
1.E+00
1.E-01
1.E-02
1.E-03
1.E-04
1.E-05
Occurrence of contact distributions less than D for each coordination number
D
y = 0.6544e^0.756x
R^2 = 0.8673
y = 0.2621e^2.0296x
R^2 = 0.9728
y = 0.1403e^2.263x
R^2 = 0.9033
Css = 4
Css = 5
Css = 6
Expon. (Css = 4)
Expon. (Css = 5)
Expon. (Css = 6)

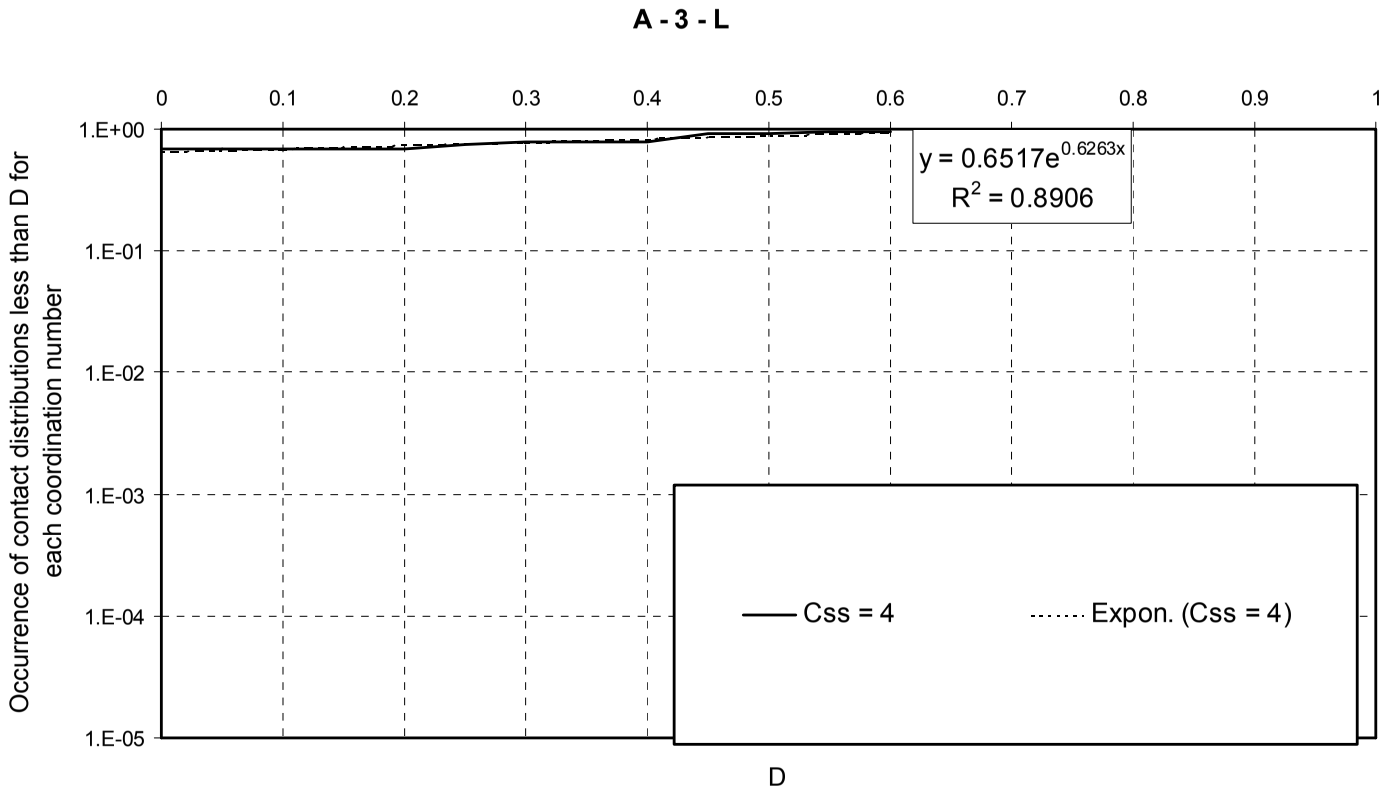
A - 3 - L
0
0.1
0.2
0.3
0.4
0.5
0.6
0.7
0.8
0.9
1
1.E+00
1.E-01
1.E-02
1.E-03
1.E-04
1.E-05
Occurrence of contact distributions less than D for each coordination number
y = 0.6517e^0.6263x
R^2 = 0.8906
Css = 4
Expon. (Css = 4)
D

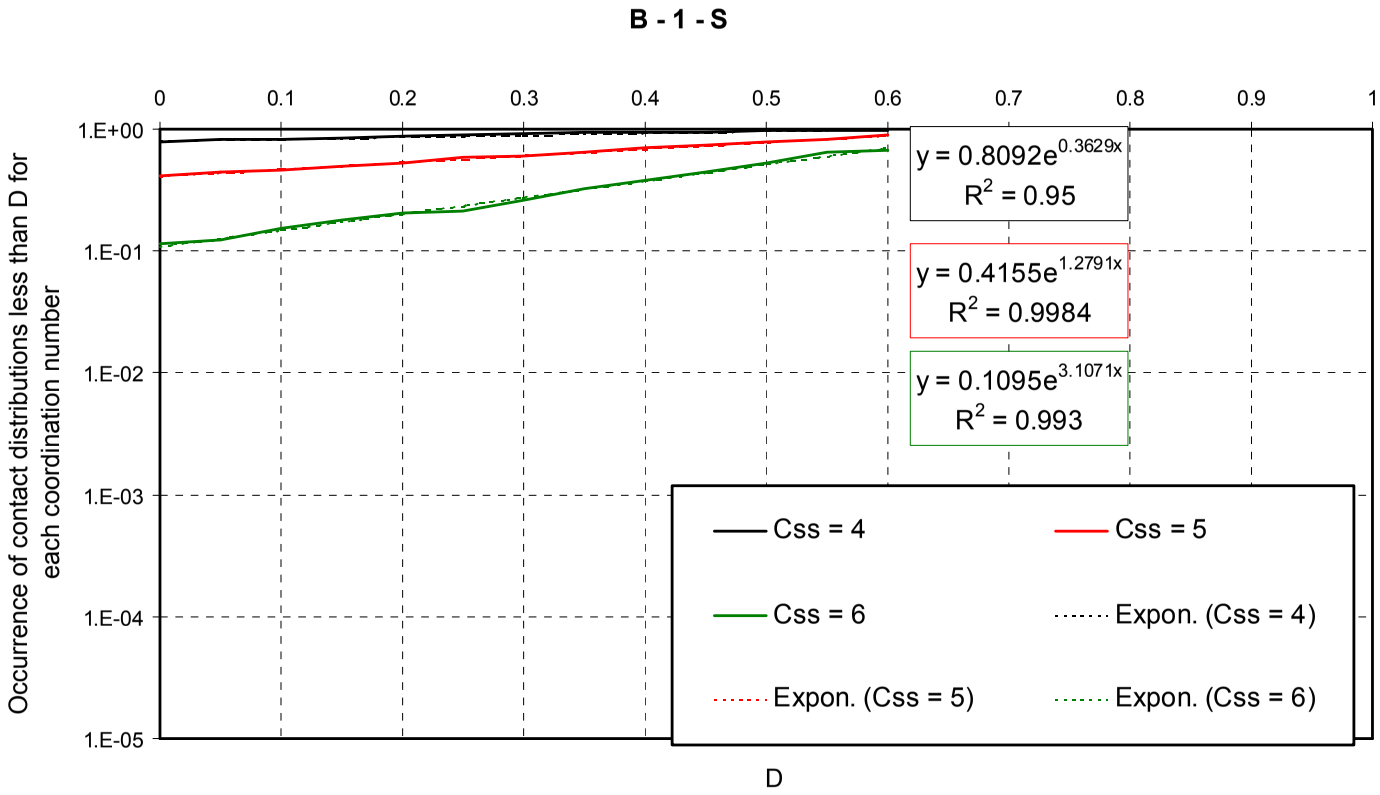
B - 1 - S
0
0.1
0.2
0.3
0.4
0.5
0.6
0.7
0.8
0.9
1
1.E+00
1.E-01
1.E-02
1.E-03
1.E-04
1.E-05
Occurrence of contact distributions less than D for each coordination number
D
y = 0.8092e^0.3629x
R^2 = 0.95
y = 0.4155e^1.2791x
R^2 = 0.9984
y = 0.1095e^3.1071x
R^2 = 0.993
Css = 4
Css = 5
Css = 6
Expon. (Css = 4)
Expon. (Css = 5)
Expon. (Css = 6)

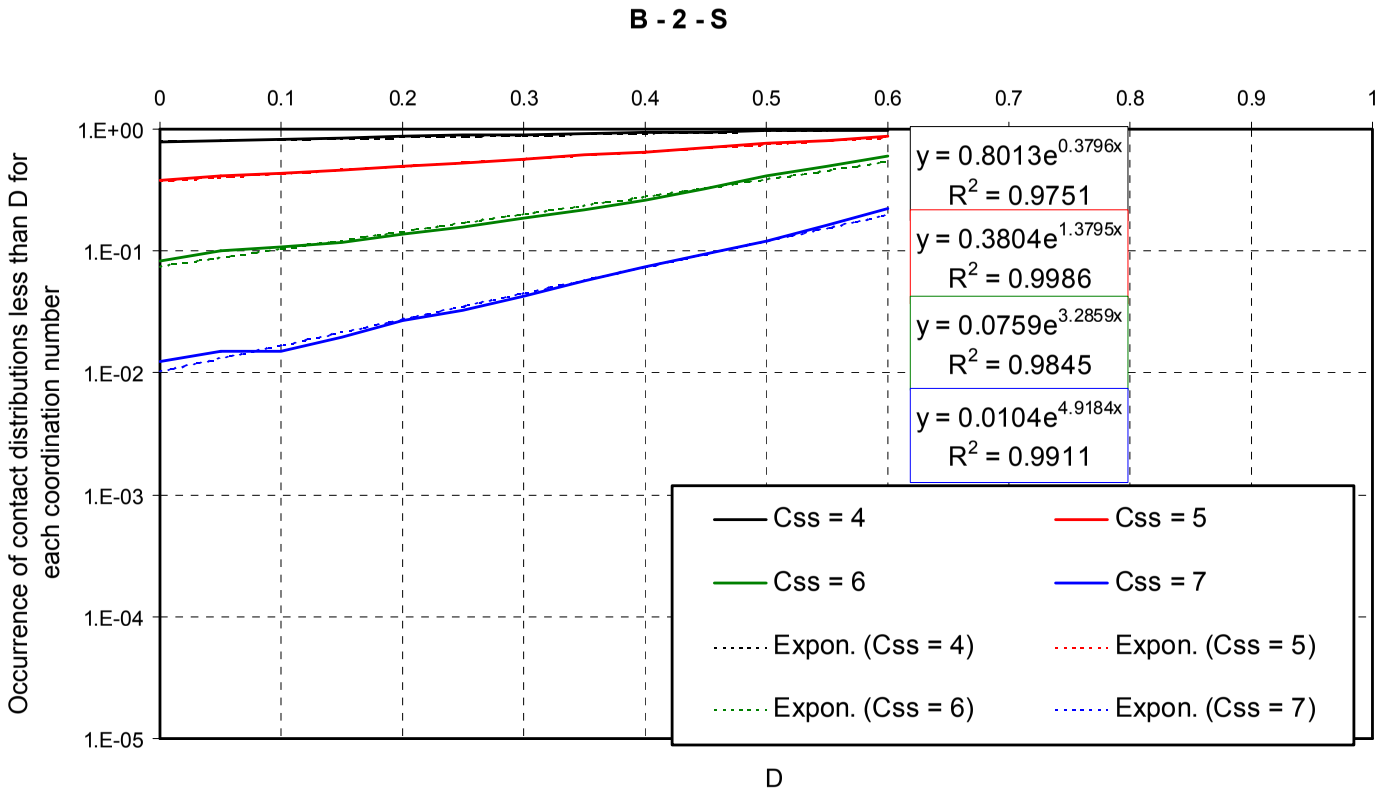
B - 2 - S
0
0.1
0.2
0.3
0.4
0.5
0.6
0.7
0.8
0.9
1
1.E+00
1.E-01
1.E-02
1.E-03
1.E-04
1.E-05
Occurrence of contact distributions less than D for each coordination number
D
y = 0.8013e^0.3796x
R^2 = 0.9751
y = 0.3804e^1.3795x
R^2 = 0.9986
y = 0.0759e^3.2859x
R^2 = 0.9845
y = 0.0104e^4.9184x
R^2 = 0.9911
Css = 4
Css = 5
Css = 6
Css = 7
Expon. (Css = 4)
Expon. (Css = 5)
Expon. (Css = 6)
Expon. (Css = 7)

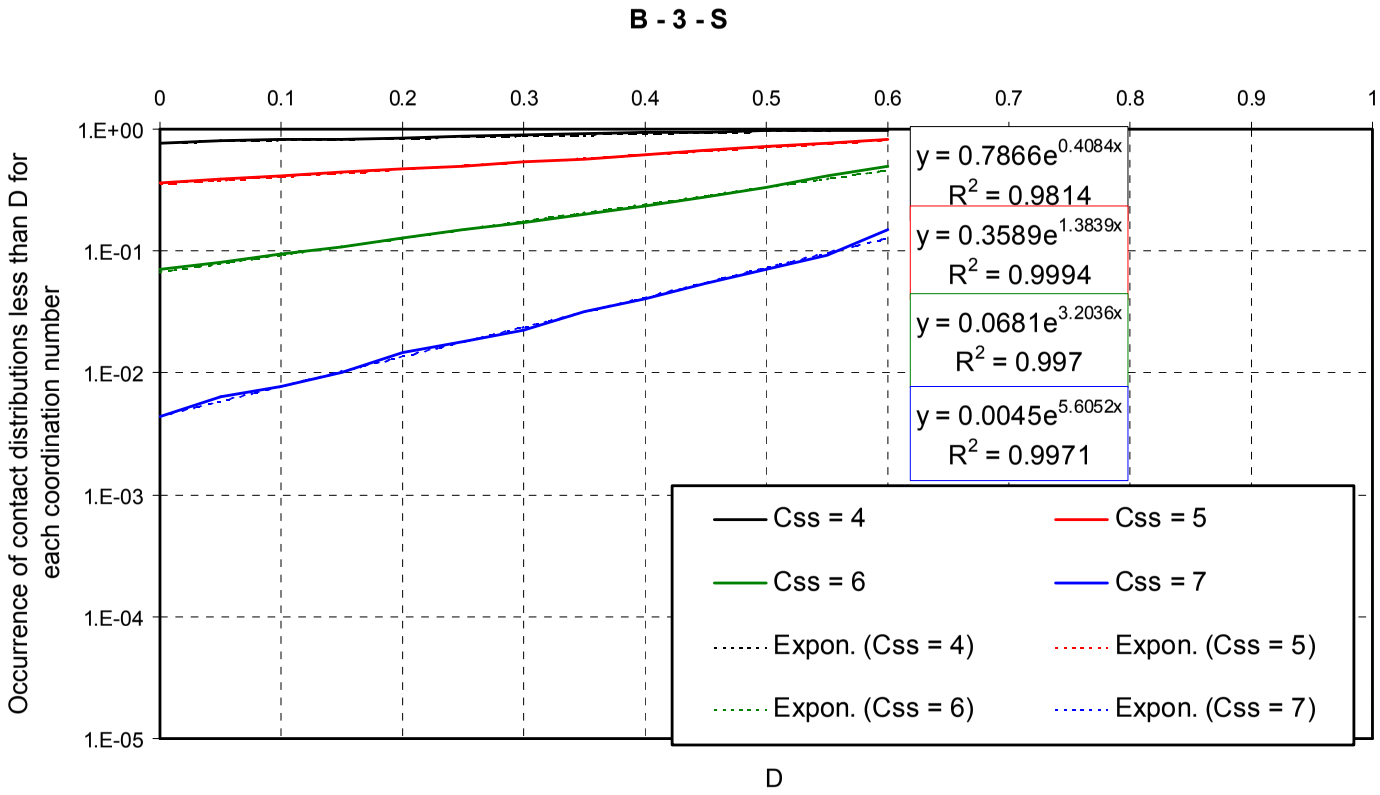
B - 3 - S
0
0.1
0.2
0.3
0.4
0.5
0.6
0.7
0.8
0.9
1
1.E+00
1.E-01
1.E-02
1.E-03
1.E-04
1.E-05
Occurrence of contact distributions less than D for each coordination number
D
y = 0.7866e^0.4084x
R^2 = 0.9814
y = 0.3589e^1.3839x
R^2 = 0.9994
y = 0.0681e^3.2036x
R^2 = 0.997
y = 0.0045e^5.6052x
R^2 = 0.9971
Css = 4
Css = 5
Css = 6
Css = 7
Expon. (Css = 4)
Expon. (Css = 5)
Expon. (Css = 6)
Expon. (Css = 7)

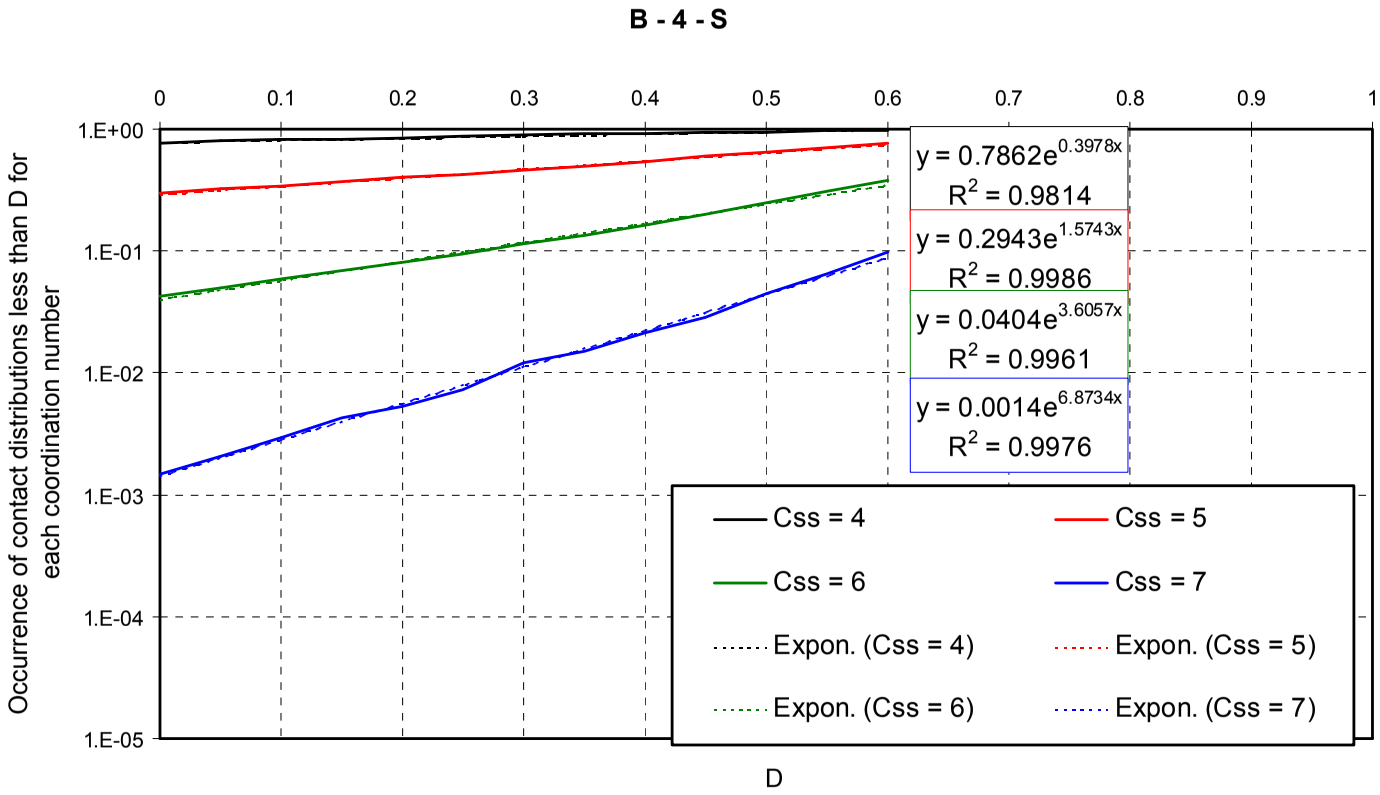
B - 4 - S
0
0.1
0.2
0.3
0.4
0.5
0.6
0.7
0.8
0.9
1
1.E+00
1.E-01
1.E-02
1.E-03
1.E-04
1.E-05
Occurrence of contact distributions less than D for each coordination number
D
y = 0.7862e^0.3978x
R^2 = 0.9814
y = 0.2943e^1.5743x
R^2 = 0.9986
y = 0.0404e^3.6057x
R^2 = 0.9961
y = 0.0014e^6.8734x
R^2 = 0.9976
Css = 4
Css = 5
Css = 6
Css = 7
Expon. (Css = 4)
Expon. (Css = 5)
Expon. (Css = 6)
Expon. (Css = 7)

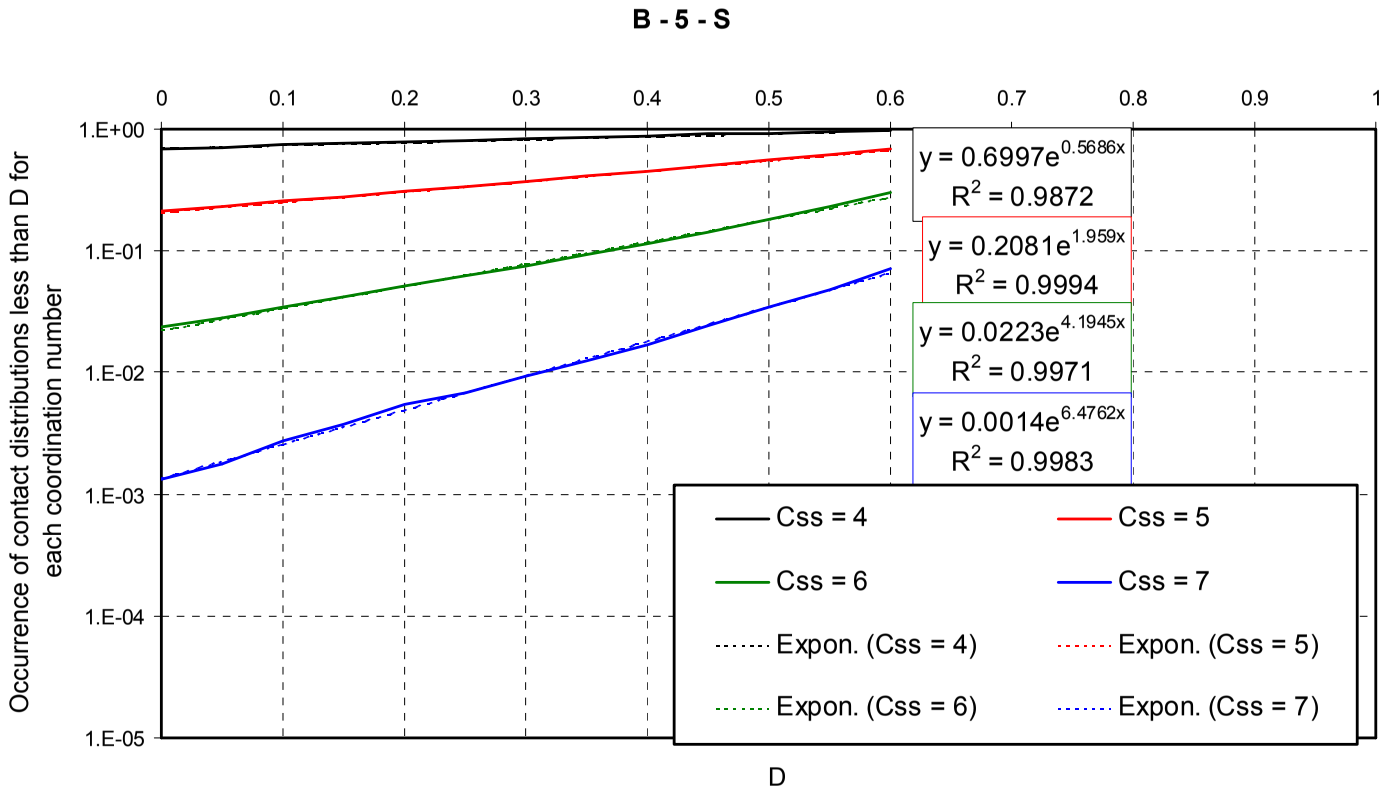
B - 5 - S
0
0.1
0.2
0.3
0.4
0.5
0.6
0.7
0.8
0.9
1
1.E+00
1.E-01
1.E-02
1.E-03
1.E-04
1.E-05
Occurrence of contact distributions less than D for each coordination number
D
y = 0.6997e^0.5686x
R^2 = 0.9872
y = 0.2081e^1.959x
R^2 = 0.9994
y = 0.0223e^4.1945x
R^2 = 0.9971
y = 0.0014e^6.4762x
R^2 = 0.9983
Css = 4
Css = 5
Css = 6
Css = 7
Expon. (Css = 4)
Expon. (Css = 5)
Expon. (Css = 6)
Expon. (Css = 7)

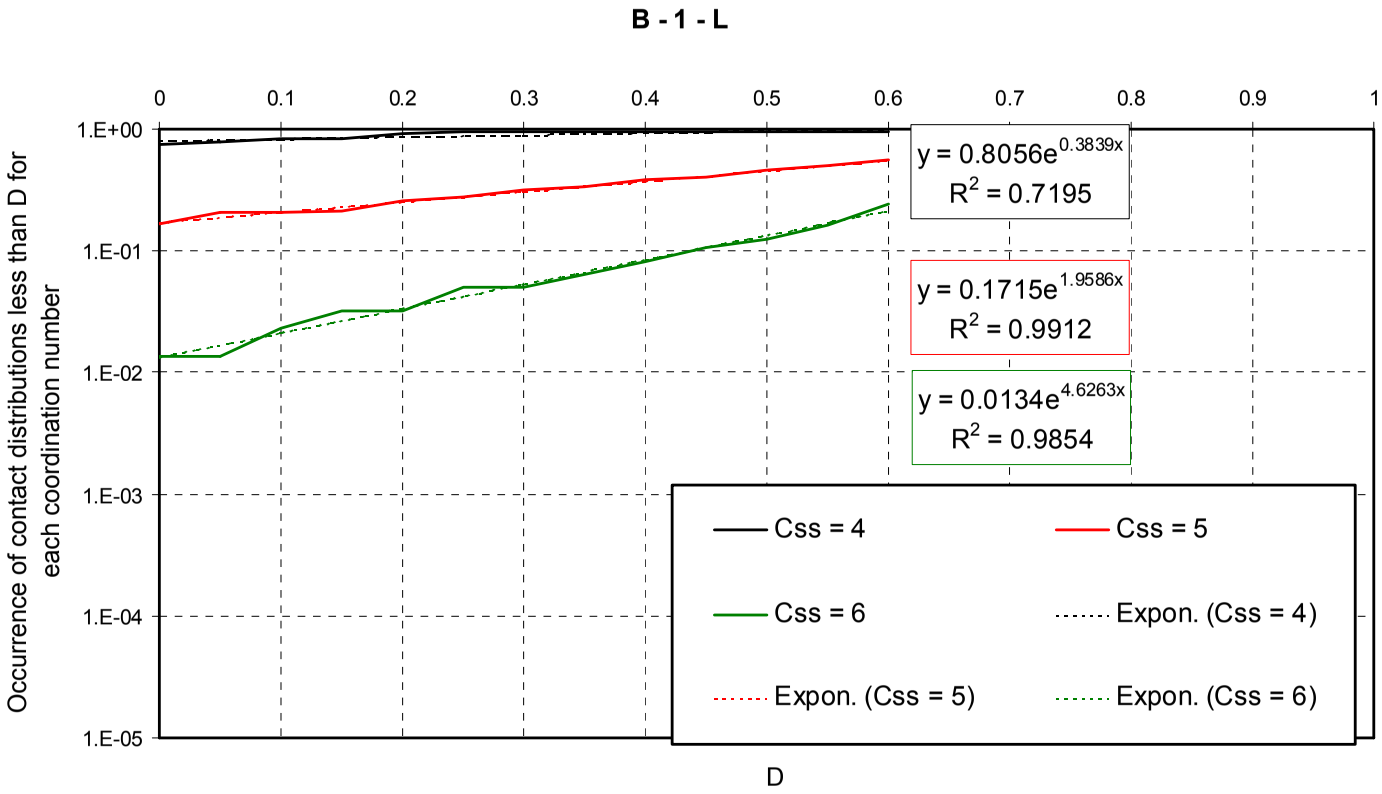
B - 1 - L
0
0.1
0.2
0.3
0.4
0.5
0.6
0.7
0.8
0.9
1
1.E+00
1.E-01
1.E-02
1.E-03
1.E-04
1.E-05
Occurrence of contact distributions less than D for each coordination number
D
y = 0.8056e^0.3839x
R^2 = 0.7195
y = 0.1715e^1.9586x
R^2 = 0.9912
y = 0.0134e^4.6263x
R^2 = 0.9854
Css = 4
Css = 5
Css = 6
Expon. (Css = 4)
Expon. (Css = 5)
Expon. (Css = 6)

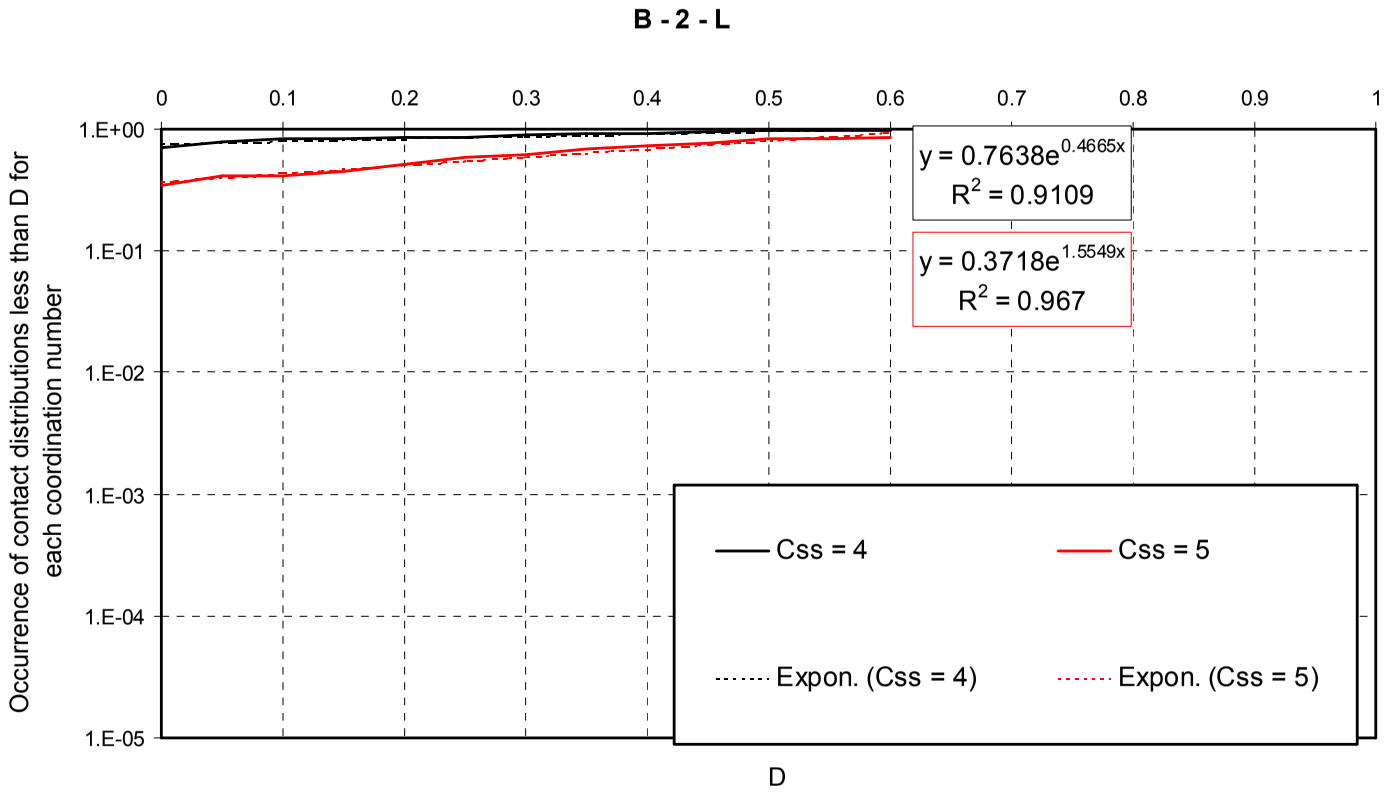
B - 2 - L
0
0.1
0.2
0.3
0.4
0.5
0.6
0.7
0.8
0.9
1
1.E+00
1.E-01
1.E-02
1.E-03
1.E-04
1.E-05
Occurrence of contact distributions less than D for each coordination number
y = 0.7638e^0.4665x
R^2 = 0.9109
y = 0.3718e^1.5549x
R^2 = 0.967
Css = 4
Css = 5
Expon. (Css = 4)
Expon. (Css = 5)
D

J EXAMPLE OF FORWARD ANALYSIS OF COORDINATION NUMBER

J.1 Introduction

Given the radii of the two types of spheres, namely large and small, and given their respective quantities in the considered bidisperse packing, estimate the distribution of the four different partial coordination numbers C_{ss}, C_{sl}, C_{ls} and C_{ll}.

In the following example, we analyse try to estimate coordination numbers for the packing A-3.

J.2 Inputs

Table 22 Input 1 to forward analysis

Input 1 – I1 Packing's Characteristics	
R_s – Radius of small spheres	1
R_l – Radius of large spheres	2
P_s – Packing density of small spheres	0.29
P_l – Packing density of large spheres	0.34

Table 23 Input 2 to forward analysis

Input 2 – I2 Useful Numbers		Derived from:
P_{ss}	8.75	Literature, I1
P_{ss}'	7.9	Figure, I1
P_{ll}	8.75	Literature, I1
P_{ll}'	8.1	Figure, I1
P_{ls}	19.7	Literature, I1
P_{ls}'	16.9	Figure, I1
C_{ssmax}	13.4	Appendix A, I1
C_{ssmax}^{L1}	11.64	Appendix A, I1
C_{llmax}	13.4	Appendix A, I1
C_{lsmax}	31.6	Appendix A, I1
C_{lsmax}^{L1}	29.5	Appendix A, I1

Table 24 Input 3 to forward analysis

Input 3 – I3 Known Distributions			Derived from:
Parameter	Mean	St Dev	
Css	3.74	1.44	Figure, I1
Cll	2.12	1.1	Figure, I1
Css'	0.635	0.12	Figure, I1
Cls'	0.71	0.1	Figure, I1

The distributions of the self-same coordination numbers Css and Cll can be directly estimated (Input 3) from Figure 4.21 and Figure 4.23, where the average value and the standard deviation of the normal distributions that describe them are plotted as functions of size ratio and grading (Input 1). The result of their estimation is shown in Tables 25 and 26 and Figures J.1 and J.2.

Table 25 Comparison between estimated distribution of Css and observed distribution of Css

Css	Estimated Total Distribution of Css	Observed Total Distribution of Css
0	0.009	0.007
1	0.045	0.049
2	0.133	0.135
3	0.243	0.252
4	0.273	0.256
5	0.190	0.187
6	0.081	0.087
7	0.022	0.024
8	0.004	0.003
9	0.000	0.000
10	0.000	0.000

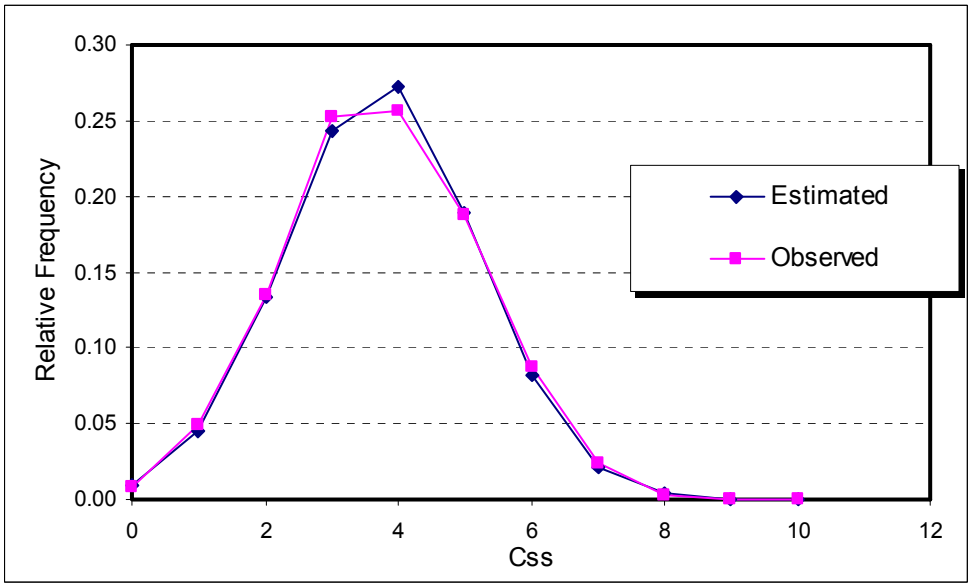

Figure J.1 Estimated and observed distributions of Css

Table 26 Comparison between estimated distribution of Cll and observed distribution of Cll

Cll	Estimated Total Distribution of Cll	Observed Total Distribution of Cll
0	0.058	0.058
1	0.218	0.231
2	0.361	0.385
3	0.265	0.202
4	0.086	0.111
5	0.012	0.014
6	0.001	0.000
7	0.000	0.000
8	0.000	0.000
9	0.000	0.000
10	0.000	0.000

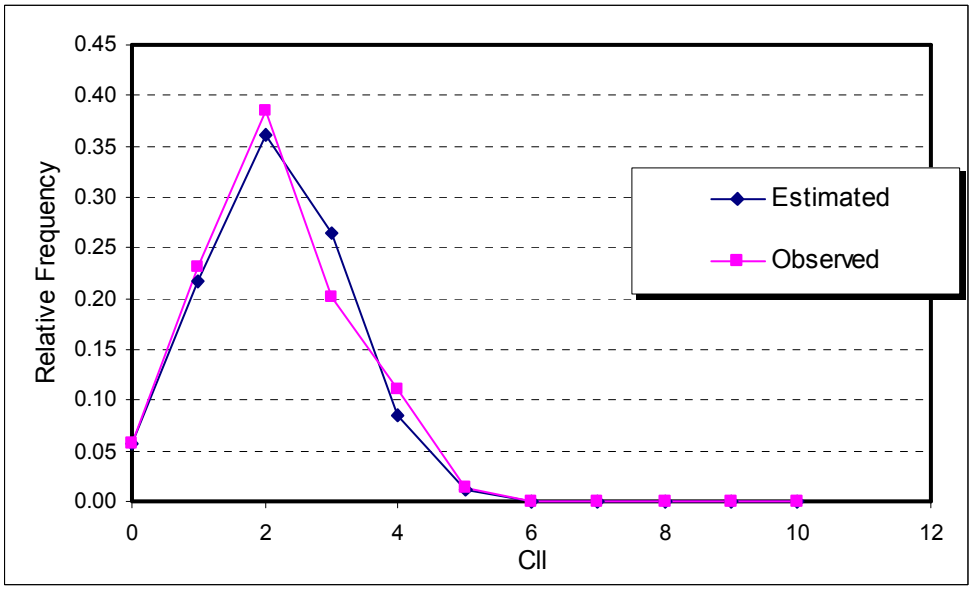

Figure J.2 Estimated and observed distributions of Cll

The next sections show how to estimate the distributions of Cls (Task A) and Csl (Task B).

J.3 Estimation of Cls – Task A

In this first case, the unknown **total distribution of Cls** is a linear combination of the known **relative distributions of Cls for each value of Cll**, where the coefficients of the linear combination are the known **occurrences of each value of Cll**, i.e. the distribution of large spheres on a large one, Cll.

Using transformation B2 we calculate the values of Cls' that, for different values of Cll, correspond to each value of Cls (Table 27):

Table 27 Values of Cls'

Cls'	Cll = 0	Cll = 1	Cll = 2	Cll = 3	Cll = 4	Cll = 5	Cll = 6	Cll = 7	Cll = 8	Cll = 9	Cll = 10
Cls = -1	-0.059	0.007	0.074	0.140	0.207	0.273	0.340	0.406	0.472	0.539	0.605
Cls = 0	0.000	0.066	0.133	0.199	0.266	0.332	0.399	0.465	0.532	0.598	0.665
Cls = 1	0.059	0.126	0.192	0.259	0.325	0.391	0.458	0.524	0.591	0.657	0.724
Cls = 2	0.118	0.185	0.251	0.318	0.384	0.451	0.517	0.584	0.650	0.716	0.783
Cls = 3	0.178	0.244	0.310	0.377	0.443	0.510	0.576	0.643	0.709	0.776	0.842
Cls = 4	0.237	0.303	0.370	0.436	0.503	0.569	0.635	0.702	0.768	0.835	0.901
Cls = 5	0.296	0.362	0.429	0.495	0.562	0.628	0.695	0.761	0.828	0.894	0.960
Cls = 6	0.355	0.421	0.488	0.554	0.621	0.687	0.754	0.820	0.887	0.953	1.020
Cls = 7	0.414	0.481	0.547	0.614	0.680	0.746	0.813	0.879	0.946	1.012	1.079
Cls = 8	0.473	0.540	0.606	0.673	0.739	0.806	0.872	0.939	1.005	1.071	1.138
Cls = 9	0.533	0.599	0.665	0.732	0.798	0.865	0.931	0.998	1.064	1.131	1.197
Cls = 10	0.592	0.658	0.725	0.791	0.858	0.924	0.990	1.057	1.123	1.190	1.256
Cls = 11	0.651	0.717	0.784	0.850	0.917	0.983	1.050	1.116	1.183	1.249	1.315
Cls = 12	0.710	0.777	0.843	0.909	0.976	1.042	1.109	1.175	1.242	1.308	1.375
Cls = 13	0.769	0.836	0.902	0.969	1.035	1.102	1.168	1.234	1.301	1.367	1.434
Cls = 14	0.828	0.895	0.961	1.028	1.094	1.161	1.227	1.294	1.360	1.427	1.493
Cls = 15	0.888	0.954	1.020	1.087	1.153	1.220	1.286	1.353	1.419	1.486	1.552
Cls = 16	0.947	1.013	1.080	1.146	1.213	1.279	1.345	1.412	1.478	1.545	1.611
Cls = 17	1.006	1.072	1.139	1.205	1.272	1.338	1.405	1.471	1.538	1.604	1.670
Cls = 18	1.065	1.132	1.198	1.264	1.331	1.397	1.464	1.530	1.597	1.663	1.730
Cls = 19	1.124	1.191	1.257	1.324	1.390	1.457	1.523	1.589	1.656	1.722	1.789
Cls = 20	1.183	1.250	1.316	1.383	1.449	1.516	1.582	1.649	1.715	1.782	1.848
Cls = 21	1.243	1.309	1.376	1.442	1.508	1.575	1.641	1.708	1.774	1.841	1.907

Calculating the value that the characteristic distribution assumes for each value of Cls' and associating this calculated value to the values of Cls and Cll that generated Cls', we obtain the relative distributions of Cls in cumulative form (columns in Table 28):

Table 28 Cumulative relative distributions of Cls

f(Cls, Cll) - cumulative	Cll = 0	Cll = 1	Cll = 2	Cll = 3	Cll = 4	Cll = 5	Cll = 6	Cll = 7	Cll = 8	Cll = 9	Cll = 10
Cls = -1	0.000	0.000	0.000	0.000	0.000	0.000	0.000	0.001	0.009	0.044	0.148
Cls = 0	0.000	0.000	0.000	0.000	0.000	0.000	0.001	0.007	0.037	0.132	0.325
Cls = 1	0.000	0.000	0.000	0.000	0.000	0.001	0.006	0.032	0.117	0.299	0.555
Cls = 2	0.000	0.000	0.000	0.000	0.001	0.005	0.027	0.103	0.274	0.526	0.767
Cls = 3	0.000	0.000	0.000	0.000	0.004	0.023	0.091	0.250	0.497	0.744	0.907
Cls = 4	0.000	0.000	0.000	0.003	0.019	0.079	0.228	0.468	0.720	0.894	0.972
Cls = 5	0.000	0.000	0.002	0.016	0.069	0.206	0.439	0.695	0.880	0.967	0.994
Cls = 6	0.000	0.002	0.013	0.060	0.186	0.410	0.669	0.865	0.961	0.992	0.999
Cls = 7	0.002	0.011	0.052	0.167	0.382	0.642	0.848	0.955	0.991	0.999	1.000
Cls = 8	0.009	0.044	0.150	0.355	0.615	0.831	0.947	0.989	0.998	1.000	1.000
Cls = 9	0.038	0.133	0.328	0.587	0.812	0.939	0.987	0.998	1.000	1.000	1.000
Cls = 10	0.118	0.302	0.558	0.791	0.930	0.984	0.997	1.000	1.000	1.000	1.000
Cls = 11	0.277	0.529	0.770	0.920	0.981	0.997	1.000	1.000	1.000	1.000	1.000
Cls = 12	0.500	0.747	0.908	0.977	0.996	1.000	1.000	1.000	1.000	1.000	1.000
Cls = 13	0.723	0.896	0.973	0.995	0.999	1.000	1.000	1.000	1.000	1.000	1.000
Cls = 14	0.882	0.968	0.994	0.999	1.000	1.000	1.000	1.000	1.000	1.000	1.000
Cls = 15	0.962	0.993	0.999	1.000	1.000	1.000	1.000	1.000	1.000	1.000	1.000
Cls = 16	0.991	0.999	1.000	1.000	1.000	1.000	1.000	1.000	1.000	1.000	1.000
Cls = 17	0.998	1.000	1.000	1.000	1.000	1.000	1.000	1.000	1.000	1.000	1.000
Cls = 18	1.000	1.000	1.000	1.000	1.000	1.000	1.000	1.000	1.000	1.000	1.000
Cls = 19	1.000	1.000	1.000	1.000	1.000	1.000	1.000	1.000	1.000	1.000	1.000
Cls = 20	1.000	1.000	1.000	1.000	1.000	1.000	1.000	1.000	1.000	1.000	1.000
Cls = 21	1.000	1.000	1.000	1.000	1.000	1.000	1.000	1.000	1.000	1.000	1.000

From these cumulative distributions we calculate the absolute distributions subtracting from each term the previous term (Table 29):

Table 29 Relative distributions of Cls'

f(Cls, Cll)	Cll = 0	Cll = 1	Cll = 2	Cll = 3	Cll = 4	Cll = 5	Cll = 6	Cll = 7	Cll = 8	Cll = 9	Cll = 10
Cls = 0	0.000	0.000	0.000	0.000	0.000	0.000	0.001	0.006	0.028	0.088	0.177
Cls = 1	0.000	0.000	0.000	0.000	0.000	0.001	0.005	0.025	0.079	0.167	0.230
Cls = 2	0.000	0.000	0.000	0.000	0.001	0.004	0.021	0.071	0.158	0.227	0.212
Cls = 3	0.000	0.000	0.000	0.000	0.003	0.018	0.064	0.147	0.222	0.218	0.140
Cls = 4	0.000	0.000	0.000	0.003	0.015	0.057	0.137	0.217	0.224	0.150	0.065
Cls = 5	0.000	0.000	0.002	0.013	0.050	0.127	0.211	0.228	0.160	0.073	0.022
Cls = 6	0.000	0.002	0.011	0.044	0.117	0.204	0.230	0.170	0.081	0.025	0.005
Cls = 7	0.001	0.009	0.038	0.108	0.196	0.232	0.179	0.090	0.029	0.006	0.001
Cls = 8	0.007	0.033	0.098	0.187	0.233	0.188	0.099	0.034	0.008	0.001	0.000
Cls = 9	0.029	0.089	0.178	0.232	0.197	0.109	0.039	0.009	0.001	0.000	0.000
Cls = 10	0.080	0.169	0.230	0.205	0.118	0.045	0.011	0.002	0.000	0.000	0.000
Cls = 11	0.159	0.227	0.212	0.128	0.051	0.013	0.002	0.000	0.000	0.000	0.000
Cls = 12	0.223	0.218	0.138	0.057	0.015	0.003	0.000	0.000	0.000	0.000	0.000
Cls = 13	0.223	0.149	0.064	0.018	0.003	0.000	0.000	0.000	0.000	0.000	0.000
Cls = 14	0.159	0.072	0.021	0.004	0.001	0.000	0.000	0.000	0.000	0.000	0.000
Cls = 15	0.080	0.025	0.005	0.001	0.000	0.000	0.000	0.000	0.000	0.000	0.000
Cls = 16	0.029	0.006	0.001	0.000	0.000	0.000	0.000	0.000	0.000	0.000	0.000
Cls = 17	0.007	0.001	0.000	0.000	0.000	0.000	0.000	0.000	0.000	0.000	0.000
Cls = 18	0.001	0.000	0.000	0.000	0.000	0.000	0.000	0.000	0.000	0.000	0.000
Cls = 19	0.000	0.000	0.000	0.000	0.000	0.000	0.000	0.000	0.000	0.000	0.000
Cls = 20	0.000	0.000	0.000	0.000	0.000	0.000	0.000	0.000	0.000	0.000	0.000
Cls = 21	0.000	0.000	0.000	0.000	0.000	0.000	0.000	0.000	0.000	0.000	0.000

Some of these distributions reach negative values of Cls, therefore we have to refer to the distribution of their non-negative part:

Table 30 Distribution of the non-negative part of relative distributions of Cls

f(Cls, Cll) – non-negative	Cll = 0	Cll = 1	Cll = 2	Cll = 3	Cll = 4	Cll = 5	Cll = 6	Cll = 7	Cll = 8	Cll = 9	Cll = 10
Cls = 0	0.000	0.000	0.000	0.000	0.000	0.000	0.001	0.006	0.029	0.092	0.208
Cls = 1	0.000	0.000	0.000	0.000	0.000	0.001	0.005	0.025	0.080	0.175	0.270
Cls = 2	0.000	0.000	0.000	0.000	0.001	0.004	0.021	0.071	0.159	0.237	0.249
Cls = 3	0.000	0.000	0.000	0.000	0.003	0.018	0.064	0.148	0.224	0.228	0.164
Cls = 4	0.000	0.000	0.000	0.003	0.015	0.057	0.137	0.217	0.225	0.157	0.077
Cls = 5	0.000	0.000	0.002	0.013	0.050	0.127	0.211	0.228	0.161	0.076	0.026
Cls = 6	0.000	0.002	0.011	0.044	0.117	0.204	0.230	0.170	0.082	0.027	0.006
Cls = 7	0.001	0.009	0.038	0.108	0.196	0.232	0.179	0.090	0.030	0.007	0.001
Cls = 8	0.007	0.033	0.098	0.187	0.233	0.188	0.099	0.034	0.008	0.001	0.000
Cls = 9	0.029	0.089	0.178	0.232	0.197	0.109	0.039	0.009	0.001	0.000	0.000
Cls = 10	0.080	0.169	0.230	0.205	0.118	0.045	0.011	0.002	0.000	0.000	0.000
Cls = 11	0.159	0.227	0.212	0.128	0.051	0.013	0.002	0.000	0.000	0.000	0.000
Cls = 12	0.223	0.218	0.138	0.057	0.015	0.003	0.000	0.000	0.000	0.000	0.000
Cls = 13	0.223	0.149	0.064	0.018	0.003	0.000	0.000	0.000	0.000	0.000	0.000
Cls = 14	0.159	0.072	0.021	0.004	0.001	0.000	0.000	0.000	0.000	0.000	0.000
Cls = 15	0.080	0.025	0.005	0.001	0.000	0.000	0.000	0.000	0.000	0.000	0.000
Cls = 16	0.029	0.006	0.001	0.000	0.000	0.000	0.000	0.000	0.000	0.000	0.000
Cls = 17	0.007	0.001	0.000	0.000	0.000	0.000	0.000	0.000	0.000	0.000	0.000
Cls = 18	0.001	0.000	0.000	0.000	0.000	0.000	0.000	0.000	0.000	0.000	0.000
Cls = 19	0.000	0.000	0.000	0.000	0.000	0.000	0.000	0.000	0.000	0.000	0.000
Cls = 20	0.000	0.000	0.000	0.000	0.000	0.000	0.000	0.000	0.000	0.000	0.000
Cls = 21	0.000	0.000	0.000	0.000	0.000	0.000	0.000	0.000	0.000	0.000	0.000

Each of these distributions (columns of Table 30) has to be weighted multiplying it by the relative occurrence of each Cll value in Table 31 (total distribution of Cll estimated earlier):

Table 31 Distribution of Cll

F(Cll)	Cll = 0	Cll = 1	Cll = 2	Cll = 3	Cll = 4	Cll = 5	Cll = 6	Cll = 7	Cll = 8	Cll = 9	Cll = 10
	0.058	0.218	0.361	0.265	0.086	0.012	0.001	0.000	0.000	0.000	0.000

Obtaining the distributions in Table 32:

Table 32 Weighted relative distributions of Cls

f(Cls, Cll) - weighted	Cll = 0	Cll = 1	Cll = 2	Cll = 3	Cll = 4	Cll = 5	Cll = 6	Cll = 7	Cll = 8	Cll = 9	Cll = 10
Cls = 0	0.000	0.000	0.000	0.000	0.000	0.000	0.000	0.000	0.000	0.000	0.000
Cls = 1	0.000	0.000	0.000	0.000	0.000	0.000	0.000	0.000	0.000	0.000	0.000
Cls = 2	0.000	0.000	0.000	0.000	0.000	0.000	0.000	0.000	0.000	0.000	0.000
Cls = 3	0.000	0.000	0.000	0.000	0.000	0.000	0.000	0.000	0.000	0.000	0.000
Cls = 4	0.000	0.000	0.000	0.001	0.001	0.001	0.000	0.000	0.000	0.000	0.000
Cls = 5	0.000	0.000	0.001	0.003	0.004	0.002	0.000	0.000	0.000	0.000	0.000
Cls = 6	0.000	0.000	0.004	0.012	0.010	0.002	0.000	0.000	0.000	0.000	0.000
Cls = 7	0.000	0.002	0.014	0.028	0.017	0.003	0.000	0.000	0.000	0.000	0.002
Cls = 8	0.000	0.007	0.035	0.050	0.020	0.002	0.000	0.000	0.000	0.000	0.007
Cls = 9	0.002	0.019	0.064	0.061	0.017	0.001	0.000	0.000	0.000	0.002	0.019
Cls = 10	0.005	0.037	0.083	0.054	0.010	0.001	0.000	0.000	0.000	0.005	0.037
Cls = 11	0.009	0.049	0.076	0.034	0.004	0.000	0.000	0.000	0.000	0.009	0.049
Cls = 12	0.013	0.047	0.050	0.015	0.001	0.000	0.000	0.000	0.000	0.013	0.047
Cls = 13	0.013	0.032	0.023	0.005	0.000	0.000	0.000	0.000	0.000	0.013	0.032
Cls = 14	0.009	0.016	0.008	0.001	0.000	0.000	0.000	0.000	0.000	0.009	0.016
Cls = 15	0.005	0.005	0.002	0.000	0.000	0.000	0.000	0.000	0.000	0.005	0.005
Cls = 16	0.002	0.001	0.000	0.000	0.000	0.000	0.000	0.000	0.000	0.002	0.001
Cls = 17	0.000	0.000	0.000	0.000	0.000	0.000	0.000	0.000	0.000	0.000	0.000
Cls = 18	0.000	0.000	0.000	0.000	0.000	0.000	0.000	0.000	0.000	0.000	0.000
Cls = 19	0.000	0.000	0.000	0.000	0.000	0.000	0.000	0.000	0.000	0.000	0.000
Cls = 20	0.000	0.000	0.000	0.000	0.000	0.000	0.000	0.000	0.000	0.000	0.000
Cls = 21	0.000	0.000	0.000	0.000	0.000	0.000	0.000	0.000	0.000	0.000	0.000

The sum of these relative distributions will be the total distribution of Cls (Table 33).

Table 33 Comparison between estimated and observed distributions of Cls

Cls	Estimated Total distribution of Cls	Observed Total Distribution of Cls
0	0.000	0.000
1	0.000	0.000
2	0.000	0.000
3	0.001	0.000
4	0.003	0.000
5	0.010	0.014
6	0.029	0.043
7	0.064	0.077
8	0.115	0.111
9	0.165	0.159
10	0.189	0.207
11	0.174	0.154
12	0.127	0.077
13	0.074	0.087
14	0.034	0.048
15	0.012	0.014
16	0.003	0.010
17	0.001	0.000
18	0.000	0.000
19	0.000	0.000
20	0.000	0.000
21	0.000	0.000

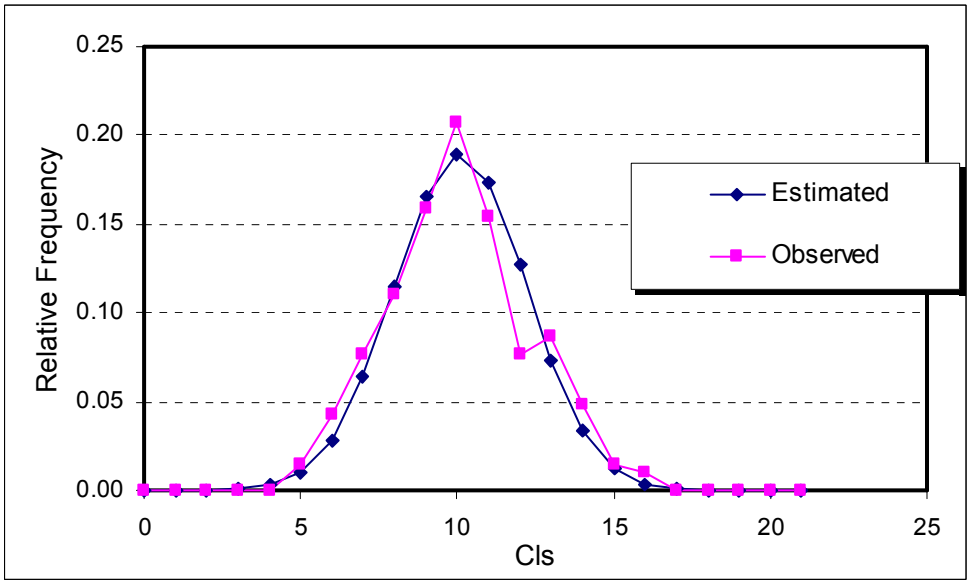

Figure J.3 Estimated and observed distributions of Cls

J.4 Estimation of Csl – Task B

In this second case, the known **total distribution of Css** is a linear combination of the known **relative distributions of Css for each value of Csl**, where the coefficients of the linear combination are the unknown **occurrences of each value of Csl**, i.e. the distribution of large spheres on a small one, Csl.

Using transformation B2 we calculate the values of Css' that, for different values of Csl, correspond to each value of Css (Table 34):

Table 34 Values of Css'

Css'	Csl = 0	Csl = 1	Csl = 2	Csl = 3	Csl = 4	Csl = 5	Csl = 6	Csl = 7
Css = -1	-0.127	0.005	0.136	0.267	0.399	0.530	0.661	0.793
Css = 0	0.000	0.131	0.263	0.394	0.525	0.657	0.788	0.919
Css = 1	0.127	0.258	0.389	0.521	0.652	0.783	0.915	1.046
Css = 2	0.253	0.385	0.516	0.647	0.779	0.910	1.041	1.173
Css = 3	0.380	0.511	0.642	0.774	0.905	1.036	1.168	1.299
Css = 4	0.506	0.638	0.769	0.900	1.032	1.163	1.294	1.426
Css = 5	0.633	0.764	0.896	1.027	1.158	1.290	1.421	1.552
Css = 6	0.759	0.891	1.022	1.154	1.285	1.416	1.548	1.679
Css = 7	0.886	1.017	1.149	1.280	1.411	1.543	1.674	1.805
Css = 8	1.013	1.144	1.275	1.407	1.538	1.669	1.801	1.932
Css = 9	1.139	1.271	1.402	1.533	1.665	1.796	1.927	2.059
Css = 10	1.266	1.397	1.529	1.660	1.791	1.923	2.054	2.185
Css = 11	1.392	1.524	1.655	1.786	1.918	2.049	2.180	2.312
Css = 12	1.519	1.650	1.782	1.913	2.044	2.176	2.307	2.438

Calculating the value that the characteristic distribution assumes for each value of Css' and associating this calculated value to the values of Css and

Csl that generated Css', we obtain the relative distributions of Css in cumulative form (columns of Table 35):

Table 35 Cumulative relative distributions of Css

f(Css, Csl) - cumulative	Csl = 0	Csl = 1	Csl = 2	Csl = 3	Csl = 4	Csl = 5	Csl = 6	Csl = 7
Css = -1	0.000	0.000	0.000	0.001	0.025	0.191	0.587	0.906
Css = 0	0.000	0.000	0.001	0.022	0.180	0.572	0.899	0.991
Css = 1	0.000	0.001	0.020	0.170	0.556	0.892	0.990	1.000
Css = 2	0.001	0.018	0.160	0.540	0.884	0.989	1.000	1.000
Css = 3	0.017	0.151	0.525	0.876	0.988	1.000	1.000	1.000
Css = 4	0.142	0.509	0.868	0.986	1.000	1.000	1.000	1.000
Css = 5	0.493	0.859	0.985	0.999	1.000	1.000	1.000	1.000
Css = 6	0.850	0.983	0.999	1.000	1.000	1.000	1.000	1.000
Css = 7	0.982	0.999	1.000	1.000	1.000	1.000	1.000	1.000
Css = 8	0.999	1.000	1.000	1.000	1.000	1.000	1.000	1.000
Css = 9	1.000	1.000	1.000	1.000	1.000	1.000	1.000	1.000
Css = 10	1.000	1.000	1.000	1.000	1.000	1.000	1.000	1.000
Css = 11	1.000	1.000	1.000	1.000	1.000	1.000	1.000	1.000
Css = 12	1.000	1.000	1.000	1.000	1.000	1.000	1.000	1.000

From these cumulative distributions we calculate the absolute distributions subtracting from each term the previous term (Table 36):

Table 36 Relative distributions of Css

f(Css, Csl)	Csl = 0	Csl = 1	Csl = 2	Csl = 3	Csl = 4	Csl = 5	Csl = 6	Csl = 7
Css = 0	0.000	0.000	0.001	0.021	0.156	0.381	0.312	0.085
Css = 1	0.000	0.001	0.019	0.148	0.376	0.320	0.091	0.009
Css = 2	0.001	0.018	0.140	0.370	0.328	0.097	0.010	0.000
Css = 3	0.016	0.132	0.364	0.336	0.104	0.011	0.000	0.000
Css = 4	0.125	0.358	0.343	0.110	0.012	0.000	0.000	0.000
Css = 5	0.351	0.350	0.117	0.013	0.000	0.000	0.000	0.000
Css = 6	0.357	0.124	0.014	0.001	0.000	0.000	0.000	0.000
Css = 7	0.132	0.016	0.001	0.000	0.000	0.000	0.000	0.000
Css = 8	0.017	0.001	0.000	0.000	0.000	0.000	0.000	0.000
Css = 9	0.001	0.000	0.000	0.000	0.000	0.000	0.000	0.000
Css = 10	0.000	0.000	0.000	0.000	0.000	0.000	0.000	0.000
Css = 11	0.000	0.000	0.000	0.000	0.000	0.000	0.000	0.000
Css = 12	0.000	0.000	0.000	0.000	0.000	0.000	0.000	0.000

Some of these distributions reach negative values of Css, therefore we have to refer to the distribution of their non-negative part (Table 37):

Table 37 Distribution of the non-negative part of relative distributions of Css

f(Css, Csl) – non-negative	Csl = 0	Csl = 1	Csl = 2	Csl = 3	Csl = 4	Csl = 5	Csl = 6	Csl = 7
Css = 0	0.000	0.000	0.001	0.021	0.160	0.471	0.755	0.906
Css = 1	0.000	0.001	0.019	0.148	0.385	0.396	0.221	0.091
Css = 2	0.001	0.018	0.140	0.371	0.336	0.120	0.023	0.003
Css = 3	0.016	0.132	0.364	0.336	0.106	0.013	0.001	0.000
Css = 4	0.125	0.358	0.343	0.110	0.012	0.001	0.000	0.000
Css = 5	0.351	0.350	0.117	0.013	0.000	0.000	0.000	0.000
Css = 6	0.357	0.124	0.014	0.001	0.000	0.000	0.000	0.000
Css = 7	0.132	0.016	0.001	0.000	0.000	0.000	0.000	0.000
Css = 8	0.017	0.001	0.000	0.000	0.000	0.000	0.000	0.000
Css = 9	0.001	0.000	0.000	0.000	0.000	0.000	0.000	0.000
Css = 10	0.000	0.000	0.000	0.000	0.000	0.000	0.000	0.000
Css = 11	0.000	0.000	0.000	0.000	0.000	0.000	0.000	0.000
Css = 12	0.000	0.000	0.000	0.000	0.000	0.000	0.000	0.000

The target is to weight each of these columns so that their sum is as close as possible to the total distribution of Css estimated earlier. These weights constitute the total distribution of Csl.

Since we know that this unknown distribution of Csl will have to be a normal distribution, this problem corresponds to finding the values of average and standard deviation of a normal distribution so that the relative frequencies of the values of Csl used as weights for the columns in Table 37 deliver a total distribution as close as possible to the estimated total distribution of Css. We can call the total distribution of Css estimated earlier as “I” and the one derived by the weighted sum of the relative distributions of Css as “II”. In this example, the normal distribution that

minimises the sum of the squares of the differences between I and II has average value of 1.50 and standard deviation of 1.04, delivering the following relative frequencies of Csl shown in Table 38 and Figure J.4 and approximating the estimated total distribution of Css as shown in Table 39 and Figure J.5.

Table 38 Comparison between estimated and observed distributions of Csl

Csl	Estimated Total distribution of Csl	Observed Total Distribution of Csl
0	0.139	0.145
1	0.350	0.368
2	0.350	0.341
3	0.139	0.129
4	0.022	0.017
5	0.001	0.000
6	0.000	0.000
7	0.000	0.000

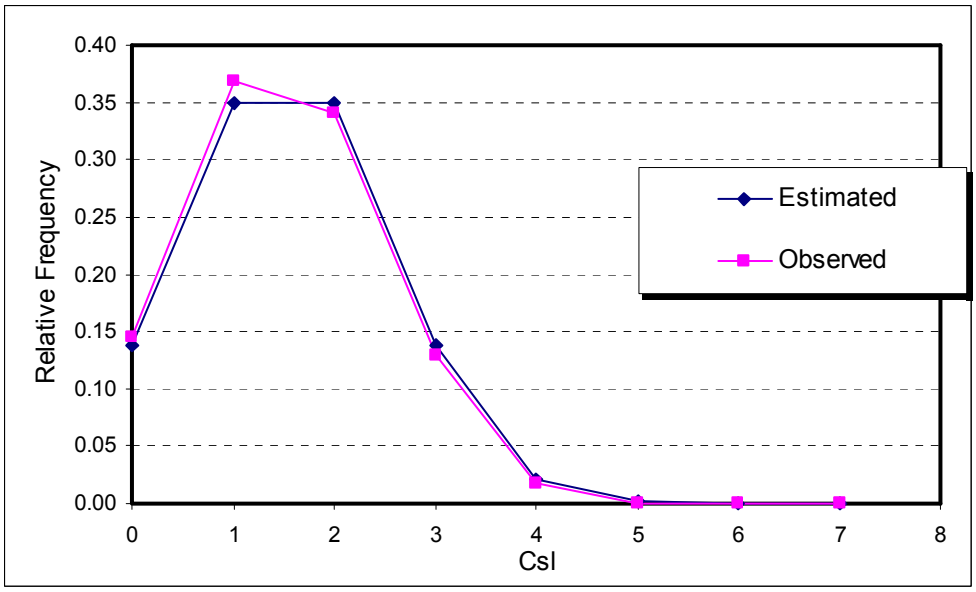

Figure J.4 Estimated and observed distributions of Csl

Table 39 Direct and indirect estimation of the distribution of Css

Css	Estimated Total Distribution of Css - I (as normal distribution)	Observed Total Distribution of Css	Estimated Total Distribution of Css - II (as sum of distributions)
0	0.009	0.007	0.007
1	0.045	0.049	0.037
2	0.133	0.135	0.114
3	0.243	0.252	0.225
4	0.273	0.256	0.278
5	0.190	0.187	0.214
6	0.081	0.087	0.098
7	0.022	0.024	0.024
8	0.004	0.003	0.003
9	0.000	0.000	0.000
10	0.000	0.000	0.000

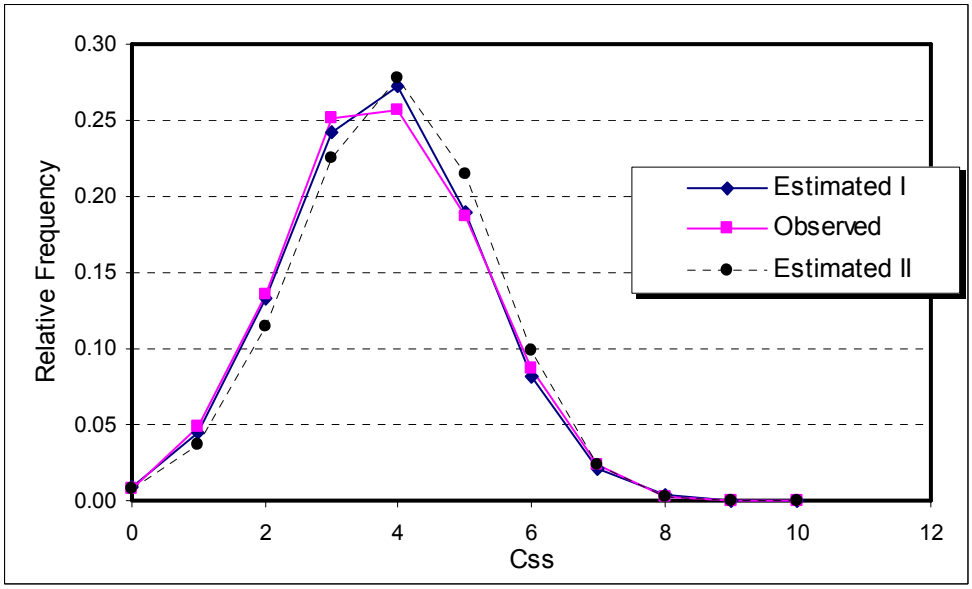

Figure J.5 Directly estimated, observed and indirectly estimated distributions of Css

K NOTES ON THE EXAMPLE DISCUSSED SECTION 4.6

K.1 Introduction

In Section 4.6 is presented an example of estimation of coordination number for a real bidisperse packing of spherical particles. The two types of particles are considered of the same size and, in order for them to be distinguished, they are called "black" and "white". During this analysis it was affirmed:

> *"Since the two types of spheres are geometrically identical, it can be shown that when the number of black and white spheres in the packing is much larger than 1, as it normally should be for a statistical approach to be valid, the average number of white spheres in contact with a white sphere, C_{ww}, is the same of white spheres in contact with a black one, C_{bw}."*

K.2 Demonstration

We have a packing formed by N_b black spheres and N_w white spheres of same size. Let's assume for every sphere a constant coordination number of 6. The total number of spheres is

$$N_{tot} = N_b + N_w \tag{36}$$

The probability for a **black** sphere to be touched only by **black** spheres (P_{bb}) can be calculated as follows:

The central sphere is black. The remaining spheres are ($N_b - 1$) black and N_w white, for a total of ($N_{tot} - 1$).

Probability for the first touching sphere to be black:

$$P_{bb}(1) = \frac{(N_b - 1)}{(N_{tot} - 1)} \tag{37}$$

Probability for the first two touching spheres to be black:

$$P_{bb}(2) = \frac{(N_b - 1)}{(N_{tot} - 1)} \cdot \frac{(N_b - 2)}{(N_{tot} - 2)} \tag{38}$$

If the coordination number is 6, the probability of a black sphere to be touched by 6 black spheres is:

$$P_{bb} = \frac{(N_b - 1)}{(N_{tot} - 1)} \cdot \frac{(N_b - 2)}{(N_{tot} - 2)} \cdot \frac{(N_b - 3)}{(N_{tot} - 3)} \cdot \frac{(N_b - 4)}{(N_{tot} - 4)} \cdot \frac{(N_b - 5)}{(N_{tot} - 5)} \cdot \frac{(N_b - 6)}{(N_{tot} - 6)} \quad (39)$$

Similarly, we can calculate the probability of a **white** sphere to be touched by 6 **black** spheres (P_{wb}):

> The central sphere is now white. The remaining spheres are N_b black and (N_w – 1) white, for a total of (N_{tot} – 1). If the coordination number is 6, with the same method as for the black sphere it is possible to say that the probability of a white sphere to be touched by 6 black spheres is:

$$P_{wb} = \frac{N_b}{(N_{tot} - 1)} \cdot \frac{(N_b - 1)}{(N_{tot} - 2)} \cdot \frac{(N_b - 2)}{(N_{tot} - 3)} \cdot \frac{(N_b - 3)}{(N_{tot} - 4)} \cdot \frac{(N_b - 4)}{(N_{tot} - 5)} \cdot \frac{(N_b - 5)}{(N_{tot} - 6)} \quad (40)$$

Comparing these two probabilities we notice that $P_{wb} > P_{bb}$. Similarly, we can come to the conclusion that $P_{bw} > P_{ww}$. These are the probabilities for coordination numbers of 6 of spheres all of the same colour, but it is reasonable to assume that a similar relationship can be calculated for mixed-colour coordination numbers and, eventually, lead to the relationship:

$$\mathbf{N_{wb} > N_{bb} > N_{bw} > N_{ww}} \quad \text{(assuming } N_b > N_w\text{)} \quad (41)$$

But this is not all. Let's consider the ratio between, for instance, P_{wb} and P_{bb}:

$$\frac{P_{wb}}{P_{bb}} = \frac{N_b}{(N_b - 6)} \qquad \text{(after simplification)} \qquad (42)$$

It can be seen that for large values of N_b the "- 6" will tend to be less important, and the two terms will, eventually, coincide. Therefore, it is also correct to state that:

(a) **if** $\mathbf{N_b >> 1}$ **then** $\mathbf{P_{wb} \approx P_{bb}}$ (43)

(b) **if** $\mathbf{N_w >> 1}$ **then** $\mathbf{P_{bw} \approx P_{ww}}$ (44)

If the number of black and white spheres is large enough, the colour of the central sphere does not influence its touching spheres' colour probability. With the same assumption used before, we are allowed to say that

if $\mathbf{N_b >> 1}$ **and** $\mathbf{N_w >> 1}$ **then**

$\mathbf{N_{wb} \approx N_{bb}}$ **and** $\mathbf{N_{bw} \approx N_{ww}}$ (45)

which is the statement in Section 4.6.

REFERENCES

Annic, C. et al. (1994). Experimental study of radical tessellations of assemblies of discs with size distribution. *Journal of Physics I France*, 4, 115-125.

Antony S.J. et al. (2005). Strength and signature of force networks in axially compacted sphere and non-sphere granular media: micromechanical investigations. *Journal of Physics D: Applied Physics,* 38, 3944-3952.

Aste, T. & Weaire, D. (2000). *The pursuit of perfect packing.* London: Institute of Physics Publishing.

Aste, T. (2005). Variations around disordered close packings. *Journal of Physics: Condensed Matter*, 17, 2361-2390.

Aste, T. et al. (1996)a. From one cell to the whole froth: a dynamical map. *Physical Review E*, 53(6), 6181-6191.

Aste, T. et al. (1996)b. Statistical properties and shell analysis in random cellular structures. *Physical Review E*, 54(5), 5482-5492.

Aste, T. et al.(2004)c. Investigating the geometrical structure of disordered sphere packings. *Physica A*, 339, 16-23.

Aste, T. et al. (2005)d. Geometrical structure of disordered sphere packings. *Physical Review E*, 71(6), 061302, 1-15.

Beck, J.M. & Volpert, V.A. (2003). *Gapped gapless packing structures.* Preprint submitted to Elsevier Science.

Bennett, C.H. (1972). Serially deposited amorphous aggregates of hard spheres. *Journal of Applied Physics*, 43(6), 2727-2734.

Berryman, J.G. (1982). Random close packing of hard spheres and disks. *Physical Review A*, 27(2), 1053-1061.

Bezrukov, A. & Stoyan, D. (2006). Simulation and statistical analysis of random packings of ellipsoids. *Particle & Particle Systems Characterization,* 23, 388-398.

Bezrukov, A. et al.(2001)a. Spatial statistics for simulated packings of spheres. *Image Anal. Stereol.,* 20, 203-206.

Bezrukov, A. et al. (2002)b. Statistical analysis of simulated random packings of spheres. *Particle & Particle Systems Characterization,* 19, 111-118.

Bouvard, D. & Lange, F.F. (1992). Correlation between random dense parking and random dense packing for determining particle coordination number in binary systems. *Physical Review A*, 45(8), 5690-5693.

Brilliantov, N.V. et al. (1996). Model for collisions in granular gases. *Physical Review E*, 53(5), 5382-5392.

Cheng, Y.P. et al. (2003). Discrete element simulation of crushable soil. *Geotechnique*, 53(7), 633-641.

Clarke, A.S. & Jonsson, H. (1993). Structural changes accompanying densification of random hard-sphere packings. *Physical Review E*, 47(6), 3975-3984.

Donev, A. et al. (2004)a. Jamming in hard spheres and disk packings. *Journal of Applied Physics*, 95(3), 989-999.

Donev, A.(2005)b. Pair correlation function characteristics of nearly jammed disordered and ordered hard-sphere packings. *Physical Review E*, 71(1), 1-14.

Elliott, J.A. et al.(2002). Recursive packing of dense particle mixtures. *Journal of Materials Science Letters*, 21, 1249-1251.

Frenkel, G. et al. (2008). Structural characterisation and statistical properties of two-dimensional granular systems. *Physical Review E*, 77, 041304-1 - 041304-10.

Fu, X. et al. (2006). Investigation of particle packing in model pharmaceutical powders using X-ray microtomography and discrete element method. *Powder Technology*, 167, 134-140.

Gan, M. et al. (2004). Predicting packing characteristics of particles of arbitrary shapes. *KONA*, 22, 82- 93.

Gervois, A. et al. (1992). Universal properties of Voronoi tessellations of hard discs. *Journal of Physics A*, 25, 6169-6177.

Gopalakrishnan, K. & Shashidhar, N. (2006). Structural characteristics of three-dimensional random packing of aggregates with wide size distribution. International *Journal of Information Technology*, 3(3), 201-208.

Hecht, C.A. (2000)a. Apollonian packing and fractal shape of grains improving geomechanical properties in engineering geology. *Pure and Applied Geophysics*, 157, 487-504.

Hecht, C.A. (2004)b. Geomechanical models for clastic grain packing. *Pure and Applied Geophysics,* 161, 331-349.

Jiang, M.J. et al. (2005). Yielding of microstructured geomaterial by distinct element method analysis. *Journal of Engineering Mechanics*, 1209-1213.

Kansal, A.R. et al. (2002). Computer generation of dense polydisperse sphere packings. *Journal of Chemical Physics*, 117(18), 8212-8218.

Kong, C.M. & Lannutti, J.J. (2000). Effect of agglomerate size distribution on loose packing fraction. *Journal of the American Ceramic Society,* 83(9), 2183-2188.

Kristiansen, K.L. et al. (2005). Simulation of random packing of binary sphere mixtures by mechanical contraction. *Physica A*, 358, 249-262.

Kumar, V.S. & Kumaran, V. (2005). *Voronoi neighbour statistics of hard disks and hard spheres* [online]. Available at <URL: http://scitation.aip.org/getabs/servlet/GetabsServlet?prog=normal&id=JCPSA6000123000007074502000001&idtype=cvips&gifs=yes> [Accessed 16 January 2008].

Lim, W.L. (2004). The application of Weibull statistics to the strength of railway ballast. *Granular Matters*, 6(4), 229-237.

Liniger, E. & Raj, R.(1987). Packing and sintering of two-dimensional structures made from bimodal particle size distributions. *Journal of the American Ceramic Society*, 70(11), 843-849.

Liu, L.F. et al. (1999). Dynamic simulation of the centripetal packing of mono-sized spheres. *Physica A*, 268, 433-453.

Luchnikov, V.A. et al. (1999). Voronoi-Delaunay analysis of voids in systems of nonspherical particles. *Physical Review E*, 59(6), 7205-7212.

Makse, H.A. et al. (2000). Packing of compressible granular materials. *Physical Review Letters*, 84(18), 4160-6143.

Mansfield, M.L. et al.(1996). The random parking of spheres on spheres. *The Journal of Chemical Physics*, 105(8), 3245-3249.

Matheson, A.J. (1974). Computation of a random packing of hard spheres. *Journal of Physics C,* 7. 2569-2576.

McDowell, G.R. (1996)a. The fractal crushing of granular materials. *Journal of the Mechanics and Physics of Solids*, 44(12), 2079-2102.

McDowell, G.R. (1998)b. On the micro-mechanics of crushable aggregates. *Geotechnique*, 48(5), 667-680.

McDowell, G. R. (2000)c. The application of Weibull statistics to the fracture of soil particles. *Soils and foundations*, 40(5), 133-141.

McDowell, G.R. & Humphreys, A. (2002). Yielding of granular materials. *Granular Matters*, 4(1), 1-8.

Nowak, E.R. et al. (1998). Density fluctuations in vibrated granular materials. *Physical Review E*, 57(2), 1971-19582.

Oda, M. (1977). Co-ordination number and its relation to shear strength of granular material. *Soils and Foundations*, 17(2).

Ohlenbush, H.M. et al. (1998). The topological structure of 2D disordered cellular systems. *The European Physical Journal B*, 2(2), 211-220.

Okubo, T. & Odagaki, T. (2004). Random packing of binary hard discs. *Journal of Physics: Condensed Matter,* 16, 6651-6659.

Onoda, G.Y. & Liniger, E.G. (1990). Random loose packings of uniform spheres and the dilatancy onset. *Physical Review Letters*, 64(22), 2727-2730.

Pfender, F & Ziegler, G.M. (2004). *Kissing numbers, sphere packings and some unexpected proofs* [online]. Available at <URL: http://www.math.tu-berlin.de/~fpfender/papers/AMS.pdf> [Accessed 16 January 2008].

Philippe, P. & Bideau, D. (2002). Compaction dynamics of a granular medium under vertical tapping. *Europhysics Letters*, 60(5), 677-683.

Philipse, A.P. (1996). The random contact equation and its implications for (colloidal) rods in packings, suspensions, and anisotropic powders. *Langmuir,* 12, 1127-1133.

Pinson, D. et al. (1998). Coordination number of binary mixtures of spheres. *Journal of Physics D*, 31, 457-462.

Plus Magazine (2003). Newton and the kissing problem [online]. Available at <URL: http://plus.maths.org/issue23/features/kissing/index.html> [Accessed 5 November 2007].

Pollastri, G. et al. (2002). Prediction of coordination number and relative solvent accessibility in proteins. *PROTEINS: Structure, Functions and Genetics*, 47, 142-153.

Richard, P. et al.(2001)a. A model of binary assemblies of spheres. *The European Physical Journal E*, 6(3), 295-303.

Richard, P. et al. (1999)b. Order and disorder in hard sphere packings. *Europhysics Letters*, 48(4), 415-420.

Richard, P. et al. (2003)c. Analysis by x-ray microtomography of a granular packing undergoing compaction. *Physical Review E*, 68(2), 020301, 1-4.

Santiso, E. & Muller, E. A. (2002). Dense packing of binary and polydisperse hard spheres. *Molecular Physics*, 100(15), 2461-2469.

Seidler, G.T. et al. (2000). Granule-by-granule reconstruction of a sandpile from x-ray microtomography data. *Physical Review E*, 62(6), 8175-8181.

Silbert, L.E. et al. (2002). Geometry of frictionless and frictional sphere packings. *Physical Review E*, 65, 031304, 1-6.

Sloane, N.J.A. (1998). *The sphere packing problem* [online]. Available at <URL: http://www.itsoc.org/publications/nltr/98_dec/08slo.pdf> [Accessed 16 January 2008].

Smith, W.O. et al. (1929). Packing of homogeneous spheres. *Physical Review*, 34, 1271-1274.

Thom, N. & Brown, S. (1988). The effect of grading and density on the mechanical properties of a crushed dolomitic limestone. Proceedings 14th ARRB Conference, part 7.

Ting, J.M. et al. (1995). Effect of particle shape on the strength and deformation mechanisms of ellipse-shaped granular assemblages. *Engineering Computations*, 12, 99-108.

To, L.T. & Stachurski, Z.H.(2004). Random close packing of spheres in a round cell. *Journal of Non-Crystalline Solids*, 333, 161-171.

Torquato, S. et al. (2000). Is random close packing of spheres well defined? *Physical Review Letters,* 84(10), 2064-2067.

Townend, R. (2006). *An investigation into x-ray computed tomography and its application into the damage evolution of dense bitumen macadam*. MEng dissertation, The University of Nottingham.

Troadec, J.P. et al. (1998)a. Statistics of Voronoi cells of slightly perturbed face-centered cubic and hexagonal close-packed lattices. *Europhysics Letters*, 42, 167-172.

Troadec, J.P. et al. (1987)b. Coordinance of a spherical impurity in a disordered packing of equal spheres. *Journal of Physics C*, 20, 993-1004.

University of Bristol (2007). Sphere packing [online]. Available at <URL: http://www.enm.bris.ac.uk/teaching/projects/2002_03/jb8355/sphere_packing.htm> [Accessed 28 February 2007].

University of Pittsburgh (1998). *The Kepler conjencture* [online]. Available at <URL: http://www.math.pitt.edu/~thales/kepler98/> [Accessed 5 November 2007].

Whistler Alley (2004). *Platonic Solids* [online]. Available at <URL: http://whistleralley.com/polyhedra/platonic.htm> [Accessed 23 June 2005].

Williams, S.R. and Philipse, A.P. (2003). Random packings of spheres and spherocylinders simulated by mechanical contraction. *Physical Review E*, 67(5), 051301. 1-9.

Wolfram (2002). *Sphere Point Picking* [online]. Available at <URL: http://mathworld.wolfram.com/SpherePointPicking.html> [Accessed 23 June 2005].

Wouterse, A. & Philipse, A.P. (2006) Geometrical cluster ensemble analysis of random sphere packings. *The Journal of Chemical Physics*, 125, 194709, 1-10.

Wouterse, A. et al.(2005). On the caging number of two- and three-dimensional hard spheres. *The Journal of Chemical Physics*, 123, 054507, 1-9.

Yang, R.Y. (2003). Numerical study of the packing of wet coarse uniform spheres. *Particle Technology and Fluidization*, 49(7), 1656-1666.

Yang, R.Y. et al.(2000)a. Computer simulation of the packing of fine particles. *Physical Review E*, 62(3), 3900-3908.

Yang, R.Y. et al.(2003)b. Effect of material properties on the packing of fine particles. *Journal of Applied Physics*, 94(5), 3025-3034.

Zou, R.P. et al.(2003)a. Packing of multi-sized mixtures of wet coarse spheres. *Powder Technology*, 130, 77-83.

Zou, R.P. et al.(2001)b. Packing density of binary mixtures of wet spheres. *Journal of the American Ceramic Society*, 84(3), 504-508.

Zou, R.P. et al. (2003)c. Coordination number of ternary mixtures of spheres – 2003. *Particle & Particle Systems Characterization,* 20, 335-341.